THEORETICAL ANALYSIS OF BUMP AND AIRBLAST EVENTS
ASSOCIATED WITH COAL MINING UNDER STRONG ROOFS

by

Xiaolin Wu

Dissertation submitted to the Faculty of the

Virginia Polytechnic Institute and State University

in partial fulfillment of the requirements for the degree of

Doctor of Philosophy

in

Mining and Minerals Engineering

APPROVED:

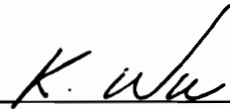<u>Dr. M. G. Karfakis, Chairman</u>

<u>Dr. C. Haycocks</u>

<u>Dr. M. Karmis, Department Head</u>

<u>Dr. E. Topuz</u>

<u>Dr. K. Wu</u>

September, 1995

Blacksburg, Virginia

Keywords: Roof, Bump, Airblast, Energy, Span

c.2

LD
5655
V856
1995
W83
c.2

THEORETICAL ANALYSIS OF BUMP AND AIRBLAST EVENTS
ASSOCIATED WITH COAL MINING UNDER STRONG ROOFS

by

Xiaolin Wu

Committee Chairman: Dr. Mario G. Karfakis

Mining and Minerals Engineering

(ABSTRACT)

This investigation was conducted to study the bump and airblast problems associated with delayed caving of competent longwall roofs. The roofs were modeled as elastic beams on continuous elastic foundations subject to exponentially distributed abutment stress. Elastic beam theory was applied to develop analytical solutions for deflection of single-layer roof models. Methods for analyzing double-layer roof and double-layer foundation models are discussed. Formulae for evaluating critical spans of the roof beds and strain energy storage in the roof and foundation are developed. The factors affecting roof caveability and energy accumulation are identified and analyzed. A comprehensive parametric analysis reveals that mechanical characteristics of roof beds, foundation properties, abutment stress concentrations, and roof configurations may interact to influence roof caveability and energy storage. Based on estimation of local Richter magnitude, criterion for pressure and shock bump events are suggested. Five case studies of bump events show that the theoretical predictions agree well with field data. The developed model solutions were implemented in a Windows-based software package CBPEP. This package facilitates determination of roof spans, stored strain energy in the roof and foundation, and the coal bump potential caused by delayed caving of strong roofs. The increases in air pressure and temperature associated with sudden roof collapse in a large area was also investigated using an adiabatic air compression model. The

presence of fragmented gob materials on the floor greatly influences the pressure and temperature variations after the recompaction of fragmented material commences. Three case studies of airblasts were analyzed, one of which was associated with a mine explosion. The investigation indicates that when a sufficiently large collapse is anticipated in a mine where flammable gas or dust may be present, it should be assumed that there exists a possibility that the high air pressure and temperature induced could trigger an explosion.

ACKNOWLEDGMENTS

TABLE OF CONTENTS

LIST OF FIGURES

LIST OF TABLES

CHAPTER 1   INTRODUCTION

1.1 Research Background

Coal bumps, or mine tremors, the violent, sudden failure of coal pillars and rock around the mine opening, are a common problem in deep underground coal mines with competent roof and floor rock.   These events may result in adverse effects such as fatalities and injuries, damage to mine facilities, economical losses from loss of production and abandonment of large reserves, and environmental concerns.   Although many factors, such as abnormal geological conditions, improper mine design, physical and mechanical properties of roof strata, and the like, may act together or separately to trigger bump events, the presence of strong, massive roofs immediately overlying the mined-out area has long been recognized to be a substantial factor in contributing to mine tremors associated with pressure and shock bumps.   This factor has been cited by numerous investigators [Avershin and Petukhov, 1964; Fine, et al., 1964; Holland, 1958; Holland and Thomas, 1954; Jacobi, 1966; Lama, 1966; Rice, 1934].   Typical competent roof strata in coal mines are sandstone, limestone, or sandy shale.   The majority of the U.S. bump-prone areas are located in the Southern Appalachian Basin of West Virginia, Kentuchy, Virginia, and the Uinta and Piceance Creek Basins of Utah and Colorado [Iannacchione and DeMarco, 1992].   Most of reserves in these areas are deep and have thick, strong, and massive sandstone or sandy shale roofs in close proximity to the coal seam.   Goode and others [1984] documented that all 20 coal bumps which occurred from 1964 to 1983 in

these areas associated with mining underneath strong sandstone or sandy shale roofs. Geological data compiled by Haramy and others [1988] indicated that 35 Colorado and 38 Utah active and abandoned coal mines had strong sandstone roof beds in the main roofs. Laboratory test data showed the average compressive strengths for the sandstone samples varying from 120 MPa to 230 MPa in the Southern Appalachian Coal Basin [Campoli, et al., 1993; Iannacchione and Mark, 1990; Khair, 1985], 70 MPa to 220 MPa in the Utah and Colorado coal mines, with a corresponding modulus of elasticity ranging from 8 GPa to 50 GPa [Haramy, et al., 1988; Haramy and McDonnell, 1988]. Of the 172 bump events comprising the USBM Coal Bump Database, lithologic descriptions of the mine roof are included for 95 bump sites. In 86 instances, reference is made to the presence of sandstone immediately above to within a few meters of the coalbed [Iannacchione and Zelanko, 1995]. There were some 2,000 bumps with Richter magnitudes between 2.5 and 3.8 occurred in China coal mines since 1949 which were associated with mining extractions taking place under strong sandstone, limestone roofs, with compressive strengths between 100 MPa and 220 MPa [Mei and Lu, 1987; Hua, 1987; Song and Xu, 1992]. Bump events caused by mining under competent roofs were also reported in other coal-producing countries, such as Poland, Russia, Australia, England, Canada, and Japan [Haramy and McDonnell, 1988; Kusznir, 1983; Lama, et al., 1984; Petulhov, 1987; Sugawara, et al., 1987; Zou and Miller, 1987]. It can be anticipated that the bump potential, as well as its severity, tend to increase with the increased production and mining depth.

It is believed that one of most important factors favoring bump conditions is the sudden release of strain energy stored in the coal seam and the surrounding rock mass [Haramy and McDonnell, 1988]. In longwall and retreat room-and-pillar mining, the removal of coal will redistribute the overburden weight around the working faces. The strong roofs tend to bridge or cantilever over adjoining gob area and transfer local stresses onto the working faces, the abutment pillars, and the unmined panels. At the same time, massive strain energy is stored both in the roof strata and the coal seam. The increased

deflection of the roof beds with the increase of the unsupported span results in the superimposition of additional stresses to the already high front abutment stress concentration. Pressure bumps may occur, if the local compressive stress concentration exceeds the local compressive strength of the coal, resulting in a violent release of stored strain energy in the form of elastic pulses radiating a considerable amount of seismic energy. Sudden catastrophic fracture of the roof strata may result in the rapid release of stored strain energy and in the rapid stress transfer to the abutments, potentially producing shock bumps.

A sudden collapse of strong roof beds in large mined-out area may be accompanied by an air blast or windblast event. The accelerated collapse of the roof strata will rapidly compress the air beneath the falling block, developing high air pressures in the mine void and the surrounding air escape ways. The devastating large-area roof collapse occurred at the Coalbrook North Colliery in South Africa on January 21, 1960 resulted in 437 fatalities, with a damage area extending even to one square mile [McPherson, 1980]. On July 16, 1986, an area of room and pillar gob estimated at some 10,000 m^2 within a larger gob area, collapsed at Moura No. 4 coal mine in Queensland, Australia. The windblast that swept through the section was followed immediately by a coal dust explosion. All twelve miners within the section were killed [McPherson, et al., 1995]. Airblast events due to violent caving of strong roof strata overhanging the mined-out area were also reported in China coal mines, causing serious accidents involving loss of life [Song and Xu, 1992].

1.2 Research Objectives

While the problem of coal bumps has been observed and extensively investigated for many years, and progress has been made in the detection of bump-prone areas and the

techniques in mitigating them, these events are still occurring at disturbing rates, and there has been little quantitative method to predict bump-prone conditions and evaluate bump intensities. Very limited work has been done in the investigation of air compression process during sudden roof caving. The objective of this investigation is to achieve a better understanding of the behavior of competent roofs, as related to bump and airblast problems caused by their delayed caving. In order to realize the objective the following specific goals are developed.

- To develop models and their analytical solutions of the cantilevering and bridging roof strata based on elastic beam principles

- To evaluate roof caveability in terms of determination of the critical spans of roof strata

- To determine the amount of strain energy stored in the roof and the coal seam prior to the roof collapse

- To develop a quantitative assessment of coal bump possibility and its severity caused by violent strain energy release

- To investigate the air compression process and its influencing factors caused by catastrophic collapse of roof strata in large areas

1.3 Research Scope

In the context of longwall and retreat room-and pillar mining system, four configurations of roof types are identified according to the locations of strong roofs and the longwall weighting stages. Analytical solutions for single-layer cantilevering and bridging roof models are developed using elastic beam theory. Following the analysis of

single-layer roof beam over single-layer foundation (coal), analytical approaches for double-layer roof beam and double-layer foundation (coal and weak roof) are discussed. A methodology to evaluate critical spans and stored strain energy in the roof and the coal seam is developed. Based on energy analysis, an evaluation of likeliness of bump problems and a quantitative assessment of the severity of these problems are proposed. Major factors influencing roof caveability and strain energy buildup are investigated. The developed analytical solutions are implemented in a Windows-based software package CBPEP. The airblast events associated with the accelerated roof collapse in large areas are also investigated. Several bump and airblast case studies are conducted to verify the developed models.

CHAPTER 2   LITERATURE REVIEW

2.1 Introduction

Although strong roof alleviates roof fall problems in panel entries, its inability to cave in a timely manner may result in a number of ground control problems. Methods to control or reduce the possibility and the severity of coal bumps are usually concerned with the behavior of the roof overhanging over mined-out areas. In coal mines, common roof formations are stratified and horizontally-bedded. This kind of the mine roof can be assumed to be continuous over plan area greater than that of any excavation created during mining. It is often considered as a "beam" or "plate" clamped at the edges by the pressure of the overburden. The voussoir beam or plate theory can be applied to analyze the performance of a jointed roof bed. In the study of ground control problems in longwall and retreat room and pillar mining, three particular important issues are roof caveability, strain energy storage and release, and the assessment of bump and accompanying windblast potential associated with delayed collapse of the competent roof beds. A brief literature review pertaining to these issues is given in the following sections of this chapter.

2.2 Investigation on Roof Caveability

As early as 1905, it had been assumed that the roof is composed of many thin beams, each beam supported by the underlying beam [Hackett, 1962]. In the case when the length of a roof bed is less than twice its width, it is treated as a plate [Adler and Sun, 1976]. The concept of a voussoir arch was introduced in 1941 to analyze the stability of mine roofs containing transverse fractures [Evans, 1941]. In more recent times, each of these theories: beam, plate and voussoir arch have been substantially improved by either more refined theoretical analysis or observations in the laboratory and in the field.

2.2.1 Beam Theory

Horizontally bedded mine roofs bounded by bedding planes are usually treated as built-in or simple supported beams [Caudle and Clark, 1955; Obert, et al., 1960]. Because of weak bond between bedding planes, the lower portion of the roof often detaches from the overlying rock and forms a layer loaded by its own weight. It is generally assumed that the beam is composed of a homogenous, isotropic, and elastic material, and that it is free from any discontinuities. In addition to these assumptions, the following geometric restrictions are also imposed: The span of the roof beam is at least twice the beam thickness; The length of the excavation is more than twice the roof span; The beam is of rectangular cross-section. The applied load is uniform and equal to the rock density multiplied by the roof thickness. The stress and the deflection are then evaluated from simple beam theory which can be found in any elementary mechanics of materials book. Because rock is much weaker in tension than in compression, only the tensile stresses are considered critical. The maximum span for a self-supporting built-in roof beam in tensile failure mode can be determined by the following expression [Adler and Sun, 1976]:

$$L_{max} = \sqrt{\frac{2T_o t}{\rho g}} \qquad (2.1)$$

7

where

L_{max} = maximum roof span,

T_o = tensile strength of rock,

ρ = rock density, and

g = gravitational acceleration.

Based on static equilibrium, an analysis of the inclined roof bed and multiple roof beds was also given by Adler and Sun [1976].

Assuming that overlying longwall roof beds are separated from each other along bedding planes with minimum tensile resistance, the cantilevering length of the roof bed behind the working face can be expressed as [Kidybinski, 1982]:

$$L_{max} = \sqrt{\frac{T_r t}{3\lambda}}$$
(2.2)

where

L_{max} = span of cantilevering roof beam,

T_r = tensile strength of roof strata,

t = roof thickness, and

λ = rock density.

In an attempt to explaining observed bump conditions presented by the different overburden depths in the Selby Coalfield where mining taking place under thick and massive limestone roof, Wilson [1986] hypothesized that the strong roofs acted as a fixed end beam under a uniform overburden pressure, and that the failure modes are governed by the overburden depth. There exists a limit of the overburden depth as determined by:

$$H = \frac{C_o - T_o}{2kg}$$
(2.3)

8

where

H = overburden depth,

Co = compressive strength of rock, and

k = ratio of horizontal stress to vertical stress.

Above this limit, the tensile failure would occur on the upside of the rock beam, remote from the excavation. Below it the severe compressive failure would take place on the underside of the rock beam, close to the excavation, causing a bump. He also proposed that in-situ horizontal stresses are of great importance in determining the caveability of strong roofs. The roof caving spans in tension and in compression can be determined by the following equations [Wilson, 1986]:

$$L_t = t\sqrt{\frac{2}{gH}(T_o + kgH)} \tag{2.4}$$

$$L_c = t\sqrt{\frac{2}{gH}(C_o - kgH)} \tag{2.5}$$

where

L_t = roof span in tension,

L_c = roof span in compression, and

t = roof thickness.

Recognizing the fact that the roof beds do not rest on completely rigid abutments and that the elastic deformation of the abutments ought to affect the stability of the roof, elastically supported beam theory, based on the differential equations of the elastic line, was proposed to provide an analytical basis for predicting the effects of elastic abutments on roof beam deflections [Hetenyi, 1946; Stephansson, 1971]. Stephansson [1971] developed the mathematical solutions of deflection, bending moment, and longitudinal

9

stresses for seven different roof configurations of single-, double- and multi-layer roofs on elastic abutments. In his analysis, the roof bed was assumed to act as a horizontal beam supported by the elastic, homogeneous, and isotropic abutments at both ends undergone a uniform loading. Model experiments and underground measurements were also conducted to verify theoretical predictions. His work showed that elastic deformations of the abutments had a great influence upon stress and deflection of the roof beam. The maximum values of deflection and stress of the roof beam followed between two extreme cases, i.e., simply supported and built-in beams [Stephansson, 1971].

In a study of strong roof performance in response to longwall mining, Haramy and others [1988] modeled the strong roof bed as a cantilever beam over an elastic foundation (coal) under a evenly distributed vertical overburden load. The deflection line of the bending roof beam and the strain energy storage in the roof and the coal seam were developed. However, the proposed cantilever roof model does not provide the method for determining the caving span of the roof strata.

For jointed roof beds, Singh and Dubey [1994] argued that the caving spans of the roof strata are controlled by joint orientation, features of bedding planes, rock density, and rock tensile strength. The following empirical expressions were proposed to determine the roof spans for the first caving and the periodic caving in longwall mining.

$$L_1 = F\sqrt{\frac{2itT_o}{\lambda}} \tag{2.6}$$

$$L_2 = F\sqrt{\frac{2itT_o}{3\lambda}} \tag{2.7}$$

where

L_1 = first caving span,

L_2 = periodic caving span,

10

F = joint orientation factor,

i = weakening coefficient,

t = roof thickness,

λ = rock density, and

T_o = rock tensile strength.

Many other specific approaches for evaluating roof caveability were proposed by other investigators as reviewed by Kidybinski [1982]. However, most of methods used so far have purely empirical feature and are hardly applicable for general use.

2.2.2 Plate Theory

When the length of a roof bed is less than twice its width, it must be analyzed by the plate theory. For a flat rectangular plate with a length of L and a width of b fixed on all sides under a uniform load, the maximum deflection and tensile stress are given by [Adler and Sun, 1976]:

$$D_{max} = \frac{A\rho gb^4}{Et^2} \tag{2.8}$$

$$\sigma_{max} = \frac{6B\rho gb^2}{t} \tag{2.9}$$

where

D_{max} = maximum deflection,

σ_{max} = maximum tensile stress,

ρ = rock density,

b = width of roof plate,

t = thickness of roof plate,

E = modulus of elasticity of rock, and

A, B = constants depended on ratios of roof length to roof width.

11

Equations 2.8 and 2.9 are valid for deflections which are small compared to the thickness of the plate. When the ratio of the length to the width of the roof bed is greater than two, the calculated maximum stress and deflection by Equations 2.8 and 2.9 approximate those for a built-in beam. The difference in maximum stresses is less than 1%, and the difference in maximum deflections is less than 12% [Obert, et al., 1960].

In the derivation of Equations 2.8 and 2.9, the neutral surface has been considered as the mid-surface of the plate, which is valid for steel-like materials, where elastic constants in compression and in tension are nearly equal. For rock material, it has been observed that the modulus of elasticity and the Poisson's ratio have different values obtained from compressive and tensile tests [Rzhevsky and Nasik, 1971; Adler, 1970]. A methodology for determination of these double elastic constants was developed by Adler [1970]. Investigation on rock plate with double elastic constants has been conducted by Singh and others [1980]. Their results showed that in bi-elasticity cases, application of Equations 2.8 and 2.9 would lead to serious errors. The actual flexural rigidity of the rock plate is lower than the corresponding value taking Young's modulus E_c under compression for the entire plate. At $E_c / E_t = 4$, the difference is more than 50 percent. The deflection of the plate is thereby significantly increased [Singh, et al., 1980].

2.2.3 Voussoir Beam and Plate Theory

Voussoir beam theory assumes that the roof beam consists of a no-tension material and carries its own weight by arching. The concept was first introduced by Evans [1941] to analyze the stability of the jointed roof strata which are far too cracked transversely to act simply as continuous and elastic beams. He investigated a beam with cracks at the center and the abutments using an assumed stress diagram as shown in Figure 2.1. However, an error in statics and the failure to handle the basic indeterminacy of the problem limited its practical application [Beer and Meek, 1982]. Subsequent significant investigations on voussoir beam behavior have been reported by Barker and Hatt [1972],

12
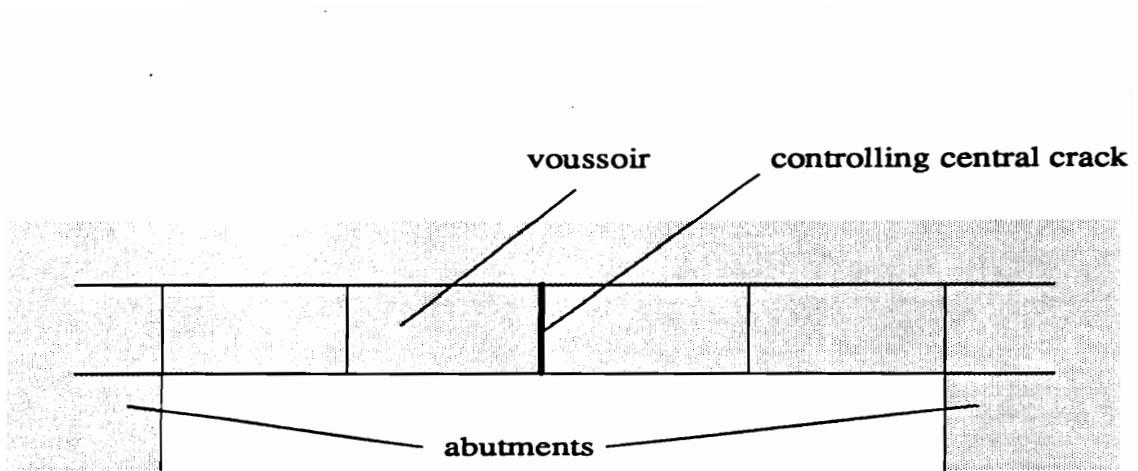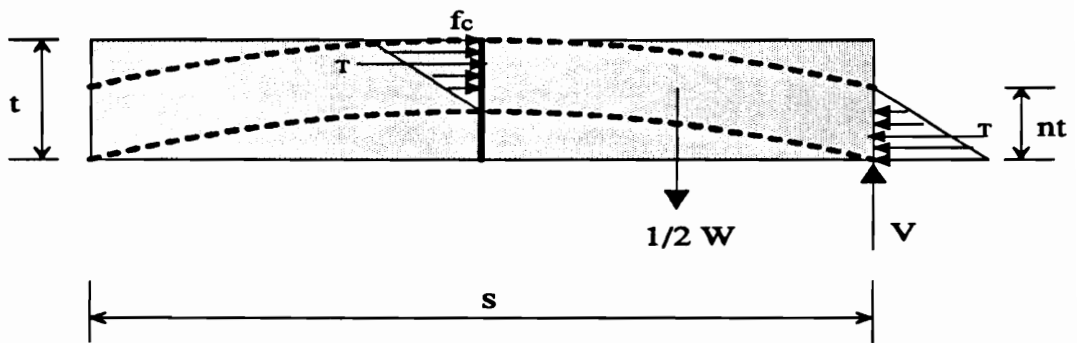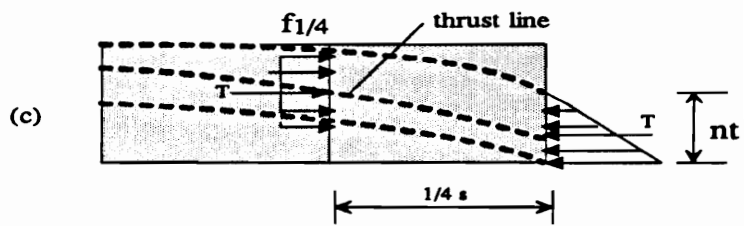
**Figure 2.1 Voussoir beam geometry and load specification
[after Brady and Brown, 1993]**

Wright [1974] and Sterling [1980]. Beer and Meek [1982] improved and extended these early work and developed a series of design curves suitable for design of underground excavations.

The basic assumptions made in voussoir beam theory include [Beer and Meek, 1982; Brady and Brown, 1993]: (1) the ground above the roof beam is completely destressed in the direction normal to the bedding plane, (2) the rock mass has parted along smooth bedding plane breaks forming a serious of beams, (3) the beam consists of no-tension material and the distribution of compressive stress at the central section and the abutments is linear and triangular, and (4) the thrust line has a parabolic shape.

A voussoir beam may fail in three ways [Brady and Brown, 1993]. For a beam with low span/thickness ratio failure may occur by shear at the abutments. For a roof with high span/thickness ratio, buckling failure of the beam may occur without significant spalling of central or abutment voussoirs. A roof with low strength or moderate span/thickness ratio may fail by compression at the center or abutments. The possibility of shear and compressive failure can be readily assessable by comparing the equilibrium distribution of stresses in the beam with the shear and compressive strength of material in question.

Brady and Brown [1993] devised a simple iterative procedure to analyze voussoir beam by the application of a relaxation scheme as expressed in a set of equations below:

$$f_c = \frac{\gamma s^2}{4nz} \tag{2.10}$$

$$f_{av} = \frac{1}{2} f_c \left(\frac{2}{3} + \frac{n}{2} \right) \tag{2.11}$$

$$L = s + \frac{16z^2}{3s} \tag{2.12}$$

$$\Delta L = \frac{f_{av}}{E'} L \qquad\qquad (2.13)$$

$$z = \left[\frac{3s}{16} \left(\frac{16 z_c^2}{3s} - \Delta L \right) \right]^{\frac{1}{2}} \qquad\qquad (2.14)$$

$$n = \frac{3}{2} \left(1 - \frac{z}{t} \right) \qquad\qquad (2.15)$$

where

f_c = maximum longitudinal stress,

γ = rock density,

s = beam span,

n = ratio of load to depth,

z = height of the incrementally deformed arch,

f_{av} = average longitudinal stress,

L = arc length of the arch,

ΔL = elastic shortening of the arch,

E' = modulus of elasticity of rock,

z_c = value of z from the previous computation cycle, and

t = thickness of beam.

The solution procedure involves sequential calculation of f_c, f_{av}, L, (L, z and n from Equations 2.10 to 2.15 [Brady and Brown, 1993]. Each sequence of computation produces new values of n, which is then introduced into Equation 2.10 to recommence the solution cycle. Iterations of the solution sequence are continued until stable values of the maximum longitudinal stress and the lateral depth ratio are obtained. A computer program of this iterative procedure was developed by Seedsman [1987].

15

For cases where the mine excavations have plan dimensions not compatible with the beam conditions, the voussoir beam theory was extended to plate by applying the concept of yield lines in the design of reinforced concrete slabs. A detailed design procedure for square and rectangular voussoir plates was given by Beer and Meek [1982], and improved by Brady and Brown [1993].

2.3 Analysis of Energy Changes due to Mining

The generation of underground excavation induces transient stresses which may be greater than the final, static stresses in the system. These transient effects on the stability of mine structures may be best studied through analysis of energy changes in the system. Rockbursts (in hard rock mining) or bumps (in coal mining) are caused by the violent release of kinetic, or seismic energy which is transformed from strain energy stored in stressed rock mass or coal, in the form of longitudinal and traverse elastic waves. Analysis of energy changes is the most effective method to study these violent events.

2.3.1 Mechanics of Bumps

The best description of the mechanics of coal bumps was given by Crouch and Fairhurst [1972], and expanded by Board and Fairhurst [1983]. Although it owes a lot to the earlier work on conventional rockburst studies summarized by Cook [1983] and Salamon [1983], the basic mechanics of bumps can be illustrated by the unloading deformation characteristics of a rock specimen under different stiff testing machines as shown in Figure 2.2 [Brady and Brown, 1993]. Suppose that the specimen is at its peak strength and is further compressed by a small amount Δs. In order to accommodate this displacement, the load on the specimen must reduced from P_A to P_B, so that an amount of energy ΔW_s, given by the area ABED in Figure 2.2 a and b, is absorbed. However, in displacing by Δs from point A, the 'soft' machine only unloads to F and releases stored
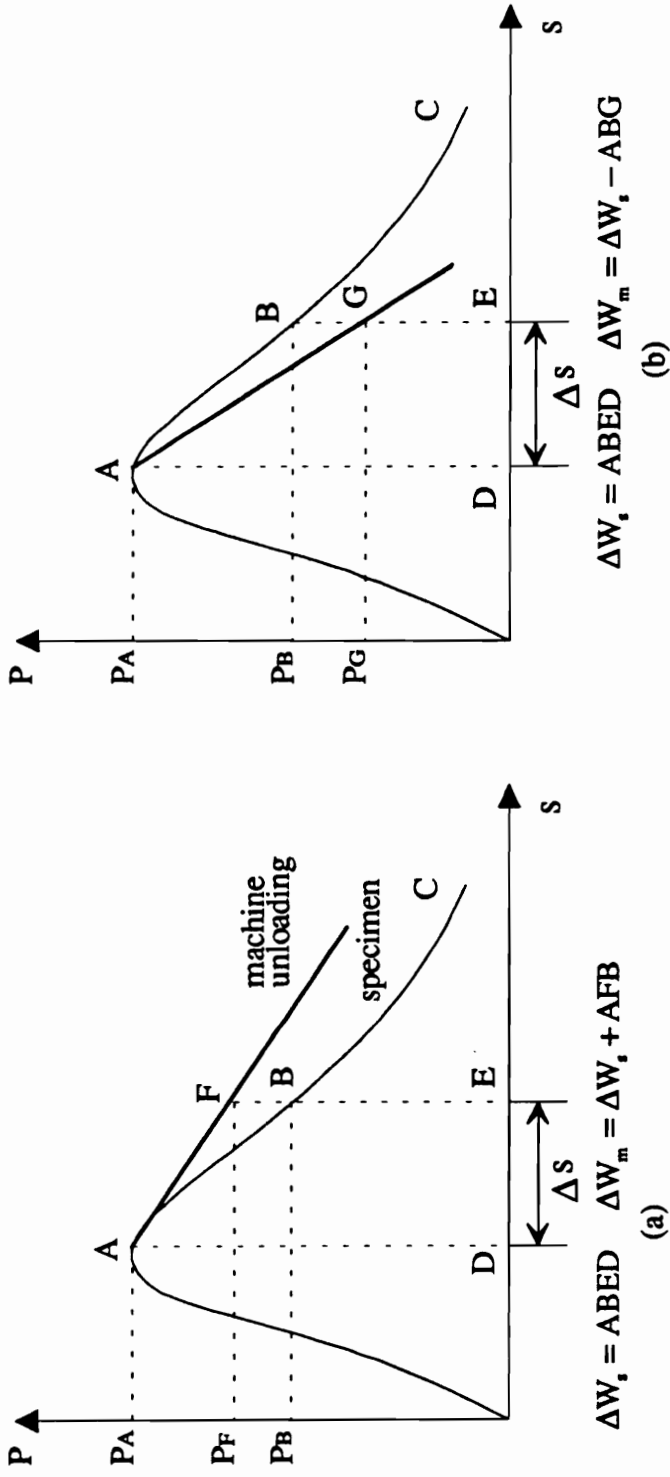
Figure 2.2   Post-peak unloading using machines: (a) soft, and (b) stiff
[after Brady and Brown, 1993]

17

energy ΔW_m, given by the area AFED. In this case $\Delta W_m > \Delta W_s$, the energy released by the machine during unloading is greater than that which can be absorbed by the specimen in following the post-peak curve from A to B. The excess of energy represented by the area AFB will be transformed into kinetic energy, causing catastrophic failure of the specimen. In the 'stiff' machine case as shown in Figure 2.2 b, the post-peak failure of the specimen is stable because $\Delta W_m < \Delta W_s$, and energy in excess of that released by the machine as stored strain energy, represented by the area ABG in Figure 2.2 b, must be supplied in order to deform the specimen along ABC.

Translated to a large scale, the bump conditions can be described as the process of stored strain energy release in the form of kinetic energy [Farmer, 1985]:

(1) The rock being loaded must be subjected to a stress of sufficient magnitude over a sufficiently large volume to release a large amount of energy if it fractures, and

(2) The loading conditions imposed by the surrounding rock must be such that their loading characteristic is less stiff than the fracturing rock.

These two factors are characterized as the energy dissipation function of the stressed rock and the energy release rate of the rock mass, and the interaction between these will determine the likelihood of bumps. The energy release rate is the rate of energy released during generation of underground excavations and is equal to the product of the mean force on the areal increment before extraction and the mean convergence after extraction. The energy dissipation function of the stressed rock is related primarily to its ability to yield or fracture, absorbing accumulated strain energy in the stress concentration zone around the excavation. Most of bump control measures are aimed at changing the energy dissipation function.

2.3.2 Energy Analysis due to Mining

A considerable amount of investigations have been attempted to answer the following two questions:

- In what way does the creation of excavations affect the energy changes and energy redistributions around excavations?

- Where does the kinetic or seismic energy come from?

2.3.2.1 Fundamental Energy Relationship in Mining Context

The general ideas of fundamental energy storage and release process during mining were proposed by Cook [1967b], Salamon [1974], and Blight [1984]. As summarized by Brady and Brown [1993], the energy redistribution caused by gradual creation of excavation follows the following pattern. As gradual remove of mine material, excavations in mines change in shape and grow in size with time, and areas of induced stress are generated around excavations. The previously stored strain energy in removed materials W_r is gradually released. Partial released energy W_r is transformed into surrounding induced stress zone, causing an increase of energy ΔW_s. The remnant of the released energy is consumed in the form of rock fracture energy W_f in the stress induced zone. Energy conservation law requires that $W_r = \Delta W_s + W_f$. In the case of sudden creation of an excavation, the work that would have been done by the host rock, exterior to the excavation periphery, appears as excess energy W_e at the excavation surface. This excess energy is subsequently released or propagated into the surrounding media in the form of kinetic energy. This process is similar to sudden loading applied to an elastic spring. Sudden loading produces imbalanced kinetic energy in the spring and radiates elastic waves. This extreme case gives an explanation of the possible source of kinetic or seismic energy.

2.3.2.2 Energy Changes for a Spherical Cavity

Research work by Hopkins [1960], Timoshenko and Goodier [1970], and Salamon [1983] showed that excess energy, W_e, induced by the sudden development of a spherical opening had the same magnitude of the energy released by excavating opening W_r. The dynamic response of this excess energy is generation of stress waves which radiate through the surrounding rock mass at the longitudinal wave velocity. It can be inferred that analysis of the released energy may constitute a basis for excavation design, since the released energy or energy release rate indicate both static and dynamic stresses imposed by the excavation.

2.3.2.3 Energy Changes for a Thin Tabular Excavation

Since this kind of excavation is common when coal seams or gold reefs are mined by longwall methods, energy changes or energy release associated with creating tabular excavations have been the subject of numerous investigations. Many of original ideas associated with energy release evolved from studies of problems in deep mining in South African goldmines [Salamon, 1984]. Using displacement-discontinuity techniques, special forms of the results for a single excavation were given by Salamon [1974, 1983, 1984] and Walsh [1977]. The important results from energy analysis for a tabular excavation include: (1) Sudden generation of a tabular excavation results in all strain energy stored in the removed materials transformed into surrounding stressed rock mass [Brady and Brown, 1993]; and (2) The amount of kinetic energy transferred from total energy released during excavating depends on how many mining steps were taken to reach the final shape and size of the excavation as shown in Figure 2.3 [Salamon, 1983].

2.3.2.4 Source of Kinetic or Seismic Energy

A close examination of energy analysis and illustrated examples of spherical cavity and thin tabular excavation discussed in Brady and Brown's textbook [1993] shows that
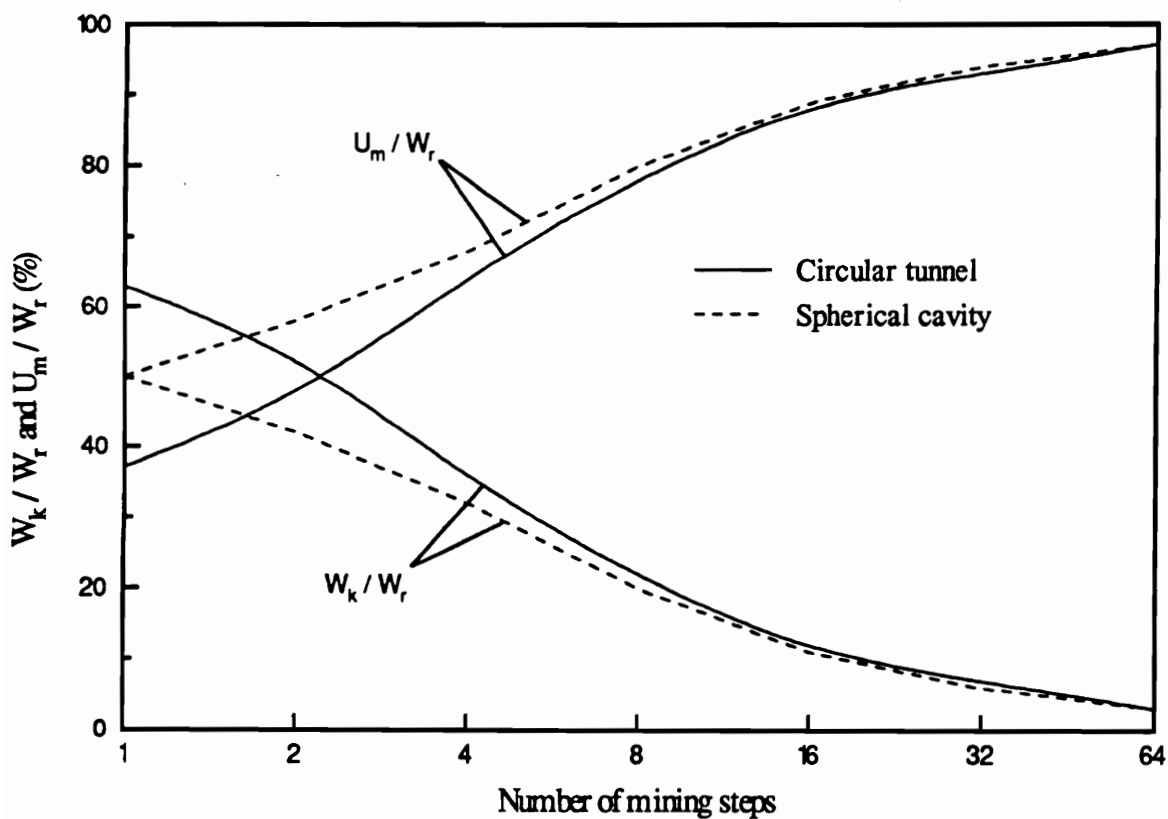
Figure 2.3 Split of the total released energy [after Salamon, 1983]
(W_r: total released energy; W_k: kinetic energy; and U_m: strain energy
removed with the excavated rock)

the source of kinetic or seismic energy accompanying by rockbursts is sudden generation of excavation, and that the induced stress waves radiate from the periphery of the excavation. This explanation for kinetic energy source is valid based on assuming that the excavation is made in one step. When the excavation is in fact expanded gradually, the estimation is grossly misleading. The error increases with the number of steps used to excavate the cavity. For instance, work done by Salamon [1983] showed that 50 percent of the released energy can be transformed into kinetic energy if a spherical cavity was made in one step, but if mining were done in 64 equal steps the kinetic energy would be only 3.4 percent of the released energy W_r (Figure 2.3). This suggests that the enlargement of mining excavations in small steps, which is the normal course of mining in most cases, does not result in the release of kinetic energy into the rock mass, therefore, it can not be the source of seismic energy. Another explanation of the kinetic energy source was given by Salamon [1983]. He suggested that the source of kinetic, or seismic energy comes from strain energy stored in stress-concentrated zone surrounding the excavation. A seismic event would occur if the following conditions pre-exist [Salamon, 1983]:

- Substantial amount of energy must be stored in the rock around the instability to provide the source of kinetic energy. The origin of this energy is work done by: (1) gravitational forces and/or (2) tectonic forces and/or (3) stress induced by mining.

- A region in the rock mass must be on the brink of unstable equilibrium.

- Some induced stresses must affect the region in question, however small, must be sufficiently large to trigger off the instability.

- Sudden stress change of sizable amplitude must take place at the locus of instability to initiate the propagation of seismic waves.

22

2.3.2.5 Strain Energy Stored in the Roof and Coal

Phillips [1944], Holland and Thomas [1954] noted that the accumulation of strain energy in the coal and the adjacent rock strata is often the driving forces behind coal bumps. They reasoned that since coal is a relatively compressible material it can store high amounts of strain energy even at fairly low stress levels, and further suggested that an overlying bed of massive sandstone contributes to both the accumulation and the release of this stored energy.

Holland [1955] analyzed the strain energy stored in the roofs and the coal. The roof beds were modeled as either cantilever or fixed-end beams. The amounts of stored strain energy in the cantilever beam, the fixed-end beam, and the coal are given by the following expressions [Holland, 1955]:

$$W_{rc} = \frac{Q^2 L^5}{40EI} \tag{2.16}$$

$$W_{rf} = \frac{Q^2 L^5}{1440EI} \tag{2.17}$$

$$W_c = \frac{1}{2E_c}\left\{ P^2 + \left(\frac{P}{M-1}\right)^2 - \frac{2}{M}\left[\left(\frac{2P^2}{M-1}\right) + \left(\frac{P}{M-1}\right)^2\right]\right\} \tag{2.18}$$

where

      W_{rc} = strain energy stored in the cantilever roof beam per unit volume,

      W_{rf} = strain energy stored in the fixed-end roof beam per unit volume,

      W_c = strain energy stored in the coal per unit volume,

      Q = load per unit length,

      P = principle stress,

      L = length of the roof beam,

      E = Young's modulus of roof,

E_c = Young's modulus of coal,

M = coal Poisson's number, the inverse of Poisson's ratio, and

I = moment of inertia.

Haramy and others [1988] presented a general analysis of strain energy accumulation associated with longwall mining by simulating the strong roof as an elastic cantilever beam over elastic foundation under uniformly distributed overburden load. With the assumption of a constant applied load, the effects of elastic modulus of the roof strata, roof thickness, and roof overhang length on the strain energy accumulated in the roof and the coal were investigated [Haramy, et al., 1988]. However, the model discounts highly concentrated abutment pressures ahead of longwall faces. This limitation prevents an accurate evaluation of the total amount of strain energy stored in the roof and the coal.

In an analysis of ground control problems associated with longwall mining under strong roofs done by Wu and Karfakis [1993, 1994, 1995], the analytical solutions for strain energies stored in the roof and the coal were developed [Wu and Karfakis 1994a]. Depending on the weighting stages induced by longwall face advances, the strong roofs were modeled as either cantilevering or bridging beams over elastic foundations under exponentially distributed stress along the front abutment [Wu and Karfakis 1993].

2.4 Evaluation of Bump Potential

A considerable amount of research work have been conducted on identifying coal bump-prone conditions. Several proposed criteria for evaluating bump potential are reviewed below.

An energy index [Neyman, et al., 1972] was proposed to estimate coal's tendency to bump based on laboratory-derived loading-unloading characteristics of a coal specimen.

The energy index can be determined by the following equation:

$$W_{et} = \frac{E_e}{E_p}$$

(2.19)

where

E_e = elastic energy stored in a rock sample during loading, and

E_p = energy losses due to permanent strain during unloading.

The larger the value of W_{et}, the greater the susceptibility to bumps. For Polish coal, a value of W_{et} greater than 5 meant the coal was liable to bump.

Many field studies have related coal bump occurrences to a definite set of geological factors, namely, thick overburden, competent roof and floor strata. Lippmann [1988] suggested that coal bumps occur only when the roof and floor rock adjacent to the coal seam are about 10 times stiffer and stronger than the coal. Analysis of field data from twelve mines [Maleiki, 1995] indicated that this criterion was inadequate to assess the bump proneness. Maleiki [1995] showed that although most bumps occurred where the Young's modulus ratios (roof / floor to coal) were greater than 8 and the corresponding strength ratios greater than 4, there were two severe bump events occurred where Young's modulus and strength ratios were as low as 5 and 3, respectively.

Cook [1978] reported a comprehensive correlation between the calculated volume rate of energy release and the number of observed damaging bursts in South African goldmines. The results showed that an increase of the energy release rate yielded increasing burst occurrences (Figure 2.4). Crouch and Fairhurst [1973] also concluded that coal bumps could be related to energy release rate during pillar yielding. South African engineers have applied energy release concept mostly based on results of Cook [1967a] and Salamon [1974] to the practical design of mine layouts and excavation procedures in the burst-prone conditions [Board and Fairhurst, 1983; Salamon, 1983].

25
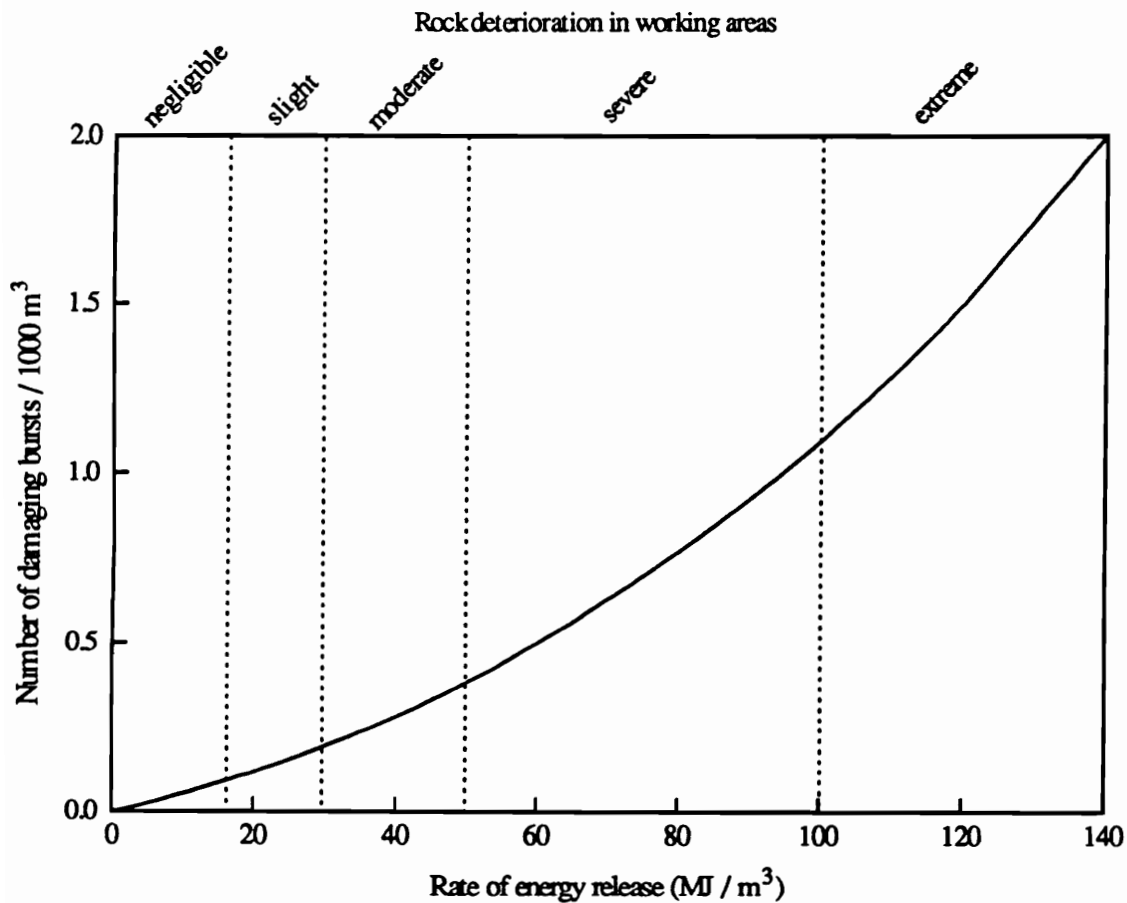
Figure 2.4 Relation between frequency of rock bursts, local ground conditions, and energy release rate in longwall mining of gold reefs [after Cook, 1978]

The optimum layout pattern is that for which the energy release rate is most nearly uniform at all stages of mining. Maleiki and others [1987] applied this method for scheduling pillar retreating activities to maintain a uniform energy release rate to avoid bump events. As noted by Zipf and Heasley [1990], the effectiveness of applying energy release rate in the prediction of bump events is limited. Since the energy release rate is inversely proportional to Young's modulus of the roof rock, a weak roof bed corresponds to a higher energy release rate or a higher possibility of bump conditions. But most bumps have occurred when mining under strong sandstone roofs.

More recently, Sames [1995] proposed a quantitative assessment of bump hazard based on evaluation of three bump contributory factors, namely, overburden depth, roof strength, and floor strength. Index scales were developed for each of these three parameters with each scale varying from 0 to 100. Three separate index values were then combined and averaged to arrive at a single relative bump hazard index. The higher the index value, the greater the degree of bump likeliness.

By estimated the local Richter magnitude and total stored strain energy when strong roof fractures, a quantitative method was proposed to identify the coal bump potential by Wu and Karfakis [1994b, 1995].

$$\log(nW_t) = 11.8 + 1.5M_L \tag{2.20}$$

where

n = seismic efficiency,

W_t = total strain energy stored in roof and coal,

M_L = local Richter magnitude.

Based on estimated local Richter magnitude, an estimation of the damage extent associated with bump events could be made by the particle velocity model suggested by Brady and Haramy [1994]:

$$\log(R^{1.5}v) = 5.50 - 0.50\log(\rho) + 2.5\log(a) + 0.75M_L \qquad (2.21)$$

where

R = radius of the damage area,

v = minimum particle velocity to initiate rock fracture,

ρ = rock density, and

a = constant.

2.5 Investigation on Airblast Phenomenon

Significant investigations on the airblast phenomenon has been attempted by McPherson [1980, 1995]. In his early work published in 1980, he developed a confined model to simulate the processes of the air compression and the recompaction of the fragmented pillar materials on the floor. In this model, the air compression under the falling roof was considered to be adiabatic, that is, during roof collapse, the heat transfer to the surrounding rock mass occurs much more slowly than the air compression process The investigation revealed that the astonishingly high air pressures that can be developed by large roof falls in confined areas [McPherson, 1980]. Recently, the air leakage model [McPherson, 1995] was developed to incorporate the dynamic air leaking through the air escape ways connected to the collapse area, and the damping effect owing to the shear resistance of the falling block. The most significant result is the prediction that the temperature of the air increases rapidly and continuously as the roof descends, reaching values that are capable of igniting a gas or dust explosion [McPherson, 1995]. Results of time stepping computer simulation by the author revealed that the damping force acted on the falling strata greatly influences the air compression process, and hence the developed peak air pressure and temperatures. Through successful trials and reasoning, the damping factor proposed by McPherson [1995] was modified to include the effects of the contact

28

area between the sides of the falling block and the intact rock mass, and the initial air volume to be compressed below the falling block [McPherson, et al., 1995]. Sensitivity analyses have been conducted to investigate the effects of the thickness of the falling block, the plan area of the collapse, the initial height of the opening, and the degree of damping of the process on the behavior of air pressures and temperatures during roof collapse [McPherson, et al., 1995].

CHAPTER 3 MODEL FORMULATION AND
SOLUTIONS OF DEFLECTION LINE

3.1 Introduction

The full size structure considered in this research is the horizontally bedded roofs that exist in most of coalbeds throughout the world. This kind of structure is often treated as either a cantilever or a fixed-end beam over rigid abutments loaded by uniformly distributed overburden pressure. Induced stresses and deflections by bending of the beam are then evaluated based on classic simple beam theory. In reality, we know, of course, that the roof beds do not rest on completely rigid abutments and that the elastic behavior of the foundation ought to influence the stability of roof beam. We also know that the applied load on the roof beam is no longer uniform due to the stress redistributions caused by mining activities. Therefore, in order to reach a reasonable solution, the influence of foundations and non-uniformly applied loading conditions must be taken into account in the analysis. In this chapter, four roof models are identified with considerations on the locations of strong roofs and the mining stages in longwall or retreat room-and-pillar extractions. The abutment stress concentration is approximated as an exponentially decaying form. Based on the elastic beam theory, analytical solutions of the deflection line for each roof model are developed. The influence of the difference in the elastic moduli of rock materials under tension and compression on the flexural rigidity of the roof beam is

investigated. By applying the composite beam principles, a methodology of analyzing double-layer roofs is also discussed.

3.2 Model Formulation

In the formulation of the models, assumptions must be made to simplify the problem and reach a reasonable solution. For the application of elastic beam theory in the problem, the following conditions are assumed:

- The strong roof beds are composed of elastic, isotropic, and homogeneous rock material, and are devoid of discontinuities. Under consideration are competent roofs found in most bump-prone coalbeds, in both U.S. and other coal-producing countries, with high compressive strengths varying from 100 to 230 MPa and with corresponding moduli of elasticity from 8 to 50 GPa.

- Each layer is assumed to be a horizontally bedded formation with a rectangular cross-section and partially supported by elastic foundations, such as weak rock beds or coal pillars. The behavior of each layer conforms to the elastic beam principle. The length of each layer is greater than twice its width. The thickness of each individual layer is less than one fifth of the roof span. Hence, within this interval the influence of shear stresses can be neglected and the deflection curve is regarded as the curvature due to the bending moment only. The deflection of a rock beam is small in comparison with the layer thickness. The neutral axis is located by considering different elastic moduli under tension and compression. The stresses developed within the rock beam are proportional to the distance from the neutral axis.

- The applied load is distributed in an exponentially decaying form along the

31

supported segment of the beam. For the unsupported part of the beam, the load is assumed to be uniformly distributed. The deflection of the roof beam does not appreciably change the load conditions.

- Two types of foundations are considered. One is coal seam, and the other consists of two layers, the coal seam and the overlying weak rock stratum, or weak floor stratum. Each foundation layer is assumed to be elastic, homogeneous, and isotropic. The foundations are presumed to rest on the underlying rigid floor strata.

Based on the locations of overlying strong roof beds and the extraction stages in longwall and retreat room-and-pillar mining, roof configurations are categorized as four models.

Model 1 Single-layer cantilevering strong roofs - A single strong bed exists either in the immediate roof or in the main roof at the periodic weighting phase in longwall extraction or at pillar retreating phase in room-and-pillar extraction . This type of roof bed acts as a cantilever beam resting on an elastic foundation (coal or weak roof) as illustrated in Figure 3.1. If the strong roof bed appears in the main roof, the weak immediate roof bed is regarded as part of a double-layer foundation.

Model 2 Single-layer bridging strong roofs - The locations of strong roof beds are the same as in Model 1. This roof model represents the initial caving phase in longwall extraction or the room development phase in retreat room-and-pillar extraction (Figure 3.2). In this type, both ends of the roof are supported by elastic foundations (coal or weak roof).

Model 3 Double-layer cantilevering strong roofs - In this roof model, both the immediate and the main roofs consist of competent roof beds with the ground movement

32

occurring at the periodic weighting phase for longwall mining and at pillar retreating phase for room-and-pillar mining (Figure 3.3).

Model 4 Double-layer bridging strong roofs - This roof model is associated with the first weighting phase for a longwall system or the room development phase for a room-and-pillar system. Double-layer strong roof beds are bridged on elastic foundations as shown in Figure 3.4.

In the following sections, the basics of the elastic beam theory are discussed and then the analytical solutions of the deflection lines for each roof model are investigated.

3.3 Fundamentals of Elastic Beam Theory

3.3.1 Differential Equation of the Bending Beam

Consider a finite straight beam supported along its length by an elastic foundation and subjected to an arbitrarily distributed load $p(x)$ as illustrated in Figure 3.5. Due to the elastic assumption on the foundation, its reaction $q(x)$ is proportional to the deflection y of the beam which is defined by the well-known fourth order differential equation:

$$D\frac{d^4y}{dx^4} = p(x) - cy$$

(3.1)

where

   D = flexural rigidity of the beam,

   $p(x)$ = arbitrarily distributed load on the beam,

   c = modulus of the foundation, and

   y = deflection of the neutral axis of the beam.

33
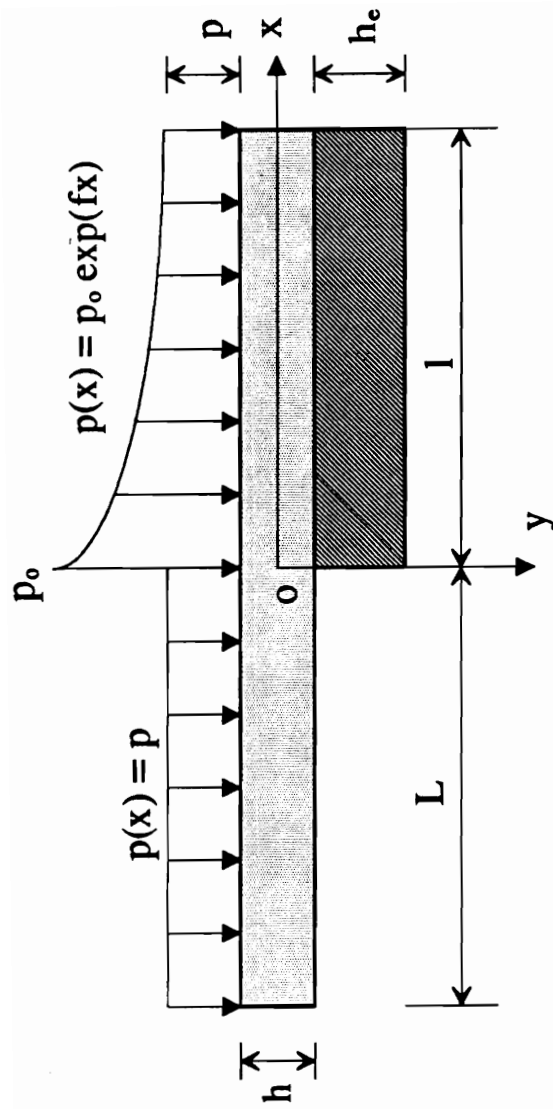
Figure 3.1 Model 1 A single-layer cantilevering beam

34
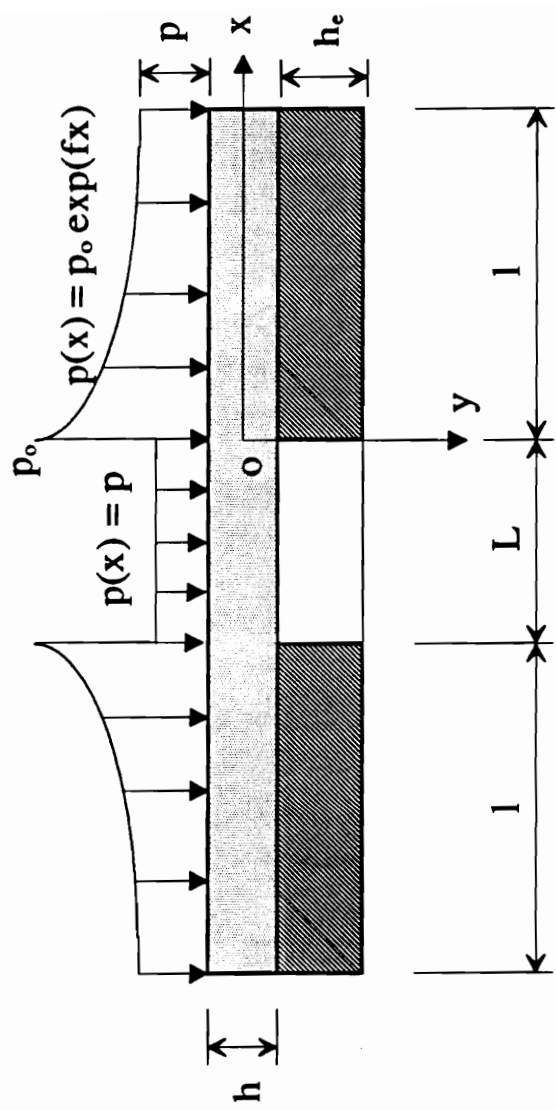
Figure 3.2 Model 2 A single-layer bridging beam
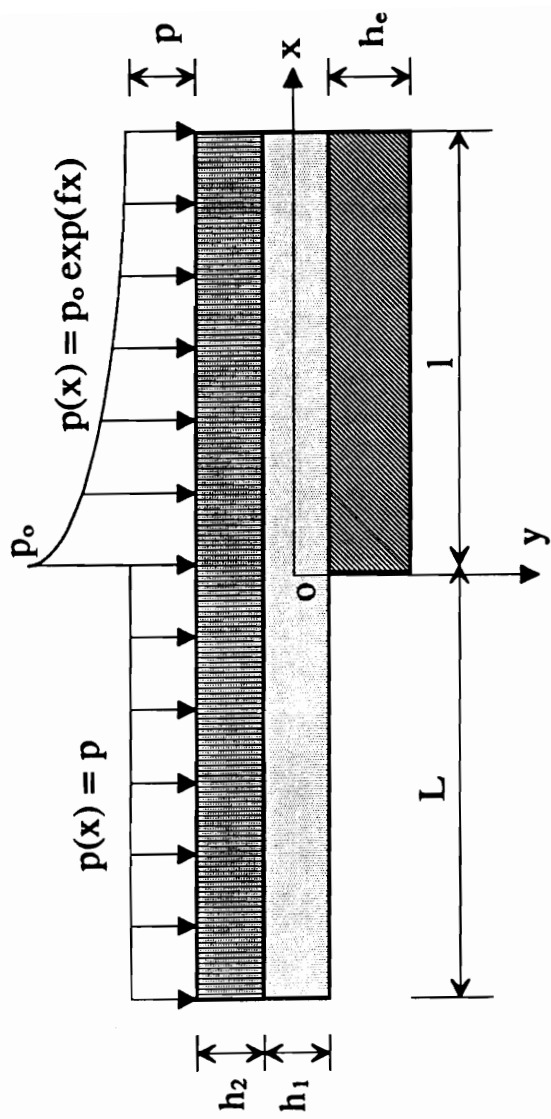
Figure 3.3 Model 3 A double-layer cantilevering beam
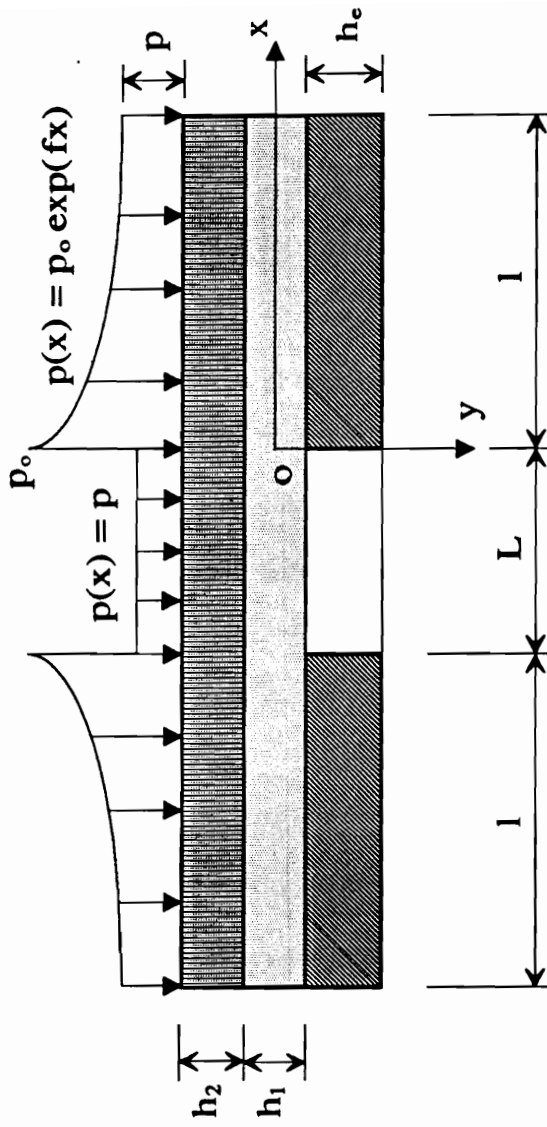
Figure 3.4 Model 4 A double-layer bridging beam
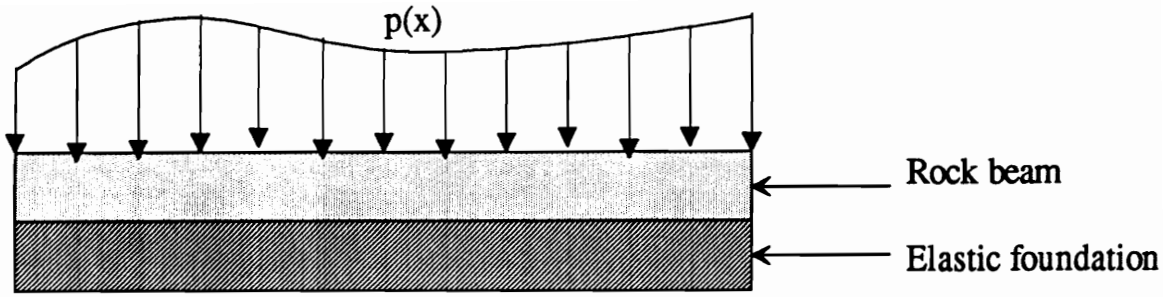
(a) A rock beam on an elatic foundation

q(x)=cy

(b) Applied load on the rock beam

Figure 3.5 A finite beam on an elastic foundation

Equation 3.1 is valid for deflections which are small compared to the thickness of the beam.

3.3.2 Foundation Characteristics

The foundation modulus, c, in Equation 3.1 is a characteristic of the elastic foundation, and is given as [Stephanson, 1971]:

$$c = \frac{E_e}{h_e\left(1-v_e^2\right)} \tag{3.2}$$

where

E_e = Young's modulus of the foundation,

h_e = height of the foundation, and

v_e = Poisson's ratio of foundation.

Using the notations in Figure 3.6, the modulus of a double-layer foundation c' can be determined by the following equations [Stephanson, 1971]:

$$c' = \frac{E_e{}'}{\left(h_{e1}+h_{e2}\right)\left(1-v_e{}'^2\right)} \tag{3.3}$$

$$E_e{}' = \frac{\left(h_{e1}+h_{e2}\right)E_{e1}E_{e2}}{h_{e1}E_{e2}+h_{e2}E_{e1}} \tag{3.4}$$

$$v_e{}' = \frac{\left(h_{e1}+h_{e2}\right)E_{e1}E_{e2}\left(v_{e1}h_{e1}+v_{e2}h_{e2}\right)}{\left(h_{e1}E_{e2}+h_{e2}E_{e1}\right)\left(h_{e1}E_{e1}+h_{e2}E_{e2}\right)} \tag{3.5}$$

39
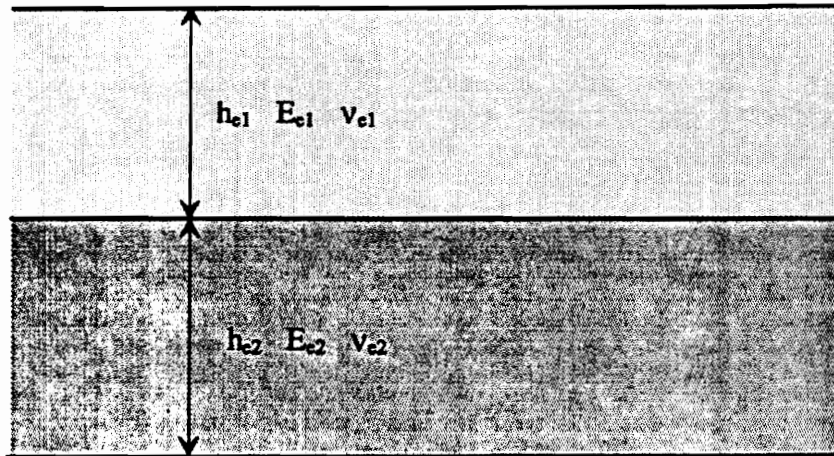
Figure 3.6 Foundations consisting of two distinct layers

where

c' = equivalent modulus of the double-layer foundation,

E_{e1}, E_{e2} = Young's moduli of lower and upper layers for the double-layer foundation, respectively,

E_e' = equivalent Young's modulus of the double-layer foundation,

h_{e1}, h_{e2} = thicknesses of lower and upper layers for the double-layer foundation, respectively,

v_{e1}, v_{e2} = Poisson's ratios of lower and upper layers for the double-layer foundation, respectively, and

v_e' = equivalent Poisson's ratio of the double-layer foundation.

3.3.3 Solutions of the Differential Equation of the Bending Beam

The solutions of differential Equation 3.1, $y(x)$, consist of two components, namely, the general solution and the specific solution.

$$y(x) = y_1(x) + y_2(x) \tag{3.6}$$

where

$y_1(x)$ = specific solution of the deflection line, and

$y_2(x)$ = general solution of the deflection line.

The specific solution of the deflection line, $y_1(x)$, is dependent upon the forms of the applied load $p(x)$.

By introducing the notation:

$$\beta = \sqrt[4]{\frac{c}{4D}} \tag{3.7}$$

where

β = characteristic of the roof-foundation system.

The general solution of the deflection line, $y_2(x)$, can be expressed as:

$$y_2(x) = e^{-\beta x}(A_1 \sin \beta x + A_2 \cos \beta x) + e^{\beta x}(A_3 \sin \beta x + A_4 \cos \beta x) \qquad (3.8)$$

in which coefficients A_1, A_2, A_3, and A_4 depend upon the manner in which the beam is subjected to loading.

3.3.4 Bending Moment and Shear Force of the Bending Beam

From the elastic beam theory, the bending moment M, the shear force V, and the deflection y, of the beam have the following relations:

$$M = -D\frac{d^2y}{dx^2} \qquad (3.9)$$

$$V = \frac{dM}{dx} = -D\frac{d^3y}{dx^3} \qquad (3.10)$$

where

M = bending moment of the beam, and

V = shear force of the beam.

3.3.5 Determination of Equivalent Elastic Constants for Rock Material

For rock materials, the modulus of elasticity in compression E_c, is generally greater than the modulus of elasticity E_t, in tension. It was reported that for sandstone $E_c = (1.5--4.0)$ E_t [Rzhevsky and Nasik, 1971]. The lower values of the modulus in tension will

42

result in a shift of the neutral axis from the center line to the concave side of the beam as shown in Figure 3.7.

For a rectangular beam with a width of b and a thickness of h, using the notations in Figure 3.7, the new position of the neutral axis is now defined by the following equations [Timoshenko, 1983]:

$$h_1 = \frac{h\sqrt{E_c}}{\sqrt{E_t} + \sqrt{E_c}} \qquad (3.11)$$

$$h_2 = \frac{h\sqrt{E_t}}{\sqrt{E_t} + \sqrt{E_c}} \qquad (3.12)$$

where

       h = thickness of the beam,

       h_1 = distance between the neutral axis to the underside of the beam,

       h_2 = distance between the neutral axis to the upside of the beam,

       E_t = modulus of elasticity in tension of the beam, and

       E_c = modulus of elasticity in compression of the beam.

Because of the shift of the neutral axis, the equivalent modulus of elasticity E_{ev}, and the equivalent moment of inertia I_{ev}, of the beam are reduced and can be evaluated as follows [Jaeger, 1979]:

$$E_{ev} = \frac{4 E_t E_c}{\left(\sqrt{E_t} + \sqrt{E_c}\right)^2} \qquad (3.13)$$

$$I_{ev} = \frac{b h_1{}^3 \left(\sqrt{E_t} + \sqrt{E_c}\right)}{3 \sqrt{E_c}} \qquad (3.14)$$
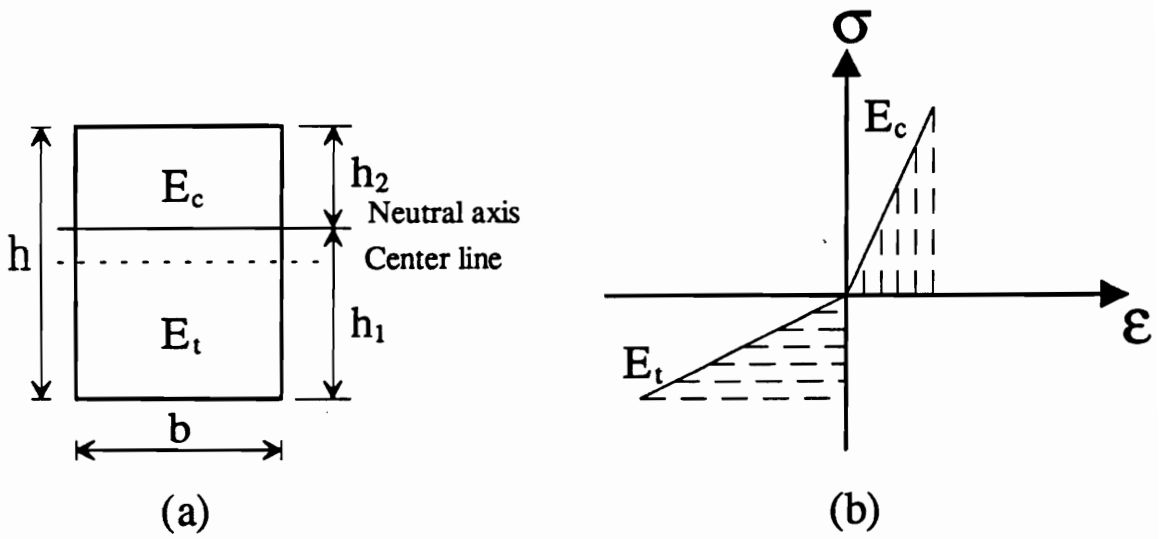
Figure 3.7 (a) Neutral axis shift $E_c > E_t$
(b) Stress-strain relationship in compression
and tension

where

b = width of the beam,

E_{av} = equivalent modulus of elasticity of the beam, and

I_{av} = equivalent moment of inertia of the beam.

Hence the equivalent flexural rigidity of the bending beam D_{av} becomes:

$$D_{av} = E_{av} I_{av} \qquad (3.15)$$

where

D_{av} = equivalent flexural rigidity of the beam.

Figure 3.8 illustrates the relationship of D_{av} / D vs E_c / E_t which indicates that the actual flexural rigidity of the rock beam at $E_c / E_t = 4$, is more than 20 percent lower than the corresponding value, when using E_c as the general modulus of elasticity for the entire beam.

3.3.6 Maximum Tensile and Compressive Stresses in the Bending Beam

The maximum tensile stress, σ_{tmax}, and the maximum compressive stress, σ_{cmax}, at the external fibers of the beam under the bending moment, M, can be determined by:

$$\sigma_{tmax} = \frac{M h_1}{I_{av}} \qquad (3.16)$$

$$\sigma_{cmax} = \frac{M h_2}{I_{av}} \qquad (3.17)$$

where
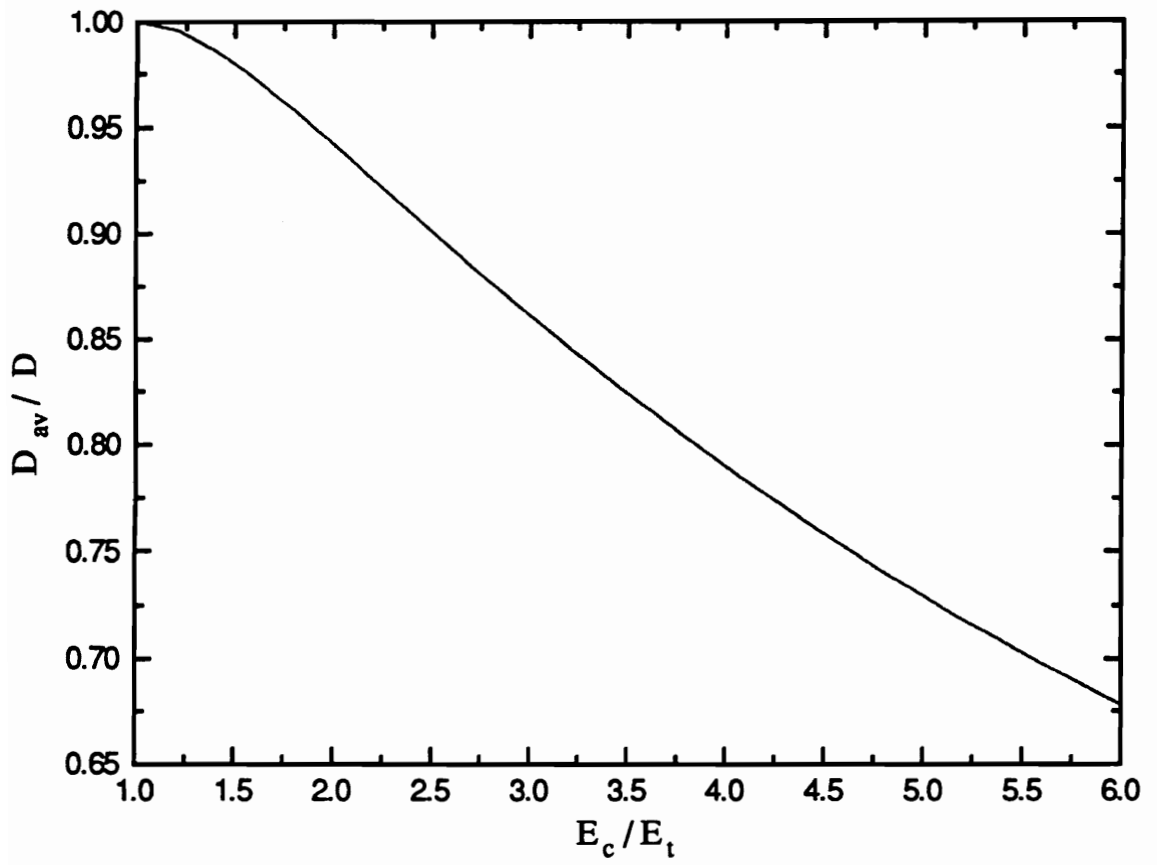
Figure 3.8 Influence of E_c / E_t on the flexural rigidity of the beam

σ_{tmax} = maximum tensile stress in the bending beam, and

σ_{cmax} = maximum compressive stress in the bending beam.

3.4 Analytical Solutions of Deflection Line

Based upon roof configurations and the beam theories discussed in the preceding sections, the solutions of deflection lines for each roof model are developed.

3.4.1 Model 1: Single-layer Cantilevering Roof Beam

This model represents a single layer roof, partially supported by an elastic foundation (coal or weak roof) as illustrated in Figure 3.1. The applied load distributions are assumed to be:

$$p(x) = \begin{cases} p_o \, e^{fx} & 0 \le x \le l \\ p & x > l, \text{ and } -L < x < 0 \end{cases} \qquad (3.18)$$

where

p = overburden pressure,

p_o = peak abutment pressure,

f = characteristic of the abutment load distribution,

l = length of the stress concentration, and

L = length of the unsupported part of the beam.

The parameter, f, in Equation 3.18, denotes the abutment load distribution characteristics. It is defined by the p, p_o and l values.

$$f = \frac{\text{Ln}\left(\dfrac{p}{p_o}\right)}{1} \tag{3.19}$$

By replacing D with D_{sv} in the differential Equation 3.1 and substituting $p(x)$ in Equation 3.18, the differential equation of the deflection line for the supported part of the beam can be written as:

$$D_{sv} \frac{d^4 y}{dx^4} = p_o e^{fx} - cy \tag{3.20}$$

If a weak roof bed exists between the roof bed and the coal pillar, the foundation modulus, c, in Equation 3.20 should be replaced by c' as defined in Equation 3.3.

From the differential equation theory, the specific solution of Equation 3.20 has the form:

$$y_1(x) = \alpha \, e^{fx} \tag{3.21}$$

where

$\alpha = $ constant.

Substituting y in Equation 3.20 with $y_1(x)$ defined in Equation 3.21 and solving α, we get:

$$\alpha = \frac{p_o}{D_{sv} f^4 + c} \tag{3.22}$$

Hence the specific solution can be expressed as follows:

48

$$y_1(x) = \frac{p_o}{D_{av} f^4 + c} e^{fx} \qquad (3.23)$$

Now let us examine the general solution, $y_2(x)$, of the deflection line of the beam which is defined in Equation 3.8. For points infinitely distant from the origin, the second term in Equation 3.8 must vanish. This condition can be satisfied only if the integration constants A_3 and A_4 in the equation are taken to equal zero. Hence $y_2(x)$ will take the form:

$$y_2(x) = e^{-\beta x}(A_1 \sin \beta x + A_2 \cos \beta x) \qquad (3.24)$$

Combing Equations 3.23 and 3.24, we get the solution for the deflection curve of the beam:

$$y = \frac{p_o}{D_{av} f^4 + c} e^{fx} + e^{-\beta x}(A_1 \sin \beta x + A_2 \cos \beta x) \qquad (3.25)$$

The remaining integration constants A_1 and A_2 are determined by the following procedure.

Denoting and substituting the following notations:

$$y_o = y\big|_{x=0} \qquad (3.26)$$

$$\dot{y}_o = \frac{dy}{dx}\bigg|_{x=0} \qquad (3.27)$$

where

y_o = deflection of the beam at $x = 0$, and

49

y'_o = slope of the deflection line at x = 0.

together with Equation 3.22, into Equation 3.25, we get:

$$y_o = \alpha + A_2 \tag{3.28}$$

$$y'_o = \alpha f + \beta(A_1 - A_2) \tag{3.29}$$

From Equations 3.28 and 3.29, values of A_1 and A_2 can be expressed as follows:

$$A_1 = \frac{y'_o - \alpha f}{\beta} + y_o - \alpha \tag{3.30}$$

$$A_2 = y_o - \alpha \tag{3.31}$$

Now the deflection line (Equation 3.25) can be rewritten as:

$$y = \alpha e^{fx} + e^{-\beta x}\left[\left(\frac{y'_o - \alpha f}{\beta} + y_o - \alpha\right)\sin \beta x + (y_o - \alpha)\cos \beta x\right] \tag{3.32}$$

The second derivative of Equation 3.32 with respect to x together with Equation 3.9 gives the bending moment equation:

$$M = -D_{av}\left[\alpha f^2 e^{fx} + 2\beta^2 e^{-\beta x}\left((y_o - \alpha)\sin \beta x - \left(\frac{y'_o - \alpha f}{\beta} + y_o - \alpha\right)\cos \beta x\right)\right] \tag{3.33}$$

The bending moment at the point x = 0 can then be evaluated:

$$M_o = D_{av} \left[2\beta^2 \left(\frac{y_o' - \alpha f}{\beta} + y_o - \alpha \right) - \alpha f^2 \right] \tag{3.34}$$

The third derivative of Equation 3.32 with respect to x combined the known relation for shearing force in the bending beam (Equation 3.10) gives:

$$V = -D_{av} \left[\alpha f^3 e^{fx} + 2\beta^3 e^{-\beta x} \left(\left(\frac{y_o' - \alpha f}{\beta} \right) \sin \beta x - \left(\frac{y_o' - \alpha f}{\beta} + 2y_o - 2\alpha \right) \cos \beta x \right) \right] \tag{3.35}$$

For x = 0, we get:

$$V_o = -D_{av} \left[\alpha f^3 + 2\beta^3 \left(\frac{y_o' - \alpha f}{\beta} + 2y_o - 2\alpha \right) \right] \tag{3.36}$$

The values of M_o and V_o can be evaluated by the following known boundary conditions of the unsupported part of the beam:

$$M_o = - \frac{p L^2}{2} \tag{3.37}$$

$$V_o = - pL \tag{3.38}$$

From Equations 3.35 and 3.36, we can express y_o and y_o' in terms of M_o and V_o as follows:

$$y_o = \alpha - \frac{V_0 + \beta M_0 + \alpha D_{av} f^2(f + \beta)}{2 D_{av} \beta^3} \tag{3.39}$$

$$y_o' = \alpha \; f + \frac{V_o + 2\beta \; M_o + \alpha \; D_{ev} \; f^2(f+2\beta)}{2 \; D_{ev} \; \beta^2} \tag{3.40}$$

3.4.2 Model 2: Single-layer Bridging Roof Beam

In this model a single layer roof bed is bridged on the elastic foundation (coal or weak roof) at both ends as shown in Figure 3.2. Due to the constraints at both ends of the beam, the boundary conditions defined in Equations 3.37 and 3.38 for the cantilevering beam are no longer valid. In order to find the solution of the deflection line, let us first examine the unsupported part of the beam.

The differential equation for the unsupported part of the bending beam is:

$$D_{ev} \; \frac{d^4 y}{dx^4} \; = \; p \tag{3.41}$$

with the following solution:

$$y = \frac{px^4}{24D_{ev}} + B_1 x^3 + B_2 x^2 + B_3 x + B_4 \tag{3.42}$$

where

B_1, B_2, B_3, B_4 = integration constants.

Inserting $y = y_o$ in $x = 0$, we obtain the constant B_4:

$$B_4 = y_o \tag{3.43}$$

Successive differentiating Equation 3.42 with respect to x and using notation for slope of the deflection line (Equation 3.27) along with moment and shear force making use of Equations 3.9 and 3.10 give the integration constants:

$$B_3 = \dot{y}_o \tag{3.44}$$

$$B_2 = -\frac{M_o}{2D_{av}} \tag{3.45}$$

$$B_1 = -\frac{T_o}{6D_{av}} \tag{3.46}$$

Substituting M_o in Equation 3.34 and V_o in Equation 3.36 into Equations 3.45 and 3.46, constants B_1 and B_2 can be expressed in terms of y_o and $\dot{y}_o$ as follows:

$$B_2 = \frac{1}{2}\alpha\ f^2 - \beta^2\left(\frac{\dot{y}_o - \alpha\ f}{\beta} + y_o - \alpha\right), \tag{3.47}$$

$$B_1 = \frac{1}{6}\alpha\ f^3 + \frac{1}{3}\beta^3\left(\frac{\dot{y}_o - \alpha\ f}{\beta} + 2\,y_o - \alpha\right) \tag{3.48}$$

Still it remains to find the deflection y and the slope of the deflection curve $\dot{y}_o$ at the point x = 0. These can, however, be evaluated applying the following boundary conditions:

$$V\big|_{x=0} = -pL \tag{3.49}$$

$$\frac{dy}{dx}\bigg|_{x=-\frac{L}{2}} = 0 \qquad (3.50)$$

By combining Equations 3.36 and 3.49 we get:

$$D_{av}\left[\alpha f^3 + 2\beta^3\left(\frac{y_o' - \alpha f}{\beta} + 2y_o - 2\alpha\right)\right] = pL \qquad (3.51)$$

Evaluating the first derivative of Equation 3.42 at the point x = 0.5 L and using Equations 3.44, 3.47, 3.48, and 3.50, we obtain:

$$\frac{3}{4}L^2\left[\frac{\alpha f^3}{6} + \frac{\beta^3}{3}\left(\frac{y_o' - \alpha f}{\beta} + 2y_o - 2\alpha\right)\right] - L\left[\frac{\alpha f^2}{2} - \beta^2\left(\frac{y_o' - \alpha f}{\beta} + y_o - \alpha\right)\right] - \frac{pL^3}{48D_{av}} + y_o' = 0$$

$$(3.52)$$

From Equations 3.51 and 3.52, we can find y_o and y_o':

$$y_o = \frac{2f\alpha\beta^2 + 4\alpha\beta^3 - \alpha f^3 - 2\beta^2 y_o'}{4\beta^3} + \frac{pL}{4D_{av}\beta^3} \qquad (3.53)$$

$$y_o' = -\frac{(5p\beta L^2 + 12pL - 24D_{av}\alpha f\beta^2 - 12D_{av}\alpha f^3 - 24D_{av}\alpha\beta f^2)\,L}{24\beta\,D_{av}(L\,\beta + 2)} \qquad (3.54)$$

For the supported part of the bending beam, the differential equation and deflection line equation are the same as the cantilevering beam which are defined by Equation 3.20 and Equation 3.32. However, due to the different boundary conditions, the y_o and y_o' are defined in Equations 3.53 and 3.54, respectively.

54

3.4.3 Model 3 and Model 4: Double-layer Roof Beam

These models represent a double-layer roof with welded contacts between layers of different thicknesses and Young's moduli resting on an elastic foundation (Figures 3.3 and 3.4).

The composite beam theory can be used to construct an equivalent layer of the same material as the lower layer (or the upper layer) as shown in Figure 3.9 for $E_{av1} < E_{av2}$. Following the notations in Figure 3.9, the relationship between the moduli and the sections is:

$$\frac{b_1}{b_2} = \frac{E_{av1}}{E_{av2}} \tag{3.55}$$

where

b_1 = width of the upper-layer,

b_2 = width of the lower-layer,

E_{av1} = equivalent modulus of elasticity of the upper-layer, and

E_{av2} = equivalent modulus of elasticity of the lower-layer.

The moment of inertia about the neutral axis for the equivalent layer becomes:

$$I_{cav} = \frac{1}{3}\left[\left(h_{c1} + h_{c2} - d_2\right)^3 - \left(1 - \frac{E_{av1}}{E_{av2}}\right)d^3 + \frac{E_{av1}}{E_{av2}} \, d_2{}^3 \right] \tag{3.56}$$

where

I_{cav} = equivalent moment of inertia for the double-layer roof beam,

h_{c1} = thickness of the upper-layer roof,

h_{c2} = thickness of the lower-layer roof,

d_2 = distance from the neutral axis to the upper fiber of the beam, and

d = distance from the neutral axis to the interface of two layers, $d = h_{c1} - d_2$.

The distance between the neutral axis and the upper fiber is given by:

(a) Cross-section

(b) Transformed cross-section
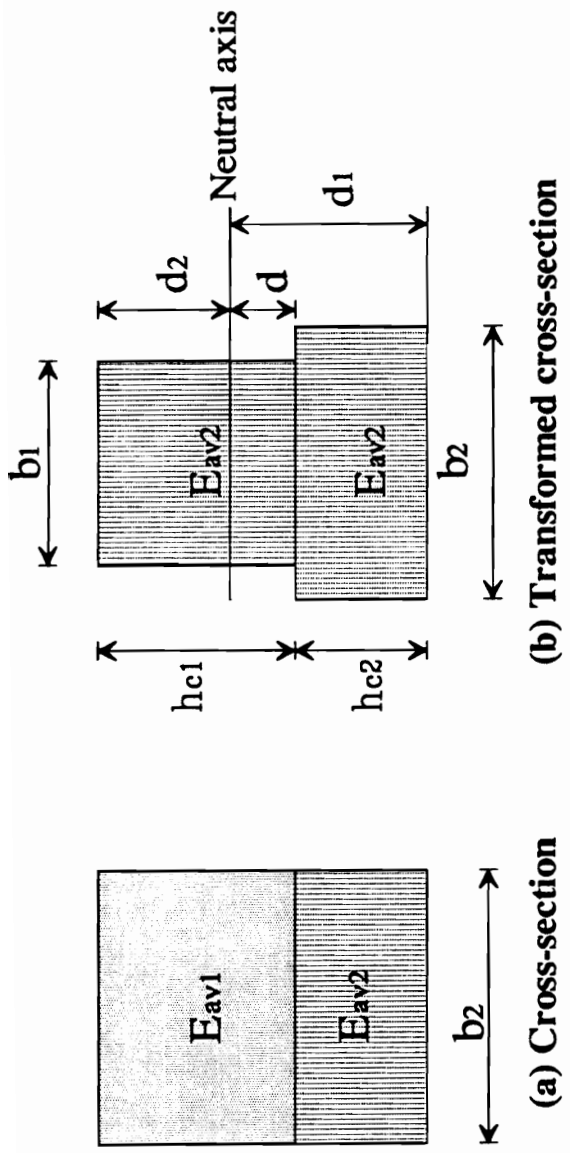
Figure 3.9 Double-layer roof with $E_{av1} < E_{av2}$

$$d_2 = \frac{\dfrac{E_{av1}}{E_{av2}} h_c^2 + \left(1 - \dfrac{E_{av1}}{E_{av2}}\right) h_{c2}^2}{2\left[\dfrac{E_{av1}}{E_{av2}} h_c + \left(1 - \dfrac{E_{av1}}{E_{av2}}\right) h_{c1}\right]} \tag{3.57}$$

where

h_c = total thickness of the double-layer beam, $h_c = h_{c1} + h_{c2}$.

The flexural rigidity now becomes:

$$D_{av} = E_{av2}\, I_{av} \tag{3.58}$$

The maximum tensile and compressive stresses can then be determined by the following equations:

$$\sigma_{tmax} = \frac{M(h_c - d_2)}{I_{av}} \tag{3.59}$$

$$\sigma_{cmax} = \frac{M d_2}{I_{av}} \tag{3.60}$$

If $E_{av2} > E_{av1}$ the new equivalent layer will have a cross-section as shown in Figure 3.10. The equivalent moment of inertia is the same as defined in Equation 3.56 by applying the notations in Figure 3.10. The equivalent flexural rigidity of the composite beam can now be expressed as:

$$D_{av} = E_{av1}\, I_{av} \tag{3.61}$$

However, the equations for the maximum tensile and compressive stresses will now become:

57

(a) Cross-section

(b) Transformed cross-section
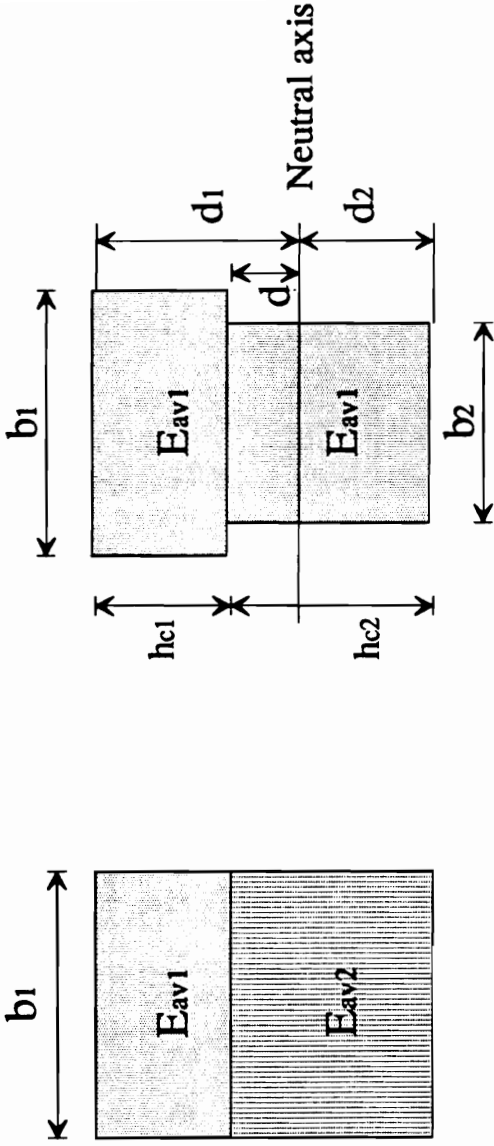
Figure 3.10 Double-layer roof with $E_{av1} > E_{av2}$

58

$$\sigma_{tmax} = \frac{M\,d_2}{I_{cav}} \tag{3.62}$$

$$\sigma_{cmax} = \frac{M(h_c - d_2)}{I_{cav}} \tag{3.63}$$

in which d_2 is the same as that in Equation 3.57.

With equivalent elastic constants, the subsequent procedures for finding the solution of the deflection line are similar to those made for the corresponding single-layer roof models.

3.5 Summary

Four structural models are formulated to simulate the locations of competent roofs and the distinct weighting stages in the longwall extraction or mining stages in the room-and-pillar extraction. In contrast to classic treatment of roof beds as an elastic beam on rigid foundation under uniformly distributed loading, the bending roofs are considered to be rested on elastic foundations, and the abutment stress concentration is approximated as an exponentially decaying form. For single-layer roof models, analytical solutions for the deflection lines of the bending beam are developed based on the elastic beam theory. These solutions are fundamentals for determination of critical spans of the roof beds and evaluation of strain energy stored in the roof beds and the foundation which are discussed in the following chapters. The double-layer roof models can be transformed to single-layer roof models by applying the composite beam principles. The difference in the elastic moduli under tension and compression for rock material alters the position of the neutral axis, decreases the actual flexural rigidity, and results in stress redistribution in the rock beams.

CHAPTER 4   CRITICAL SPANS DETERMINATION AND ROOF CAVEABILITY ANALYSIS

4.1 Introduction

In this chapter, the critical span equations will be developed based on analytical solutions presented in chapter 3. Because the tensile strength of rock materials is much less than its compressive strength, the failure mode is hence anticipated to be tensile. Therefore, only tensile failure is considered in the following discussion. The critical spans are the roof spans for which the maximum tensile stress developed in the beam equates the tensile strength of the rock materials. The influence of a number of parameters on the roof caveability is analyzed in order to assess the behavior of the major dependent variables. A set of design curves are developed for typical mechanical characteristics of the competent roof, foundation, and overburden.

4.2 Determination of the Critical Spans of Roof Beds

4.2.1 Critical Spans for a Single-layer Cantilevering Roof

When the maximum tensile stresses in the bending beam equals to the tensile strength of rock material, the cantilevering length of the roof beam reaches its critical

values. The following relations illustrate this condition:

$$\sigma_{tmax} = -T_o \tag{4.1}$$

$$M_{max} = -\frac{pL_t^2}{2} \tag{4.2}$$

where

σ_{tmax} = maximum tensile stress (negative),

M_{max} = maximum bending moment, and

L_t = critical span of the beam.

Applying stress-moment relation defined in Equation 3.16, we obtain:

$$T_o = \frac{pL_t^2 h_1}{2I_{av}} \tag{4.3}$$

where

h_1 = distance between the neutral axis to the underside of the beam, and

I_{av} = eqivalent moment of inertia of the beam.

Substitution of h_1 in Equation 3.11 and I_{av} in Equation 3.14 in Equation 4.3 results in:

$$L_t = 0.816h\sqrt{\frac{T_o}{p}\frac{\sqrt{E_c}}{\sqrt{E_c}+\sqrt{E_t}}} \tag{4.4}$$

Equation 4.4 indicates that for a given overburden pressure p and tensile strength T_o,

61

the critical spans of a single-layer cantilevering roof are dependent on the beam thickness h and the ratio of E_c / E_t of rock materials.

4.2.2 Critical Spans for a Single-layer Bridging Roof

For this kind of roof configuration, both ends of the beam are rested on foundation (coal or weak roof). Prior to roof failure, the applied load $p(x)$ acting on the beam should be continuous and evenly distributed as shown in Figure 4.1. The deflection line is defined by the following equation for the unsupported part of the bending beam [Stephanson, 1971]:

$$ y = \frac{p}{c} \left[\beta^4 \, x \left(\frac{x^3}{6} - \frac{x^2 L}{3} - \frac{L x}{\beta} - \frac{L}{\beta^2} \right) + L \, \beta^3 \, k \, (1 + \beta \, x)^2 + 1 \right] \tag{4.5} $$

where the parameter, k, is given by [Stephanson, 1971]:

$$ k = \frac{\beta^2 L^2 + 6\beta L + 6}{6\beta^2 \, (2 + L \, \beta)} \tag{4.6} $$

The bending moment, M, in the beam is given as:

$$ M = - \frac{p \, x^2}{2} + \frac{p \, L}{2} \left(x + \frac{1}{\beta} - k \, \beta \right) \tag{4.7} $$

The maximum moment M_{max} occurs at $x = 0.5 \, L$ and has the value:

$$ M_{max} = \frac{p \, L^2}{8} + \frac{p \, L}{2} \left(\frac{1}{\beta} - k \, \beta \right) \tag{4.8} $$

Combining Equations 4.6 and 4.8 together, we arrive at:
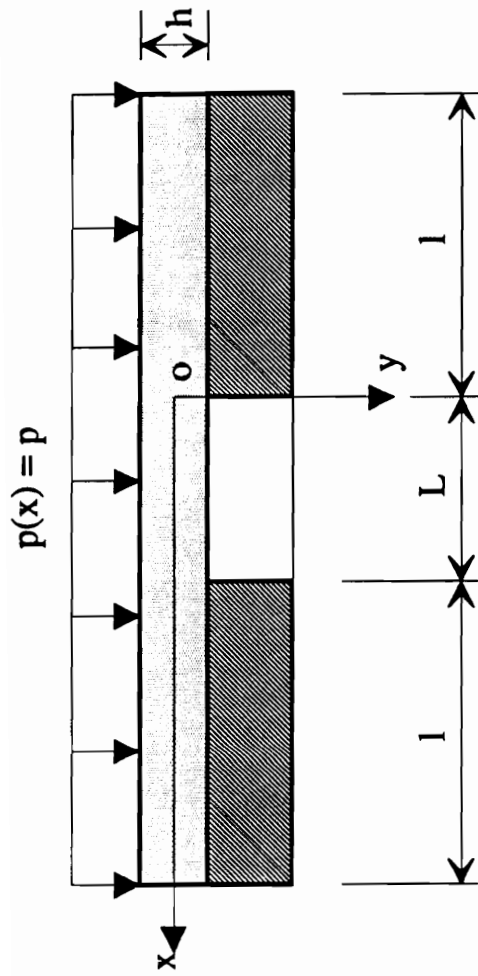
Figure 4.1 A single-layer bridging roof beam prior to failure

$$M_{max} = \frac{p\,\beta^2\,L^3 + 6\,p\,\beta\,L^2 + 12\,p\,L}{24\,\beta\,(2 + \beta\,L)} \qquad (4.9)$$

Assuming that the in situ horizontal stress is zero and using Equations 3.16 and 4.9, the critical span, L_t, for tensile failure, can be determined by the following equation:

$$p\,\beta^2\,L_t^3 + 6\,p\,\beta\,L_t^2 + \left[12\,p - \frac{8\,\beta^2\,T_o\,\sqrt{E_c}\,h^2}{\sqrt{E_c} + \sqrt{E_t}}\right]L_t - \frac{16\,\beta\,T_o\,\sqrt{E_c}\,h^2}{\sqrt{E_c} + \sqrt{E_t}} = 0 \qquad (4.10)$$

If the in situ horizontal stress is non-zero and has a magnitude of σ_h, Equation 4.10 becomes:

$$p\,\beta^2\,L_t^3 + 6\,p\,\beta\,L_t^2 + \left[12\,p - \frac{8\,\beta^2\,(T_o + \sigma_h)\,\sqrt{E_c}\,h^2}{\sqrt{E_c} + \sqrt{E_t}}\right]L_t - \frac{16\,\beta\,(T_o + \sigma_h)\,\sqrt{E_c}\,h^2}{\sqrt{E_c} + \sqrt{E_t}} = 0 \qquad (4.11)$$

Equation 4.11 shows that the critical spans of the bridging roof are not only dependent on overburden pressure, and mechanical properties of the roof beds, but also on the in-situ horizontal stress, and roof-foundation system characteristics, β.

4.2.3 Critical Spans for a Double-layer Cantilevering Roof

Following the same procedure for finding the critical span for a single-layer cantilevering roof, together with the stress-moment relationships defined in Equations 3.59 and 3.62, the critical span equations can be established.

Case 1: The upper layer has a higher value of modulus of elasticity

$$L_t = \sqrt{\frac{2\,T_o\,I_{av}}{h_c - d_2}} \qquad (4.12)$$

Case 2: The lower layer has a higher value of modulus of elasticity

$$L_t = \sqrt{\frac{2T_o I_{cav}}{d_2}}$$ (4.13)

The expressions for I_{cav} and d_2 are defined in Equations 3.56 and 3.57, respectively.

4.2.4 Critical Spans for a Double-layer Bridging Roof

By equating the tensile stress σ_t in Equations 3.59 and 3.62 to the tensile strength T_o and substituting for M_{max} in Equation 4.9, the critical spans under tensile failure can be determined as:

Case 1: The upper layer has a higher value of modulus of elasticity

$$p \beta^2 L_t^3 + 6 p \beta L_t^2 + \left[12 p - \frac{24 \beta^2 T_o I_{cav}}{h_c - d_2} \right] L_t - \frac{48 \beta T_o I_{cav}}{h_c - d_2} = 0$$ (4.14)

Case 2: The lower layer has a higher value of modulus of elasticity

$$p \beta^2 L_t^3 + 6 p \beta L_t^2 + \left[12 p - \frac{24 \beta^2 T_o I_{cav}}{d_2} \right] L_t - \frac{48 \beta T_o I_{cav}}{d_2} = 0$$ (4.15)

The expressions for I_{cav} and d_2 are defined in Equations 3.56 and 3.57, respectively.

4.3 Parametric Analysis of Roof Caveability

Based on the critical span equations developed in the preceding section, a number of selected variables which affect roof caveability are further examined in this section. The analyzed parameters include overburden depth, E_c / E_t ratio of rock materials, tensile

strength, stress concentration factor, foundation (coal) height, and foundation (coal) modulus. Since double-layer models can be transformed into corresponding single layer models using the composite beam principles, the following analyses are focused on single-layer cantilevering and bridging roofs.

4.3.1 Overburden Depth

Figure 4.2 shows the critical span variations for the cantilevering and bridging roof models for a range of roof thicknesses under different overburden depths. For both roof models, the spans increase with increasing roof thickness and decreasing overburden depth. However, the bridging spans are always greater than the cantilevering spans under the same conditions. As the overburden depth increases, this difference in spans between two roof models decreases.

4.3.2 E_c / E_t Ratio of Roof Beds

As discussed in chapter 3, for brittle rock materials like sandstone, the modulus of elasticity in compression, E_c, is generally greater than the modulus of elasticity in tension, E_t. This difference will affect the equivalent flexural rigidity of the roof beam, caving spans, and the energy storage capacity. Figure 4.3 illustrates the effects of E_c / E_t ratio on the roof spans. The spans tend to increase with an increase of this ratio for both roof models. However, the bridging roofs are more sensitive to variations in E_c / E_t values.

4.3.3 Tensile Strength

The tensile strength of rock materials is the most important factor affecting the roof caveability as compared with other parameters (Figure 4.4). For the same roof thickness and the tensile strength, the spans for the bridging beam are much greater than the spans for the cantilevering beam. As the roof thickness increases, the difference in spans between two models becomes even larger.
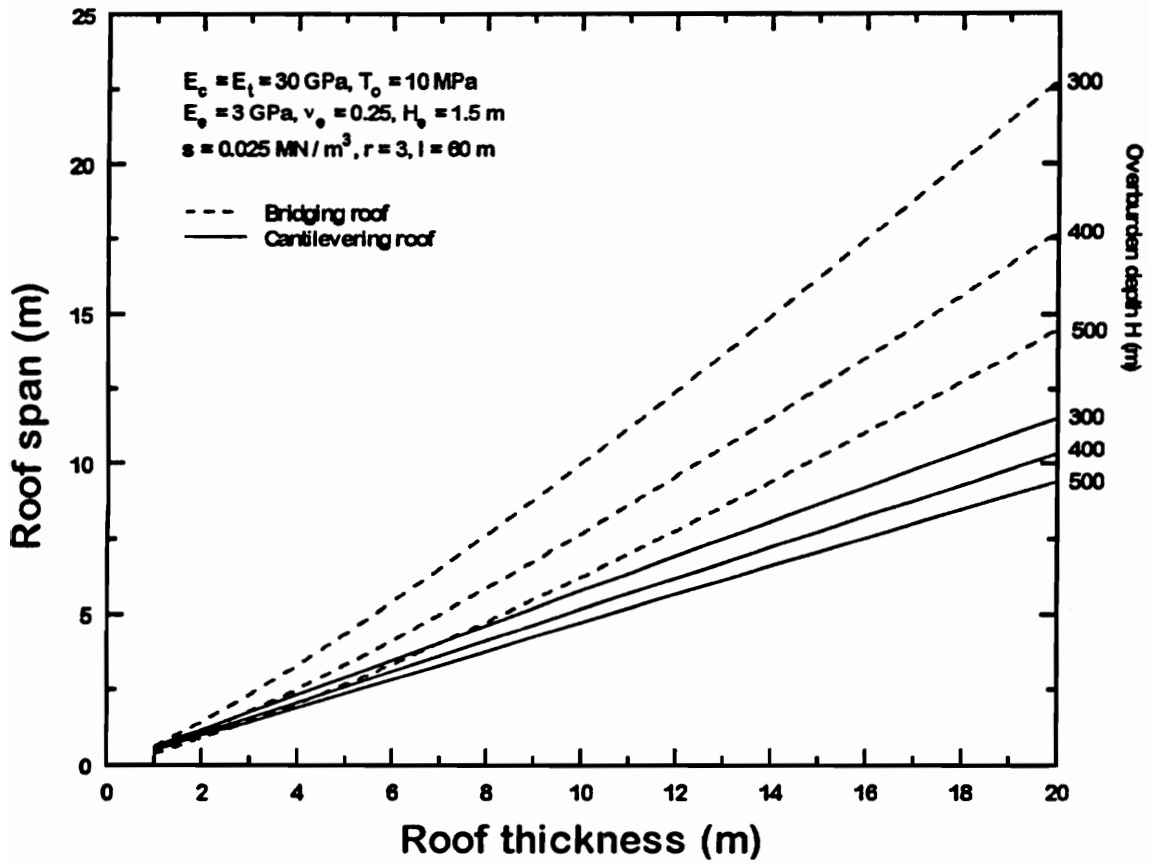
Figure 4.2 Effect of overburden depth on roof spans
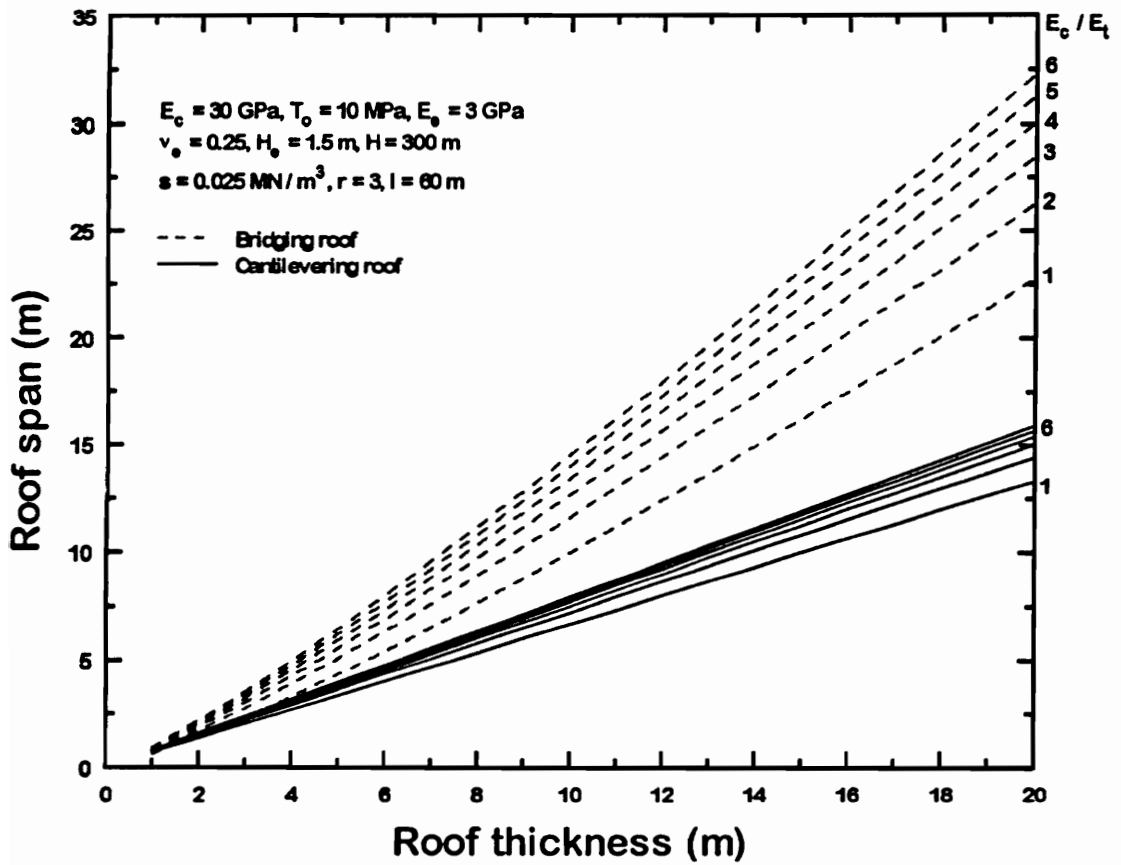
Figure 4.3 Effect of E_c / E_t on roof spans
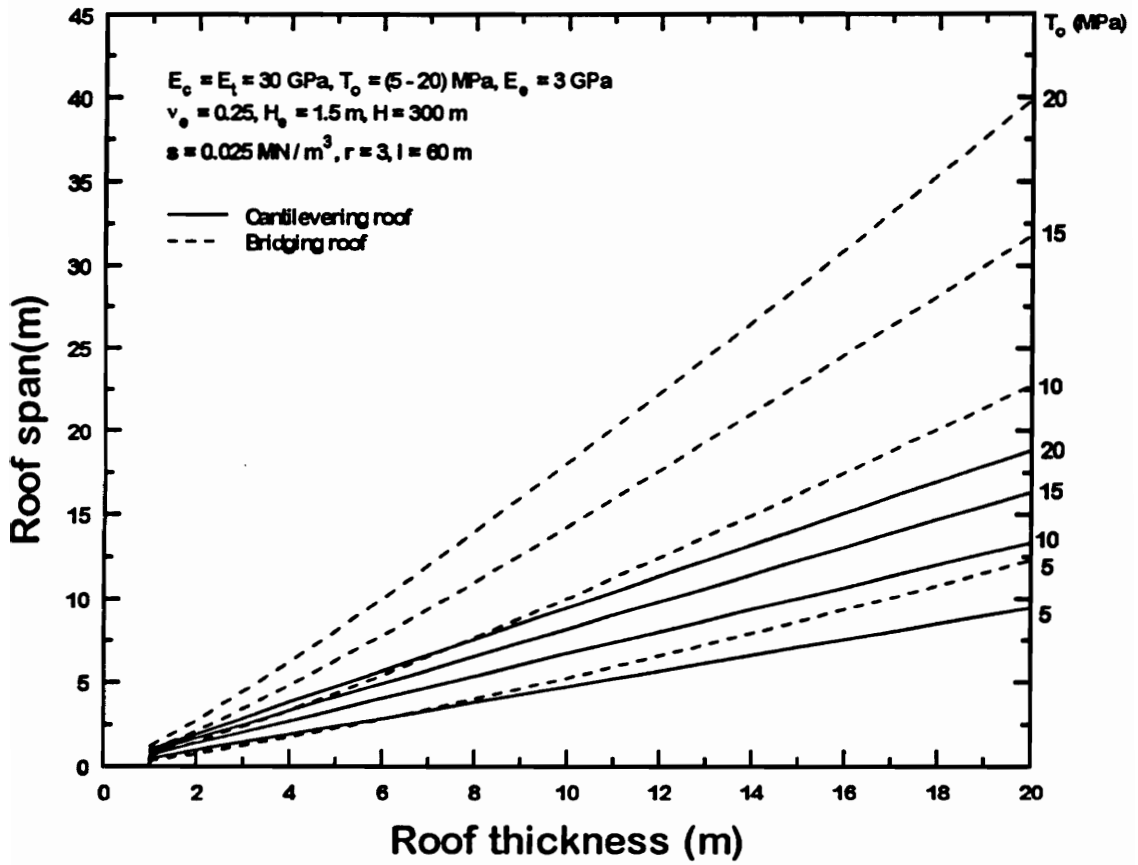
Figure 4.4 Effect of tensile strength on roof spans

4.3.4 Stress Concentration Factor

The stress concentrations on the supported part of the roof beam do not affect the critical spans of the unsupported roof as illustrated in Figure 4.5. However, for the same stress concentration factor, the spans of the bridging beam are greater than the cantilevering beam. The difference in spans for different roof configurations tends to increase with an increase of the roof thickness.

4.3.5 Foundation (coal) Height

The bridging spans increase as the foundation (coal) heights decrease as illustrated in Figure 4.6. However, the cantilevering spans are not affected by the foundation height as indicated in Equation 4.4.

4.3.6 Foundation (coal) Modulus

The foundation (coal) modulus will not affect the roof caveability of the cantilevering roof model, however, as the foundation modulus increases, roof spans for the bridging beam increases as shown in Figure 4.7.
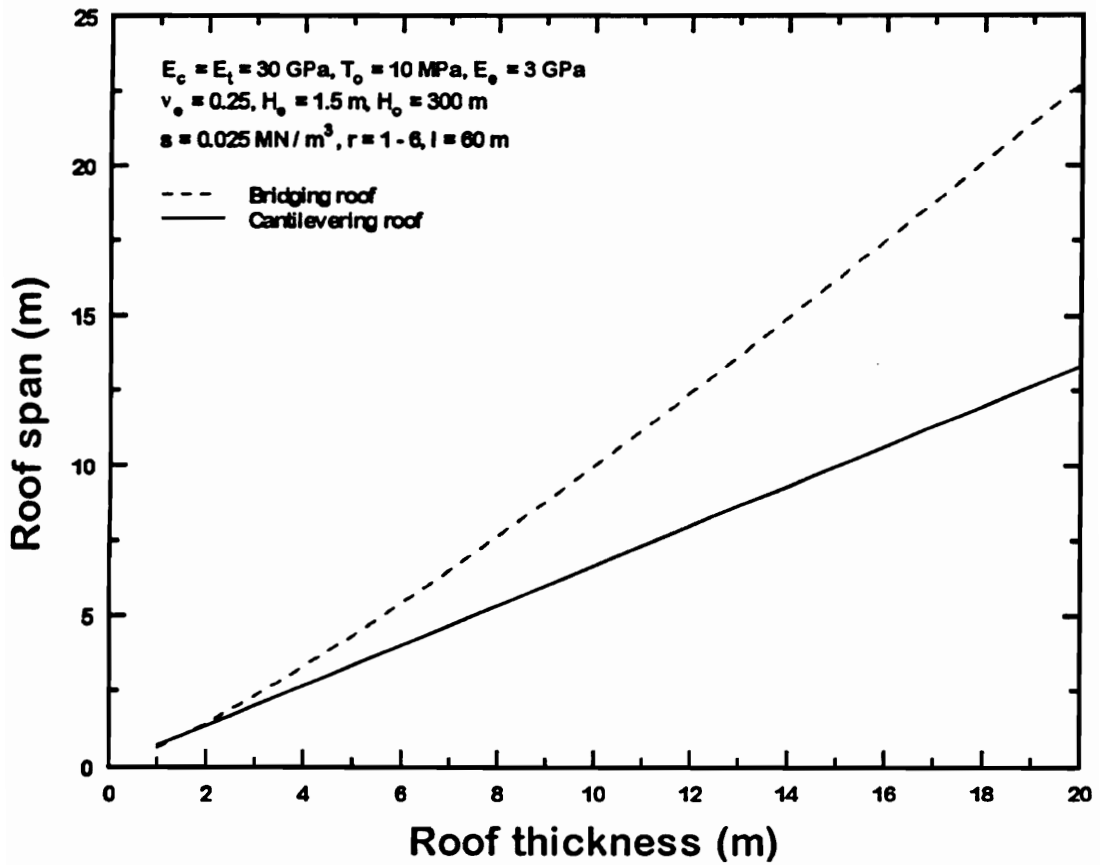
Figure 4.5 Effect of stress concentration factor on roof spans
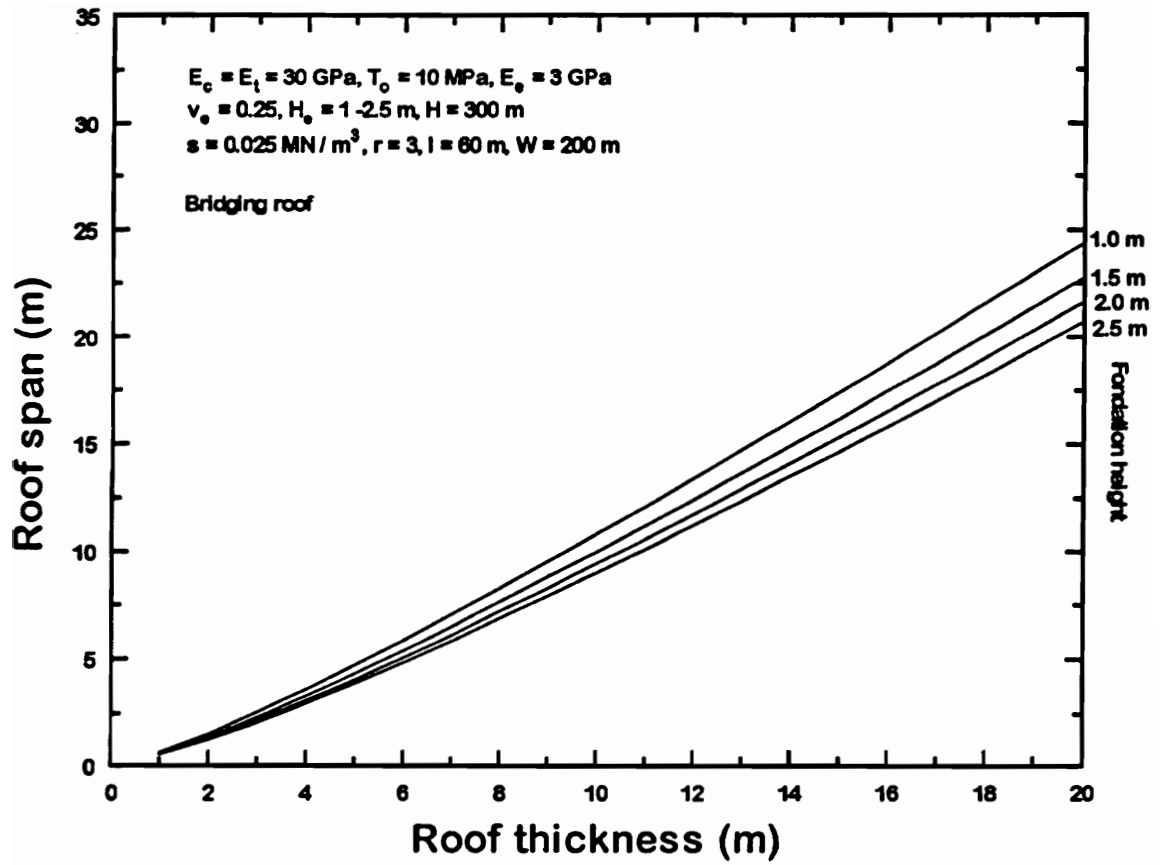
Figure 4.6 Effect of foundation (coal) height on roof spans

$E_c = E_t = 30\,GPa,\ T_o = 10\,MPa,\ E_o = (1\text{-}4)\,GPa$
$v_o = 0.25,\ H_o = 1.5\,m,\ H_o = 300\,m$
$s = 0.025\,MN/m^3,\ r = 3,\ l = 60\,m$

—— Bridging roof
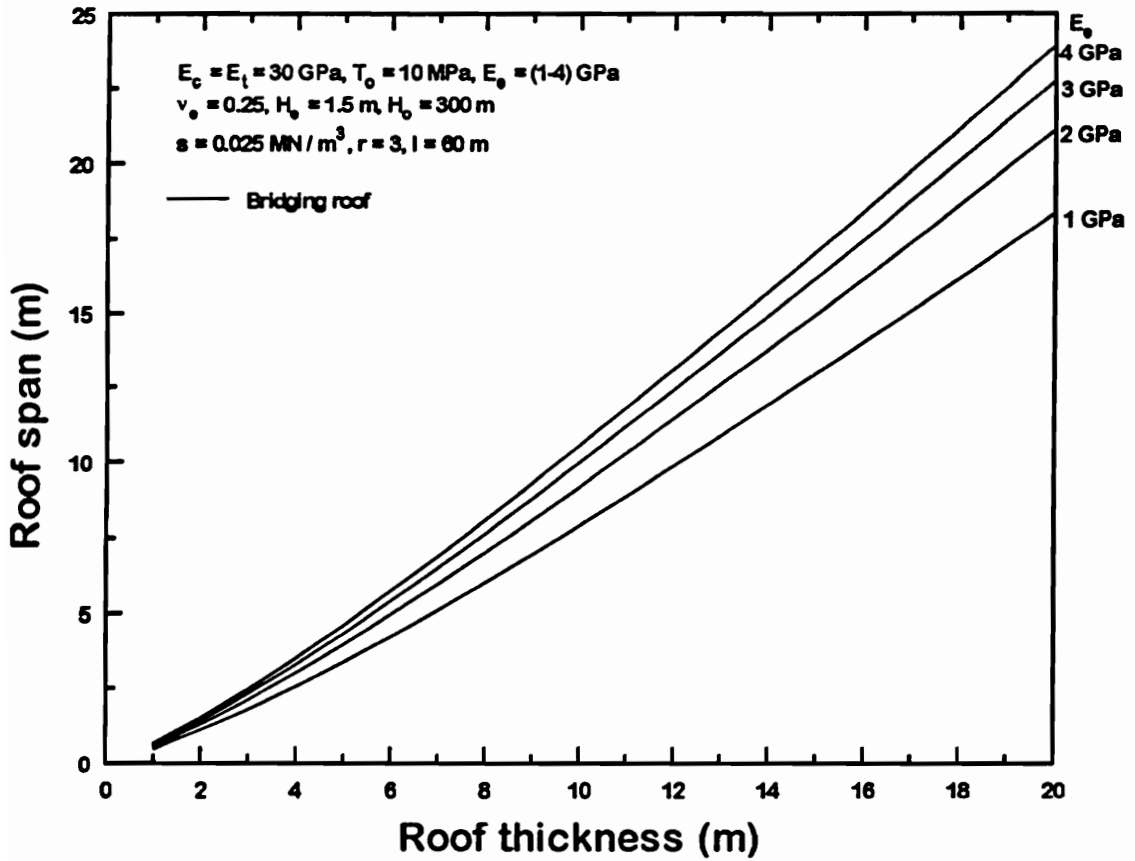
Figure 4.7 Effect of foundation (coal) modulus on roof spans

4.4 Span Curves for Single-layer Roof Models

Based on critical span Equation 4.4 the design curves for a single-layer cantilevering roof model are illustrated in Figure 4.8. Using span equations defined in Equations 4.10 and 4.11, a set of design curves (Figures 4.9(a) to 4.9(I)) for the single-layer bridging roof model are developed for the following typical values of parameters.

Foundation (coal) characteristics: modulus of elasticity E_e = 2 GPa, thickness h_e = 1.5 m, Poisson's ratio v_e = 0.25.

Roof properties: modulus of elasticity under compression E_c = 10 GPa, 20 GPa, and 30 GPa, ratio of E_c / E_t = 1, and 2.

Overburden properties: average specific gravity γ = 0.025 MN / m³, thickness H = 100, 200, 300 m. Horizontal stress σ_h = 0.

If the properties of the roof and the foundation, or their geometries differ from the above parameter values, the design curves can be calculated individually by the Mathcad program.
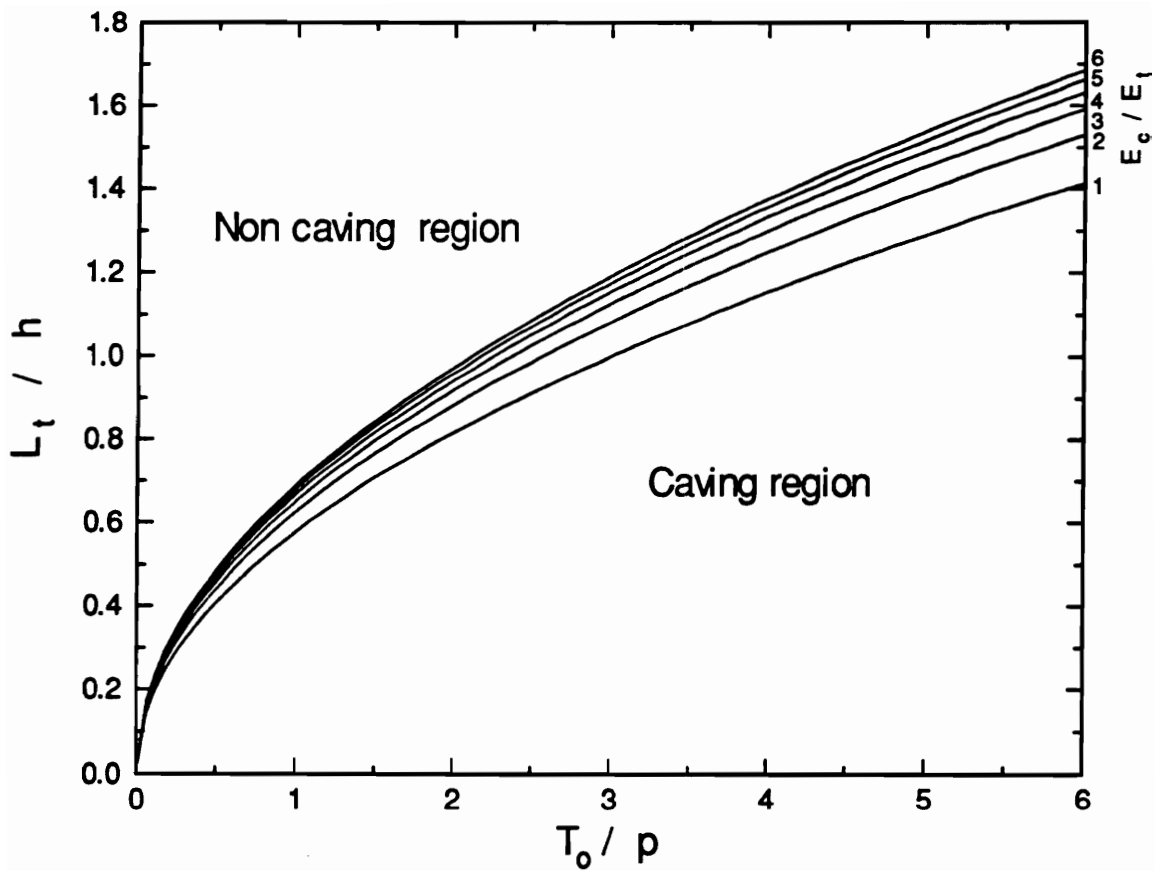
Figure 4.8 Critical spans for the cantilevering roof model
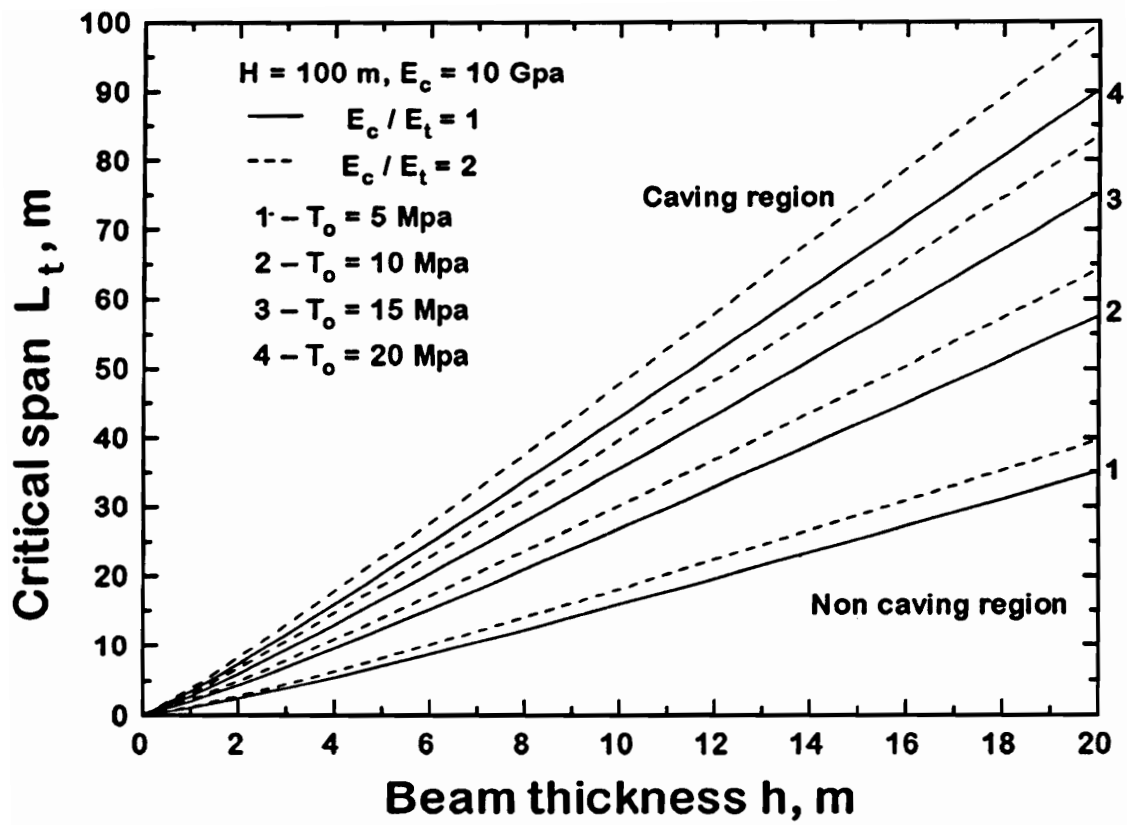
Figure 4.9 (a)
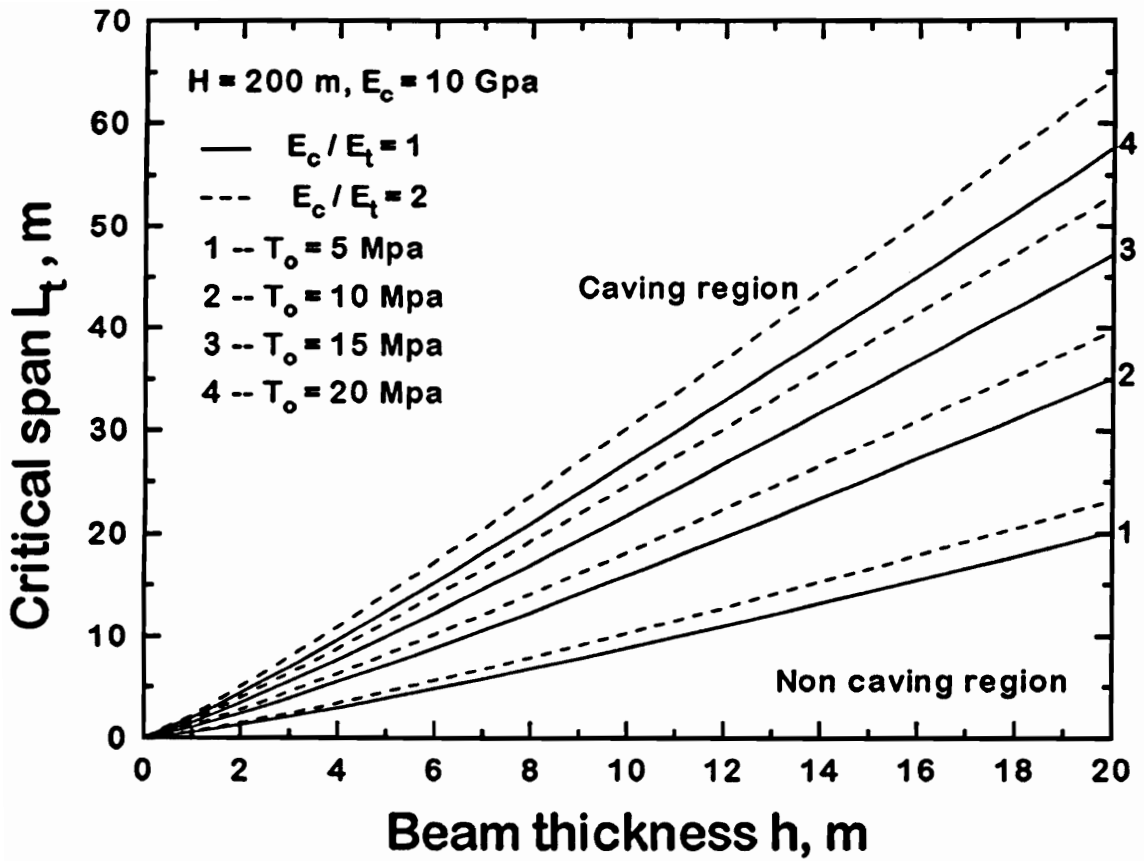
Figure 4.9 (b)
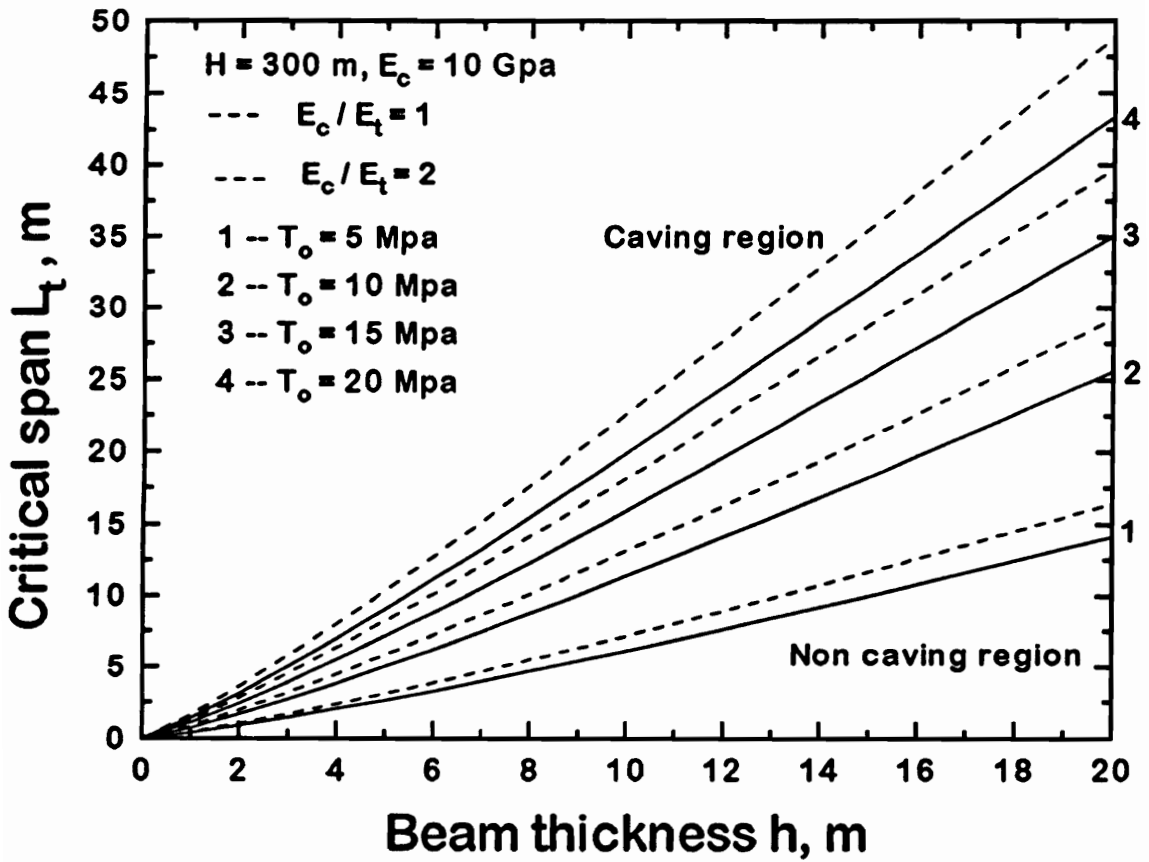
Figure 4.9 (c)
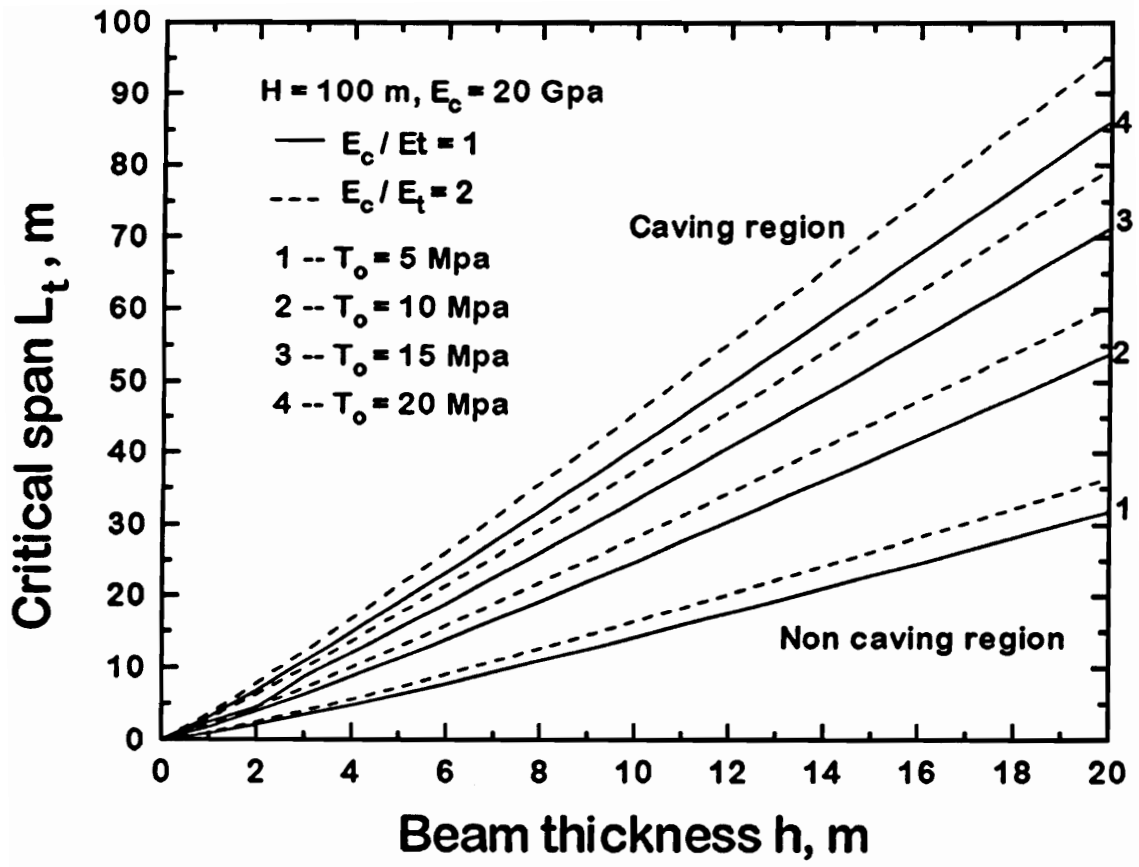
Figure 4.9 (d)
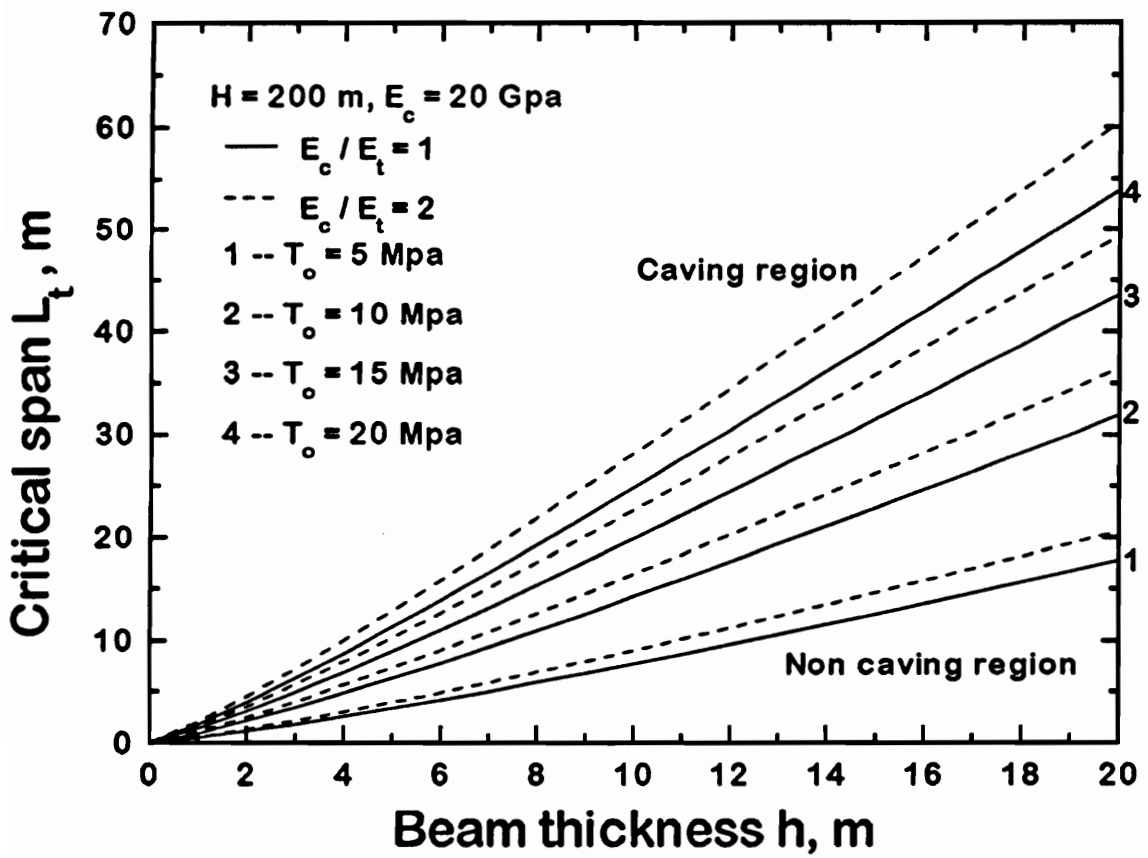
Figure 4.9 (e)
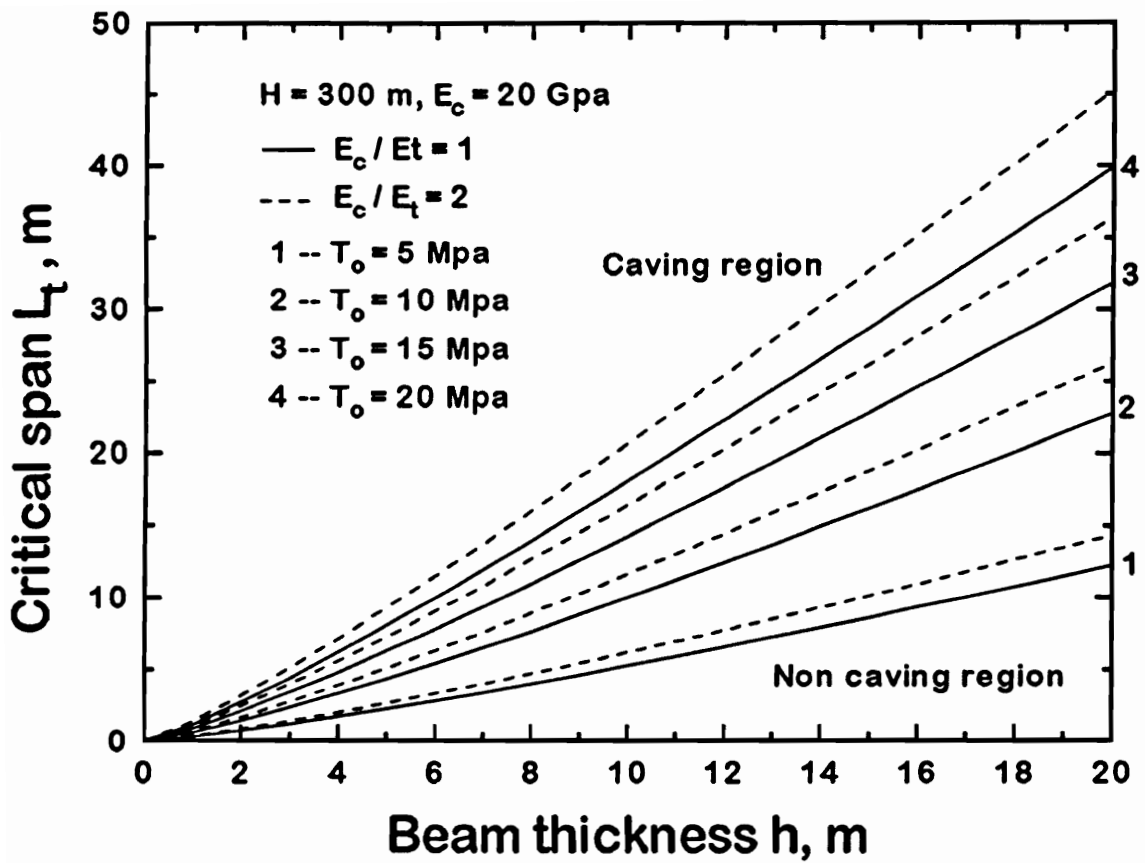
Figure 4.9 (f)
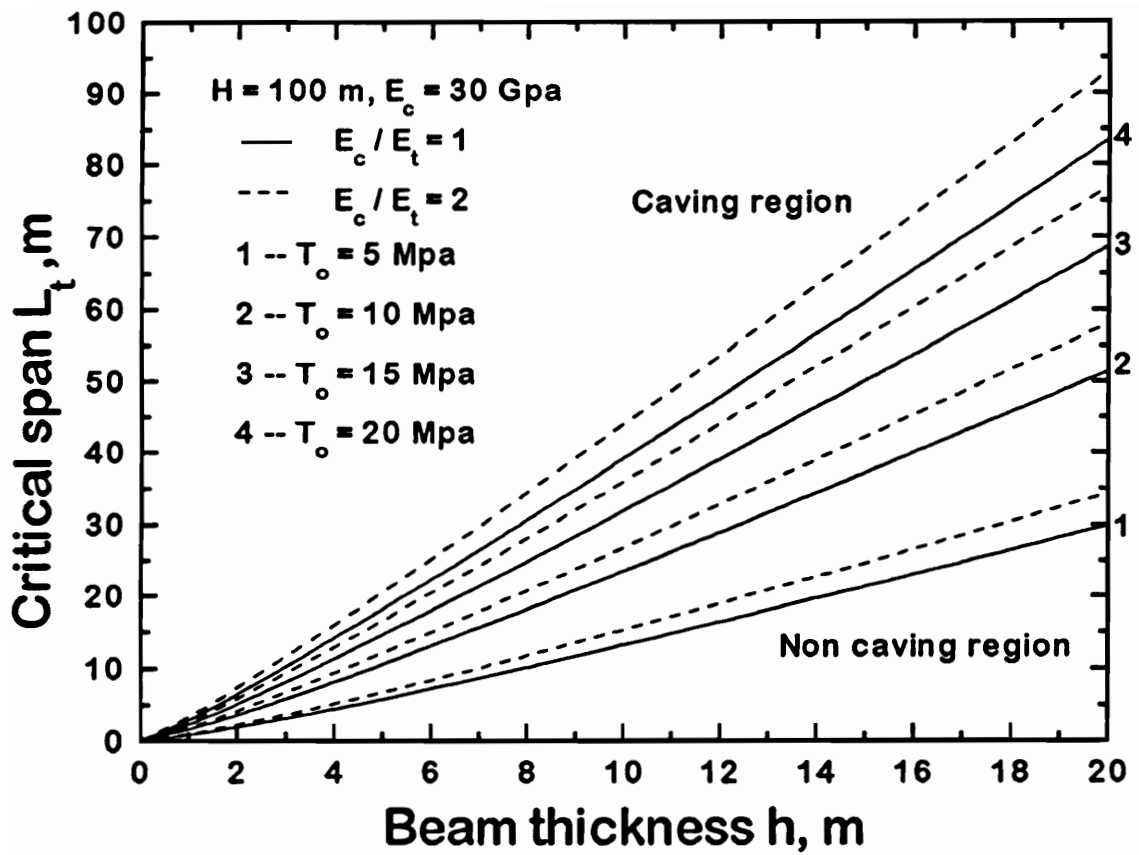
Figure 4.9 (g)
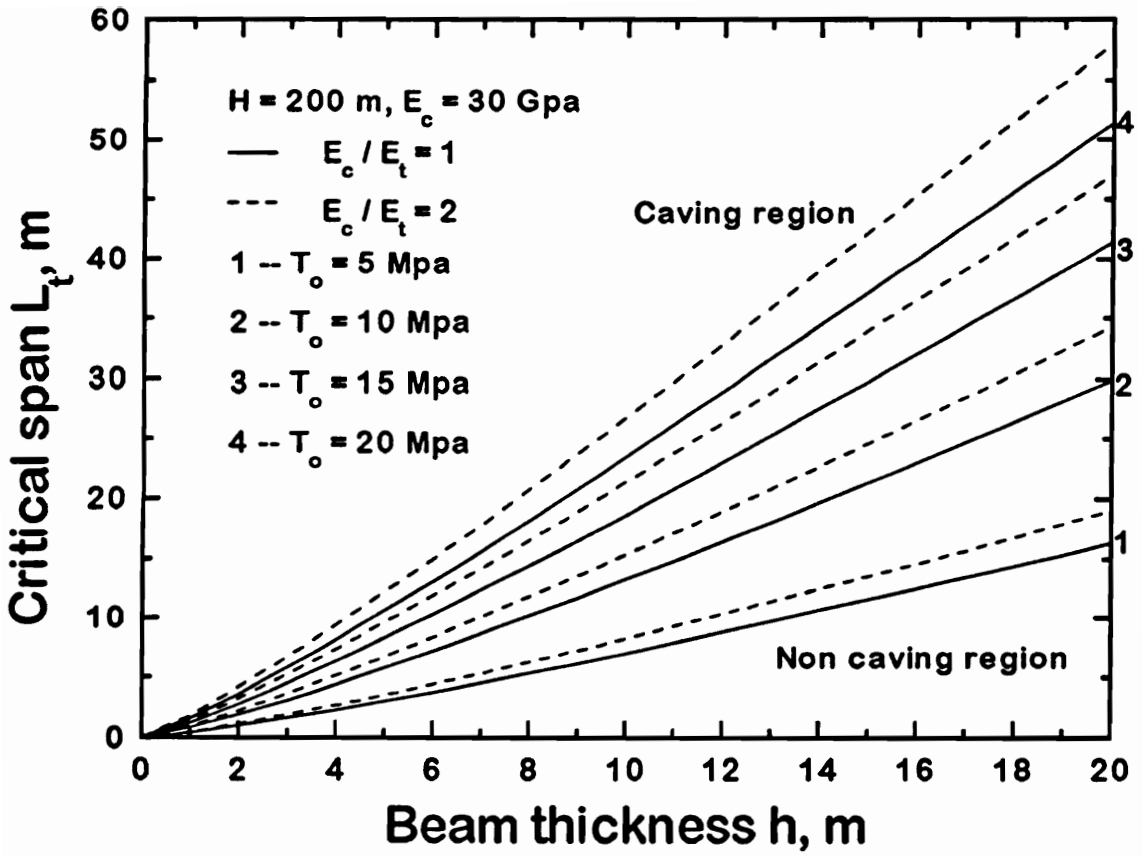
Figure 4.9 (h)
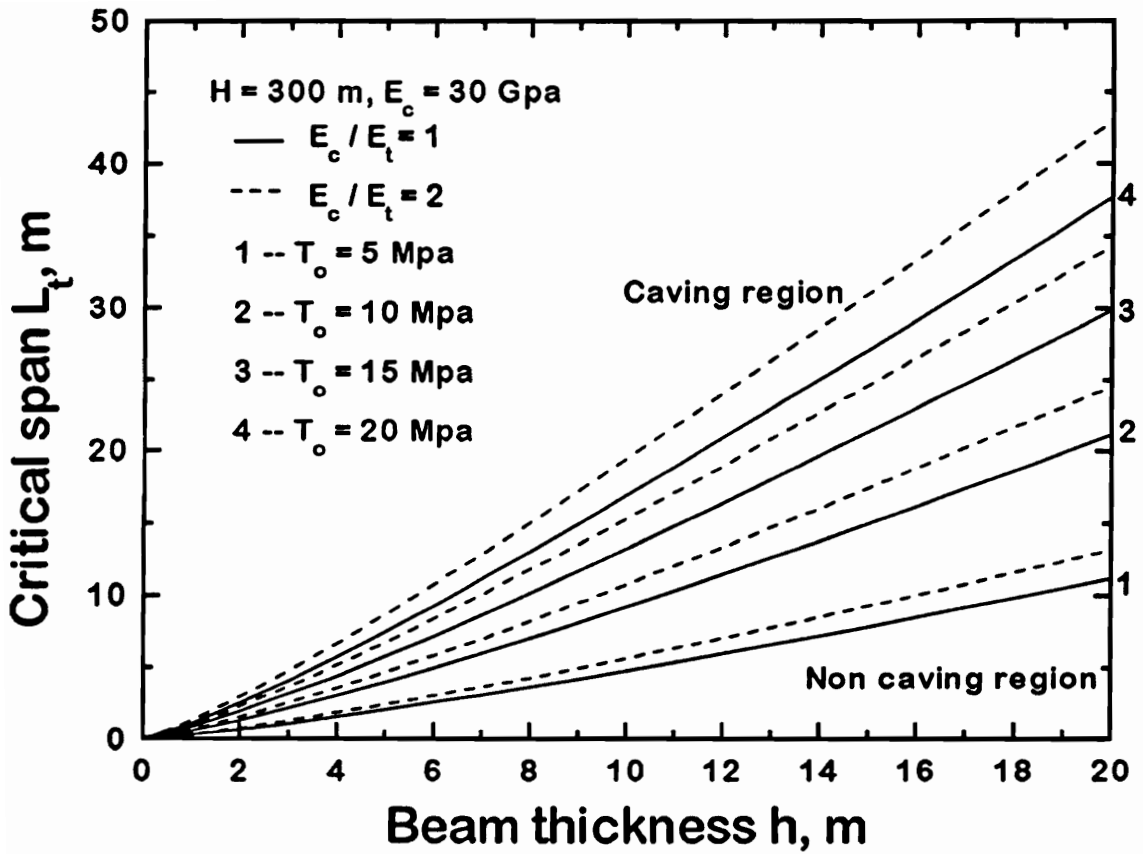
Figure 4.9 (i)

Figure 4.9 Design curves for bridging roof beam

4.5 Summary

Design formulae and design curves for tensile failure have been developed to determine the critical spans for strong roof beds directly overlying working faces based on elastic beam theories. The parametric analysis indicates that the caveability of cantilevering strong roofs, in terms of critical spans, is controlled, not only by the roof thickness but also by the overburden loading, tensile strength of rock materials, and the ratio of the elastic modulus in compression to the elastic modulus in tension. For bridging strong roofs, the caveability is also affected by the foundation characteristics such as foundation height and foundation modulus. For both cantilevering and bridging models, critical spans increase with increasing tensile strength of rock materials, E_c / E_t ratios, and decreasing overburden. Due to the assumption of uniform load distributions along the unsupported roof part, variations in stress concentration on the supported roof part do not affect the critical spans. The critical spans for the bridging roof model tend to increase with decreasing foundation height or increasing foundation modulus. For a given roof formation under the same overburden loading, the bridging roofs have a greater span than the cantilevering roofs. In the context of longwall mining, this indicates that the initial caving intervals are greater than the periodic caving intervals. The developed design curves provide a quick and simple method for determining critical spans of the roof beds.

CHAPTER 5 STRAIN ENERGY ANALYSIS

5.1 Introduction

It has been recognized that a bump event may be induced by the violent release of seismic energy which is transformed from strain energy gradually accumulated in the coal seam and the surrounding rock mass. As mining operations proceed, the virgin stress field is disturbed, resulting in stress concentrations around the working faces. At the meantime, a considerable amount of strain energy, which is proportional to the square of the stresses, is accumulated both in the roofs and the coal seam. Either roof breakage or foundation (coal or weak roof) failure may trigger rapid release of the stored strain energy. Therefore, an understanding of the strain energy accumulation behavior around the working faces, and factors contributory to the energy accumulation, are of great importance to a safe and productive mining operation. This understanding can also provide a sound basis for the assessment of bump likeliness and its severity. In this chapter, an attempt is made to analytically evaluate the strain energy accumulations caused by the cantilevering or bridging of competent roofs over the working faces. Strain energy formulae for cantilevering and bridging roof models are developed using elastic beam theory. Parameters which may affect the energy storage are identified and investigated. The parameters analyzed include roof geometry, mechanical properties of the roof beds, foundation (coal) characteristics, and the overburden loading.

86

5.2 Strain Energy Stored in the Roof and the Foundation

5.2.1 Basic Energy Equations

For elastic materials, the strain energy per unit volume, or strain energy density, can be expressed in terms of stress and strain components assuming that the stress-strain relation follows Hooke's law [Buchanan, 1988]:

$$w = \frac{1}{2}\left(\sigma_x \varepsilon_x + \sigma_y \varepsilon_y + \sigma_z \varepsilon_z + \tau_{xy}\gamma_{xy} + \tau_{yz}\gamma_{yz} + \tau_{zx}\gamma_{zx}\right) \tag{5.1}$$

where

    w = strain energy density,

    $\sigma_x, \sigma_y, \sigma_z, \tau_{xy}, \tau_{yz}, \tau_{zx}$ = stress tensor, and

    $\varepsilon_x, \varepsilon_y, \varepsilon_z, \gamma_{xy}, \gamma_{yz}, \gamma_{zx}$ = strain tensor.

If the entire volume of the structural member is considered, the total stored strain energy is the integral of Equation 5.1 over the volume of the member, that is:

$$W = \frac{1}{2} \int_{volume}\left(\sigma_x \varepsilon_x + \sigma_y \varepsilon_y + \sigma_z \varepsilon_z + \tau_{xy}\gamma_{xy} + \tau_{yz}\gamma_{yz} + \tau_{zx}\gamma_{zx}\right) dV \tag{5.2}$$

where

    W = total stored strain energy in the structural member with a volume of V, and

    V = volume of the structural member.

For the bending beam, the nonzero stress components are the flexural stress, σ_x, and the shear stress, τ_{xy}, therefore, the strain energy due to bending, neglecting shear strain energy, is:

$$W_b = \frac{1}{2} \int_{volume} \sigma_x \varepsilon_x \, dV = \frac{1}{2} \int_{volume} \frac{\sigma_x^2}{E} \, dV \qquad (5.3)$$

where

W_b = total strain energy stored in the bending beam,

σ_x, ε_x = flexural stress and strain, respectively, and

E = modulus of elasticity.

For the bending beam, flexural stress and strain can be evaluated by the following equations:

$$\sigma_x = \frac{M\,y}{I} \qquad (5.4)$$

$$\varepsilon_x = \frac{\sigma_x}{E} \qquad (5.5)$$

$$I = \int_{area} y^2 dA \qquad (5.6)$$

where

M = bending moment of the beam,

y = distance from the neutral axis,

A = cross-section area of the beam, and

I = moment of inertia of the beam.

Substituting above expressions into Equation 5.3, we obtain:

$$W_b = \frac{1}{2} \int_0^L \int_{area} \frac{M^2 y^2}{E\,I^2} \, dA \, dx = \frac{1}{2} \int_0^L \frac{M^2}{D} \, dx \qquad (5.7)$$

88

where

L = length of the beam, and

D = flexural rigidity of the beam.

Applying Equations 5.1 to 5.7, the stored strain energy in the roof beds and the coal can be evaluated.

5.2.2 Strain Energy for the Cantilevering Roof Model

The strain energy stored in this kind of roof configuration is composed of three components, that is, energy stored in the unsupported roof portion, W_{r1}, energy stored in the supported roof portion, W_{r2}, and energy stored in the foundation (coal), W_c. Based on Equations 5.1 to 5.7, each energy component can be evaluated.

5.2.2.1 Strain Energy Stored in the Unsupported Roof Part

The bending moment, M, for the unsupported roof part is given by:

$$M = \frac{1}{2}px^2 \tag{5.8}$$

Combining Equations 5.7 and 5.8 gives:

$$W_{r1} = \frac{p^2 L^5}{40 D_{av}} \tag{5.9}$$

where

W_{r1} = strain energy per unit width stored in the unsupported roof part.

5.2.2.2 Strain Energy Stored in the Supported Roof Part

The second derivative of deflection line (Equation 3.25) with respect to x together

with Equation 3.9 gives the bending moment expression for the supported roof segment:

$$M = D_{sv}\left[2\beta^2 e^{-\beta x}\left(A_1 \cos\beta x - A_2 \sin\beta x\right) - \alpha f^2 e^{fx}\right]$$ (5.10)

Substituting Equation 5.10 for Equation 5.7, we get:

$$W_{t2} = \left[\begin{array}{l} \dfrac{D_{sv}\alpha^2 f^3}{4}e^{2fx} + \dfrac{D_{sv}\beta^3}{4}e^{-2\beta x}(A_2^2 - A_1^2 + 2A_1A_2)\cos 2\beta\,x \\[2mm] -\dfrac{D_{sv}\beta^3}{2}(A_1^2 + A_2^2)e^{-2\beta x} + \dfrac{D_{sv}\beta^3}{4}e^{-2\beta x}(A_1^2 - A_2^2 + 2A_1A_2)\sin 2\beta\,x \\[2mm] +\dfrac{2D_{sv}\alpha f^2\beta^2 e^{(f-\beta)x}}{(f-\beta)^2 + \beta^2}\left[(A_2 f - A_2\beta - A_1\beta)\sin\beta\,x + (A_1\beta - A_2\beta - A_1 f)\cos\beta\,x\right] \end{array}\right]_0^1$$ (5.11)

where

W_{t2} = strain energy per unit width stored in the supported roof part.

5.2.2.3 Strain Energy Stored in the Foundation (coal)

According to the Hooke's law, the stress and strain components are related as follows:

$$\varepsilon_x = \frac{1}{E}\left[\sigma_x - \nu(\sigma_y + \sigma_z)\right]$$ (5.12)

$$\varepsilon_y = \frac{1}{E}\left[\sigma_y - \nu(\sigma_x + \sigma_z)\right]$$ (5.13)

$$\varepsilon_z = \frac{1}{E}\left[\sigma_z - \nu(\sigma_x + \sigma_y)\right]$$ (5.14)

$$\gamma_{xy} = \frac{\tau_{xy}}{G}$$ (5.15)

90

$$\gamma_{yz} = \frac{\tau_{yz}}{G} \tag{5.16}$$

$$\gamma_{zx} = \frac{\tau_{zx}}{G} \tag{5.17}$$

where

      E = modulus of elasticity,

      G = shear modulus, and

      v = Poisson's ratio.

By substituting Equations 5.12 to 5.17 into Equation 5.1, the strain energy density can be expressed as:

$$w_c = \frac{1}{2E_e}\left(\sigma_x^2 + \sigma_y^2 + \sigma_z^2\right) - \frac{v_e}{E_e}\left(\sigma_x\sigma_y + \sigma_y\sigma_z + \sigma_z\sigma_x\right) + \frac{1}{2G_e}\left(\tau_{xy}^2 + \tau_{yz}^2 + \tau_{zx}^2\right) \tag{5.18}$$

where

      w_c = strain energy density in the coal,

      E_e = modulus of elasticity of the coal,

      G_e = shear modulus of the coal, and

      v_e = Poisson's ratio of the coal.

The stress conditions in the coal are assumed to be biaxial, that is:

$$\sigma_y = cy \tag{5.19}$$

$$\sigma_x = \sigma_z = \frac{v_e}{1-v_e}\sigma_y = \frac{v_e}{1-v_e}cy \tag{5.20}$$

91

$$\tau_{xy} = \tau_{yz} = \tau_{zx} = 0 \tag{5.21}$$

By combining Equations 5.18 to 5.21 and integrating, we obtain the strain energy per unit width in the coal seam:

$$W_c = \frac{h_e c^2}{2E_e}\left[\frac{(1+v_e)(1-2v_e)}{1-v_e}\right]\int_0^1 y^2 dx \tag{5.22}$$

Substituting the deflection y, given in Equation 3.25, into Equation 5.22, and integrating gives:

$$W_c = \frac{h_e c^2}{2E_e}\left[\frac{(1+v_e)(1-2v_e)}{1-v_e}\right]\left[\begin{array}{l} \dfrac{\alpha^2}{2f}e^{2fx} - \dfrac{A_1^2 + A_2^2}{4\beta}e^{-2\beta x} \\[2ex] + \dfrac{A_1^2 - A_2^2}{8\beta}e^{-2\beta x}(\cos 2\beta x - \sin 2\beta x) \\[2ex] + \dfrac{2\alpha\, e^{(f-\beta)x}}{(f-\beta)^2 + \beta^2}\left[(A_2 f - A_2\beta - A_1\beta)\cos\beta x\right] \\[2ex] \dfrac{2\alpha\, e^{(f-\beta)x}}{(f-\beta)^2 + \beta^2}\left[(A_2\beta + A_1 f - A_1\beta)\sin\beta x\right] \\[2ex] - \dfrac{A_1 A_2}{4\beta}e^{-2\beta x}(\cos 2\beta x + \sin 2\beta x) \end{array}\right]_0^1 \tag{5.23}$$

where

W_c = strain energy per unit width stored in the coal.

Therefore, the total strain energy stored in the roof and the coal is given by:

$$W_t = W_{r1} + W_{r2} + W_c \tag{5.24}$$

where

W_t = total strain energy per unit width for the cantilevering roof model.

92

5.2.3 Strain Energy Stored in the Bridging Roof Model

The formula for evaluating the strain energy stored in the supported part of the bending beam, W_{r2}, and the strain energy stored in the coal, W_c, are the same as those for the cantilevering beam, with different initial values y_o, and y_o' which are defined in Equations 3.53 and 3.54, respectively.

For the unsupported roof part, the moment equation can be established by second derivative of deflection line expression given in Equation 3.42 and putting it into Equation 3.9:

$$M = -\frac{p\,x^2}{2} - 6\,B_1\,D_{av} - 2\,B_2\,D_{av}$$

(5.25)

Combining Equation 5.7 and 5.25 gives:

$$W_{r1} = \frac{p^2\,L^5}{40\,D_{av}} - \frac{3}{4}\,p\,B_1\,L^4 + \frac{1}{6}\left(2p\,B_2 + 36\,B_1{}^2\,D_{av}\right)L^3 - 6\,B_1\,B_2\,D_{av}\,L^2 + 2\,B_2{}^2\,D_{av}\,L$$

(5.26)

where

W_{r1} = strain energy per unit width stored in the unsupported roof part.

The total strain energy stored in the roof and the coal for the bridging model is hence given by:

$$W_t = W_{r1} + 2W_{r2} + 2W_c$$

(5.27)

where

W_t = total strain energy per unit width for the bridging roof model.

5.3 Parameter Analysis and Discussions

Based on the strain energy expressions developed in the previous section, the parameters influencing the strain energy accumulation and its distributions in the roof and the foundation (coal) are analyzed in order to observe the behavior of the major contributory variables.

5.3.1 Overburden Depth

The effects of overburden depth on the strain energy accumulation for a range of roof thicknesses are illustrated in Figure 5.1. For both roof models, total stored energy increases with increasing overburden depth and roof thickness. However, energy increase rate of the bridging model is higher than that of the cantilevering model. At the same overburden depth and roof thickness, the bridging roof accumulates more energy than the cantilevering roof.

An examination of Figure 5.2 showing energy distributions for the cantilevering roof model reveals that even though both the roof energy and the foundation (coal) energy increase with the overburden depth and the roof thickness, nearly all energy is stored in the coal. The relative values of the roof energy to the total energy as plotted in Figure 5.3, W_r / W_t, are very small (less than 10 percent).

Energy distributions for the bridging model are quite different from the cantilevering model as shown in Figure 5.4. In general, both the roof energy and the foundation (coal) energy increase as the overburden depth and the roof thickness increase. However, the increase of the roof energy is at a relatively higher rate in contrast to the foundation (coal) energy. The energy distributions in the roof and the coal are dependent upon the overburden depth and the roof thickness (Figure 5.5). For a thin roof bed under a deep
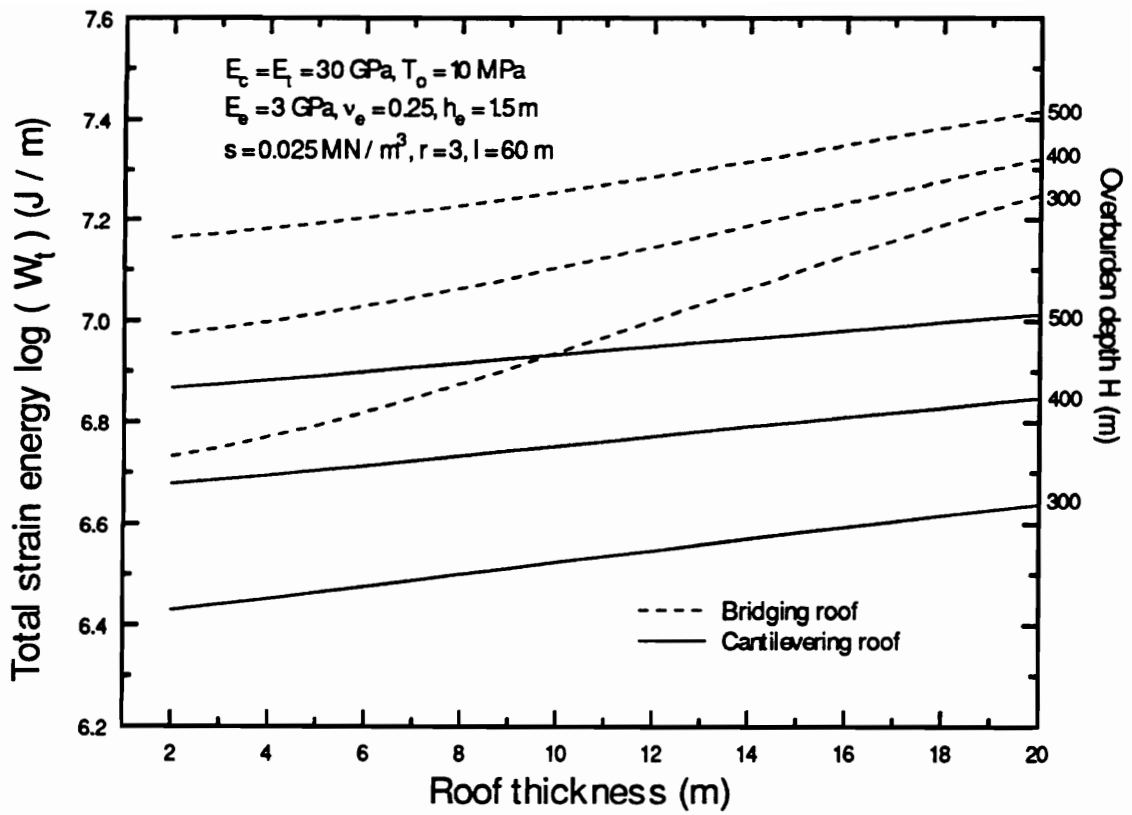
Figure 5.1 Effect of overburden depth on total strain energy
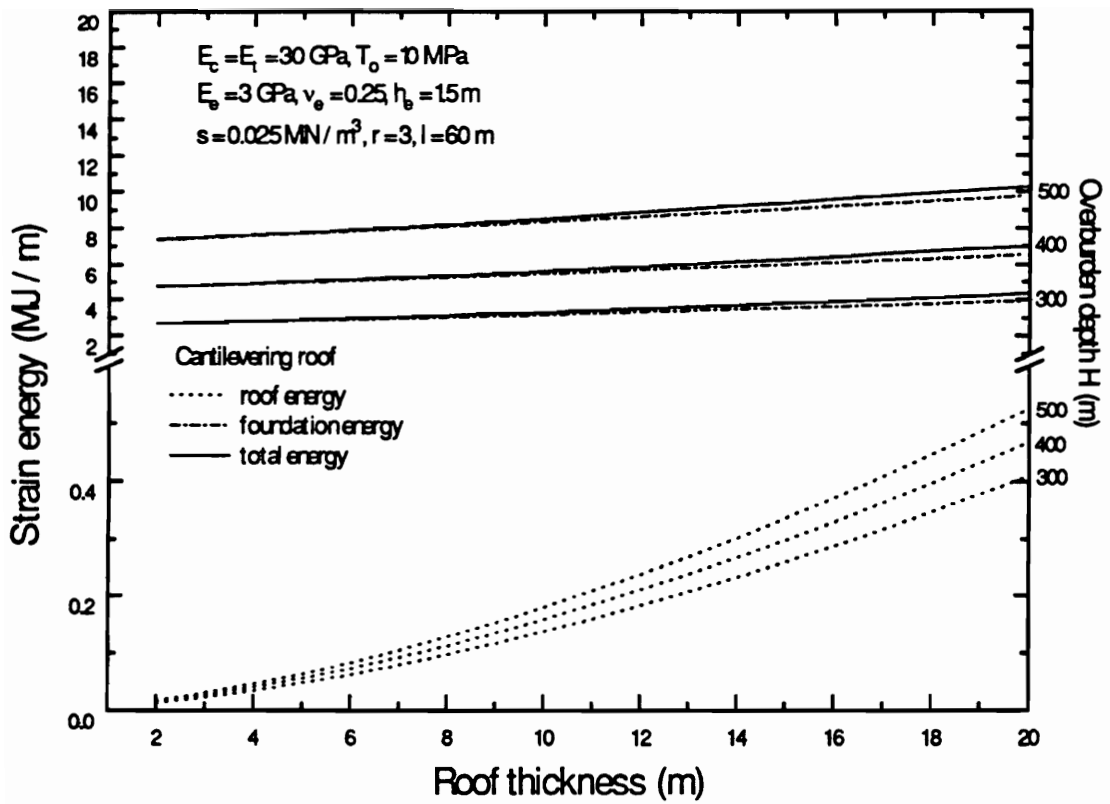
Figure 5.2 Strain energy distributions for cantilevering roof
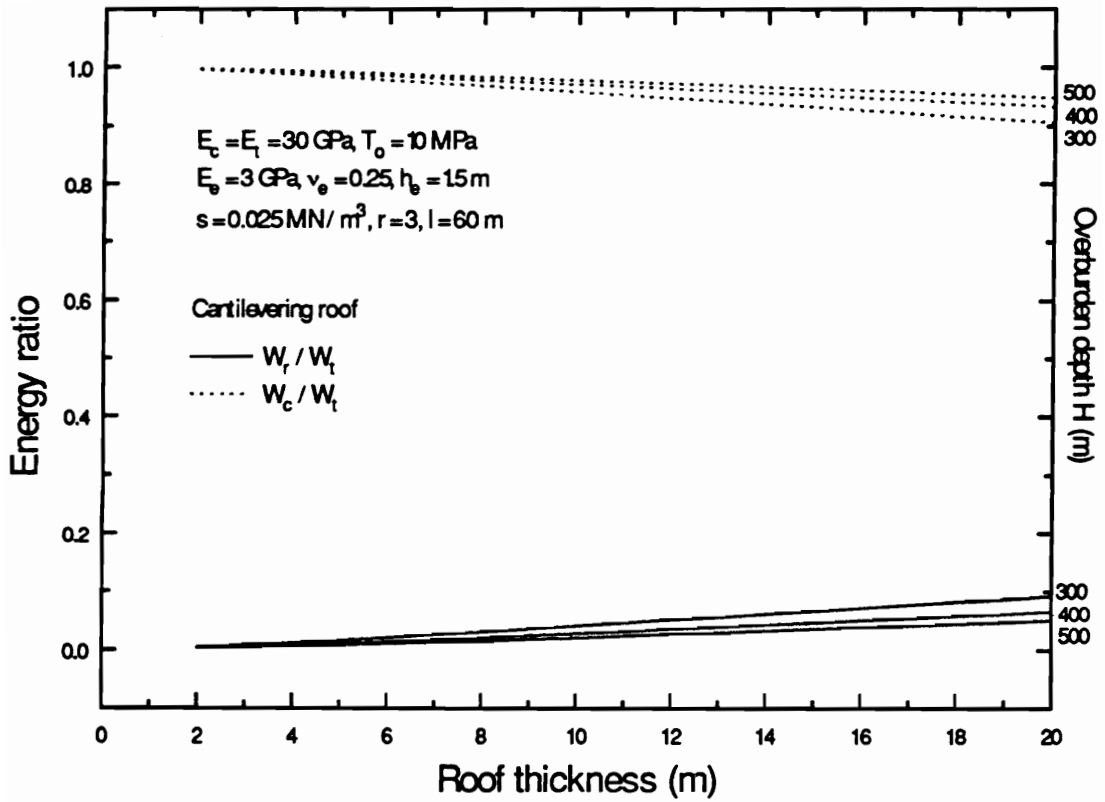
Figure 5.3 **Energy percentages stored in roof and foundation (coal) for cantilevering roof**
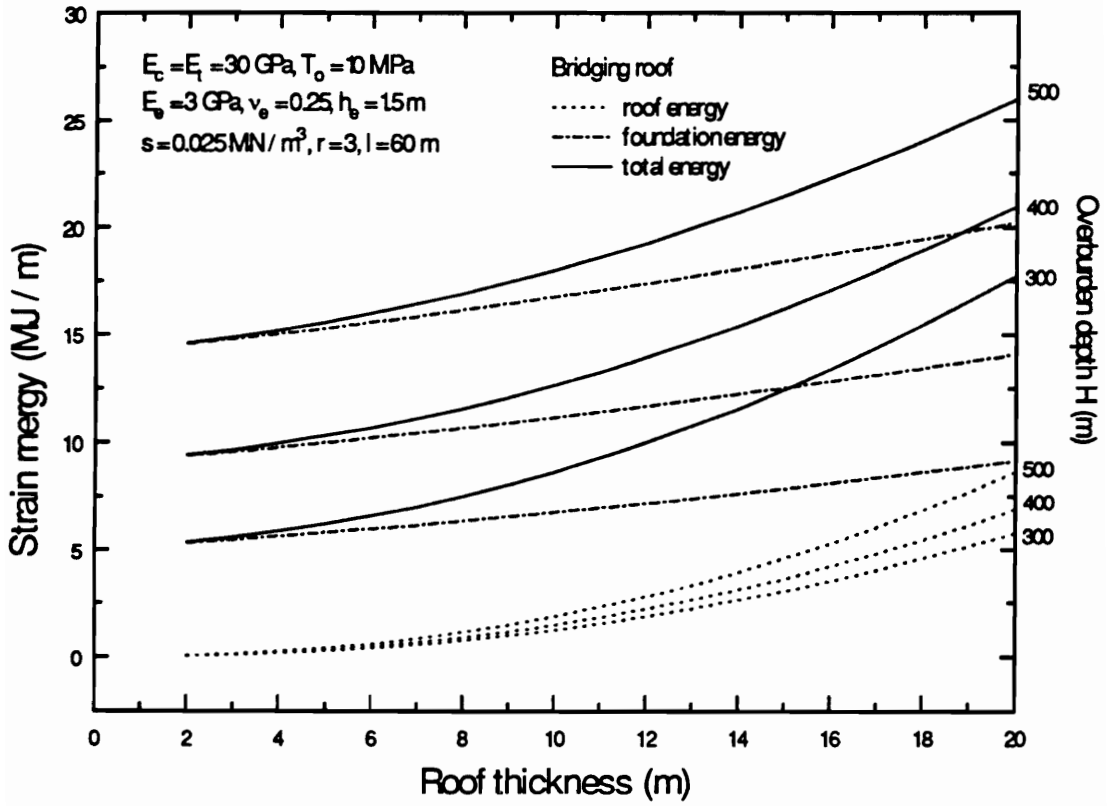
Figure 5.4 Strain energy distributions for bridging roof

**Figure 5.5 Energy percentages stored in roof and foundation
(coal) for bridging roof**

overburden, most of the energy is stored in the coal. Increasing the roof thickness or decreasing the overburden give a rise in roof energy and a decrease in foundation energy. The roof energy and the foundation energy reach to almost same magnitude at a overburden depth of 300 m and a roof thickness of 20 m.

5.3.2 Tensile Strength

As illustrated in Figure 5.6, in both roof models, the stored energy increases with the increase of the tensile strength of the roof materials. The bridging roofs accumulate much more energy than the cantilevering roofs. The difference in the energy storage between two roof models increments as the roof thickness increases.

An examination of energy distributions (Figure 5.7) in the cantilevering roof model indicates that most of energy is stored in the coal foundation. The roof carries only less than 15% of total energy for tensile strengths varying from 5 MPa to 15 MPa (Figure 5.8).

Energy distributions for the bridging roof model are presented in Figure 5.9. As the increase of tensile strength and roof thickness, the energy stored in the roof increases more rapidly than the energy stored in the coal. For a stiffer and thicker roof, the roof energy will exceed the foundation energy (Figure 5.10).

5.3.3 Foundation (coal) Modulus

Influence of the foundation (coal) modulus on the total strain energy accumulation is shown in Figure 5.11. For both models, increasing foundation modulus or decreasing the ratio of roof modulus to the coal modulus, E_r / E_c, results in decreasing the amount of stored energy. Under the same conditions the bridging roof tends to store more energy than the cantilevering roof. This fact indicates that minimization of the energy buildup could be achieved by reducing the roof modulus, that is, reducing the values of E_r / E_c.

Although variations in coal modulus affect the energy distributions as shown in

100
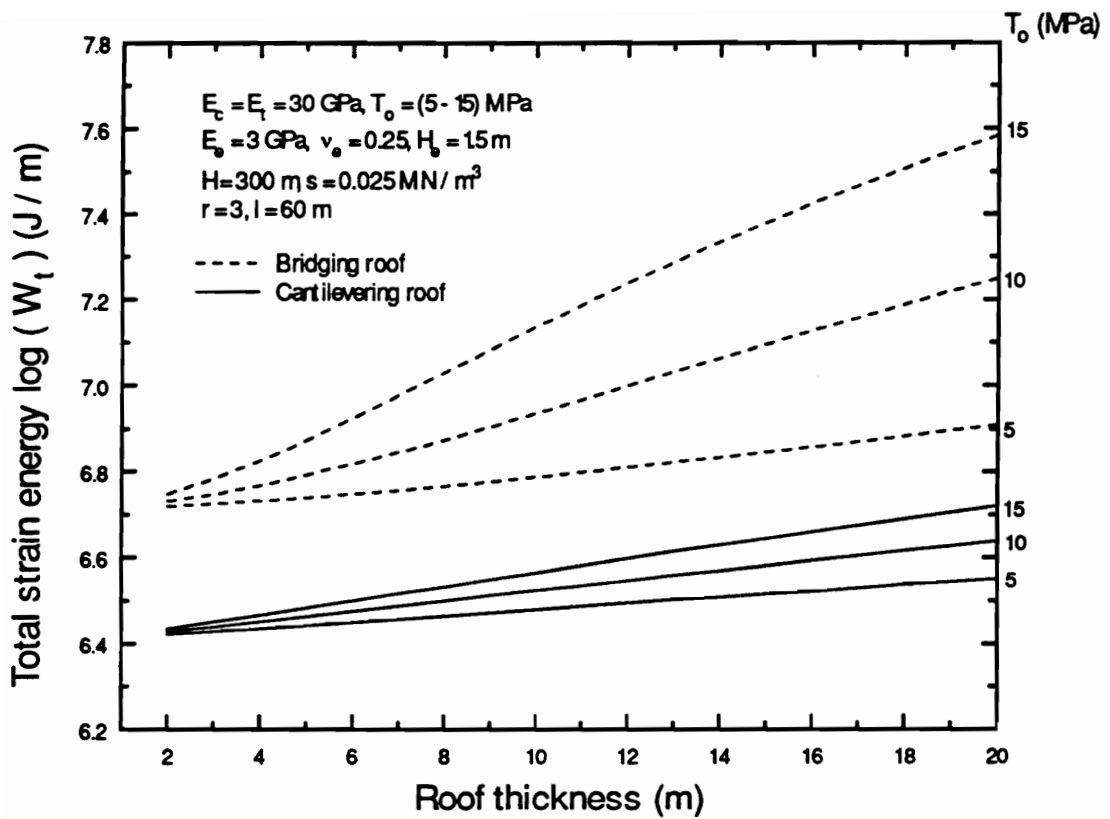
Figure 5.6 Effect of tensile strength on total strain energy
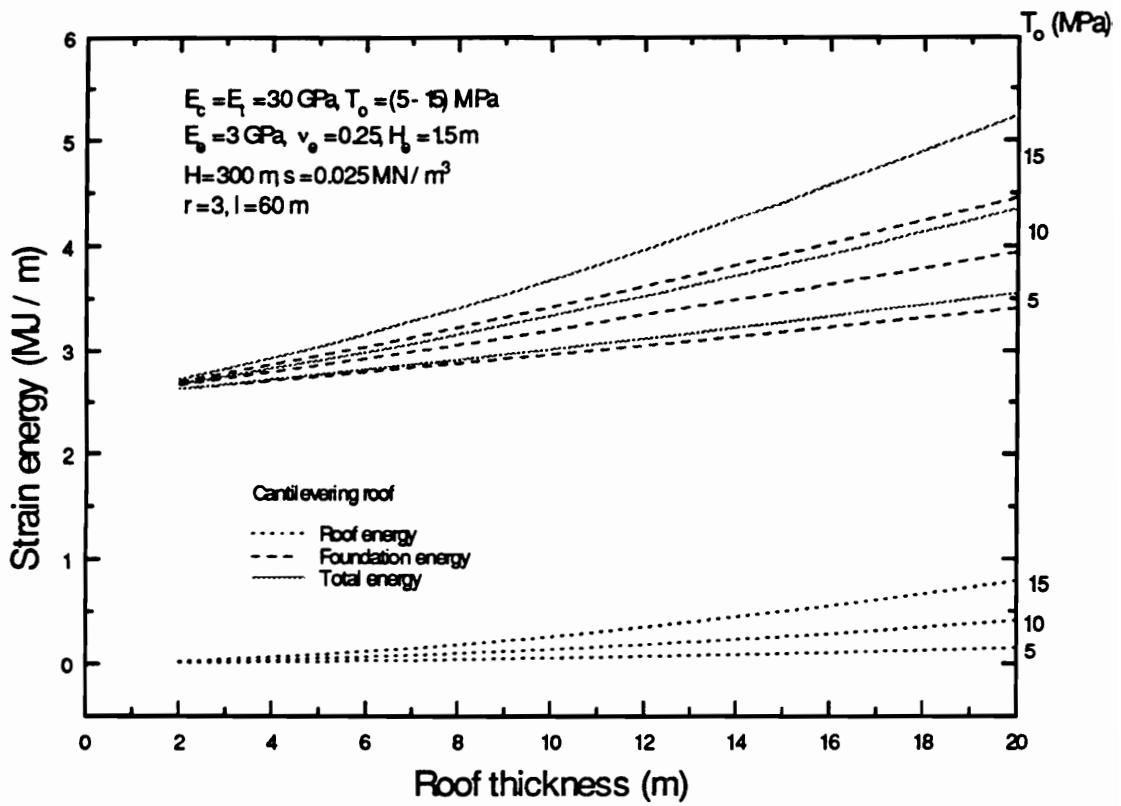
Figure 5.7 Strain energy distributions for cantilevering roof
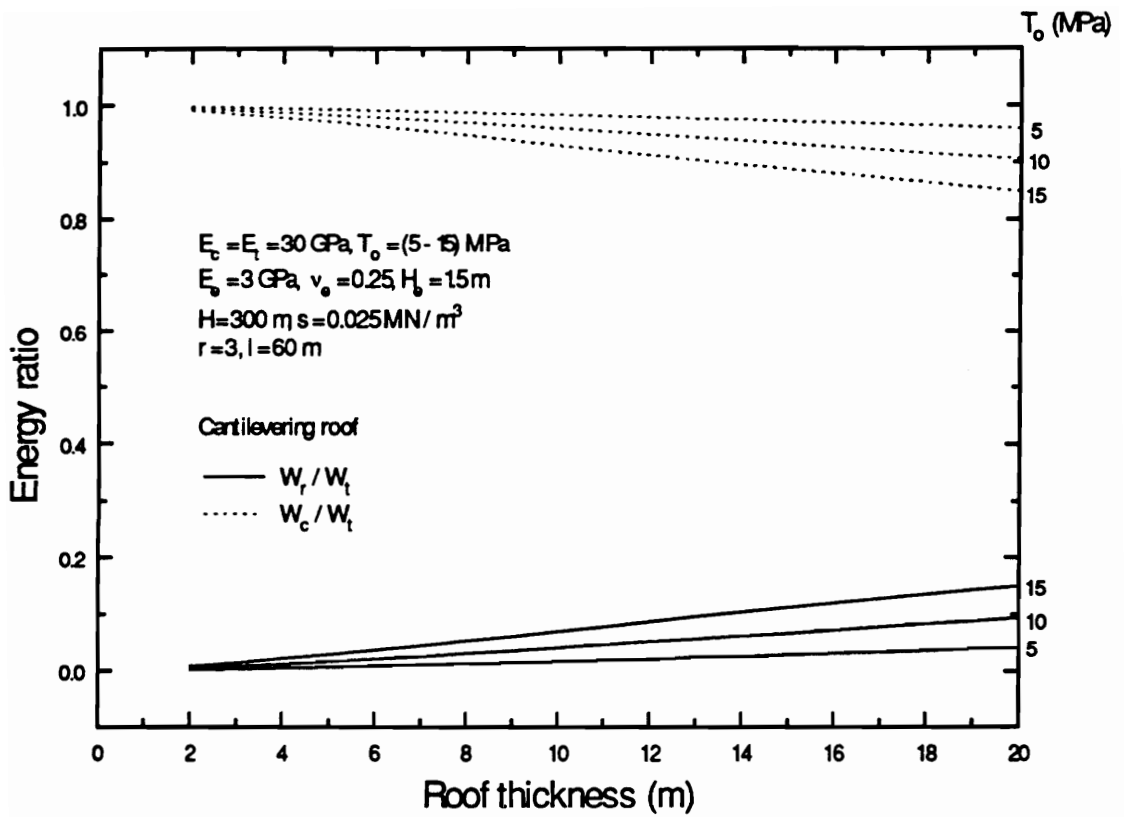
Figure 5.8 Energy percentages stored in roof and foundation (coal) for cantilevering roof
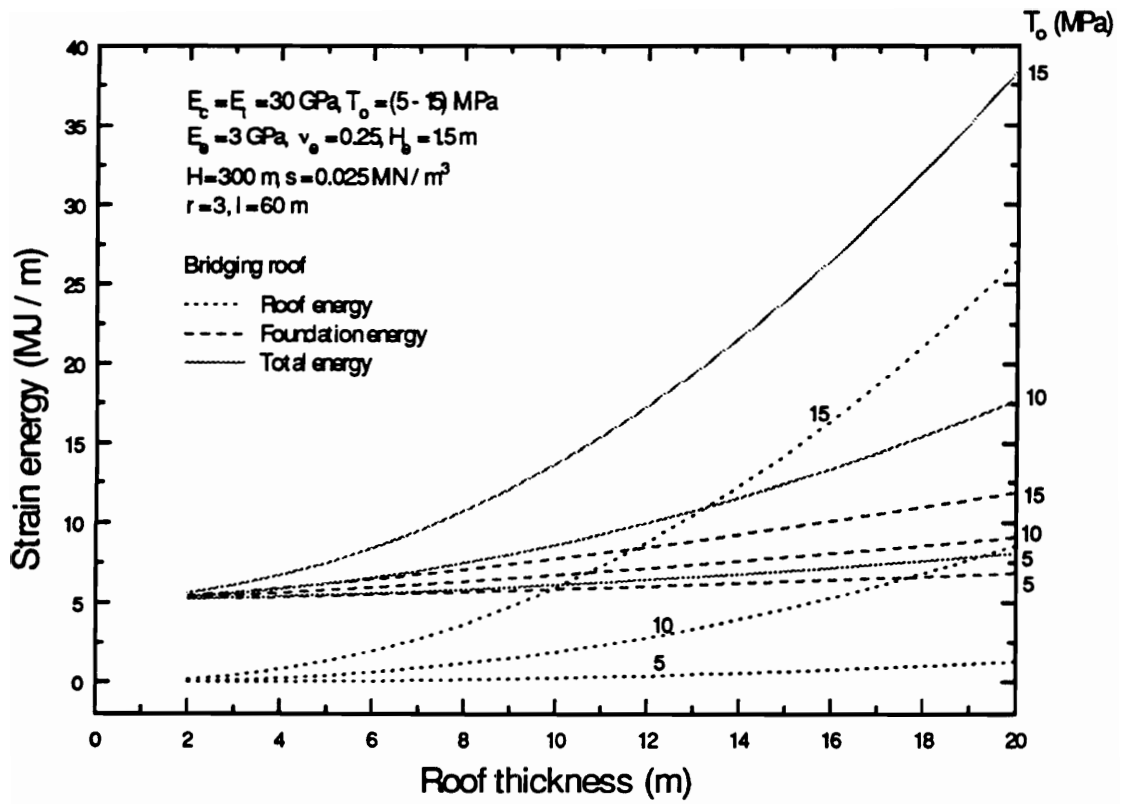
Figure 5.9 Strain energy distributions for bridging roof

104
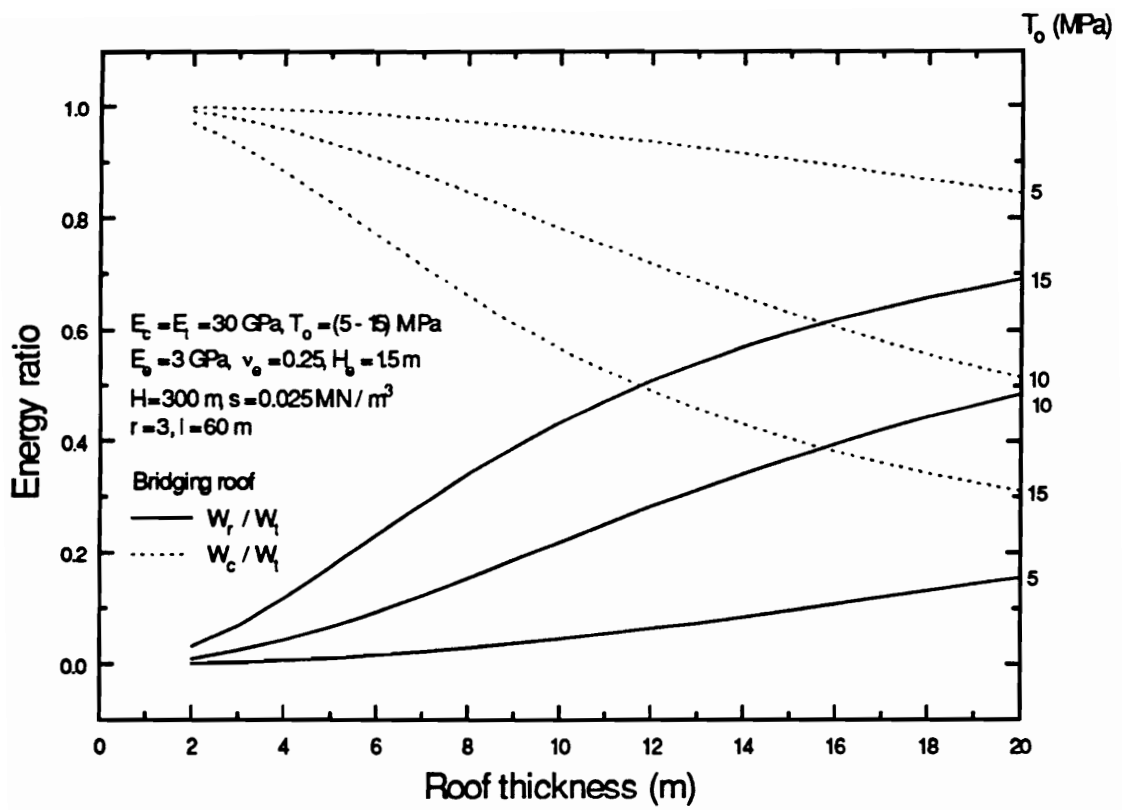
Figure 5.10 Energy percentages stored in roof and foundation (coal) for bridging roof

Figure 5.12, the majority of energy is stored in the coal for the cantilevering model. In the bridging roof model, the energies stored in the roof and the foundation are greatly affected by the roof thickness and the foundation modulus as illustrated in Figure 5.13. As the roof thickness and the coal modulus increase, the energy stored in the roof will increase, corresponding to the rapid decrease of energy in the coal.

5.3.4 Foundation (coal) Height

Variations in total stored energy for a range of foundation (coal) heights are combined in Figure 5.14. For both roof models, the total energy increases with increasing foundation height. For the same foundation height, the energy stored in the bridging model is always greater than the energy in the cantilevering model.

For the cantilevering roof, most of energy is stored in the coal (Figure 5.15). Decreasing foundation height yields an increase in roof energy and a decrease in coal energy. However, in the bridging model, as the foundation height decreases, the foundation energy decreases at a rapid rate, corresponding to a sharp increase in roof energy (Figure 5.16).

5.3.5 Stress Concentration Factor

Increasing the stress concentration factor gives an increase of total stored energy in both roof models as shown in Figure 5.17. The amount of energy stored in the bridging roof, as well as its rate of increase, are generally greater than those in the cantilevering roof.

Figure 5.18 shows a comparison of energy components in the roof and the coal for the cantilevering roof model. The effect of this factor on energy distributions is limited. The roof stores only small percentage of total energy. In contrast to the cantilevering model, the energy distributions in the roof and the coal for the bridging model are greatly dependent upon the roof thickness (Figure 5.19). As the roof becomes thicker, the energy
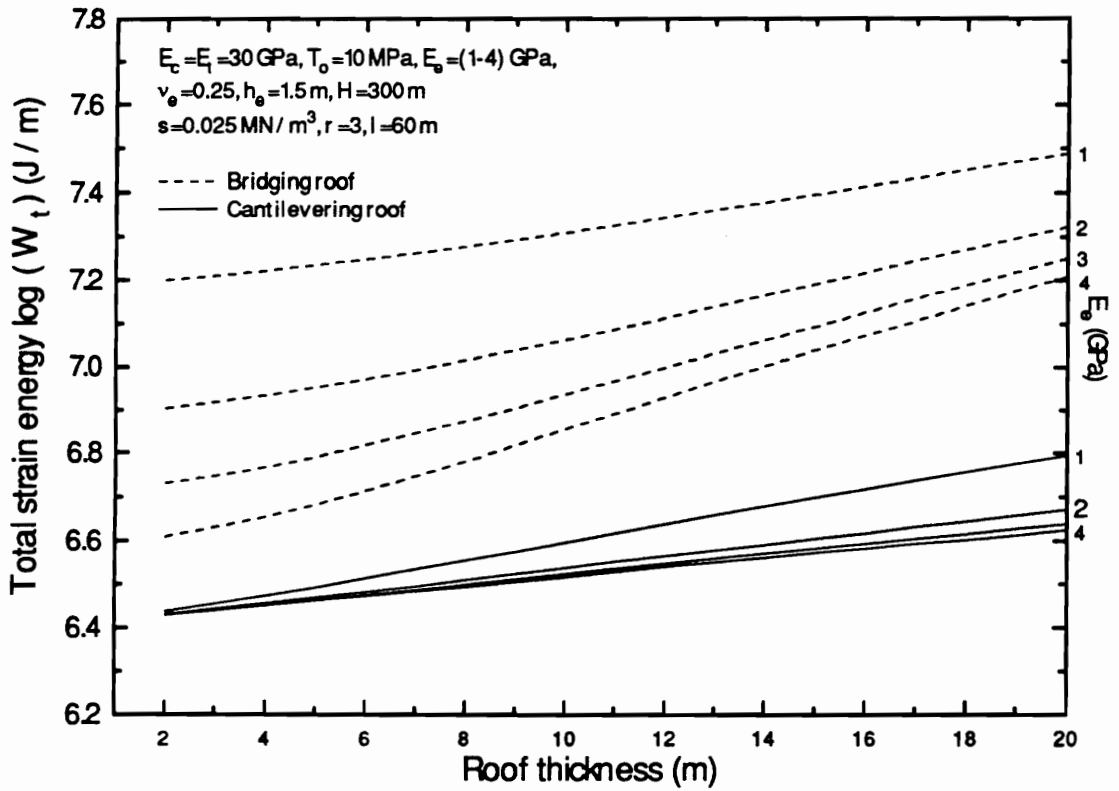
Figure 5.11 Effect of foundation (coal) modulus on total strain energy
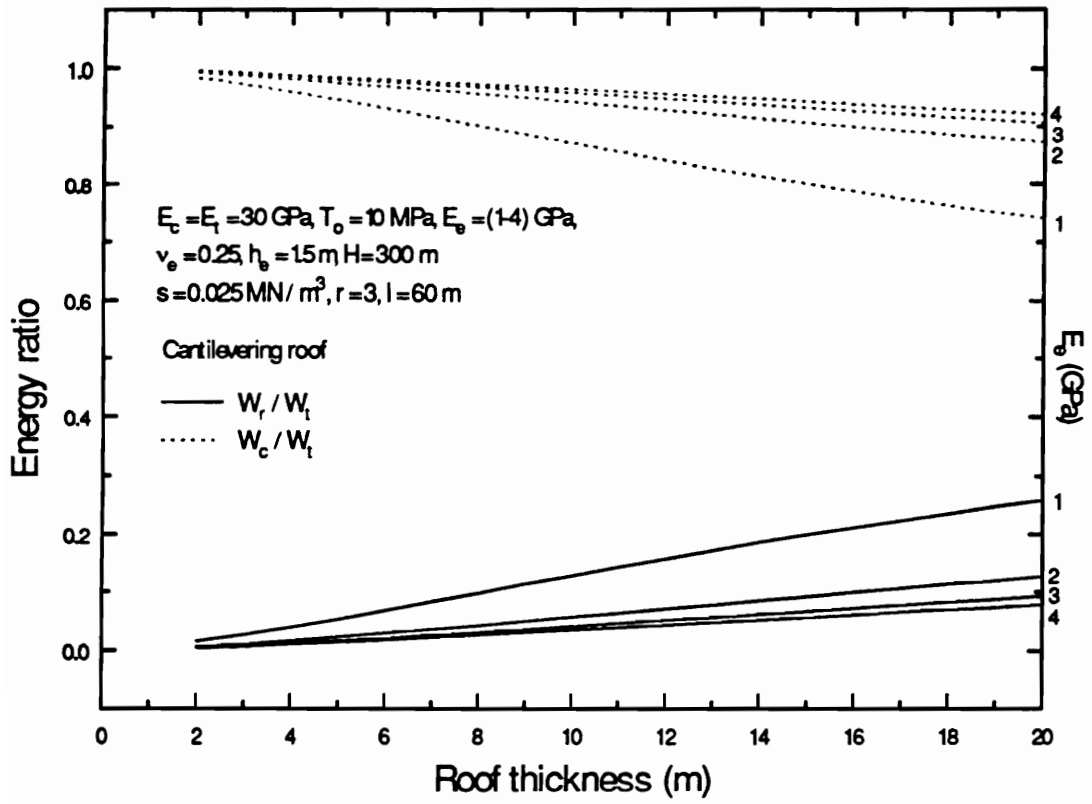
Figure 5.12 Energy percentages stored in roof and foundation (coal) for cantilevering roof
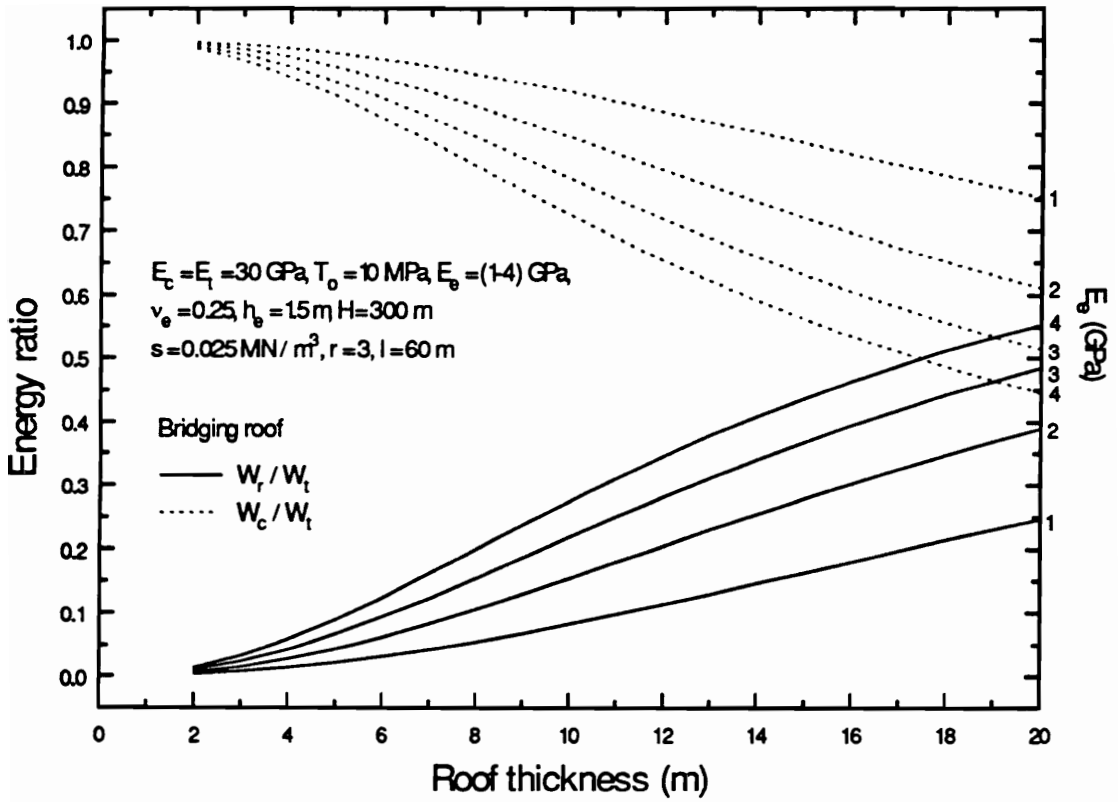
Figure 5.13 Energy percentages stored in roof and foundation (coal) for bridging roof
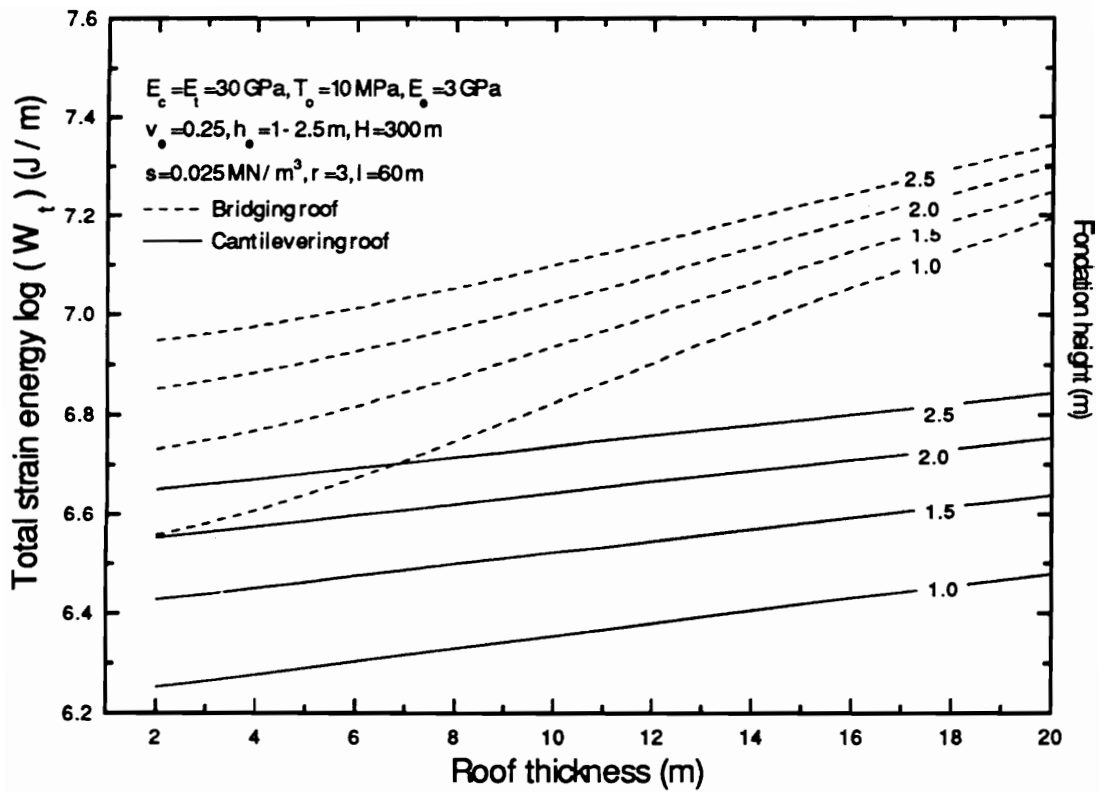
Figure 5.14 Effect of foundation (coal) height on total strain energy
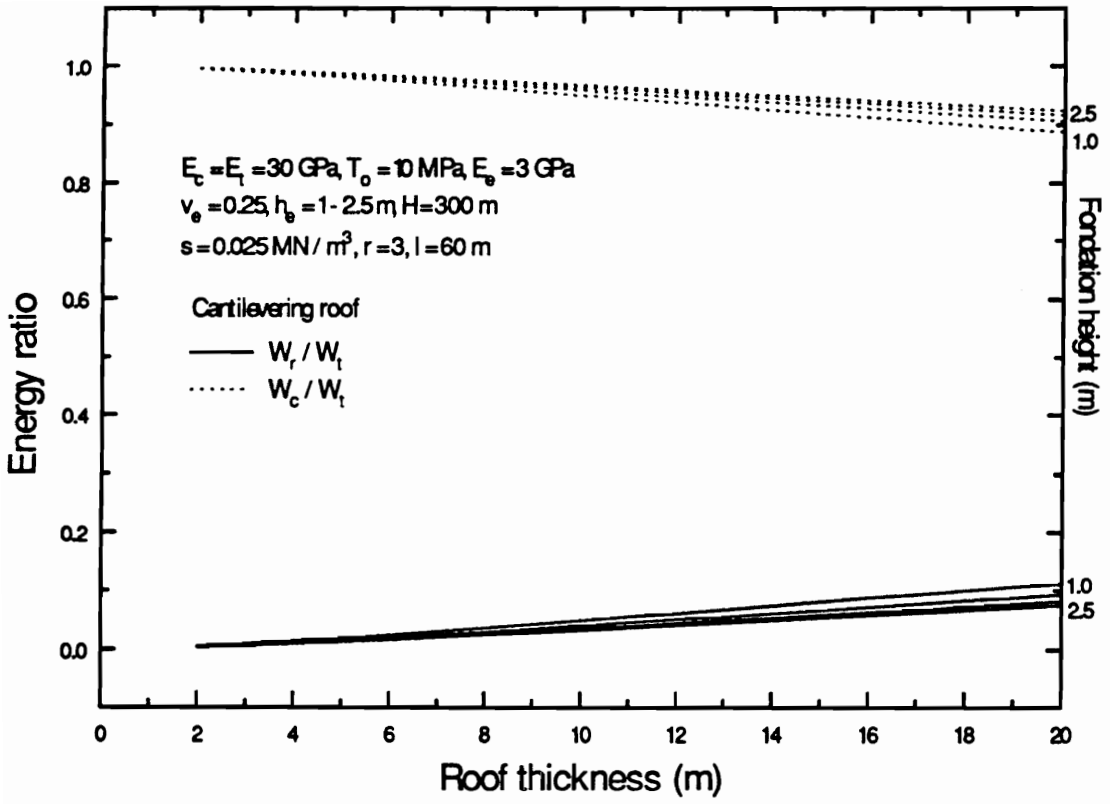
**Figure 5.15 Energy percentages stored in roof and foundation
(coal) for cantilevering roof**
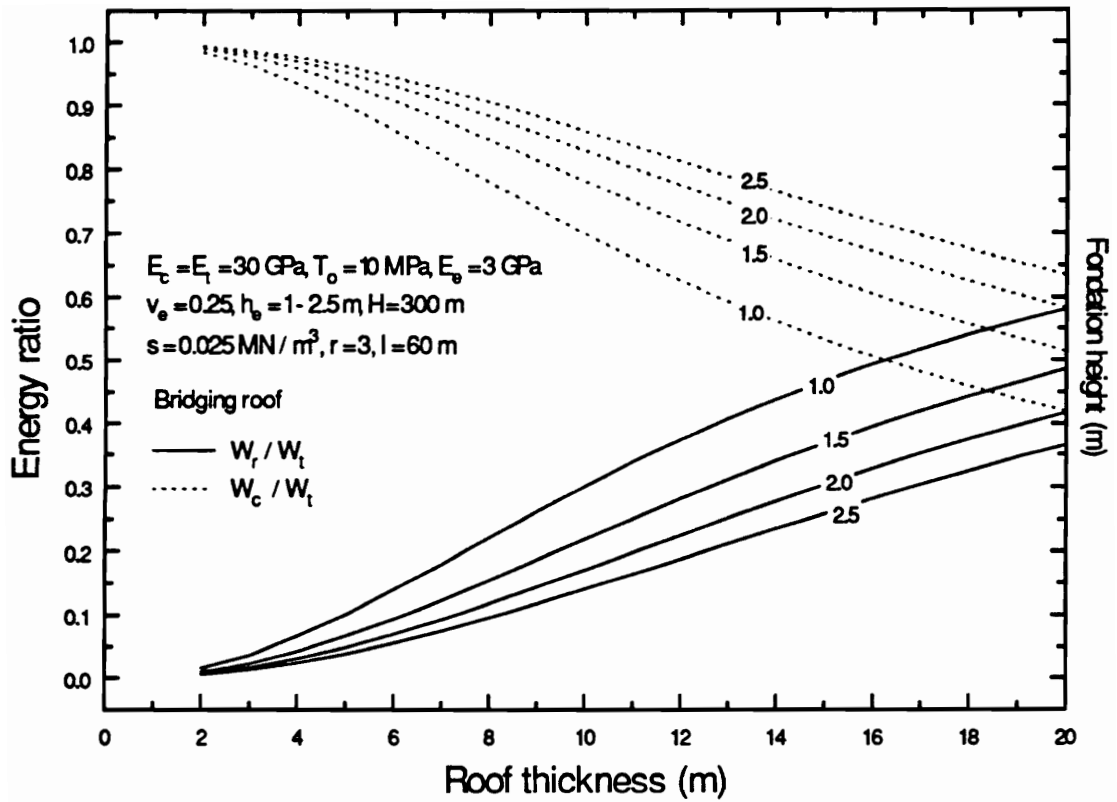
Figure 5.16 Energy percentages stored in roof and foundation (coal) for bridging roof
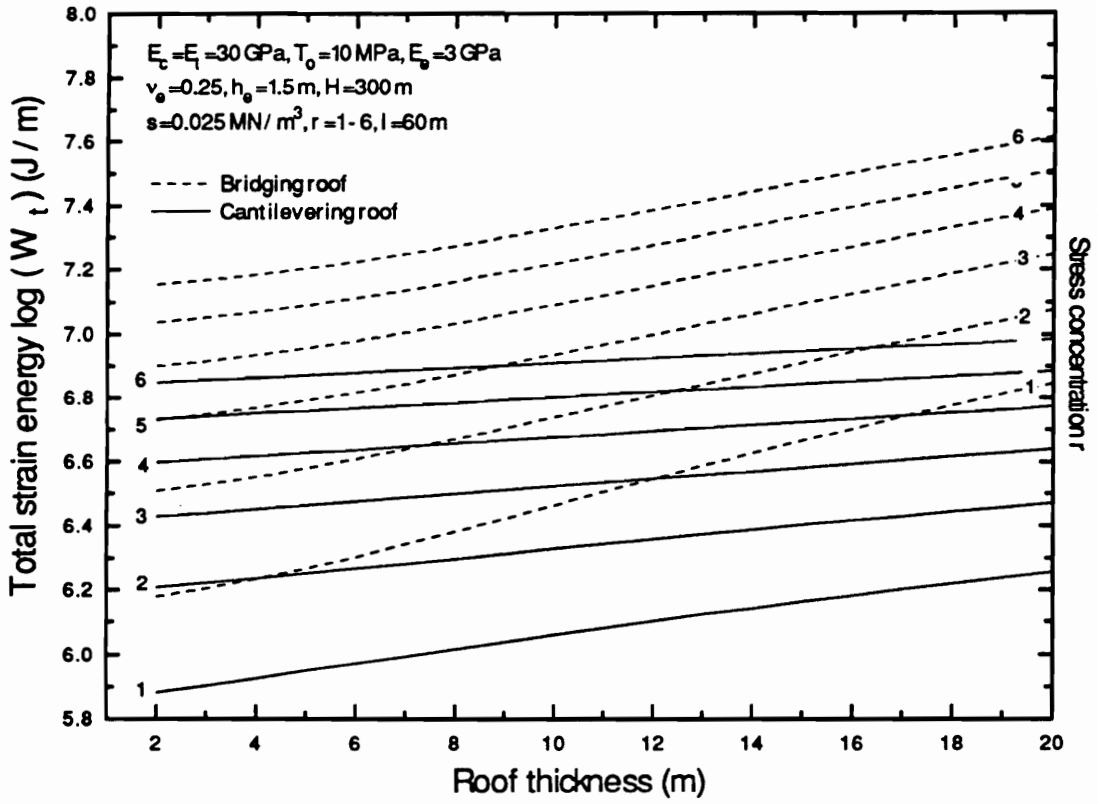
Figure 5.17 Effect of stress concentration factor on total strain energy
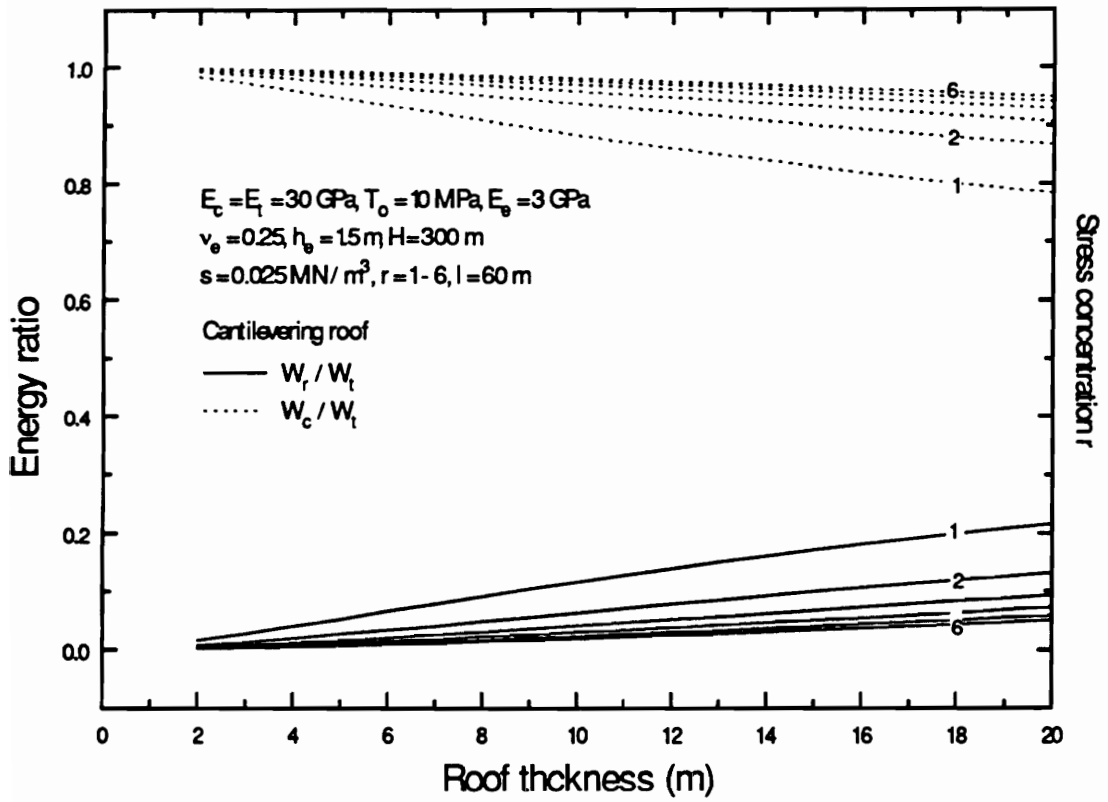
Figure 5.18 Energy percentages stored in roof and foundation (coal) for cantilevering roof
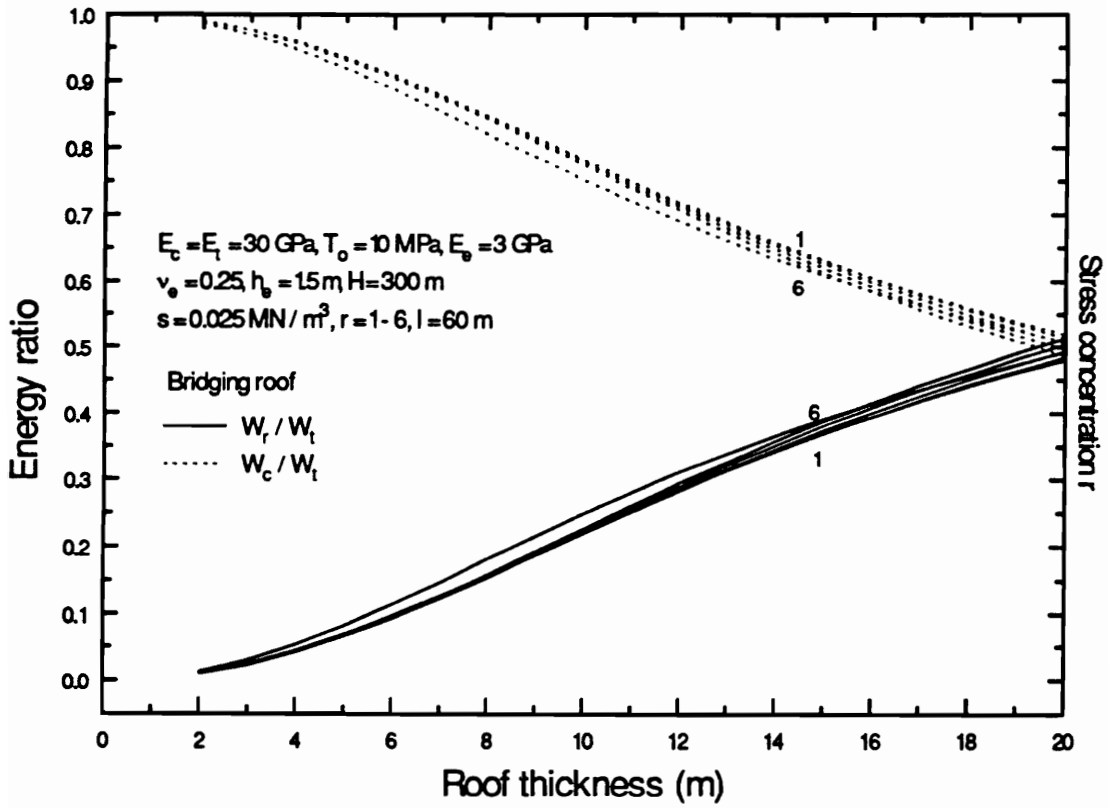
Figure 5.19 Energy percentages stored in roof and foundation (coal) for bridging roof

stored in the roof increases, the energy in the foundation, however, decreases. For a very thick roof bed, the roof energy and the foundation energy will reach the same multitude.

5.3.6 E_c / E_t Ratio

An increase in the E_c / E_t values results in increasing the total energy for both roof models. The bridging roof is more sensitive to this factor as illustrated in Figure 5.20. The energy stored in the roof is only a small fraction of the total energy for the cantilevering roof model (Figure 5.21). However, for the bridging roof model, variations in this factor greatly influence the energies stored in the roof and the coal as shown in Figure 5.22. Decreasing values of E_c / E_t gives a rise in foundation energy and a decrease in roof energy.

5.4 Summary

The formulae to evaluate the strain energy stored in the roof and the foundation are developed based on the elastic beam theory. The factors influencing the energy buildup and distributions caused by the cantilevering and bridging of strong roofs are identified and analyzed. These factors fall into four categories: the mechanical properties of the strong roofs (tensile strength and E_c / E_t ratio), the foundation properties (elasticity modulus and height), the applied stress characteristics (overburden depth and stress concentration), and the roof configurations. From parametric analysis, the following observations regarding the relevant parameters can be established. The stored strain energy increases with increasing roof thickness, overburden depth, E_c / E_t ratio, tensile strength, stress concentration factor, foundation height, and decreasing foundation modulus. It is also revealed that under the same conditions the energy storage associated with the bridging roof model is always greater than that for the cantilevering roof model, which translates into a greater bump potential for the first weighting stage as compared to

116
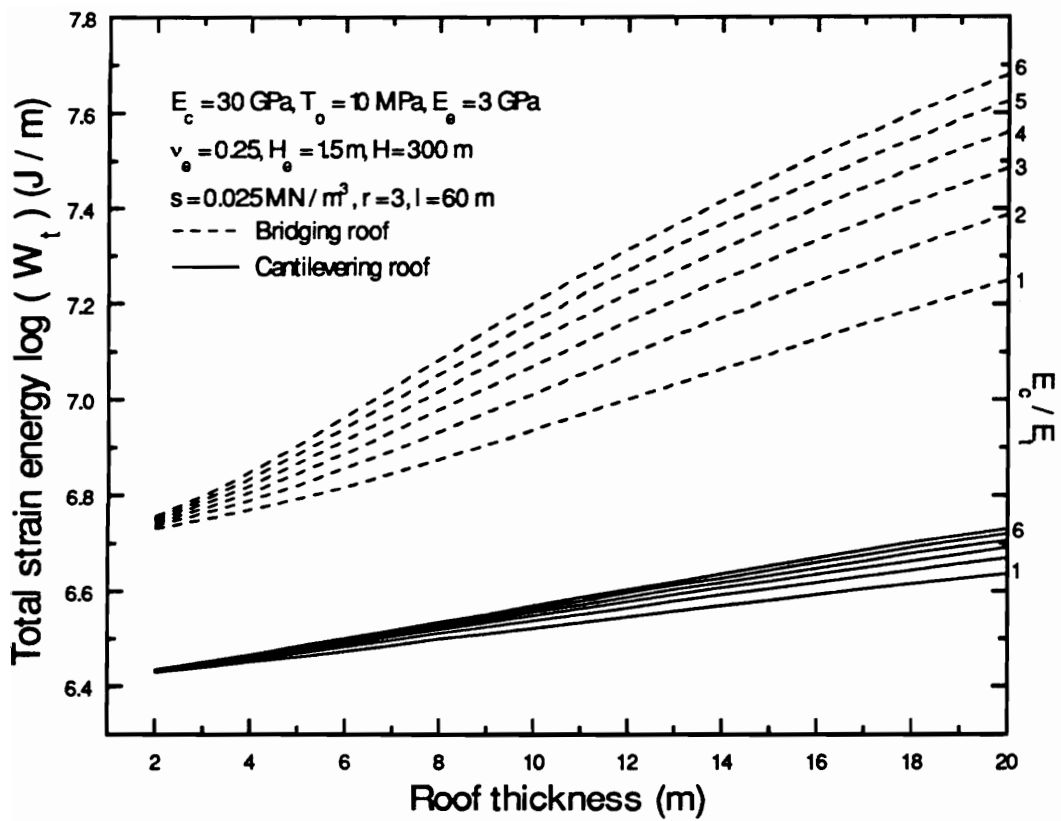
Figure 5.20 Effect of E_c / E_t ratio on total strain energy

117

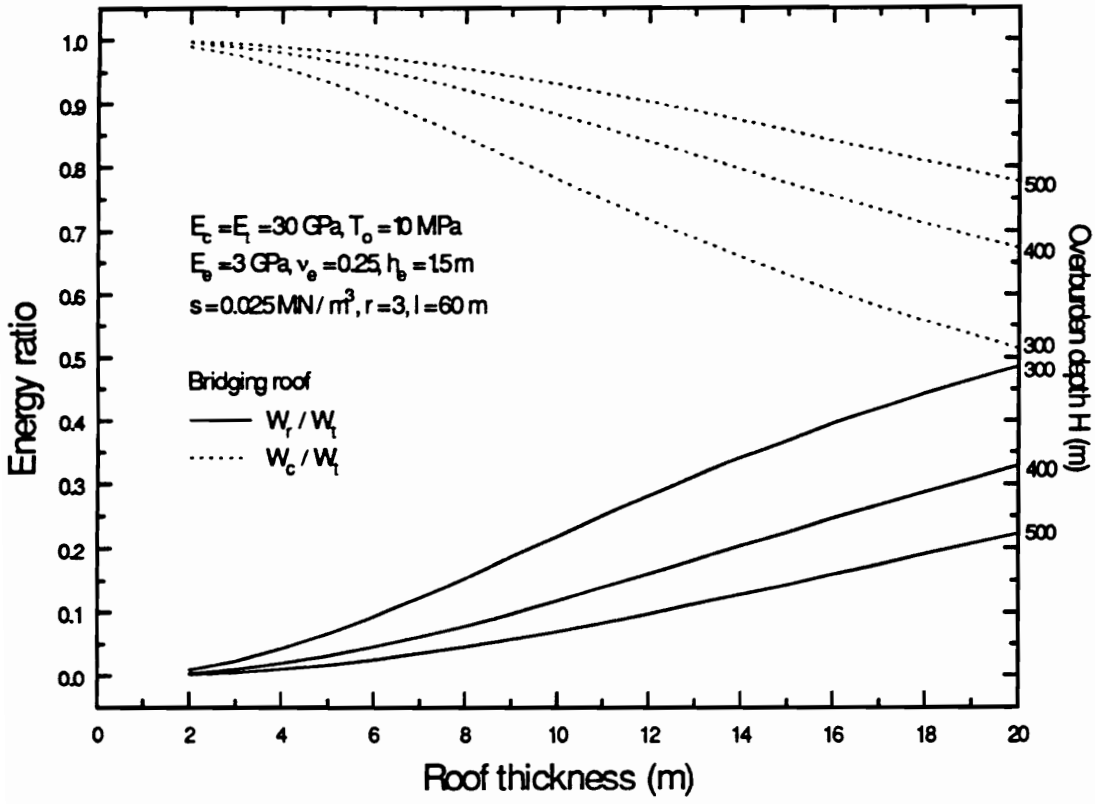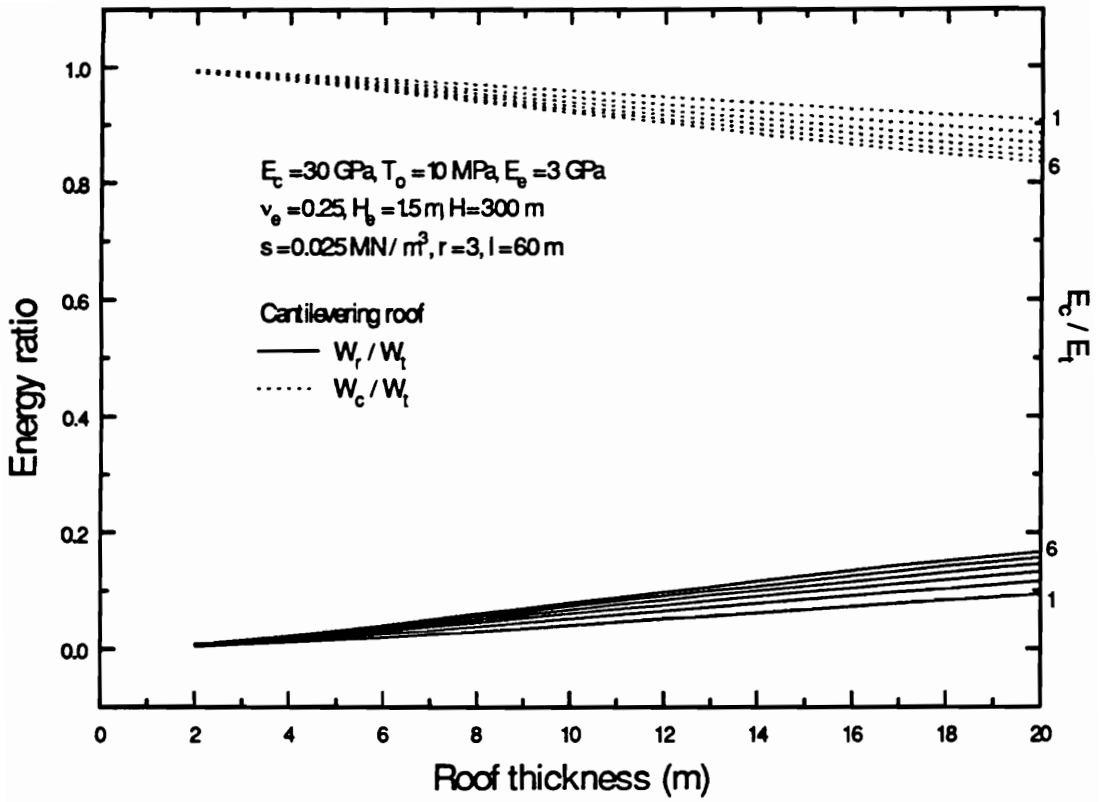**Figure 5.21 Energy percentages stored in roof and foundation (coal) for cantilevering roof**
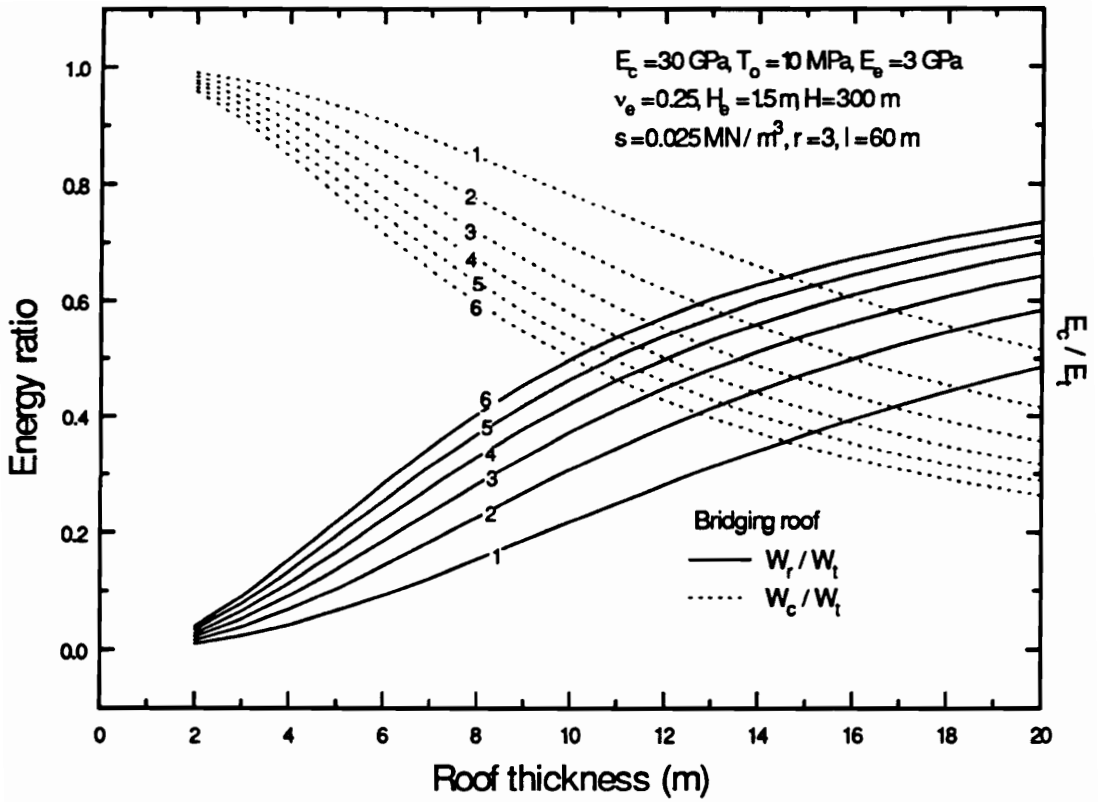
**Figure 5.22 Energy percentages stored in roof and foundation
(coal) for bridging roof**

the periodic weighting stages during longwall extraction. Distinctive energy distributions in the roof and the coal for different roof models may guideline the design of practical bump control measures. Bump control methods, such as destressing and hydraulic fracturing are aimed at releasing energy in the stress concentrated zones by artificially inducing cracks in the roof or the coal ahead of the working faces. From the parameter analysis, for the cantilevering models, the roof carries only small part of the total energy, therefore, efforts should be focused on control of the energy stored in the coal. The energy stored in the thicker bridging roof with a high strength may exceed the energy in the foundation, control of both the roof and the foundation energy accumulation should be taken into account.

CHAPTER 6   COAL BUMPS PREDICTION AND CASE STUDIES

6.1 Introduction

Upon failure of strong roofs, the stored strain energy in highly-stressed regions may be released in the form of high-intensity-and-low-frequency elastic stress waves radiating a significant amount of seismic energy, producing seismic events. The intensity of the seismic events is dependent on the amount of the seismic energy transformed from the strain energy. Extensive rockburst studies in South African gold mines [McGarr, 1984] have shown that rockburst phenomenon is similar to earthquakes with regard to stress drops, seismic moment and magnitude, source dimensions, and so on. Furthermore, the local magnitude scale, devised by Richter [1956] for earthquakes, may be used to measure the rockburst intensities caused by the release of strain energies [McGarr, 1984; Salamon, 1983]. In coal mining industry, the Richter magnitude was sometimes included as a important parameter in the bump occurrences reports [Mei and Lu, 1987; Kusznir, 1983]. This parameter was also used by Iannacchione and Mark [1990] to assess possible mine tremors caused by the strong roof collapse in a West Virginia abandoned coal mine. In this chapter, a quantitative parameter, based on an estimation of the local Richter magnitude, is proposed as a predictive index for the likeliness and severity of coal bumps associated with mining under strong roofs. Criteria for pressure and shock bumps are suggested. Several case studies from five U.S. bump-prone coal mines are conducted to

verify the theoretical predictions. A Windows-based software package "Coal Bump Potential Evaluation Program" (CBPEP) is developed to provide a tool for determination of roof spans, strain energy stored in the roof and the foundation, and bump likeliness.

6.2 Evaluation of Bump Possibility

The relationship between the local Richter magnitude, M_L, and the total strain energy, W_t, can be expressed as [Richter, 1956; Brady and Haramy, 1994]:

$$\log(nW_t) = 11.8 + 1.5M_L \tag{6.1}$$

where

n = seismic efficiency,

W_t = total strain energy, erg, and

M_L = local Richter magnitude.

The seismic efficiency, n, denotes the percentage of total strain energy being transformed into seismic energy. Depending on rock brittleness, the seismic efficiency could vary from 5 to 100 percent [Ortlepp, 1983; Iannacchione and Mark, 1990]. The term nW_t in Equation 6.1 is the seismic energy transformed from the strain energy. In a study of the relationship between the Modified Mercalli intensity and the Richter magnitude for Northern American earthquakes, Sibol and others [1987] indicated that the smallest recorded event resulting in a Modified Mercalli intensity VI which is the structural damage threshold corresponds to M_L value equal to 2.0. Data presented by Mei and Lu [1987] from Chinese coal mines also showed that the bump occurrences which caused mine facility damages, or miner fatalities, had Richter magnitudes ranging from 1.7 to 3.8. Therefore, the local Richter magnitude of 2.0 could be considered as a damage criterion to evaluate whether bump may cause safety problems.

6.2.1 Pressure Bump Possibility

Pressure bumps are associated with the violent failure of foundations under high compressive stresses. Prior to roof failure, if the local stress concentration on the foundation exceeds its compressive strength, C_o, the foundation will undergo a rapid progressive failure until the roof span reaches its critical values. During this process, considerable amounts of stored energy may be released, potentially triggering pressure bumps. Knowing the maximum deformation of the foundation in the supported roof segment, y_{max}, the corresponding induced maximum compressive stress of the foundation, σ_{cmax}, can be readily determined by the following equation:

$$\sigma_{cmax} = \frac{E_e \, y_{max}}{h_e} \tag{6.2}$$

where

E_e = elastic modulus of the foundation (coal or weak roof),

h_e = foundation height, and

y_{max} = maximum deformation of the foundation.

The value of y_{max} can be obtained by setting the first order derivative of the deflection line defined in Equation 3.25 to zero. The pressure bump may occur provided that:

$$\sigma_{cmax} \geq C_o \quad \text{and} \quad M_L \geq 2.0 \tag{6.3}$$

6.2.2 Shock Bump Possibility

Shock bumps may occur when the roof spans to its critical values, and the released strain energy results in seismic events with a local Richter magnitude greater than 2.0. The following conditions, therefore, indicate the shock bump potential:

$$\sigma_{mmax} \geq T_o \quad \text{and} \quad M_L \geq 2.0 \tag{6.4}$$

where

σ_{rmax} = maximum tensile stress in the bending roof beam, and

T_o = tensile strength of the rock material.

6.2.3 Estimation of Damage Area Caused by Energy Release

Solid experimental evidence implies that the dynamic fracture of brittle materials under compressive stresses is initiated by tensile stresses localized in the source zone [Ortlepp, 1992; Brady and Rowell, 1986; Gay and Ortlepp, 1979]. Ortlepp [1992] discovered that several rockbursts in South African mines had features of tensile failure. The transmission process of the generated tensile stress waves can be described by Taylor's equation which is based on an analysis of a series of photographs from the explosive experiment of the expanding fireball and observed process of a strong shock transmitting into the undisturbed medium [Brady and Haramy, 1994]. The radius of radiated stress waves at any moment, t, is dependent on the source energy, W_s, and the density of the undisturbed medium, ρ, as shown in Equation 6.5 [Brady and Haramy, 1994].

$$r(t) = a\left(\frac{W_s}{\rho}t^2\right)^{0.2} \tag{6.5}$$

where

$r(t)$ = radius of radiated stress waves at any moment, t,

W_s = source energy, $W_s = n\, W_t$,

t = time,

a = transformation coefficient, and

ρ = density of the medium.

124

The transformation coefficient for the medium needs to be evaluated for each site.

By differentiating Equation 6.5, we obtain the expression for the particle velocity at any time as follows:

$$v(t) = a \left(\frac{W_s}{\rho} \right)^{0.2} t^{-0.6}$$

(6.6)

where

$v(t)$ = particle velocity at any moment, t.

Setting $r(t) = R$ and solving t in Equation 6.5, then inserting t value into Equation 6.6, the particle velocity at certain distance from the location of the sensor to the source, R, can be expressed as:

$$v(R) = 0.4a^{1.5} \sqrt{\frac{W_s}{\rho}} R^{-1.5}$$

(6.7)

where

$v(R)$ = particle velocity at certain distance from the source, R, cm / s, and

R = distance from the sensor location to the source, cm.

This simple mathematical model allows determination of the particle velocity from a seismic event once the radiated energy and the medium density are known. Measurements of peak ground velocity for laboratory sized failures, mine tremors, quarry blasts, nuclear explosions, and earthquakes with local magnitudes ranging from 1.7 to 7.7 have been examined with this model and shown to be in close agreement with observations [Brady and Haramy, 1994].

By combining and arranging Equations 6.1 and 6.7, Equation 6.7 becomes [Brady and Haramy, 1994]:

$$\log\left(R^{15}v\right) = 5.50 - 0.50\log(\rho) + 2.5\log(a) + 0.75M_L \qquad (6.8)$$

where

R = distance from the sensor location to the source, cm.

v = particle velocity, cm / s, and

ρ = density of the medium, gm / cm^3.

Equation 6.8 has been applied to a wide range of cases ranging from large earthquakes to small mine tremors, and laboratory samples. However, this model does not predict a significant change in the characteristics of failure behavior as a function of seismic magnitude or moment as suggested by McGarr [1984]. Using Equation 6.8 the radius of the damage area, R, could be estimated if the minimum particle velocity required to initiate tensile fractures is known [Brady and Haramy, 1994]. Typical values of particle velocity needed to induce tensile fracture in coal were found to range from 0.05 to 0.3 m / s [Rupert and Clark, 1977; Langefors and Kihlstrom, 1963].

Equation 6.8 can be rewritten as following equation in SI units:

$$R = 0.4142 \sqrt[3]{\frac{nW_t a^5}{\rho\,v^2}} \qquad (6.9)$$

where R is measured in m, ρ in kg / m^3, v in m / s. W_t in Joule. Figure 6.1 shows relationship between the estimated damage area and the released total strain energy for a range of seismic efficiencies.
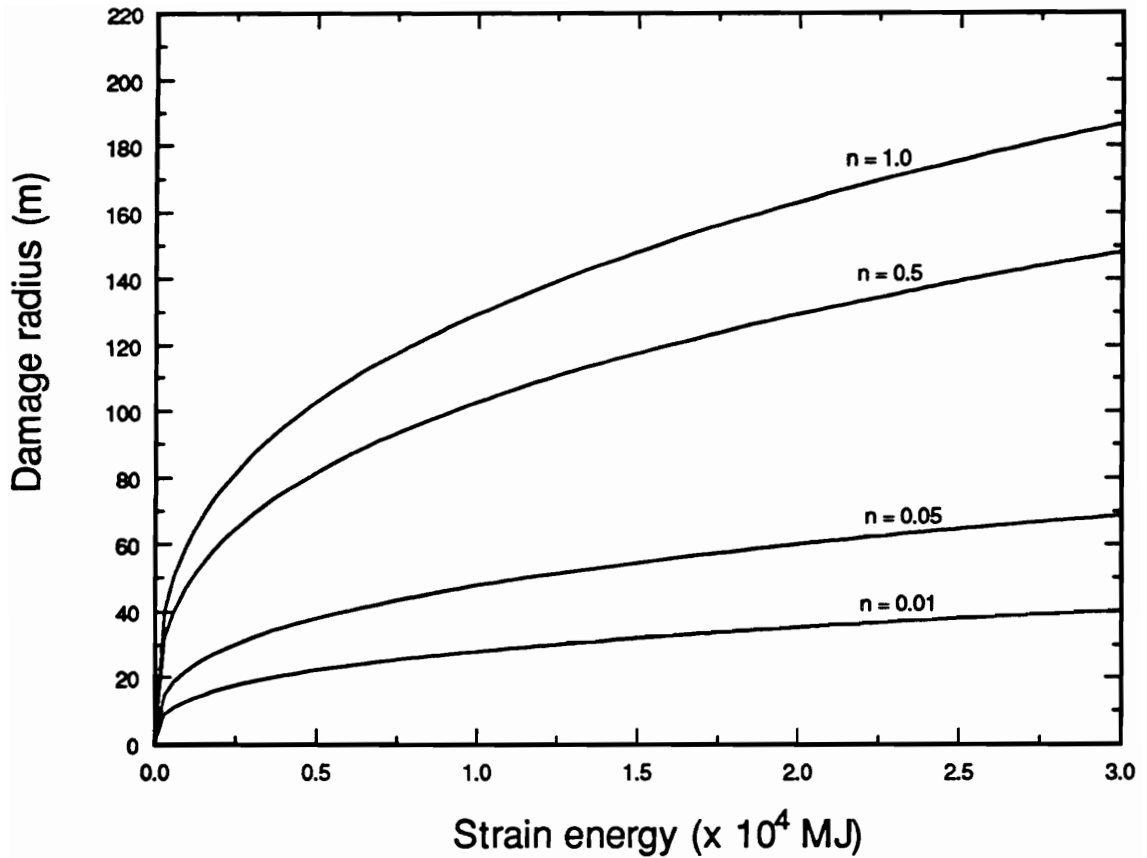
Figure 6.1 Relationship between damage area and strain energy (Parameters: a = 0.77, v = 0.30 m/s, rock density = 2200 kg/m³)

6.3 Case Studies

Data from coal mines with bump problems published in the literature have been used for model verification. Using the analytical approaches developed in chapter 4 and chapter 5, five case studies are discussed below. In the analysis of bridging roof models, the confinement provided by the horizontal stresses is of importance in the determination of roof spans as indicated in Equation 4.11. The horizontal stress is estimated by the following equation:

$$\sigma_h = \frac{\nu}{1-\nu}\sigma_v \qquad (6.10)$$

where

σ_h = horizontal stress,

σ_v = vertical stress, and

ν = average Poisson's ratio of the overburden.

6.3.1 Case Study 1

This case study presents an analysis of bump hazard in a deep coal mine (Soldier Canyon Mine) located approximately 14 miles east of Price, Utah. The mine utilized the room-and-pillar method to extract a 3-m thick Rock Canyon Coal Seam. A recent devastating bump caused a damage area that extended approximately 76,000 m^2, producing a seismic tremor with a registered Richter magnitude of 3.6 [Brady and Haramy, 1994]. The total roof caving length reached up to 276 m. The immediate roof consisted of a 3 m thick weak siltstone layer which was overlain by a competent 12.2 m thick sandstone main roof. At the damage area, the overburden depth was about 600 m. A close examination of the mine plan at the bump site identifies that the sandstone roof acted as a bridging beam rested on the 73.4-m-long abutment pillars prior to its collapse.

128

The length of the working face was approximately 128.5 m. Based on the results of finite element analysis on the relationship between the stress concentration and the location of the strong roofs [Song, et al., 1982], the stress concentration factor is chosen to be 3.0 for this analysis. The input parameters are summarized in Table 6.1.

Table 6.2 gives the roof span and the energy outputs of this case study. The predicted span of the sandstone roof is 11.1 m. The bridging of the sandstone roof will result in a maximum foundation deformation of 14.2 cm, inducing a maximum compressive stress of 65.1 MPa in the foundation. The total strain energy is estimated to be 2.22×10^4 MJ. The corresponding Richter magnitude values for seismic efficiencies from 0.01 to 1.0 are shown in Figure 6.2. Figure 6.2 indicates possibilities of tremors with estimated Richter magnitudes ranging from 2.38 to 3.70. Comparison of the peak stress (65.1 MPa) on the foundation with the compressive strength of the coal (31.73 MPa) indicates pressure bump conditions. Using a particle velocity of 0.3 m / s [Naismith, 1984], as the velocity required to initiate coal fracture and a = 0.77 [Rupert and Clark, 1977] the damage area radius R is estimated to be 142.5 m, which agrees well with the observed caving length (2R) of approximately 276 m.

6.3.2 Case Study 2

The selected mine was located in Virginia. A four-entry retreat longwall mining system was used to mine a 1.68-m-thick Pocahontas seam under 670.5-m overburden [Khair, 1985]. The roof strata consisted of 33.5-m-thick strong sandy shale overlain by a 27.4-m-thick sandstone stratum. The panel was about 200 m wide. From December 1972 to August 1979, 13 bumps occurred in this mine. The physical and mechanical properties of mine materials were fully investigated by Khair [1985]. Typical stress concentration lengths ahead of longwall working face vary from 30 m to 60 m [Unrug, 1982]. In this case, the stress concentration length is chosen to be 60 m. The finite element results [Song, et al., 1982] showed that the applied load on the roof beam reached to a uniform

Table 6.1 Input parameters for case study 1

Roof model	bridging
Sandstone roof:	
Modulus of elasticity (GPa)	6.90
Compressive strength (MPa)	107.25
Tensile strength (MPa)	10.73
Thickness (m)	12.2
Siltstone roof:	
Compressive strength (MPa)	44.80
Thickness (m)	3.0
Coal seam:	
Modulus of elasticity (GPa)	2.76
Compressive strength (MPa)	31.73
Poisson's ratio	0.25
Thickness (m)	3.0
Other parameters:	
Overburden depth (m)	600.0
Specific gravity of overburden (MN/m^3)	0.025
Stress concentration length (m)	73.44
Stress concentration factor	3.0
Length of working face (m)	128.5

Table 6.2 Output for case study 1

Output parameter	
Roof span (m)	11.10
Maximum deformation (cm)	14.15
Maximum foundation stress (MPa)	65.1
Total strain energy (x 10^4 MJ)	2.221
Bump potential	pressure
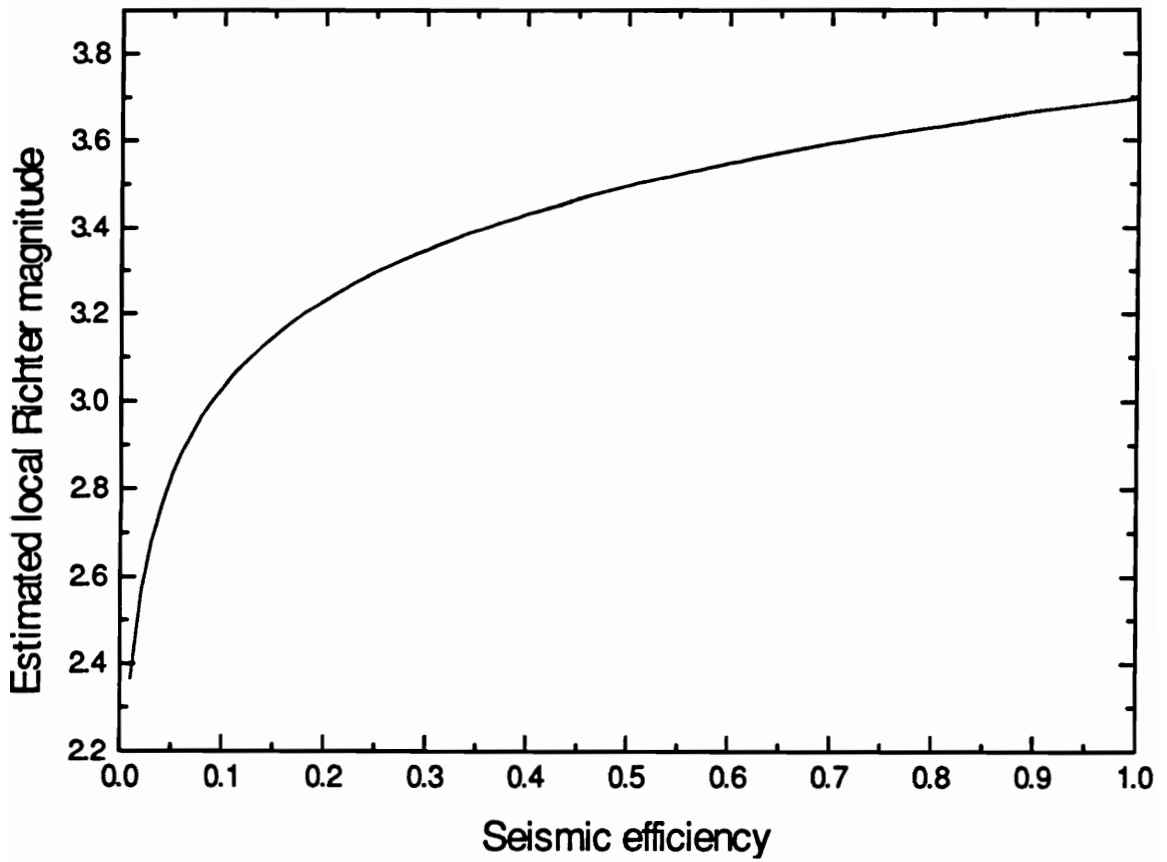
Figure 6.2 Estimated local Richter magnitudes for case study 1

distribution when the strong roof was located 17 meters away from the working face. The stress concentration factor is chosen as 1.0 for our analysis. The input data are given in Table 6.3.

Table 6.4 gives the output of the analysis. The estimations of the local Richter magnitudes corresponding to the first and the periodic weighting stages are shown in Figure 6.3. The critical spans for the first and the periodic weighting stages are estimated to be 26.7 m and 13.6 m, respectively. The maximum stresses on the foundation induced by the roof bending are 28.85 MPa and 28.38 MPa for the periodic and the first weighting stages, respectively. Although these stresses are less than the average compressive strength of coal (32.75 MPa), when the variability of coal strength data is considered, the values are too close to ignore the possibility of pressure bump events. Nevertheless, for both initial and periodic caving stages, the estimated Richter magnitudes, for all seismic efficiencies greater than 5%, are above 2.0, indicating a potential for shock bump events. A comparison of Richter magnitudes in Figure 6.3 shows that the first weighting is more dangerous than the periodic weighting.

6.3.3 Case Study 3

This case study gives a bump potential analysis in a deep bump-prone coal mine in the Southern Appalachian Basin, namely VP No. 3 Mine of Island Creek Coal Co. in Vansant, Virginia [Campoli, et al., 1993]. The mine extracted the Pocahontas No. 3 coalbed, which was located in the Pocahontas Formation and averaged 1.68 m. The overburden depth varied from 365.7 m to 670.7 m. The immediate roof consisted of a jointed siltstone layer overlain by a very stiff, massive sandstone. The siltstone formation ranged from a maximum thickness of 33.5 m down to being nonexistent. The massive sandstone in the main roof varied from a maximum thickness of 137.2 m to a minimum of 41.1 m. The longwall panel was roughly 182.9 m wide and 1828.8 m long. Many heavy tailgate and face bumps were recorded during past few years. A NX-size corehole was

Table 6.3 Input parameters for case study 2

Roof model	cantilevering bridging
Sandy shale roof:	
Modulus of elasticity (GPa)	35.80
Compressive strength (MPa)	119.70
Tensile strength (MPa)	8.23
Thickness (m)	33.5
Coal seam:	
Modulus of elasticity (GPa)	2.08
Compressive strength (MPa)	32.75
Poisson's ratio	0.25
Thickness (m)	1.68
Other parameters:	
Overburden depth (m)	670.5
Specific gravity of overburden (MN/m^3)	0.025
Stress concentration length (m)	60.0
Stress concentration factor	1.0
Length of working face (m)	200.0

Table 6.4 Output for case study 2

Output parameter	First caving	Periodic caving
Roof span (m)	26.70	13.60
Maximum deformation (cm)	2.33	2.29
Maximum foundation stress (MPa)	28.38	28.85
Total strain energy (x 10^3 MJ)	8.124	2.242
Bump potential	shock	shock

133
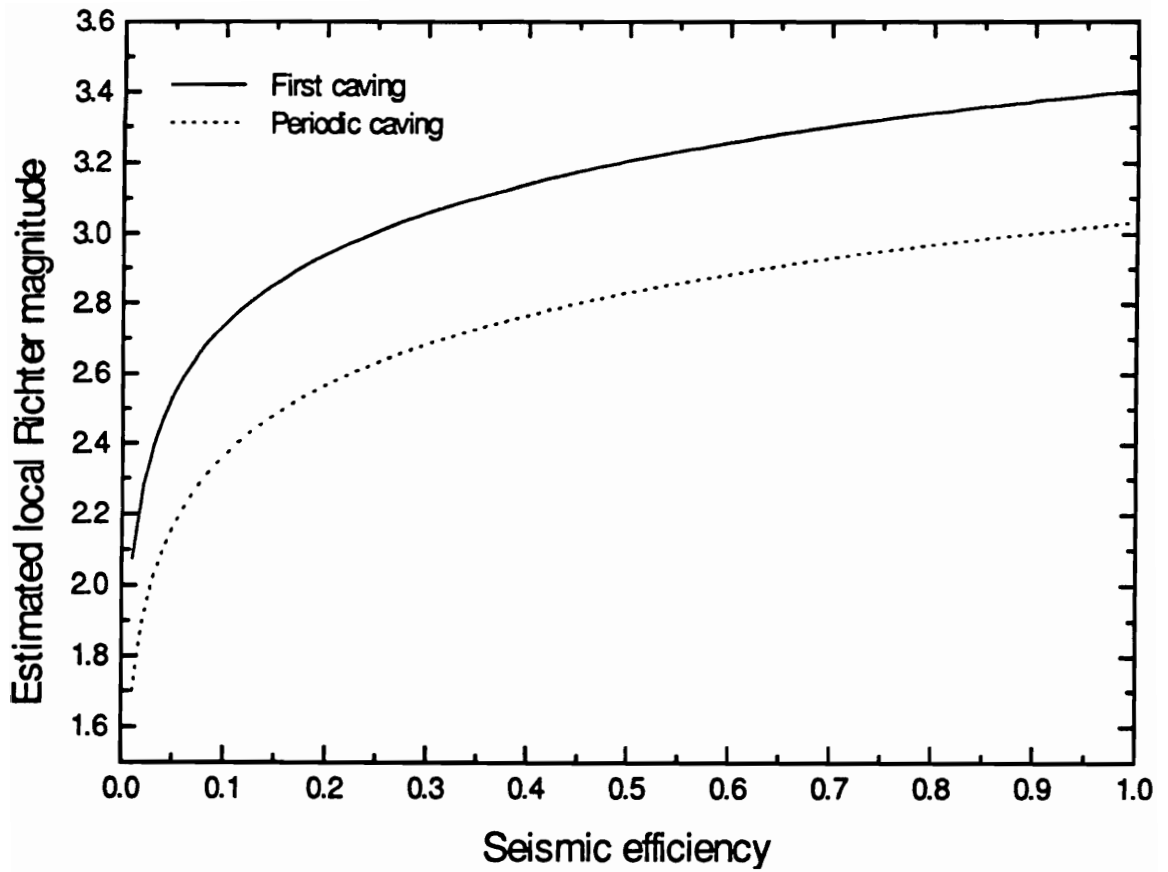
Figure 6.3 Estimated local Richter magnitudes for case study 2

drilled and logged near the center of the S-9 panel, from the surface to a depth of 685.5 m. The quality and strength of several rock units above and below the Pocahontas No. 3 Coalbed were comprehensively tested for mechanical properties in the laboratory. From the lithographic log at the bump location [Campoli, et al., 1993], the immediate roof consisted of 12.2 m strong sandy shale overlain by a relative weak shale layer and Pocahontas No. 4 coalbed. In some area, the sandstone roof with an average thickness of approximately 90 m was directly overlain over the working face. The mechanical properties of sandy shale, sandstone, and coal are summarized in Table 6.5 [Campoli, et al., 1993]. Bump possibilities caused by overlying sandy shale and sandstone roofs are analyzed below.

Sandy shale roof: As discussed in case 2, the front abutment stress distribution is assumed to have a length of 60 m and a concentration factor of 3.0. The estimated roof spans are 10.0 m and 6.3 m for the first caving and the periodic caving, respectively. As illustrated in Figure 6.4, the estimated local Richter magnitudes vary from 2.14 to 3.47 for the bridging model and from 1.88 to 3.22 for the cantilevering model. A comparison of the induced maximum compressive stresses (first caving: 59.64 MPa, periodic caving: 64.64 MPa) on the coal foundation to the compressive strength of the coal (32.75 MPa) indicates pressure bump possibilities (Table 6.6).

Sandstone roof: In this case, the roof formation is 90 m thick, therefore, the applied load on the roof beam is considered to be uniformly distributed. The stress concentrated length on the coal seam is assumed to be 60 m. The average depth of the overburden is approximately 520 m. The predicted critical spans for the bridging and the cantilevering models are 127.8 m and 53.5 m, respectively. Figure 6.4 shows estimated local Richter magnitude ranges based on energy analysis. For both cantilevering and bridging models, the induced maximum foundation stresses (Table 6.6) are greater than the compressive strength of the coal (32.75 Mpa), indicating pressure bump potential.

135

Table 6.5 Input parameters for case study 3

Roof model	cantilevering bridging
Sandy shale roof:	
Modulus of elasticity (GPa)	39.51
Compressive strength (MPa)	126.80
Tensile strength (MPa)	12.68
Thickness (m)	12.2
Sandstone roof:	
Modulus of elasticity (GPa)	37.23
Compressive strength (MPa)	137.9
Tensile strength (MPa)	13.79
Thickness (m)	90.0
Coal seam:	
Modulus of elasticity (GPa)	2.08
Compressive strength (MPa)	32.75
Poisson's ratio	0.25
Thickness (m)	1.68
Other parameters:	
Overburden depth (sandy shale, m)	638.5
Overburden depth (sandstone, m)	520.0
Specific gravity of overburden (MN/m^3)	0.025
Stress concentration length (m)	60.0
Stress concentration factor (sandy shale)	3.0
Stress concentration factor (sandstone)	1.0
Length of working face (m)	182.9

Table 6.6 Output for case study 3

Output parameter	First caving	Periodic caving
Sandy shale roof:		
Roof span (m)	10.04	6.27
Maximum deflection (cm)	4.82	5.22
Maximum foundation stress (Mpa)	59.64	64.64
Total strain energy (x 10^3 MJ)	10.124	4.221
Bump potential	pressure	pressure
Sandstone roof:		
Roof span (m)	127.80	53.48
Maximum deformation (cm)	6.24	4.12
Maximum foundation stress (Mpa)	77.24	51.00
Total strain energy (x 10^3 MJ)	70.44	5.27
Bump potential	pressure	pressure
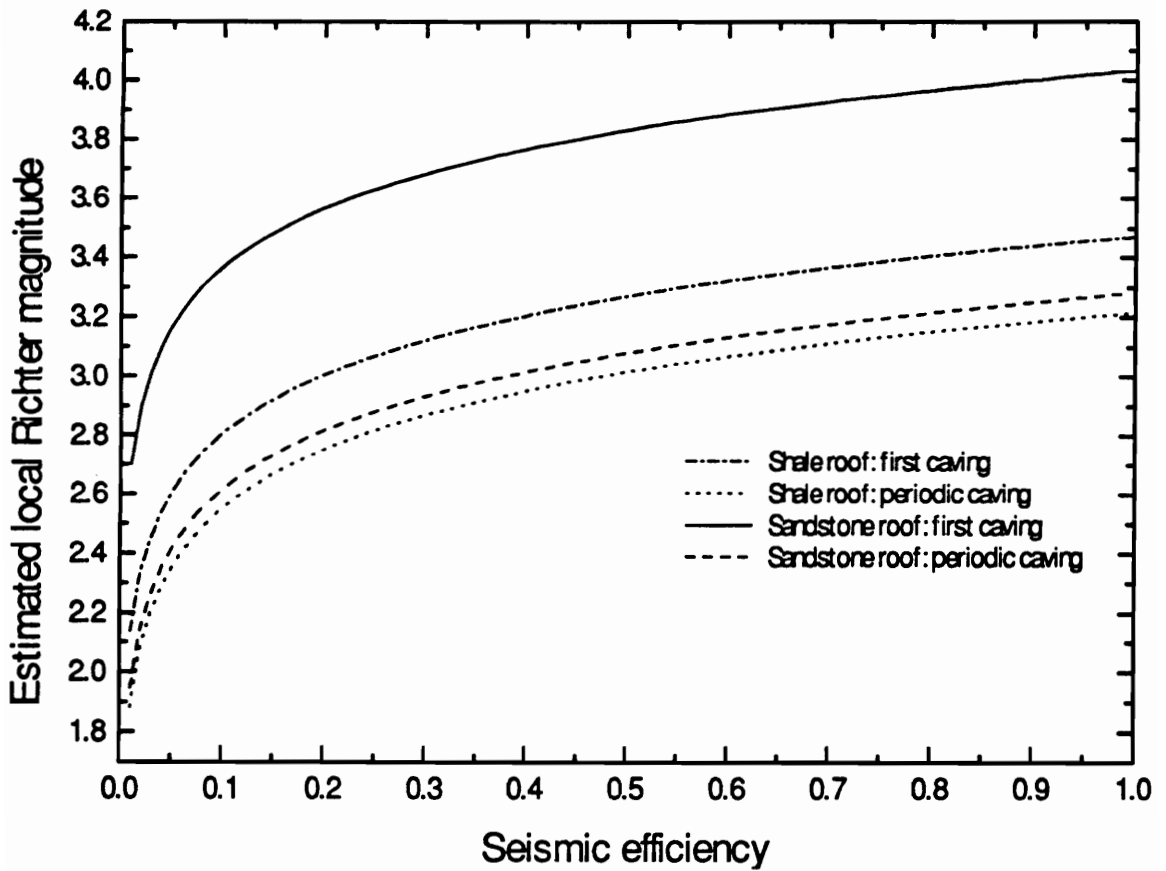
Figure 6.4 Estimated local Richter magnitudes for case study 3

6.3.4 Case Study 4

This coal mine was located in western Colorado [Haramy and McDonnell, 1988]. It utilized the advancing longwall system and extracted a 3-m-thick coal seam under nearly 900 m of overburden. The immediate roof, approximately 1.5 m thick, was composed of strong siltstone, shale, and sandstone layers which was overlain by a 2.7-m competent sandstone formation. The panel is 243.8 m wide and 1188.7 m long. The floor stratum was a 3 m strong shale layer with sandstone stringers and coal spars. Between January 1983 and July 1984, nine face, floor and rib bumps were recorded. On April 20, 1983, the bump occurred that affected the tailgate entries and the face. The bump resulted in a rapid floor heave and extended approximately 365 m along the tailgate and 90 m along the face. In addition, it disrupted ventilation, stopped production, and damaged 40 longwall shield supports. The floor heaved to within 0.3 m of the roof in some areas. Investigators from U.S. Bureau of Mines conducted a detailed monitoring and measurement of field stress, rock properties, and support pressure before and after coal bumps [Haramy and McDonnell, 1988]. Table 6.7 summarizes the roof and coal properties and other relevant parameters.

The results of roof spans, stored energies, and peak foundation stresses are given in Table 6.8. The magnitudes of the induced foundation stresses caused by roof cantilevering and bridging are 168.00 MPa and 161.36 MPa, respectively, well exceeding the compressive strength of the coal. The predicted foundation pressures are in close agreement with the measured peak abutment stress (172.4 MPa) [Haramy and McDonnell, 1988]. The estimated local Richter magnitudes for seismic efficiencies from 0.01 to 1.0 are plotted in Figure 6.5. For both initial weighting and periodic caving, energy analysis identifies a potential for pressure bump events.

Table 6.7 Input parameters for case study 4

Roof model	cantilevering bridging
Sandstone roof:	
Modulus of elasticity (GPa)	27.00
Compressive strength (MPa)	154.74
Tensile strength (MPa)	12.40
Thickness (m)	10.0
Coal seam:	
Modulus of elasticity (GPa)	3.28
Compressive strength (MPa)	32.00
Poisson's ratio	0.30
Thickness (m)	3.00
Other parameters:	
Overburden depth (m)	900.0
Specific gravity of overburden (MN/m^3)	0.0256
Stress concentration length (m)	90.0
Stress concentration factor	7.0
In-situ horizontal stress (MPa)	14.50
Length of working face (m)	243.8

Table 6.8 Output for case study 4

Output parameter	First caving	Periodic caving
Roof span (m)	8.02	4.23
Maximum deformation (cm)	14.76	15.34
Maximum foundation stress (MPa)	161.36	168.00
Total strain energy (x 10^4 MJ)	11.72	5.18
Bump potential	pressure	pressure
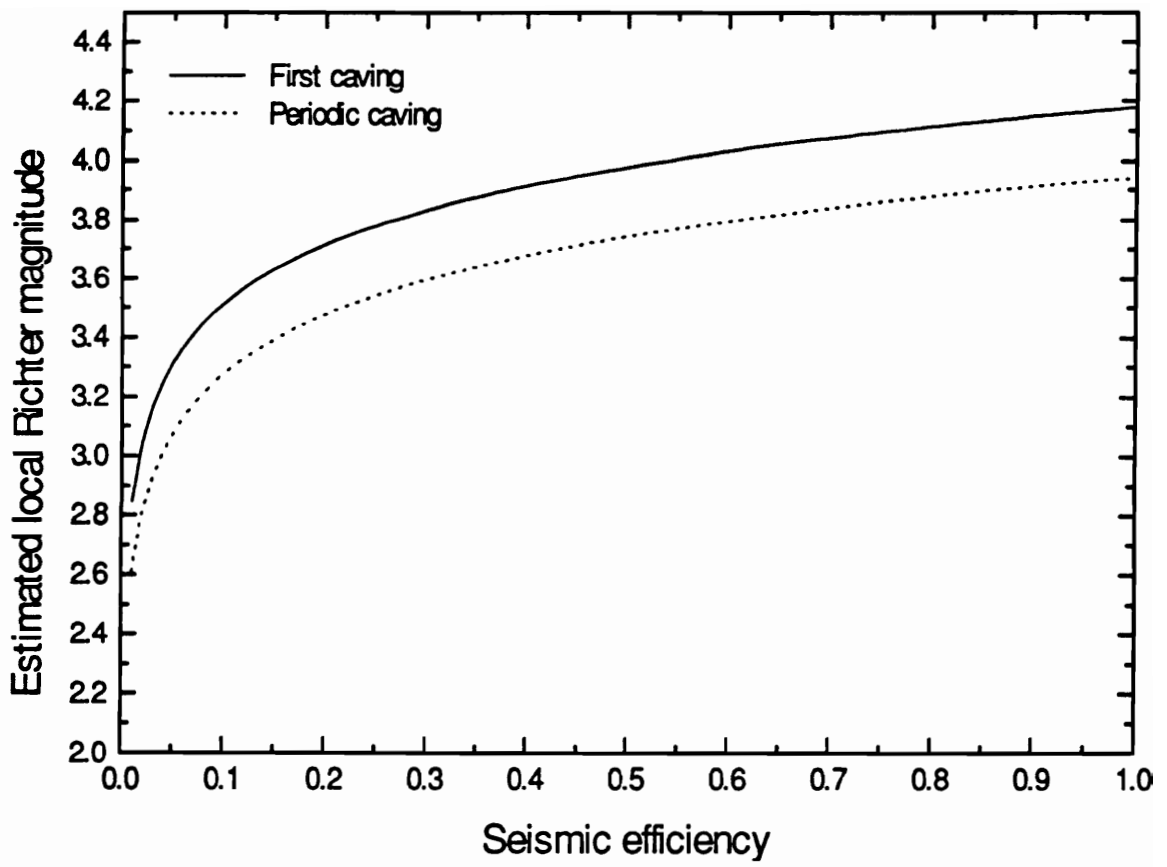
Figure 6.5 Estimated local Richter magnitudes for case study 4

6.3.5 Case Study 5

This case study presents an analysis concerning longwall panel failure in a West Virginia coal mine. A sudden sandstone roof fall resulted in damage of 60 powered supports and temporary abandonment of the panel [Hsiung and Peng, 1985]. The panel was 183.6 m wide under an overburden of about 284.6 m. The working height was 1.68 m. The immediate roof over the panel was 1.68-m-thick shale which was overlain by a 11 m strong sandstone bed. There was a 1.5 m sandy shale layer overlying the sandstone stratum and above the sandy shale layer another thick layer (12.2 m) of sandstone was present. The physical and mechanical properties of mine materials are detailed in Table 6.9 [Hsiung and Peng, 1985].

The results of this case analysis are summarized in Table 6.10. It can be noticed that the predicted roof spans associated with the first caving (19.2 m) and the periodic caving (10.3 m) agree well with the field observations (first caving: 15.9 m, and periodic caving: 7.3 ~ 9.8 m) [Hsiung and Peng, 1985]. The induced peak foundation pressures (initial caving: 20.87 MPa, periodic caving: 19.57 MPa) are very close to the compressive strength of the coal (18.5 MPa). Although these stresses are slightly above the coal strength, when the variability of strength data and in-situ confinement of the coal pillars are considered, the values are too close to ignore the shock bump possibility. As illustrated in Figure 6.6, for a lower seismic efficiency (less than 0.1), the bump may not happen. However, for the seismic efficiencies being greater than 0.3, the estimated Richter magnitudes are above 2.0, indicating that both pressure and shock bump events may occur.

Table 6.9 Input parameters for case study 5

Roof model	cantilevering bridging
Sandstone roof:	
Modulus of elasticity (GPa)	17.24
Compressive strength (MPa)	60.54
Tensile strength (MPa)	3.30
Thickness (m)	11.0 (lower layer)
	12.2 (upper layer)
Sandy shale roof:	
Modulus of elasticity (GPa)	9.58
Compressive strength (MPa)	52.67
Tensile strength (MPa)	2.20
Thickness (m)	1.68
Shale roof:	
Modulus of elasticity (GPa)	6.79
Compressive strength (MPa)	48.92
Tensile strength (MPa)	2.10
Thickness (m)	1.68
Coal seam:	
Modulus of elasticity (GPa)	3.45
Compressive strength (MPa)	18.51
Poisson's ratio	0.21
Thickness (m)	1.68
Other parameters:	
Overburden depth (m)	284.6
Specific gravity of overburden (MN/m^3)	0.025
Stress concentration length (m)	60.0
Stress concentration factor	3.0
Length of working face (m)	183.6

Table 6.10 Output for case study 5

Output parameter	First caving	Periodic caving
Roof span (m)	19.16	10.33
Maximum deformation (cm)	1.02	0.95
Maximum foundation stress (MPa)	20.87	19.57
Total strain energy (x 10^3 MJ)	0.78	0.22
Bump potential	pressure or shock	pressure or shock
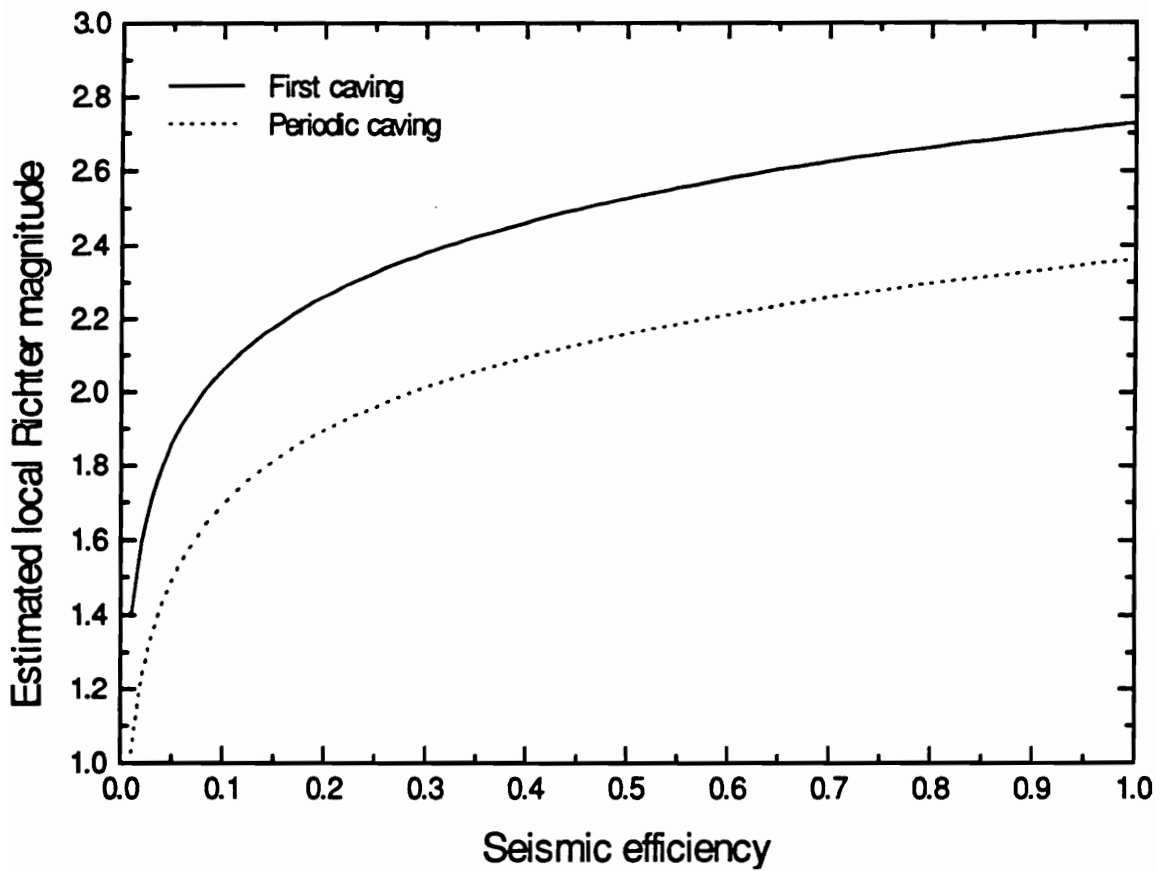
Figure 6.6 Estimated local Richter magnitudes for case study 5

6.4 Development of Windows-based Software Package

The software package "Coal Bump Potential Evaluation Program" (CBPEP) has been developed to evaluate the bump possibility associated with mining under strong roofs. CBPEP is a graphical user interactive application created by event-driven programming language, Visual Basic (Version 3.0), for Microsoft Windows operating system. The package implements the analytical solutions for single- or double-layer roof beams on single- or double-layer elastic foundations and allows for determination of roof critical span, induced foundation stress, and strain energies stored in the roof and the foundation. The criteria for assessing shock and pressure bump possibility are those described earlier in section 6.2. Figure 6.7 shows the program flowchart.

Program execution follows three major steps: (1) Model selection; (2) Input data; and (3) Output results. The following is a list of eight roof models implemented in the program:

- Model 1: single-layer cantilevering beam on single-layer foundation

- Model 2: single-layer bridging beam on single-layer foundation

- Model 3: double-layer cantilevering beam on single-layer foundation

- Model 4: double-layer bridging beam on single-layer foundation

- Model 5: single-layer cantilevering beam on double-layer foundation

- Model 6: single-layer bridging beam on double-layer foundation

- Model 7: double-layer cantilevering beam on double-layer foundation

- Model 8: double-layer bridging beam on double-layer foundation.

146
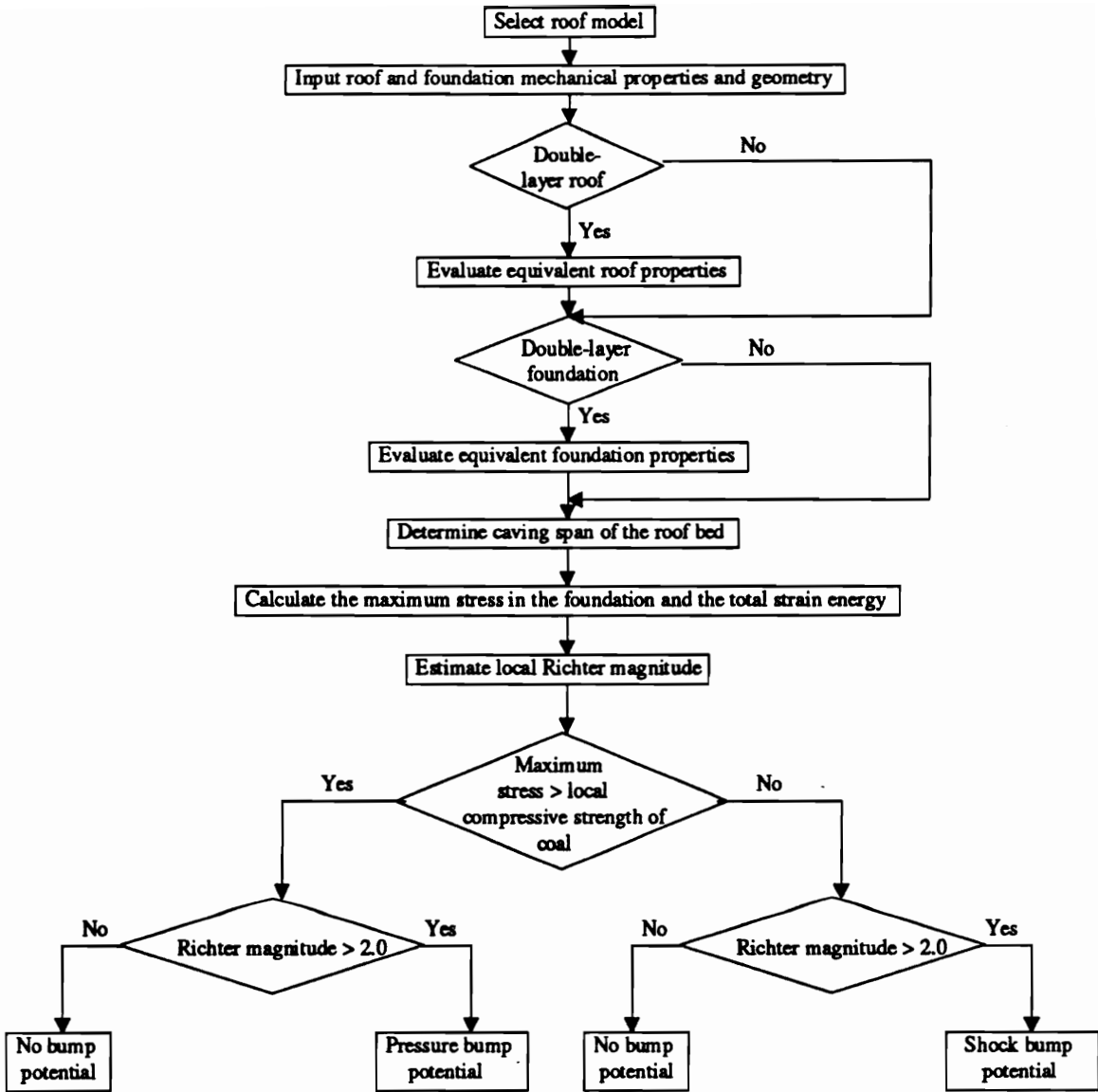
Figure 6.7 Program flowchart

147

To select a roof model, click the left button of the mouse on one of "Model" command buttons. Then click the "Continue" button on the model form to bring up the form for input data. Input to the CBPEP is designed from the keyboard. All input parameters must be in international metric units. To input a parameter value, select the text box using the mouse and type the value. Pressing the "Tab" key on the keyboard moves to the next input box. Finally by clicking the "Output" command button on the input form the program outputs the analysis results. The output from the program includes: (1) Critical span of the roof bed, (2) Strain energy stored in the roof bed, (3) Strain energy stored in the foundation, (4) Total strain energy, (5) Maximum induced foundation stress, (6) Local Richter magnitude, and (7) Comments on coal bump potential. A sample program run is shown in Figures 6.8 to 6.10.

During program execution, the user can move backward and forward to reselect the roof models or change input data by choosing "Back" or "Continue" command buttons on each form. The execution of the program can be terminated at any stage by clicking "Exit" button. The on-line help is available to the user at most of stages of program execution. The help forms give the user general information on the program, method of inputting data, and explanation of terminology. To access help screens, select the "Help" buttons. To leave a help screen, click the "Exit" button on the help form. Included in each input form is error checking for each parameter designed to prevent invalid input data. If an input error occurs, the error trapping procedure coded in CBPEP will pop up a warning message window identifying error type and suspend the program execution. Clicking "OK" button on the error message window returns the focus of control to the input form. Then you can input the correct value where the error was detected. Figure 6.11 shows an example of error checking. A list of the program is given in the Appendix.

Figure 6.8 An example of program run -- model selection form

Figure 6.9 An example of program run -- input form

Output Form: Analysis Results

Analysis Results: Single Layer Bridging Roof - Double Layer Foundation

Case Name: Case Study I

Critical Span of Roof Beds (m)	11.06	
Strain Energy in Roof Beds (MJ)	4.22E+03	
Strain Energy in Foundation (MJ)	1.80E+04	
Total Strain Energy (MJ)	2.22E+04	
Seismic efficiency (%)	100.00%	
Local Richter Magnitude	3.70	
Maximum Foundation Stress (MPa)	65.08	

Comments

Foundation failure is predicted. Local Richter magnitude is over 2.0. Pressure bump condition exists.

Help   Another Case   Back   Print   Exit

Figure 6.10 An example of program run -- output form
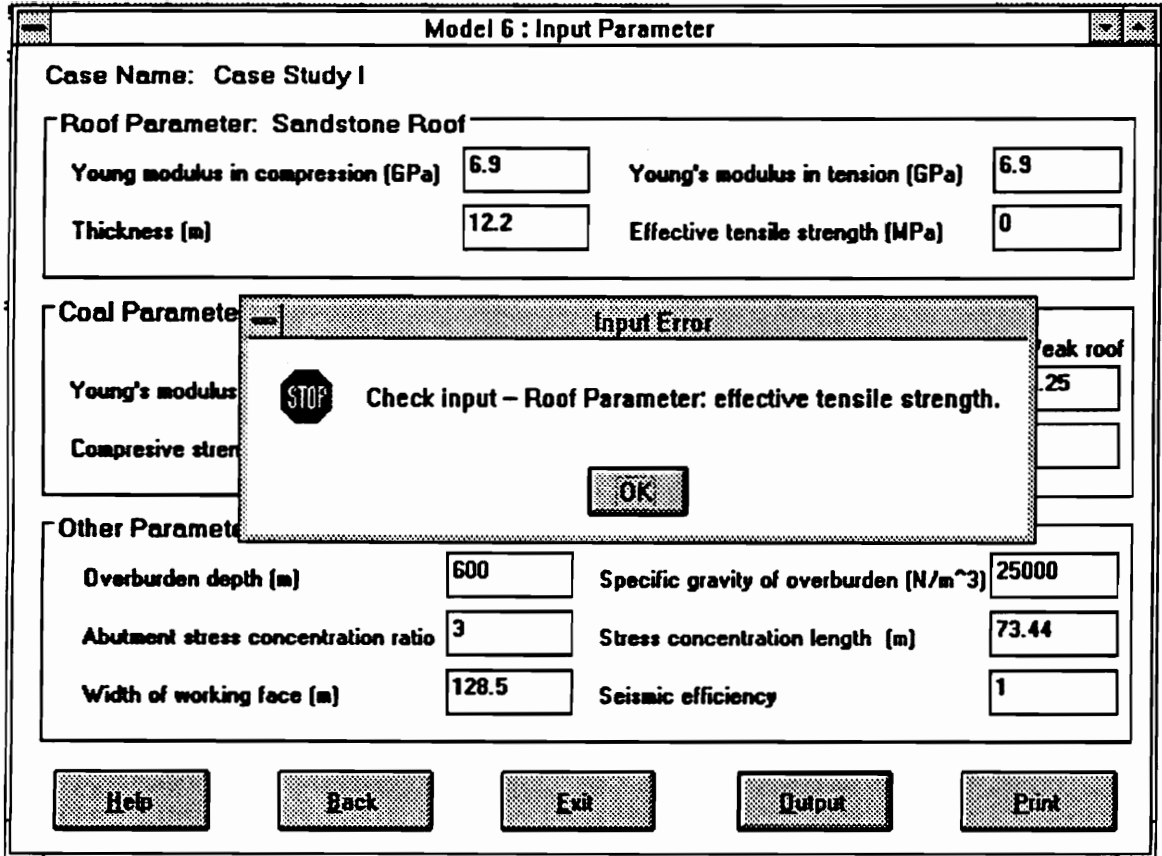
Figure 6.11 An example of error checking

6.5 Summary

A quantitative parameter, the local Richter magnitude, is proposed as a predictive index for the likeliness and severity of coal bumps associated with mining under competent roofs. Criterion for pressure and shock bump events are suggested. Evaluation of the amount of released energy together with the particle velocity damage model provides a quantitative estimate of the possibility and intensity of shock and pressure bumps. Five case studies from U.S. bump-prone coal mines are analyzed for model verification. The results of case analyses show that the bump intensities associated with the first weighting phase are higher than those at the periodic weighting phase during longwall extraction. The case studies also show that the theoretical predictions agree well with the field data. However, considering the variability and uncertainty related to the parameters used, a probabilistic approach should be applied in order to improve the prediction process. A Windows-based software package CBPEP implements the roof models and model solutions discussed in earlier chapters. The package provides a tool for determination of roof spans, strain energy stored in the roof and the foundation, and evaluation of possibility of bump events.

CHAPTER 7   AIRBLAST ANALYSIS CAUSED BY LARGE ROOF FALLS

7.1 Introduction

Mining under strong roofs may cause hazardous airblast events associated with sudden roof collapse in large areas. Early work done by McPherson [1980] revealed that the astonishingly high air pressures can be developed by large roof collapses in confined old room and pillar areas. A recent analysis [McPherson, 1995] has indicated that compression of the air under a roof fall of large areal extent could produce air temperatures that may be well above those necessary to trigger a gas or dust explosion. Based upon the adiabatic models developed by McPherson [1980, 1995], this chapter extends the analysis to include the recompaction of the fragmented material on the floor. The system damping is examined and a new damping factor is proposed.   Sensitivity analyses are conducted to investigate the effects of thickness of the falling strata, plan area of the collapse, height of workings and the degree of damping. Three case studies are included, one of which was associated with a mine explosion.

7.2 Theoretical Models of Air Compression

The air compression process under a falling mass suggested by McPherson [1980,

1995] was considered to be adiabatic. That is, during roof falls, heat transfer to the surrounding rock mass occurs slowly compared with the air compression process and, hence, is considered to be negligible during the rapid progression of a roof fall. In the McPherson's investigation reported in 1980, the resistance provided by the re-compaction of fragmented pillars materials on the floor based on laboratory testing results on carboniferous rock was considered. In the more recent investigation [McPherson, 1995], the dynamic air leakage and the shear resistance of the falling block have been considered, but with no broken materials on the floor. In this section, the bounded and the air leakage models developed by McPherson [1995] are described. Then the air leakage recompaction model is proposed to include the analysis of recompaction of fragmented materials on the floor.

7.2.1 Bounded Model

In this idealized situation the air is completely confined in the space under the falling mass as illustrated in Figure 7.1. If there are no frictional effects, the movement of the falling block follows Newton's second law of motion and is given by [McPherson, 1995]:

$$m_r \frac{du}{dt} = m_r g + (P_o - P) A_r \qquad (7.1)$$

where

m_r = mass of the falling block, $m_r = A_r h_r \rho_r$, kg,

A_r = plan area of the falling block, m^2,

h_r = thickness of the falling block, m,

ρ_r = density of roof material, kg/m^3,

P_o = air pressure over the falling block, Pa,

P = air pressure under the falling block, Pa,

g = gravitational acceleration, $g = 9.81$ m/s^2,

z = distance between the falling block and the floor, m,

155
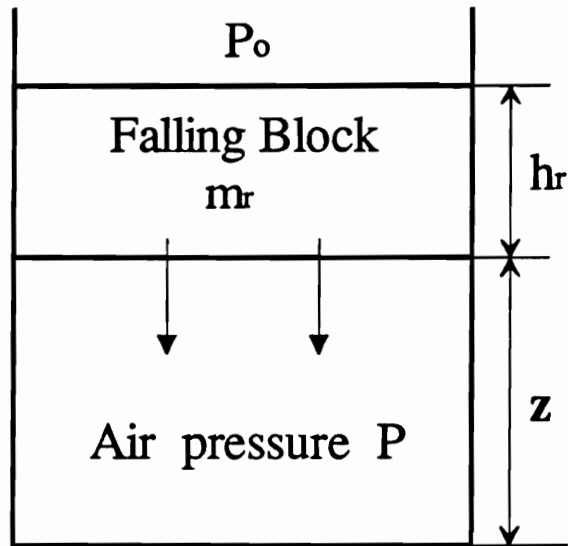
Figure 7.1 Air compressed beneath a falling block

$\dfrac{du}{dt}$ = acceleration of the falling block, m/s^2, and

u = velocity of the falling block, $u = \dfrac{dz}{dt}$, m/s.

After the collapse commences, the air beneath the falling slab will be compressed rapidly, resulting in a considerable increase in temperature. As heat transfer between surrounding rock surfaces and the air occurs much more slowly than the air compression, the process is near adiabatic and will approximate to the law:

$$PV^k = C'$$
(7.2)

where

V = volume of air, m^3,

C' = constant, and

k = adiabatic index, $k = 1.4$ for dry air.

At any moment the volume of compressed air can be expressed by:

$$V = A_r z$$
(7.3)

Therefore, Equation 7.2 can be rewritten as:

$$P = \frac{C}{z^k}$$
(7.4)

The constant, C, can be determined from the initial conditions: $P = P_o$ and $z = z_o$, i.e.

$$C = P_o z_o^k$$
(7.5)

Substituting for $m_r = A_r\, h_r\, \rho_r$ and $P = \dfrac{C}{z^k}$ into Equation 7.1 gives [McPherson, 1995]:

157

$$\frac{du}{dt} = \left[g + \left(P_o - \frac{C}{z^k} \right) \frac{1}{h_r \rho_r} \right] \tag{7.6}$$

Equation 7.6 describes the motion of the falling slab in an undamped and totally sealed system. In such a situation, the falling slab would compress the underlying air and bounce back to its initial position, repeating the process indefinitely. In reality, shear resistance at the sides of the falling slab, coupled with turbulence generated within the compressed air will cause the system to be damped. McPherson [1995] proposed a dumping factor to characterize the system damping behavior. The damping factor was expressed as:

$$DF = 1.3 + 0.044 h_r$$

By considering the system damping, Equation 7.6 can be modified as [McPherson, 1995]:

$$\frac{du}{dt} = \left[g + \left(P_o - \frac{C}{z^k} \right) \frac{1}{h_r \rho_r} - (\pm) DF \, u \right] \tag{7.7}$$

where $\pm$ means that damping forces always oppose the motion of the falling block.

Further computer simulations have indicated that when the initial falling height of the block is less than 2 m, the motion of the falling block (Equation 7.7) becomes unstable. It was found that the system damping depends not only on the thickness of the roof block, but also on the contact area between the sides of the falling block and the surrounding intact rock mass, and the initial air volume to be compressed beneath the falling block. Through successive trials, a reasonable damping factor was found to be:

$$DF = 1.80 + 5 \times 10^{-5} A_s + \frac{2.0}{z_o} \tag{7.8}$$

where A_s is the side surface area of the falling block (m^2).

158

The corresponding air temperatures are given by the adiabatic process equation [McPherson, 1995]:

$$T = T_o \left(\frac{P}{P_o} \right)^{\frac{k-1}{k}}$$ (7.9)

where

T = Absolute temperature under the falling block, K, and

T_o = Initial temperature when roof fall commences, K.

Equations 7.4, 7.7 to 7.9 can be tracked numerically to show the variations of roof height, z, pressure, P, velocity, u, and temperature, T, with respect to time, t.

7.2.2 Air Leakage Model

In an actual roof fall situation, the air to be compressed will be dissipated through leakage paths connected to the collapse area. The rate of air leakage is affected by the resistance to air movement actually within the diminishing space that exists under the falling roof, and the additional resistance offered against airflow as air dissipates through the connecting leakage paths.

From the square law for compressible flow, the rate at which of air mass is displaced from under the falling roof, $\frac{dm_a}{dt}$, is governed by the difference in air pressure between the collapsing area, P, and the main infrastructure of the mine ventilation system (assumed to be at P_o), and is also dependent upon the resistance of the leakage paths, R_t [McPherson, 1995]:

$$\frac{dm_a}{dt} = \left[\frac{(P - P_o) \rho_a}{R_t} \right]^{0.5}$$ (7.10)

where

ρ_a = prevailing air density, kg/m^3,

m_a = air mass, $m_a = \rho_a V$, kg, and

R_t = total resistance, m^{-4}.

Assuming that the falling roof is a rectangular plate with plan dimensions of X by W, and that the air is displaced in the X direction, the total resistance is composed of three components, turbulent resistance of the flowpath under the falling roof, shock losses at entries from the collapse zone to the airways, and airway length resistance. These resistances can be determined by following expressions for a single connecting airway [McPherson, 1995]:

$$R_{fall} = \frac{f X}{2W^2 z^3} \qquad (7.11)$$

$$R_{shock} = \frac{1}{2 A_a^2} \qquad (7.12)$$

$$R_{length} = \frac{f L_a S}{2A_a^3} \qquad (7.13)$$

$$R_t = R_{fall} + R_{shock} + R_{length} \qquad (7.14)$$

In the case of multiple airways connected into the collapse zone, total resistance can be assessed by assuming that they act in parallel [McPherson, et al., 1995]:

$$R_t = R_{fall} + \left(\sum \frac{1}{\sqrt{R_{length} + R_{shock}}} \right)^{-2} \qquad (7.15)$$

where

R_{fall} = rational turbulent resistance of the flowpath under the falling roof, m^{-4},

R_{length} = rational turbulent length resistance, m^{-4},

R_{shock} = rational shock loss resistance at entry from the collapse zone to the airway, m^{-4},

f = Darcy coefficient of friction, dimensionless,

X = length of the falling block, m,

W = width of the falling block, m,

A_a = cross sectional area of the leakage airpath, m^2,

L_a = length of the leakage airpath, m, and

S = perimeter of the leakage airpath, m.

From the general gas law, the reduction in pressure caused by this loss of air is [McPherson, 1995]:

$$dP = dm_a \frac{RT}{V}$$

(7.16)

where

R = gas constant, R = 287.04 J / kg °C for air, and

V = volume of space beneath the falling roof, V = z x A (m^3).

From the equations describing the motion of the falling roof, and the thermodynamic and aerodynamic processes undergone by the air, a computer model of the system was developed [McPherson, 1995]. During the time stepping procedure of the numerical simulation, stability was achieved at time increments of 0.001 seconds. At each increment, the increase in air pressure due to the falling roof was first calculated, followed immediately by a decrease of dP due to the leakage of mass dm_a.

7.2.3 Air Leakage - Recompaction Model

In certain conditions, for instance, failure of a relative weak roof underneath the strong roof or pillar failure prior to a large roof fall, the fragmented materials from

collapsed weak roof or failured pillar will accumulate to a certain height on the floor. After the falling block strikes the broken material, there exists a upward resisting force acted on the falling block due to the re-compaction of the broken materials. Pappas and Mark [1993] have conducted extensive recompaction tests on the fragmented gob materials. The results of compaction tests for weak shale, weak sandstone, and strong sandstone are summarized in Figure 7.2 [Pappas and Mark, 1993]. The average stress-strain relationship approximates to be (Figure 7.2):

$$\sigma(z) = \frac{9.3772 \times 10^6 \, \varepsilon}{1 - 2.36 \, \varepsilon} \tag{7.17}$$

where

$\sigma(z)$ = resistance (stress) of the fragmented gob material, Pa, and

ε = strain developed during recompaction process, m / m.

Now, the motion of the falling block (Equation 7.7) can be described by:

$$\frac{du}{dt} = \left[g + \left(P_o - \frac{C}{z^k} - \sigma(z) \right) \frac{1}{h_r \, \rho_r} - (\pm)DF \, u \right] \tag{7.18}$$

A computer simulation program was developed to numerically track the dynamic air leakage and the re-compaction process of the broken gob material. Stability was achieved at time increments of 0.001 seconds.

7.3 Simulation Results and Discussions

The air leakage and air leakage - recompaction models discussed in the preceding section have been simulated for a variety of conditions in order to observe the behavior of the major dependent variables.
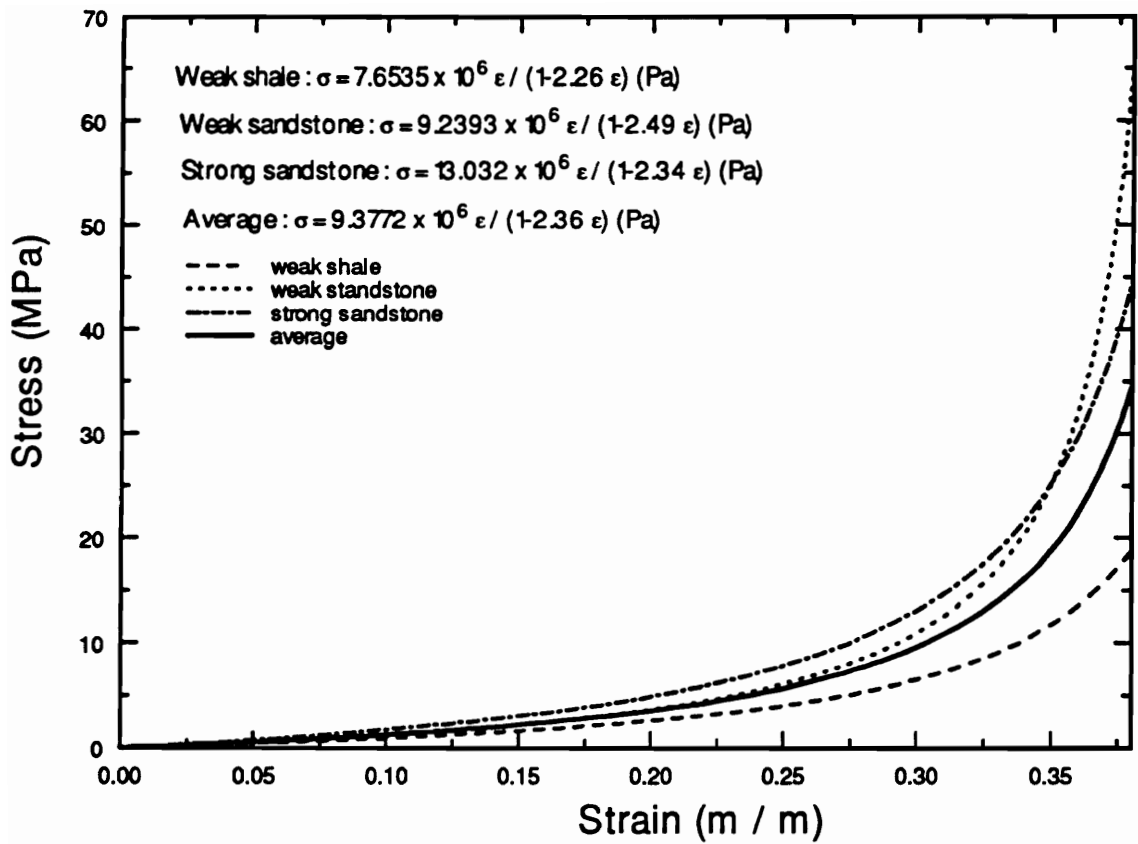
Figure 7.2 Recompaction curves of fragmented gob materials [after Pappas and Mark, 1993]

163

7.3.1 Effect of Thickness of the Falling Block

Selected simulation results are illustrated in Figure 7.3 for block thicknesses of 5, 15, and 25 m falling through an extraction height of 2 m and over a plan area of 100 m x 100 m. An examination of Figure 7.3 reveals that: After the descent commences, the roof block rapidly comes to rest on the floor. When the block is close to the floor, the height-time curves (Figure 7.3 a) show oscillations. The height at which this occurs decreases with increasing block thickness. In the very short period during the roof fall, the air pressure builds up quickly and reaches peak values. As might be expected, the thicker the falling block, the higher the values of peak pressure. Following the initial pressure build-up period, the pressures fluctuate with decreasing amplitude but increasing frequency and converge finally to the weight of the falling block (Figure 7.3 c). At this stage, the gauge pressure is simply that of the weight of the block distributed over the floor area (ρ_r g h_r). The absolute pressure is gauge pressure + P_o.

In contrast to the pressure curves, the temperature-time curves (Figure 7.3 d) show that the temperatures continue to increase, with minor oscillations, as the gap between the descending block and the floor diminishes. This is a most intriguing result and differs markedly from the convergent temperature behavior of a totally sealed system such as a pneumatic shock absorber [McPherson, 1995]. The initial rise in air temperature is not so pronounced. However, as the escape of air allows the roof to descend closer to the floor, the temperature continues to escalate upwards rapidly.

This phenomenon demands a physical explanation. In contrast to a sealed system, additional potential energy is now released. The slab falls more rapidly. Furthermore, this additional work is expended against a decreasing mass of air under the descending roof. The specific internal energy of that decreasing mass soars and, with it, the temperature [McPherson, et al., 1995].

164
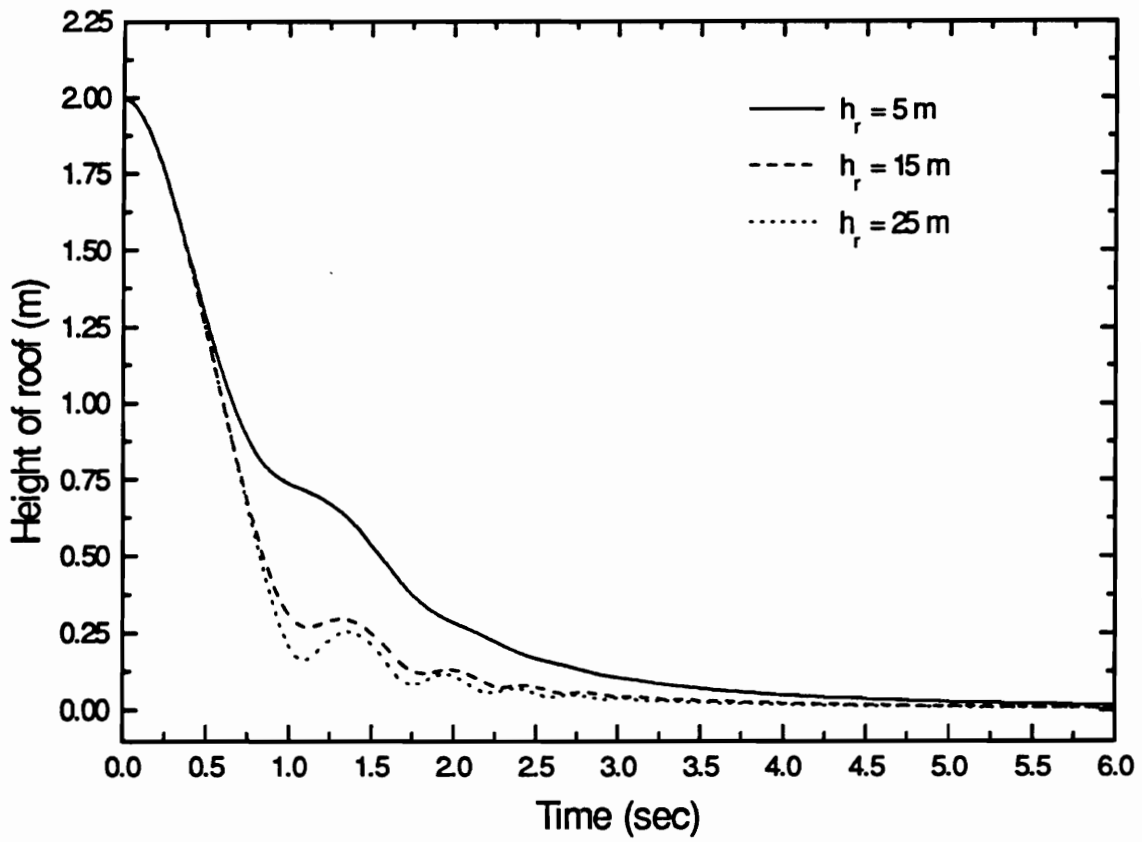
Figure 7.3(a) Predicted height of roof vs time
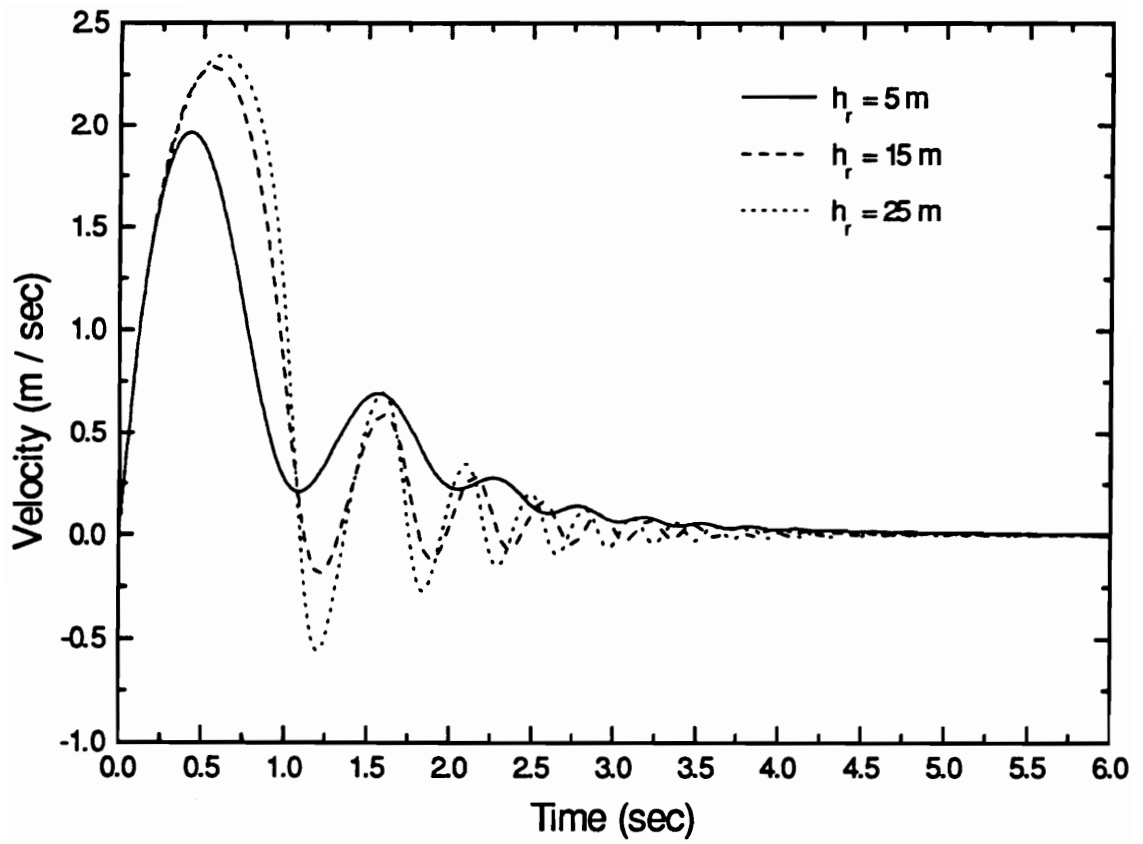
Figure 7.3(b) Predicted velocity vs time

166
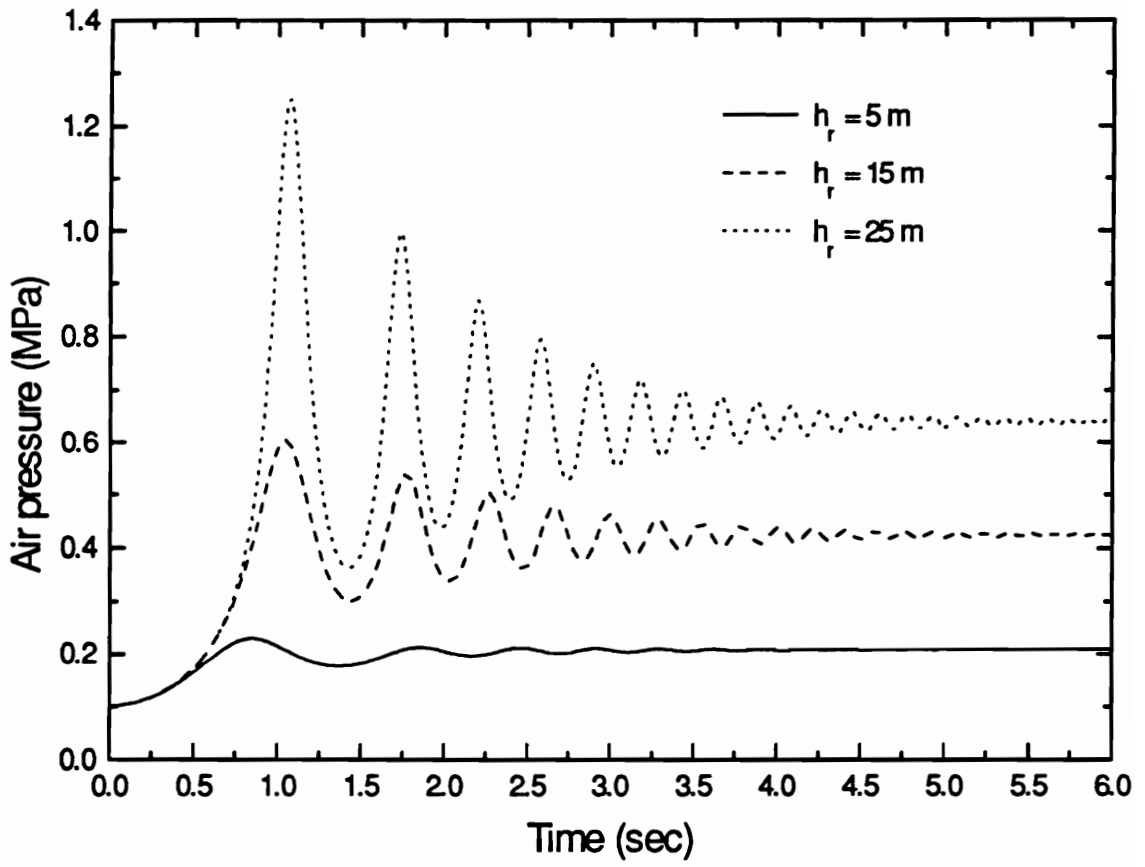
Figure 7.3(c) Predicted air pressure vs time
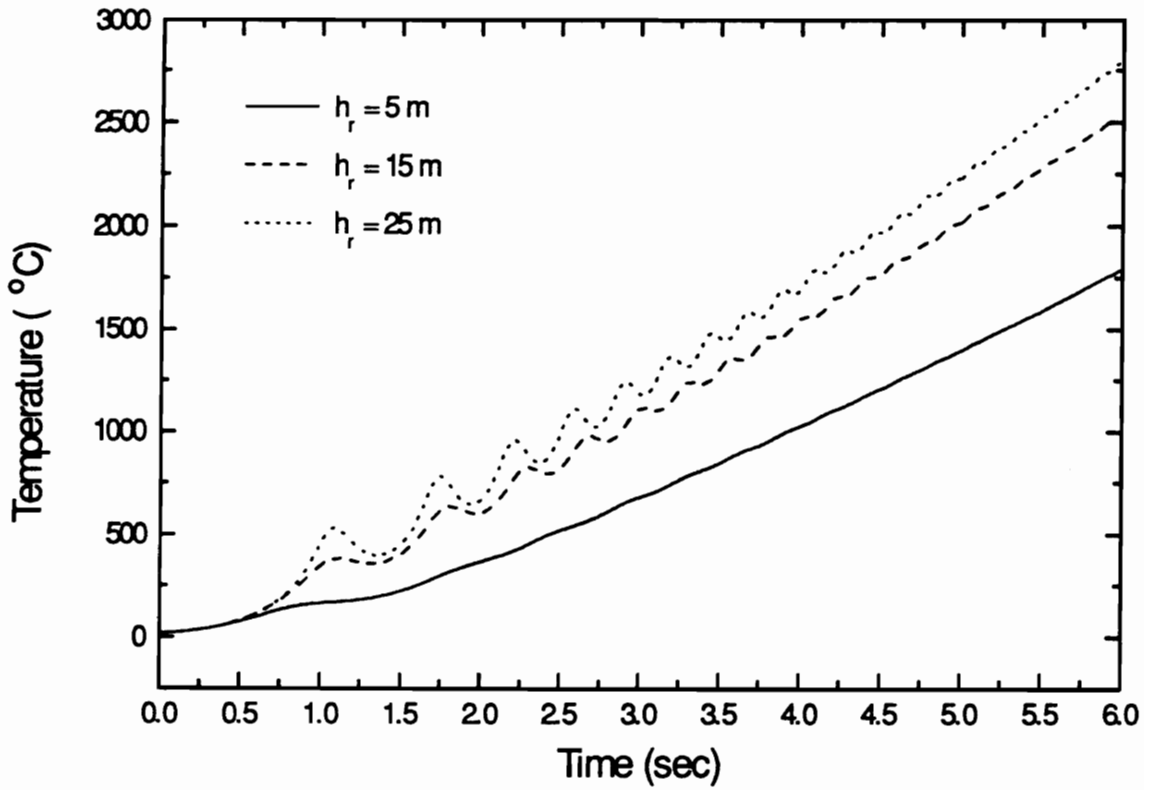
Figure 7.3(d) Predicted temperature vs time

Figure 7.3 Effect of thickness of the falling block

(simulation parameters: initial height of workings = 2 m, plan area = 100 m x 100 m, rock density = 2200 kg/m^3, and resistance of connecting airways = 0.0006 m^{-4})

7.3.2 Effect of the Damping Factor

The damping factor is dependent not only on shear resistance at the sides of the falling slab, but also on the turbulence generated within the compressed air under the falling slab. A reasonable range of this factor was found to be from 2.0 to 5.0. The effect of damping is shown on Figure 7.4. Increasing values of the damping factor yields decreasing peak pressures and after-peak pressure oscillations (Figure 7.4 c). The periods for the maximum pressure build-up are longer for a greater damping value. This factor has little significant effect on the overall behavior of the temperature curves (Figure 7.4 d).

7.3.3 Effect of Plan Area of the Falling Block

In the case of a totally bounded system (no leakage), it has been shown that the peak pressure developed is independent of either the plan area or the extracted height [McPherson, 1995]. The situation is somewhat different in the real condition of air displacement from the collapsing zone.

A comparison is made in Figure 7.5 for a 25 m-thick roof block with a range of plan areas (100 m x 100 m, 150 m x 150 m, 200 m x 200 m) falling from an initial height of 2m. The initial peak pressures tend to increase with decreasing roof dimensions (Figure 7.5 c). Furthermore, the pressure oscillations after the peak values are greatly affected by the areal dimensions. Both the amplitudes and frequencies of the oscillating pressures increase with decreasing area. For a larger area of falling roof, the temperatures increase at a slower rate (Figure 7.5 d).

These results follow from the fact that air escapes from beneath the falling roof more readily in smaller plan areas. Hence, the roof approaches the floor more rapidly (Figure 7.5 a). Accordingly, the rate of conversion of potential energy to thermal energy is also higher resulting in a greater rate of temperature increase. In considering these results, it should be recalled that these analyses pertain only to falls of large plan area and do not
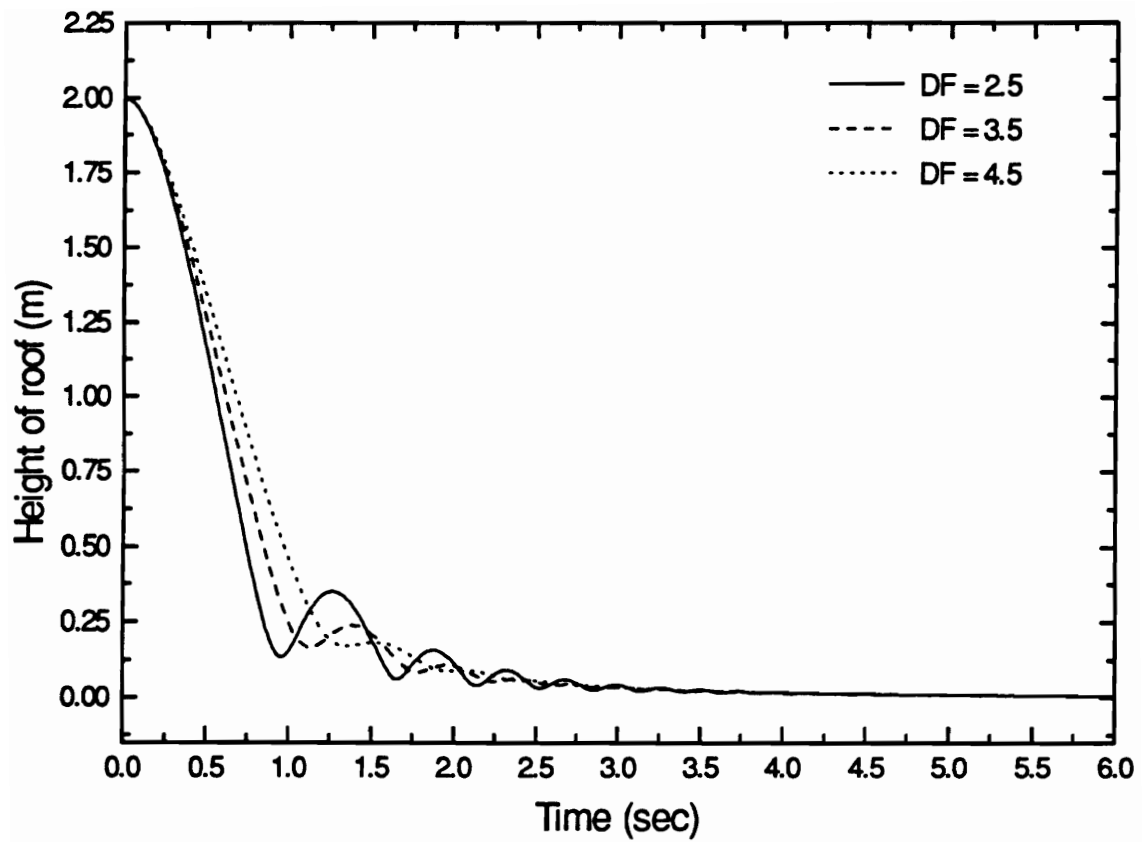
Figure 7.4 (a) Predicted height of roof vs time

170
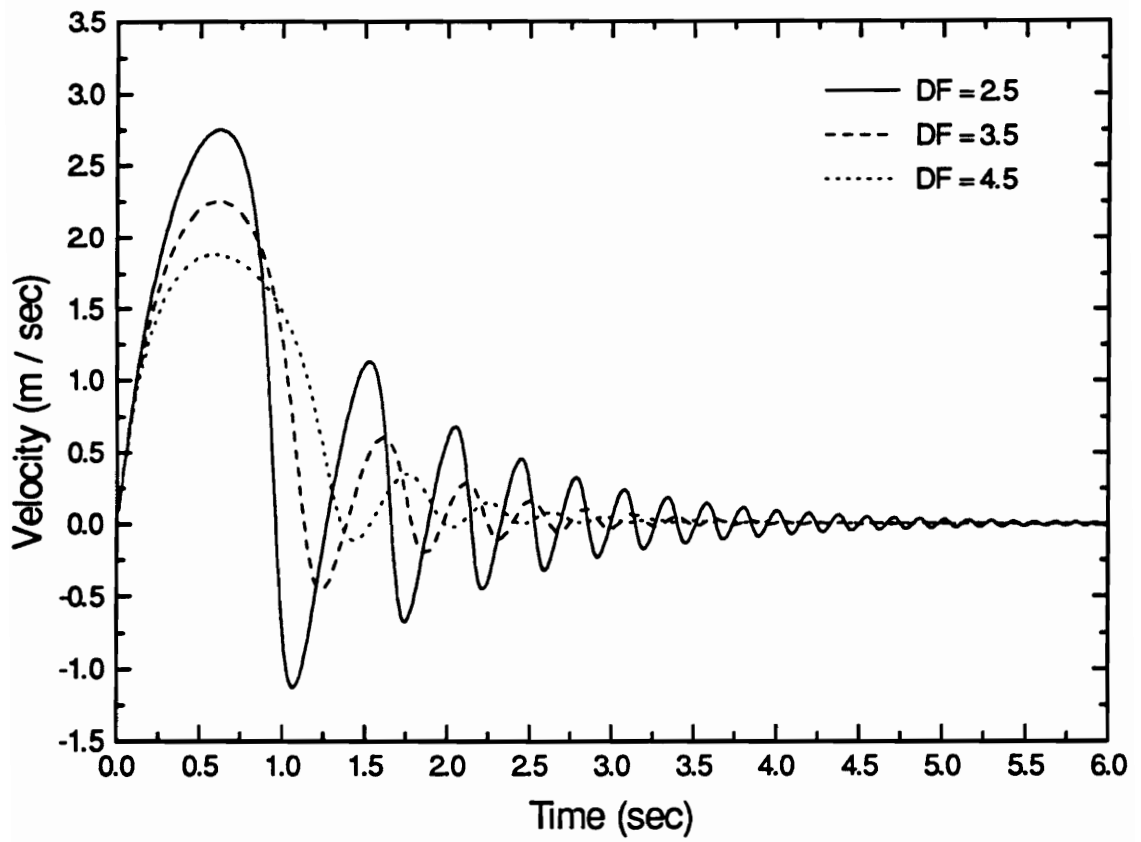
Figure 7.4 (b) Predicted velocity vs time
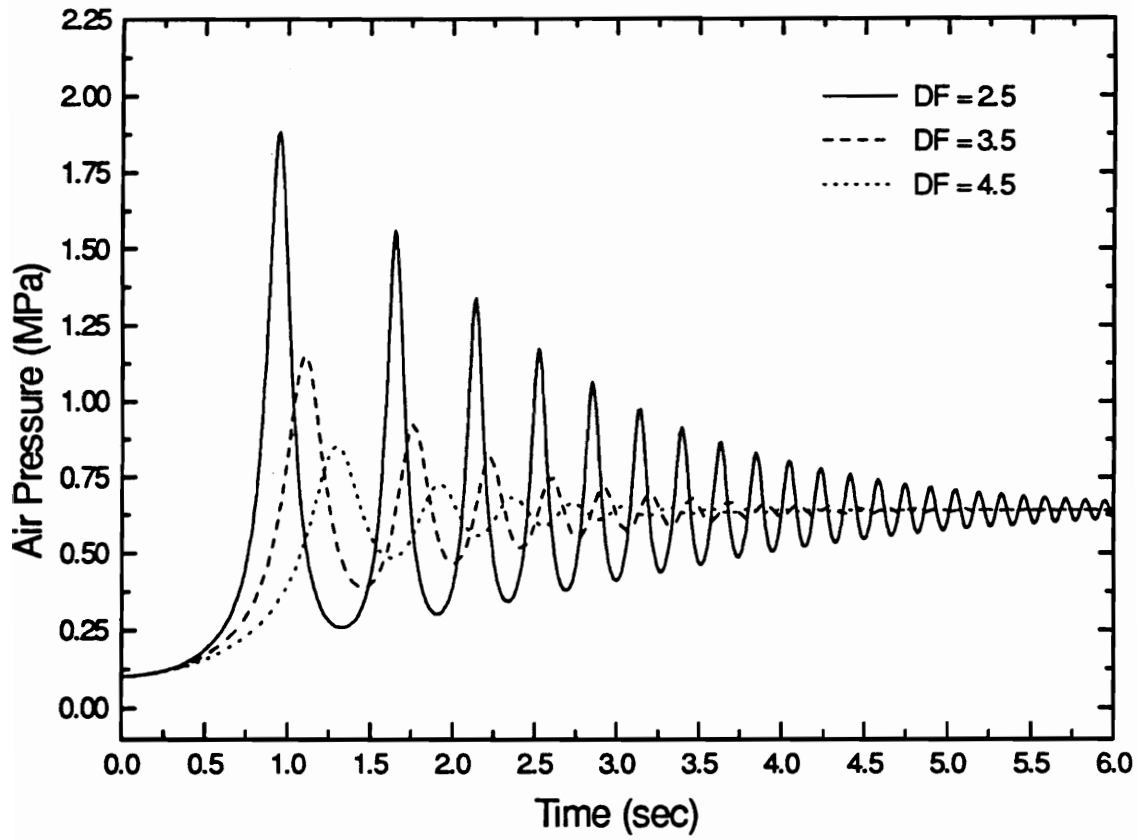
Figure 7.4 (c) Predicted air pressure vs time

172
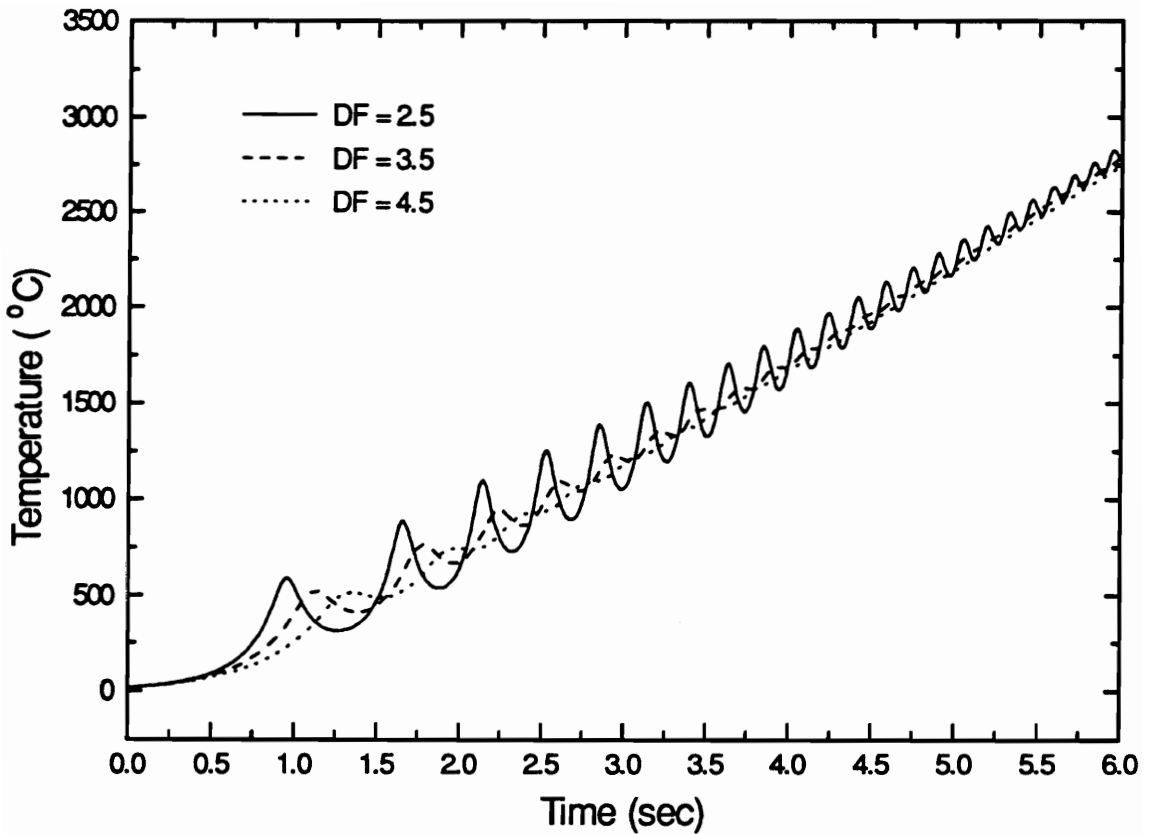
Figure 7.4 (d) Predicted temperature vs time

Figure 7.4 Effect of damping factor

(simulation parameter: initial height of workings = 2 m, plan area = 100 m x 100 m, thickness of the falling block = 25 m, rock density = 2200 kg / m^3, and resistance of connecting airways = 0.0006 m^{-4}).
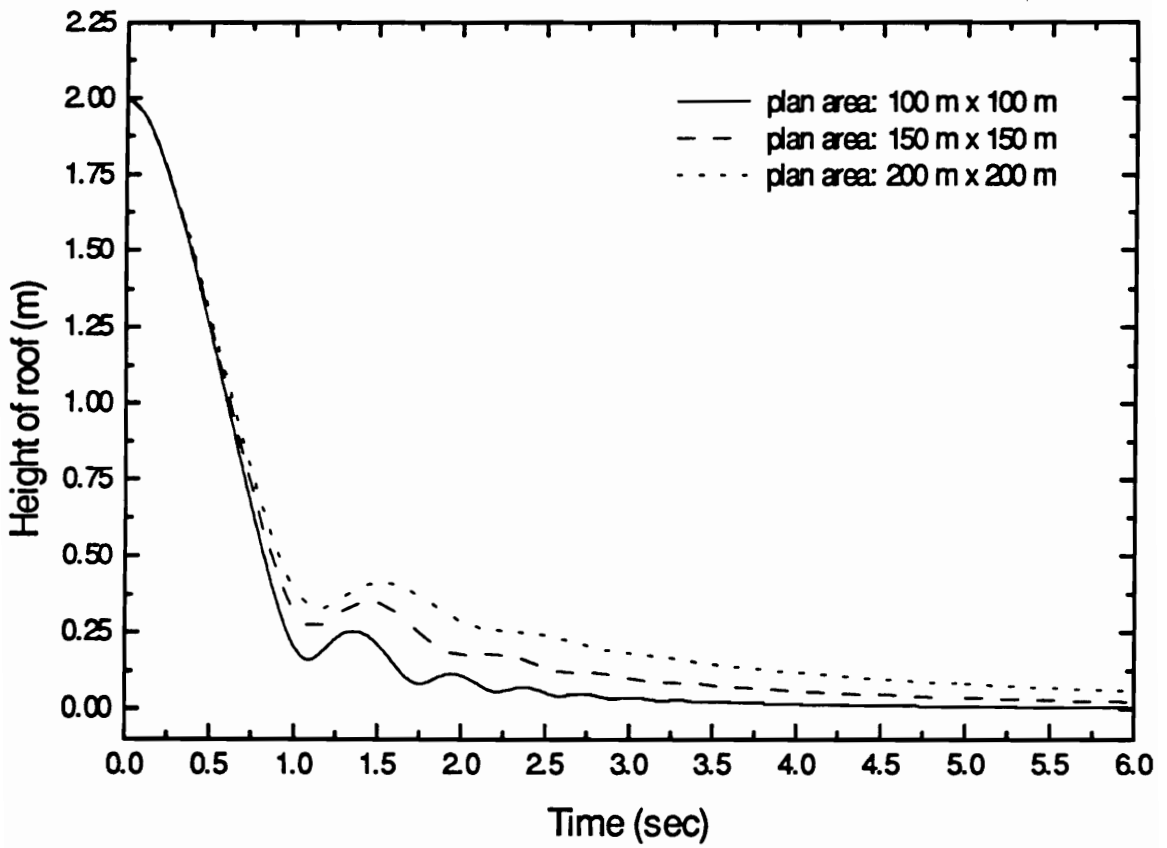
Figure 7.5 (a) Predicted height of roof vs time

174
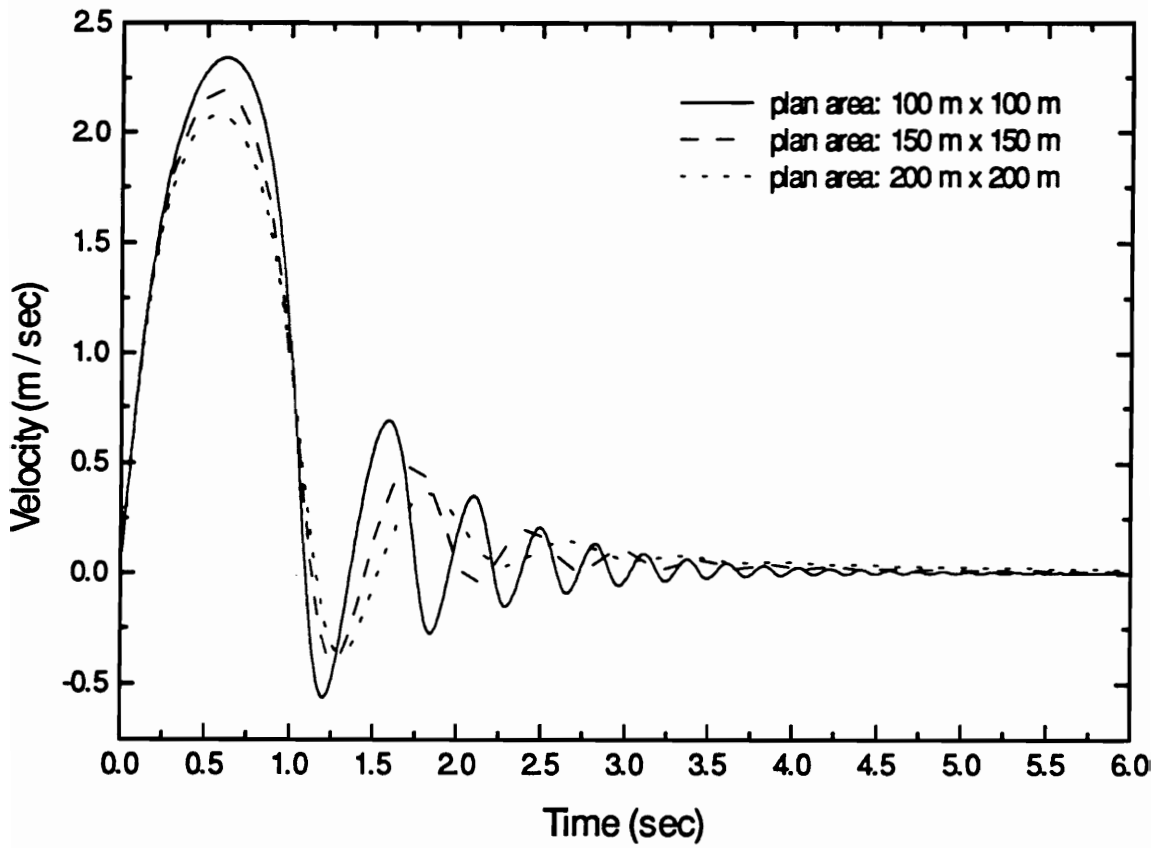
Figure 7.5 (b) Predicted velocity vs time

175

Figure 7.5 (c) Predicted pressure vs time
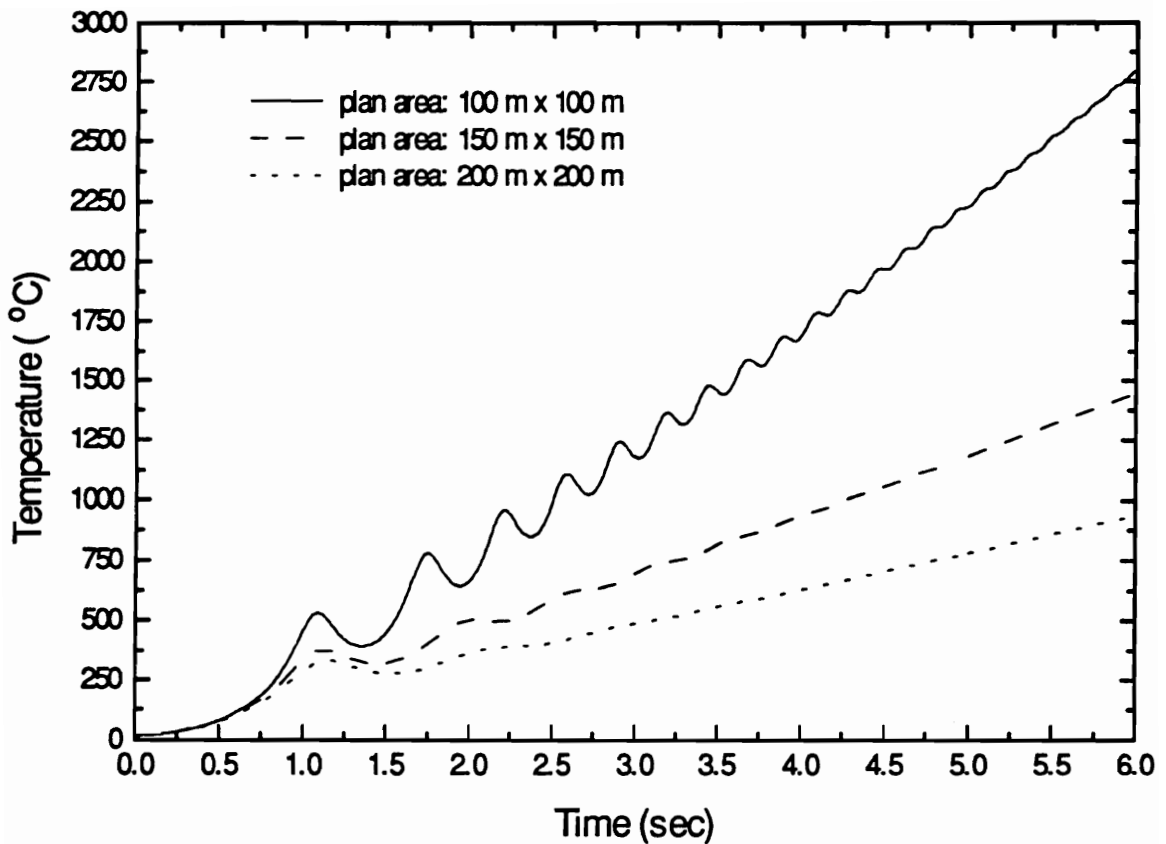
Figure 7.5 (d) Predicted temperature vs time

Figure 7.5 Effect of plan dimension of the falling block

(simulation parameters: initial height of workings = 2 m, thickness of the falling block = 25 m, rock density = 2200 kg/m^3, and resistance of connecting airways = 0.0006 m^{-4}).

apply to small localized falls where resistance to air escape from under the falling material is negligible. Indeed, the numerical simulation has been found to become unstable at plan areas of less than 20 m x 20m.

7.3.4 Effect of Initial Collapsing Height

For a given plan dimension of the falling slab, variation in the extracted height changes the total volume of air to be compressed and displaced from under the falling roof. An analysis of this parameter is presented in Figure 7.6. The block has a plan dimension of 100 m x 100 m and a thickness of 25 m with falling heights of 2 m, 3 m, and 4 m, respectively.

Again, for the no-leakage case, the peak pressure is independent of the height of seam extraction [McPherson, 1995]. For the leakage situation, Figure 7.6 reflects the fact that for a smaller extraction height, the resistance to air displacement is greater at any given time after the collapse commences. Hence, the air pressure builds up more rapidly and reaches a higher initial peak value than for greater extraction heights (Figure 7.6 c). The overall effect of extracted height on the temperature behavior is somewhat limited but exhibits slightly higher rates of temperature rise for the larger heights of extraction (Figure 7.6 d).

7.3.5 Effect of the Existence of the Fragmented Materials

Figure 7.7 shows the influence of the fragmented material for a 100 m x 100 m x 15 m block collapsing from an initial height of 2 m. The broken material has a bulking height of 0.45 m. After the roof fall initiates, the roof block rapidly comes to rest on the surface of the broken material. When the block descends closer to the fragmentation surface, the height of roof curve (Figure 7.7 a) shows bouncing-up-and-down oscillations with diminishing amplitudes, and the air pressure (Figure 7.7 c) builds up rapidly to peak value. Then the roof block continues to accelerates into the broken debris, the recompaction

178
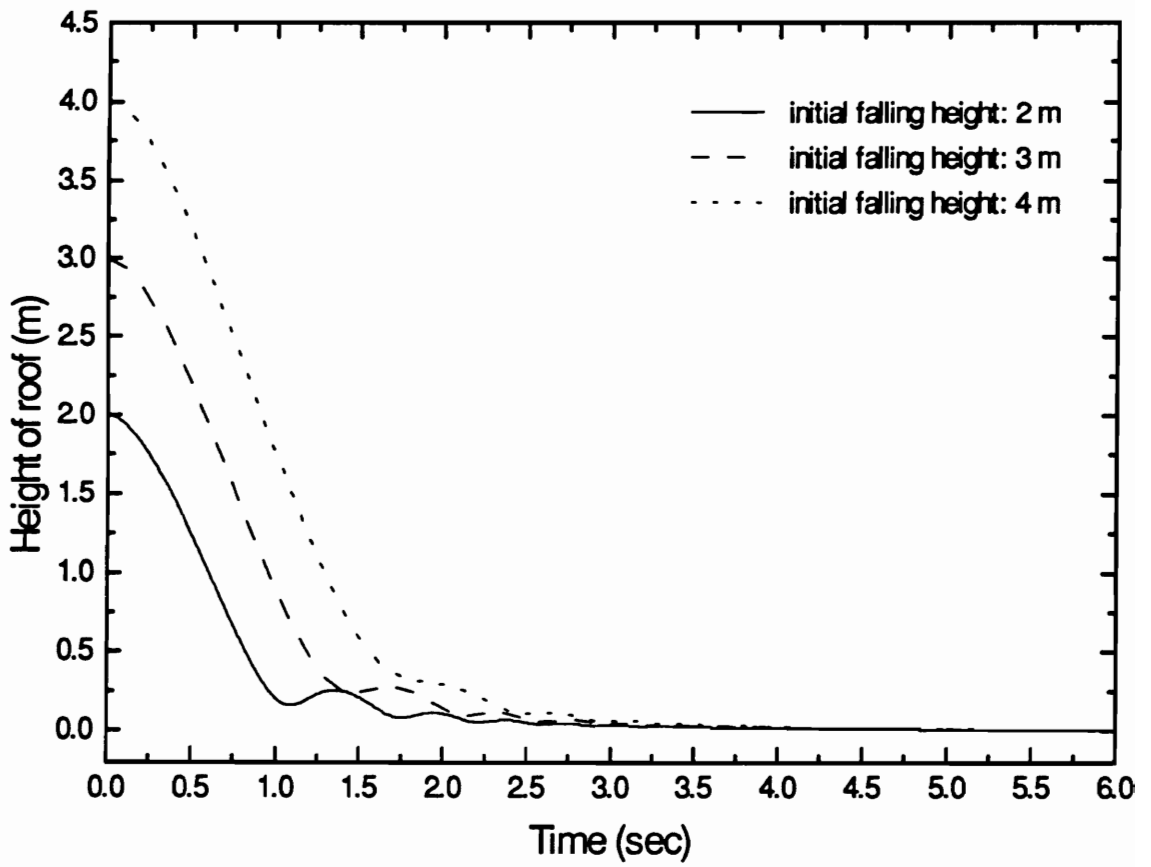
Figure 7.6 (a) Predicted height of roof vs time
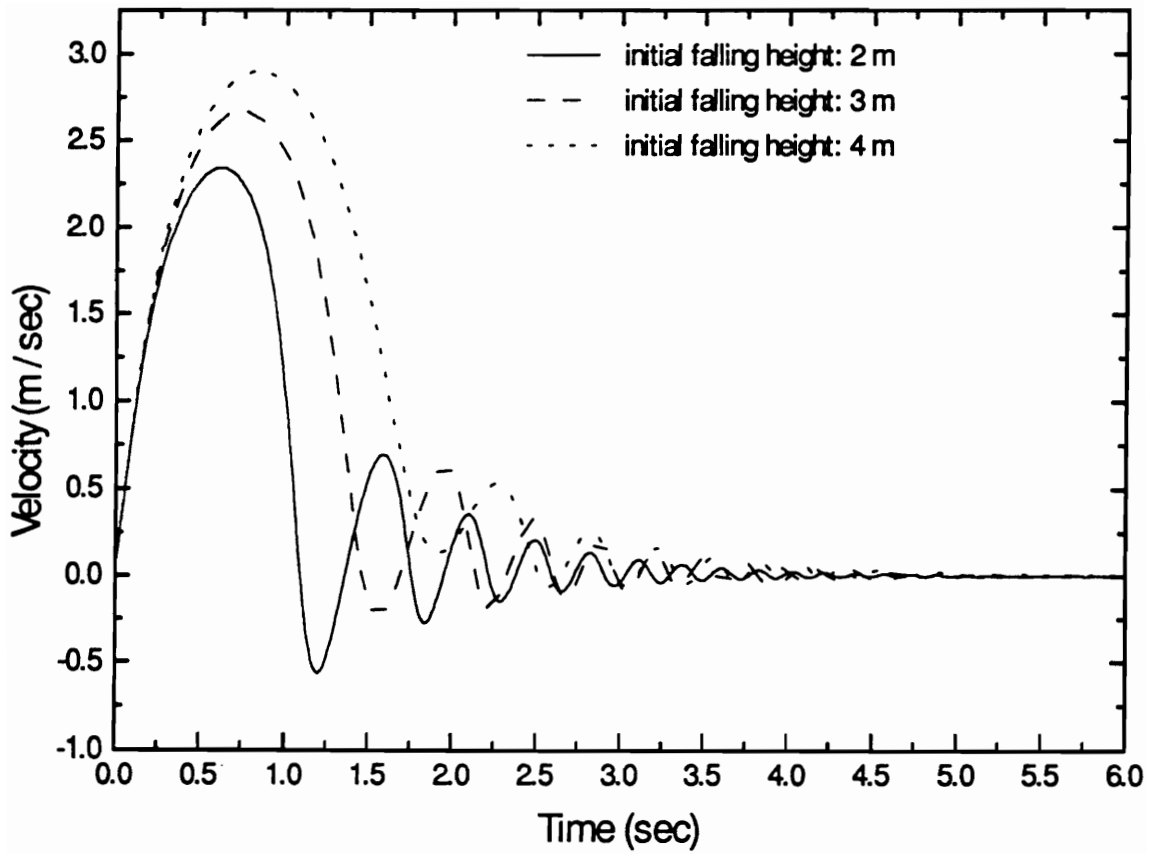
Figure 7.6 (b) Predicted velocity vs time
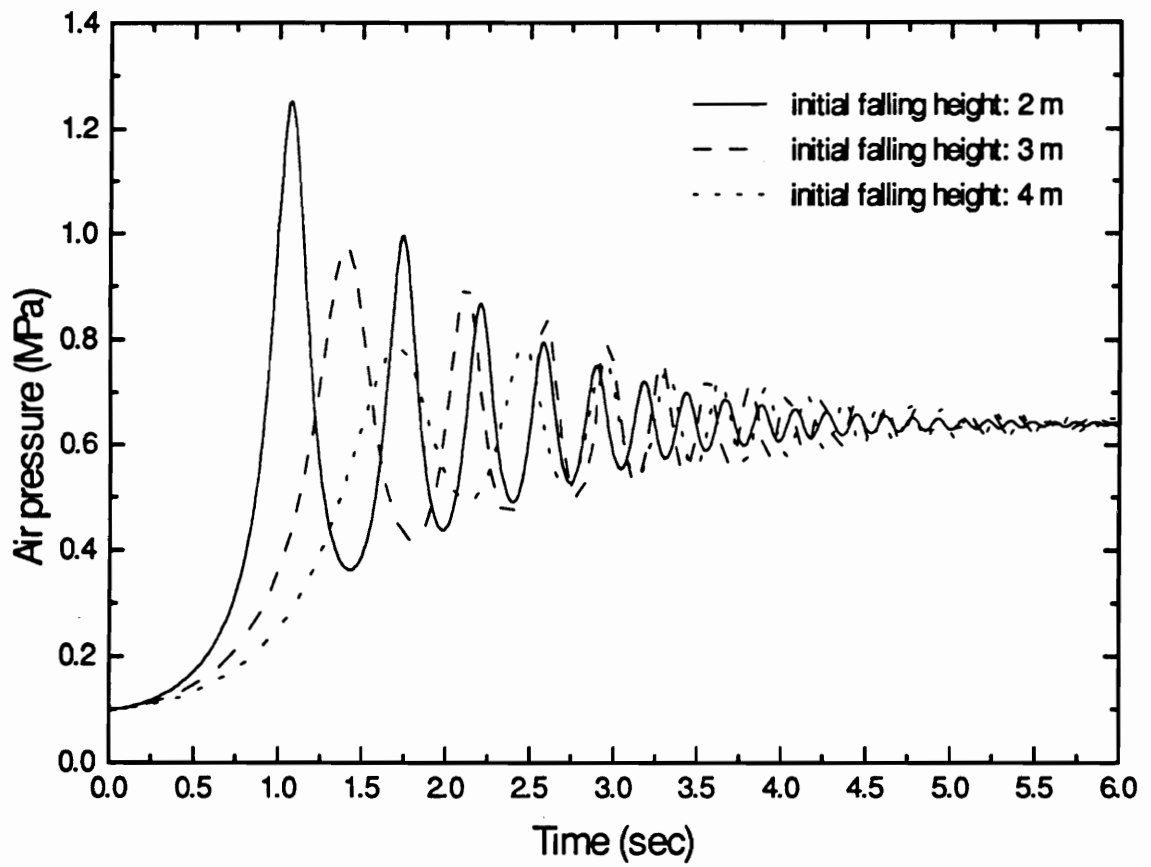
Figure 7.6 (c) Predicted air pressure vs time
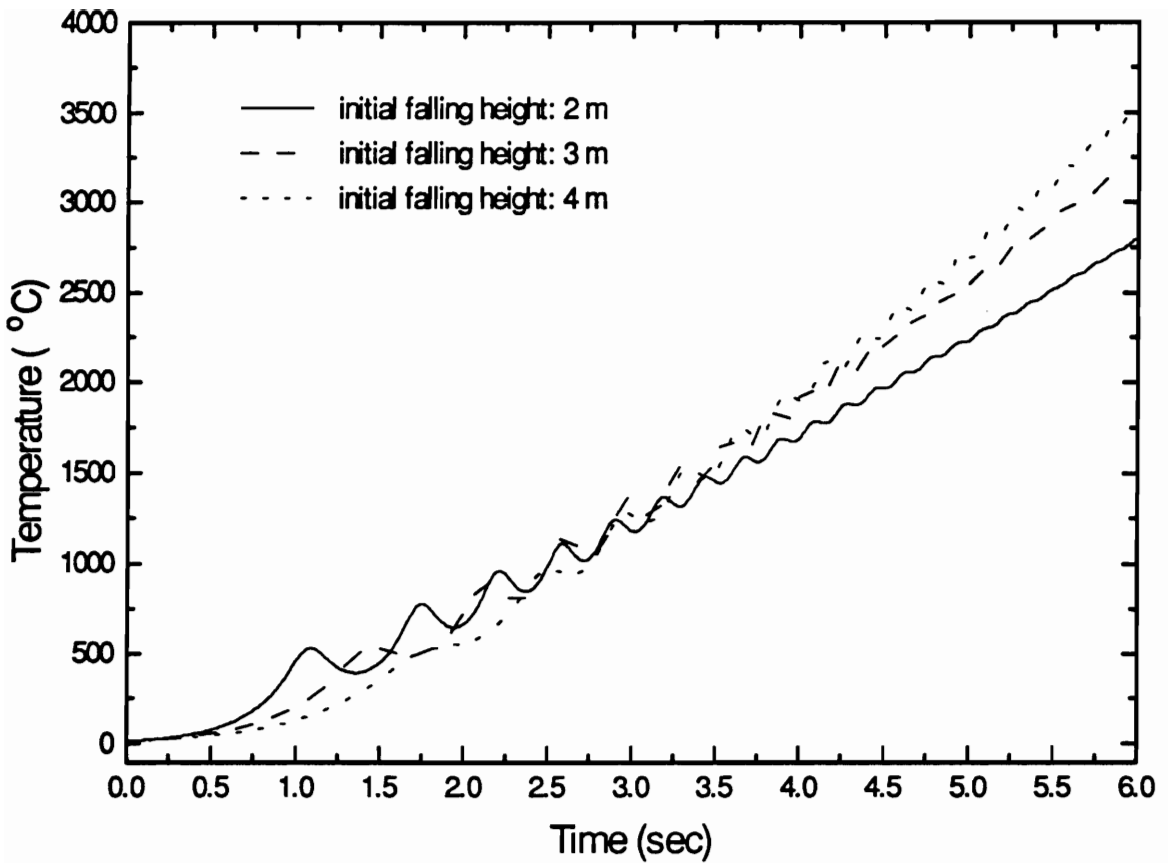
Figure 7.6 (d) Predicted temperature vs time

Figure 7.6 Effect of initial height of workings

(simulation parameter: plan area = 100 m x 100 m, thickness of the falling block = 25 m, rock density = 2200 kg / m^3, and resistance of connecting airways = 0.0006 m^{-4}).
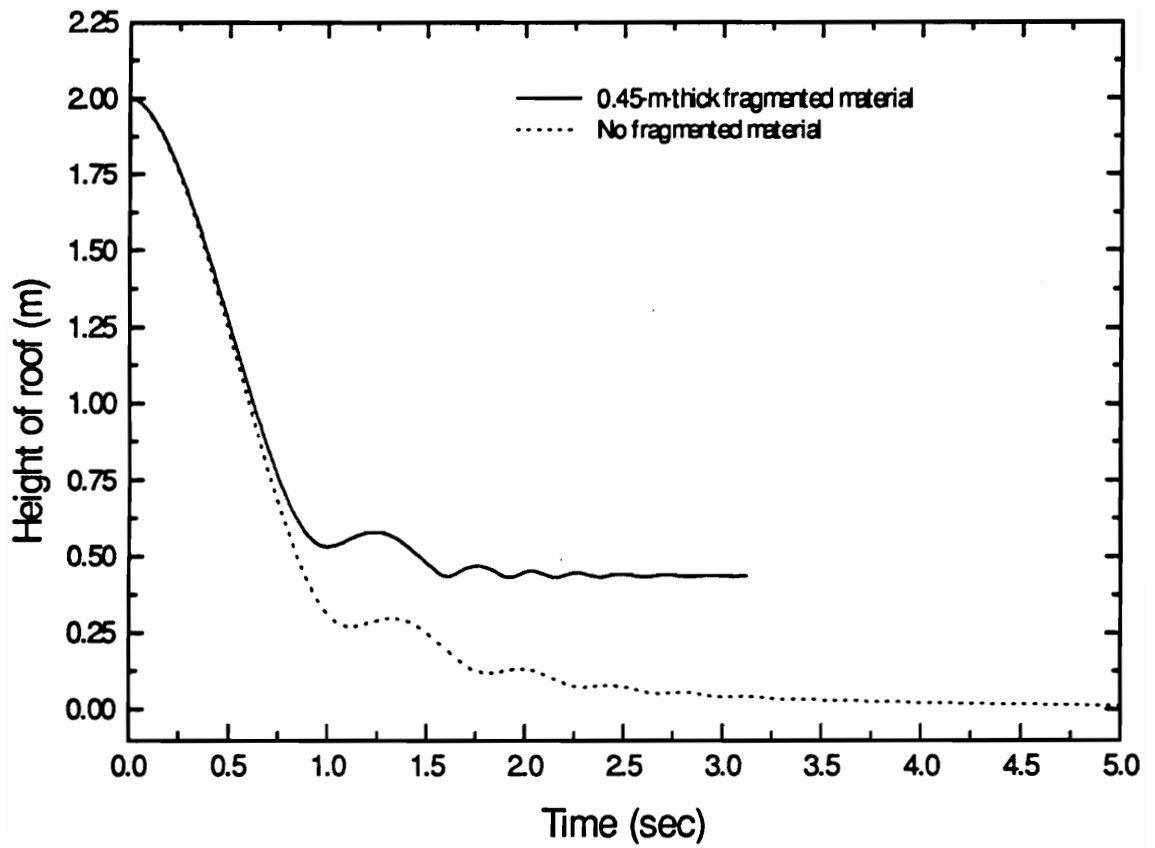
Figure 7.7 (a) Predicted height of roof vs time
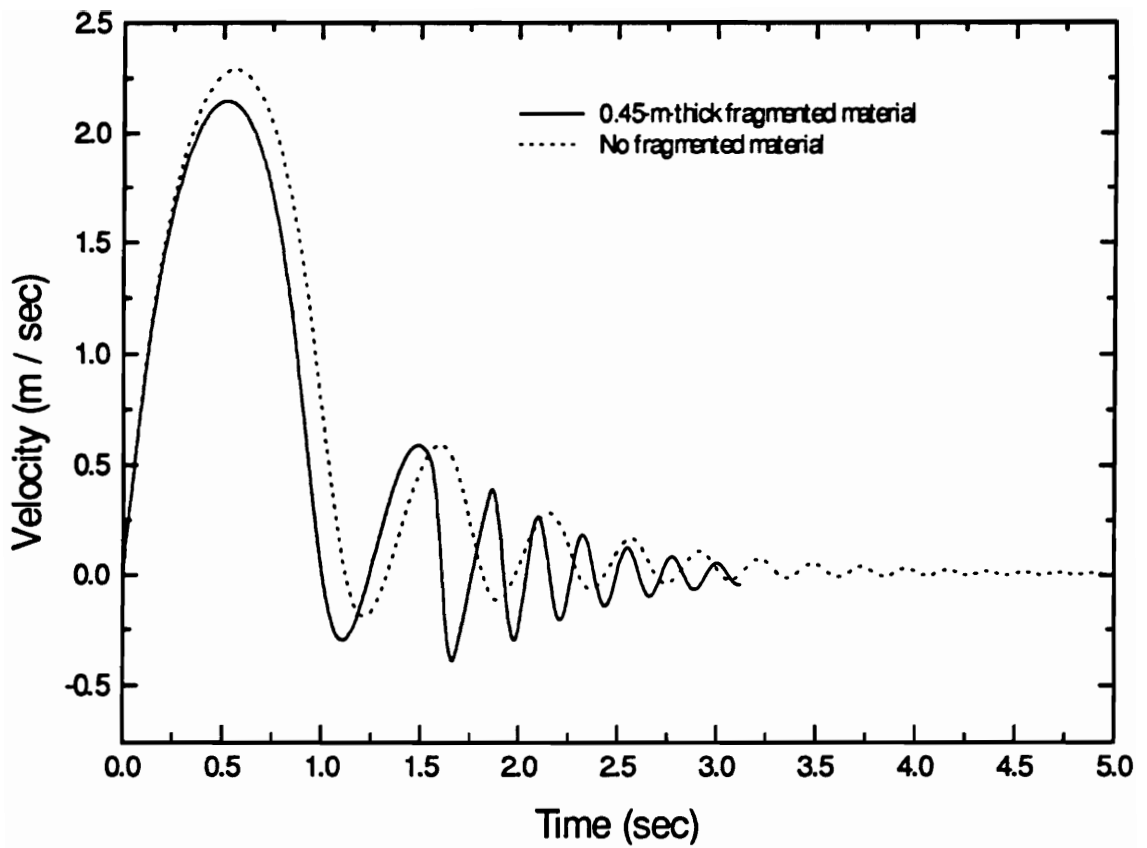
Figure 7.7 (b) Predicted velocity vs time

184
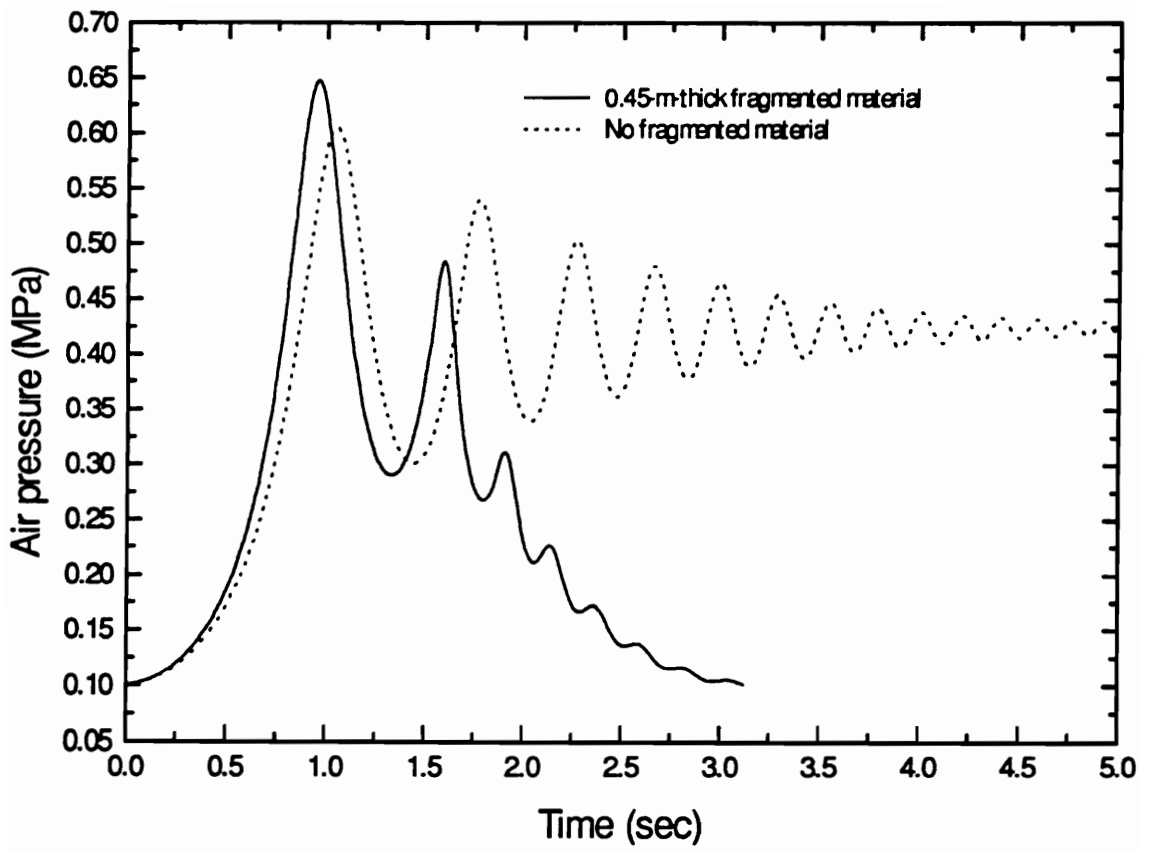
Figure 7.7 (c) Predicted pressure vs time

185
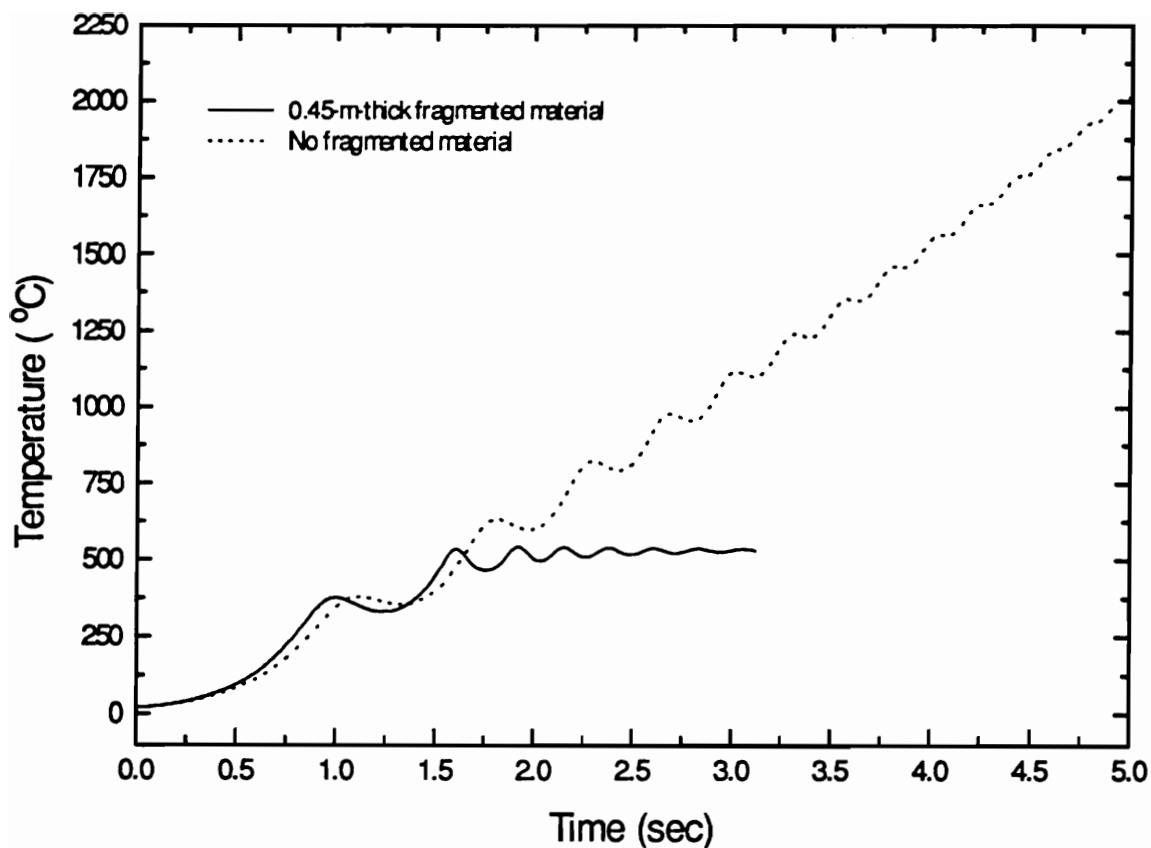
Figure 7.7 (d) Predicted temperature vs time

Figure 7.7 Effect of fragmented material on the floor prior to roof fall

(simulation parameters: initial height of workings = 2 m, thickness of the falling block = 15 m, rock density = 2200 kg/m³, and resistance of connecting airways = 0.0006 m⁻⁴).

process commences. The increased resistance of the fragmented material decelerates the roof movement. The recompaction process ceases in a short period when the resistance reaches the weight of the falling block. The initial rises in air pressure and temperature (Figures 7.7 c and d) are not so pronounced as compared with the no broken material case. However, the peak pressure associated with recompaction model is higher than that for no gob material leakage model. This follows that the broken material takes some space under the falling block, hence, the height for the block to fall through is decreased and the resistance to air displacement is increased. The most fascinating results of this analysis are the behavior of pressure and temperature curves following the peak pressure buildup period. In contrast to no-gob-material condition, the air pressure (Figure 7.7 c) drops to the initial air pressure, P_o, within a very short time after the recompaction process begins, and the corresponding temperature (Figure 7.7 d) approaches to a stable value with minor oscillations. These markedly results follow from the fact that the upward resistance of the fragmented material increases rapidly to balance the gravitational force of the falling block which must be supported by the air pressure underneath the block without the presence of gob materials.

7.3.6 Effect of Heights of the Fragmented Materials

A comparison for varying heights of broken materials (0.15 m, 0.30 m, and 0.45 m) is combined in Figure 7.8. The block has a plan area of 100 m x 100 m, and a thickness of 15 m, falling through a height of working of 2 m. In all cases, the air pressures and temperatures continue to increase to the peak values before the falling slab strikes the fragmented material (Figure 7.8 c). This factor has limited influence on the initial rises in pressure and temperature. However, after the recompaction process of fragmentation commences, the air pressures drop rapidly to the initial pressure, P_o, and corresponding temperatures becomes stable (Figure 7.8 d). It is also noticed that a thicker broken material has a higher peak pressure but a lower peak temperature and that the moment at which this occurs is affected by the thickness of the broken material. This behavior
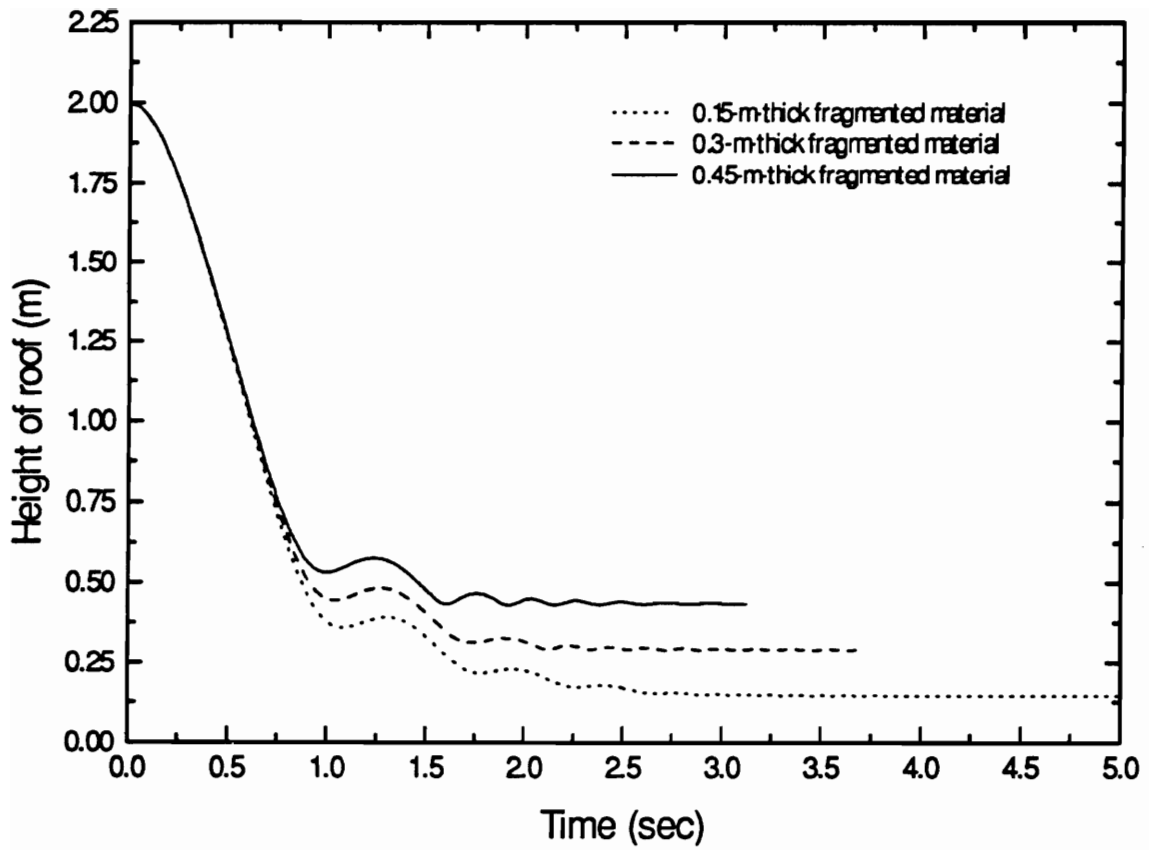
Figure 7.8 (a) Predicted height of roof vs time

188
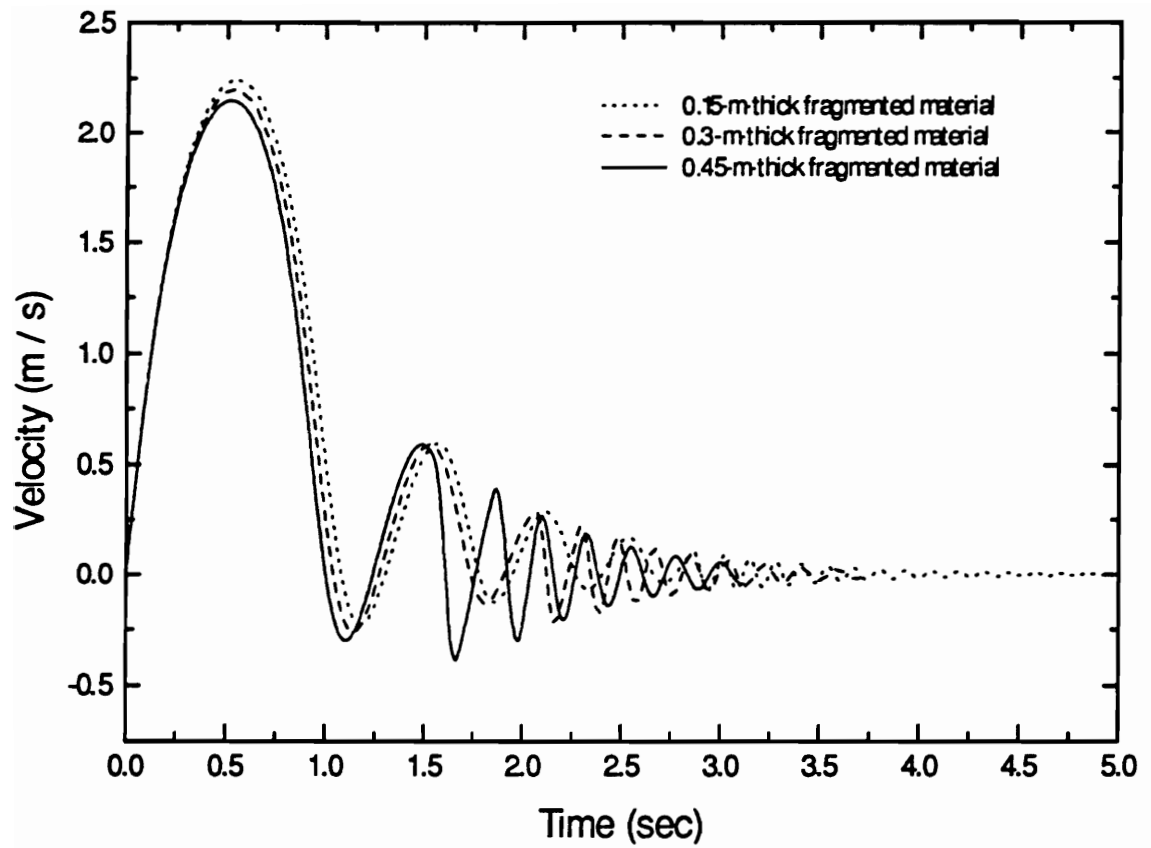
Figure 7.8 (b) Predicted velocity vs time

189
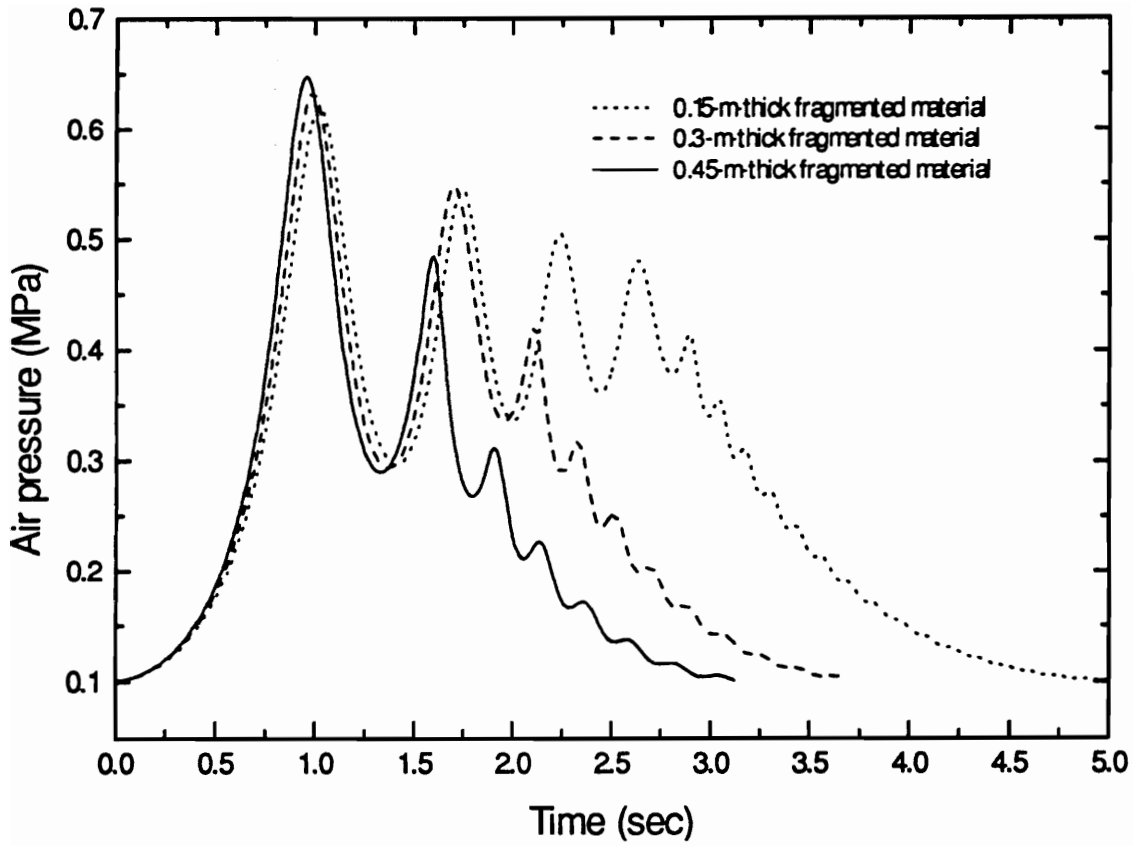
Figure 7.8 (c) Predicted pressure vs time
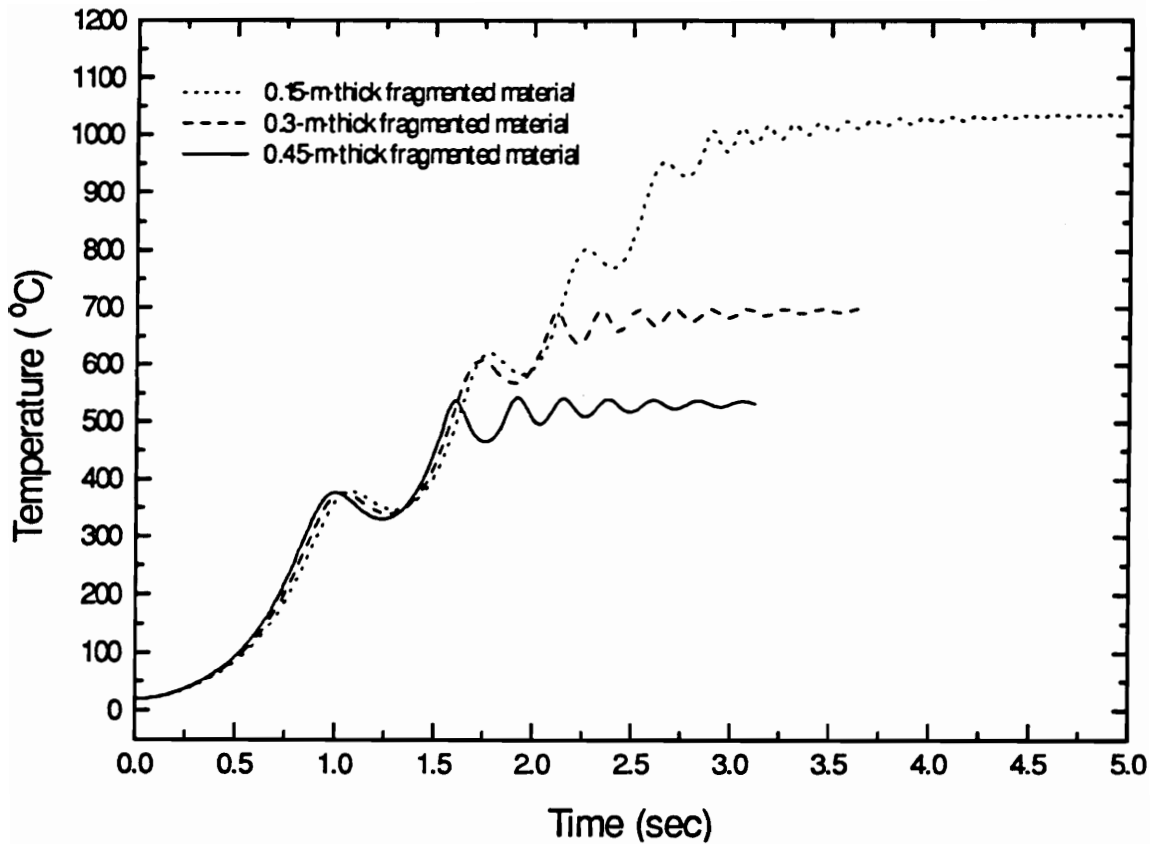
Figure 7.8 (d) Predicted temperature vs time

Figure 7.8 Effect of heights of fragmented material on the floor prior to roof fall

(simulation parameters: initial height of workings = 2 m, plan area = 100 m x 100 m, thickness of the falling block = 15 m, rock density = 2200 kg/m^3, and resistance of connecting airways = 0.0006 m^{-4}).

reflects the fact that in a thicker fragmentation situation, the less time is required for the descending slab to reach the surface of the broken material, and hence lower temperature is developed before the recompaction process starts. During the recompaction process, the resistance of the broken material increases rapidly to offset the gravitational force of the falling slab. The air pressure under the falling slab continues to drop. The adiabatic compression assumes no heat transfer during the recompaction process, therefore, the temperature becomes stable rather than increasing. In a real situation, the considerable amount of surface areas of the broken material will encourage heat transfer, and reduce the levels of temperature that will be produced. However, the roof collapsing and recompaction process takes only few second, the influence of heat transfer if it exists is anticipated to be limited.

7.3.7 Potential for Initiating a Coal Dust Explosion

Table 7.1 shows coal dust explosibility [Holden, 1982]. Comparing the ignition temperatures with those shown on Figures 7.3 to 7.8, it is clear that in the air beneath a large area of falling roof, temperatures can be generated that are considerably in excess of those required to ignite coal dust. However, the higher temperatures occur in a decreasing gap size between roof and floor. The question remains whether the air reaches dust ignition temperature while the gap is still sufficiently wide to permit propagation of the explosion to the surrounding atmosphere. As shown in Figure 7.9, it is revealed that the air temperature increases as the roof-floor gap decreases but is independent of the thickness and the plan area of the falling slab. Figure 7.9 also indicates that ignition temperatures, at which the air temperature reaches 600 °C, a mid-range value for dispersed dust on Table 7.1 can be generated while the gap under a falling roof remains sufficiently wide for an explosion flame to propagate.

192

Table 7.1 Variation of coal dust explosibility with respect to volatile content (after Holden, 1982)

Volatile Content(%)	Minimum Ignition Temperature(°C)	
	Cloud	Layer
12	670	240
25	605	210
43	575	180
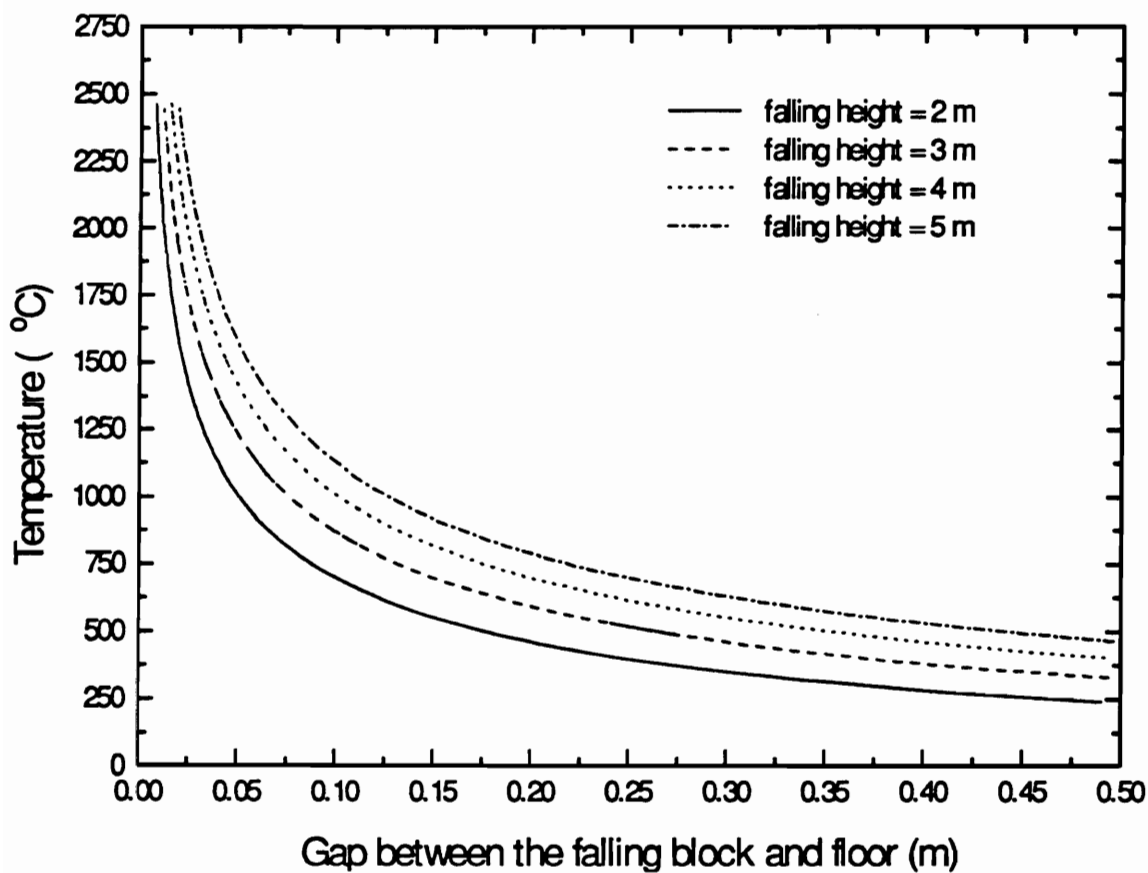
Figure 7.9 Relationship between the temperature and the roof-floor gap falling through different heights of workings

7.4 Case Studies

There were numerous recorded cases of severe windblasts caused by the sudden collapse of mine workings. The consequences have varied from personnel being knocked over to the extensive damage and 437 fatalities in the Coalbrook collapse [McPherson, 1980; Song and Xu, 1992). Three cases are outlined below in order to illustrate the influence of adiabatic air compression.

7.4.1 Case 1 and 2: Wa Jing Wan Colliery

Wa Jing Wan Colliery is one of the operating mines of the Datong Mineral Bureau in China [Song and Xu, 1992]. The mine utilized room-and-pillar method to extract a Jurassic coal seam to an extraction height of 4.0 m to 4.3m. The immediate roof was composed of strong sandstone conglomerate with a compressive strength of over 100 MPa. Its thickness varied from 5 m to 10 m, and occasionally, up to 40 m. In the early 1960s, this mine experienced severe airblasts caused by the caving of large areas of roof [Song and Xu, 1992]. In July, 1960 an area of 22,310 m^2 roof caved causing one fatality and twelve injuries. The damage extended even to the surface, inducing surface cracks ranging from 60 m to 70 m in length, and surface subsidence of 0.3 m to 0.7 m. When the mined area reached to approximately 163,000 m^2 on October 22, 1961, the roof caved entirely. The devastating windblast event resulted in 14 deaths, 19 injuries, and severe damage to the mine facilities and ventilation system. Applying the relevant data for these collapses, the results of adiabatic compression analysis are illustrated in Figure 7.10 and 7.11, respectively. The predicted peak pressures for both cases are approximately 0.4 MPa. In order to alleviate the windblast problems, the air stopping which can withstand the impact of 1.0 MPa air pressure was designed and installed in each of the separated mined-out area, and other ground control measures such as softening massive roof strata by water infusion and inducing caving by blasting boreholes were implemented during
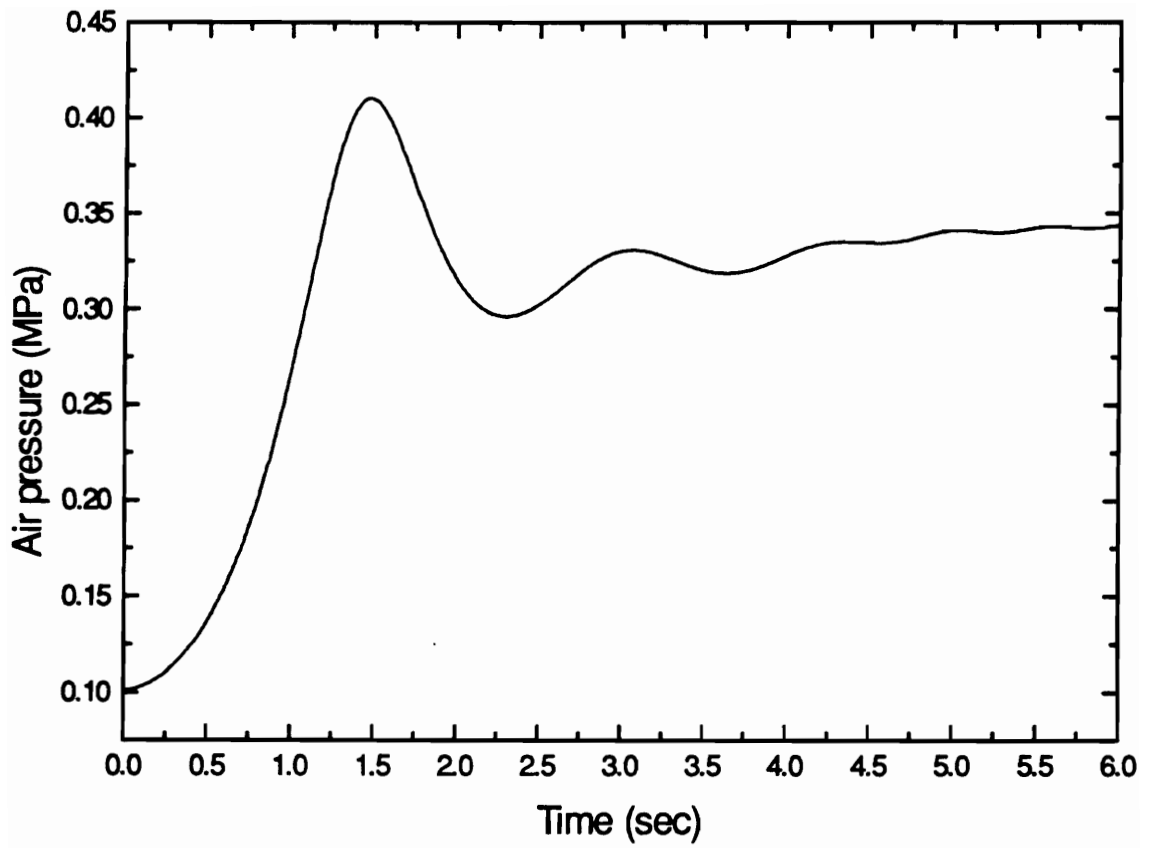
Figure 7.10 (a) Predicted air pressure vs time

196
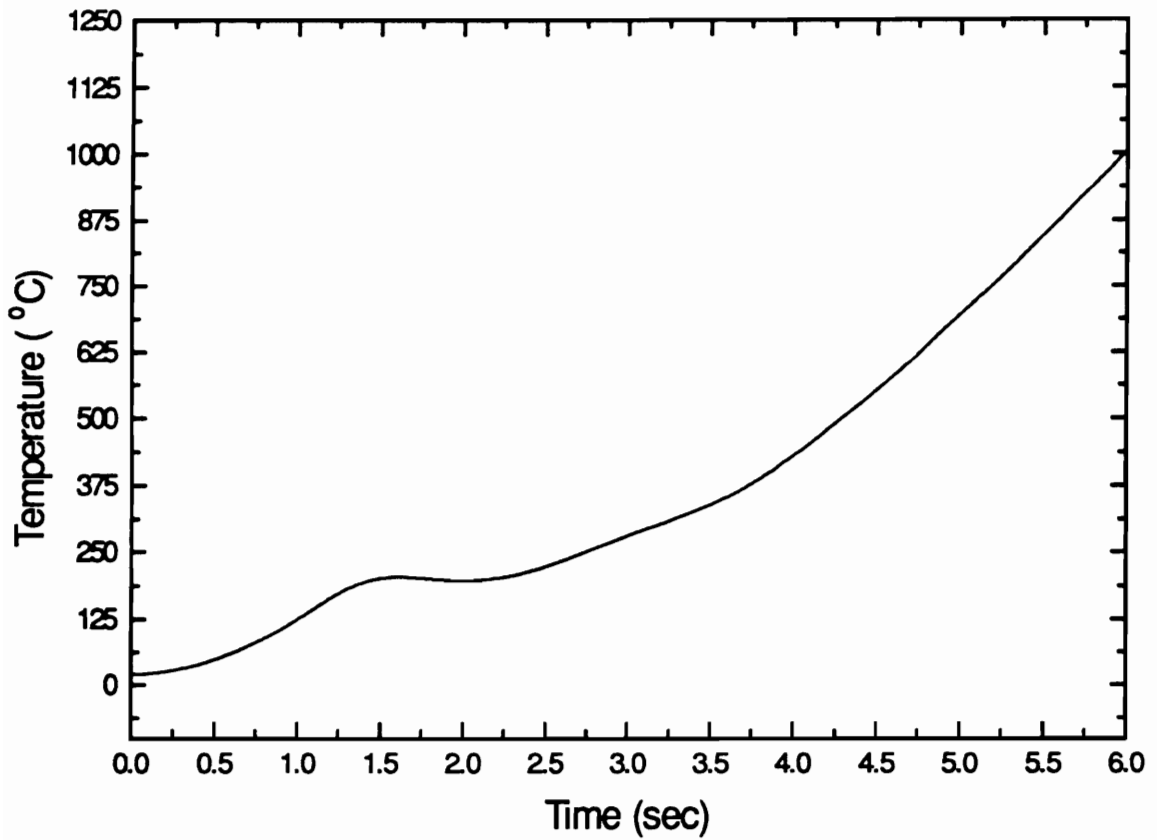
Figure 7.10 (b) Predicted temperature vs time

Figure 7.10 Variations in air pressure and temperature for Wa Jing Wan Colliery: case 1

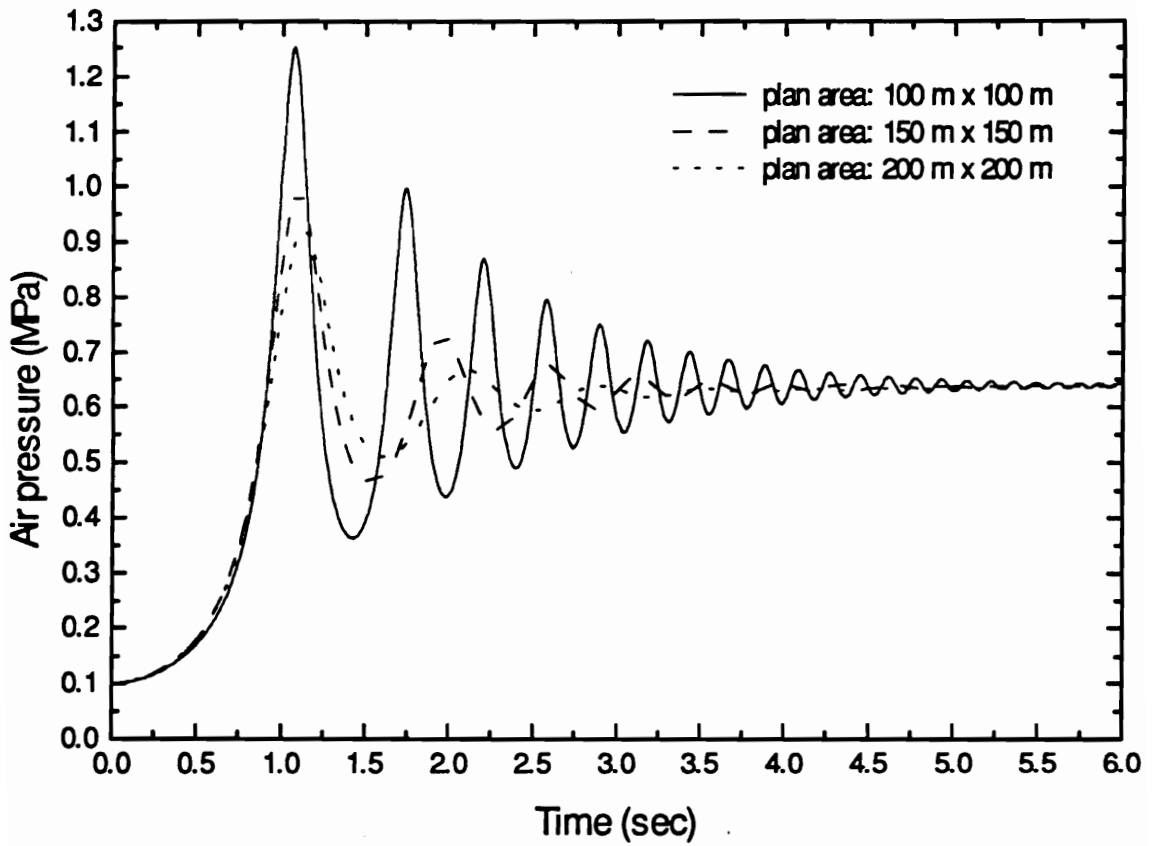(Input parameters: initial height of workings = 4 m, plan area = 150 m x 150 m, thickness of the falling block = 10 m, rock density = 2500kg/m^3. and resistance of connecting airways = 0.0006 m^{-4})

197
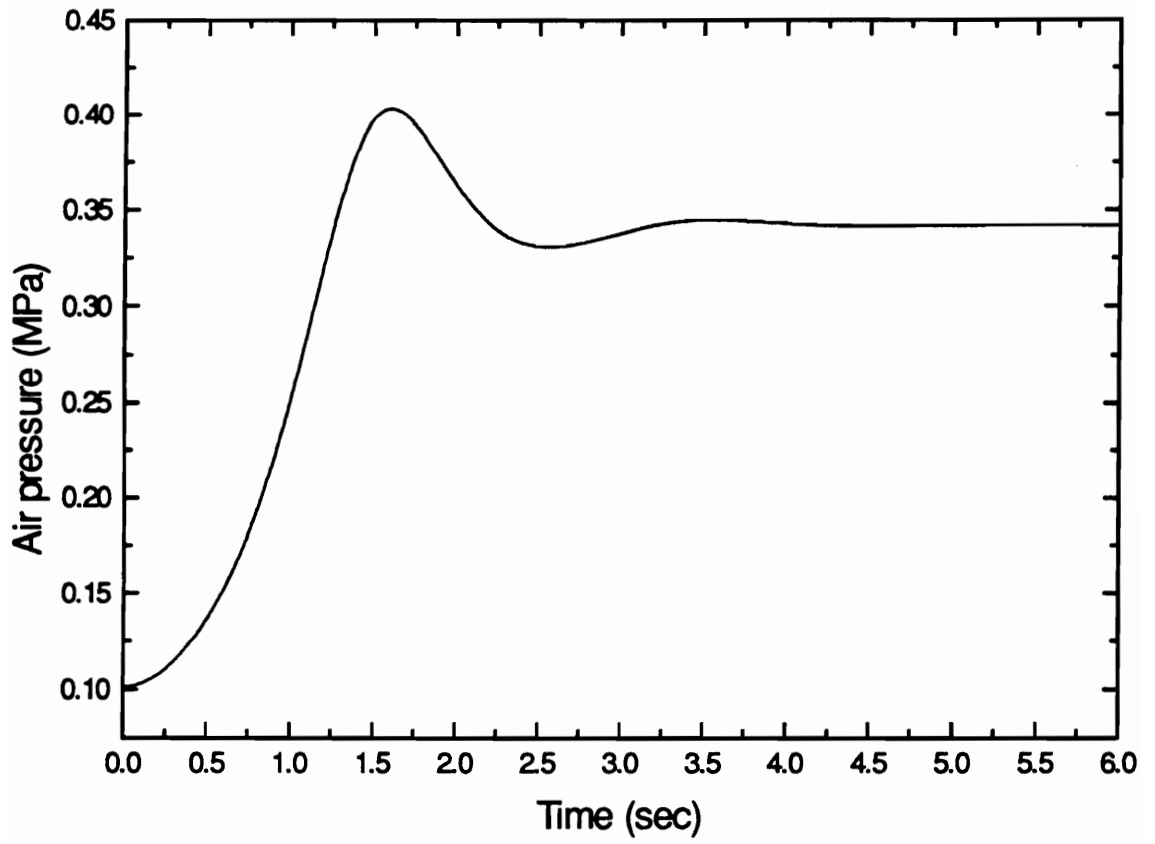
Figure 7.11 (a) Predicted air pressure vs time
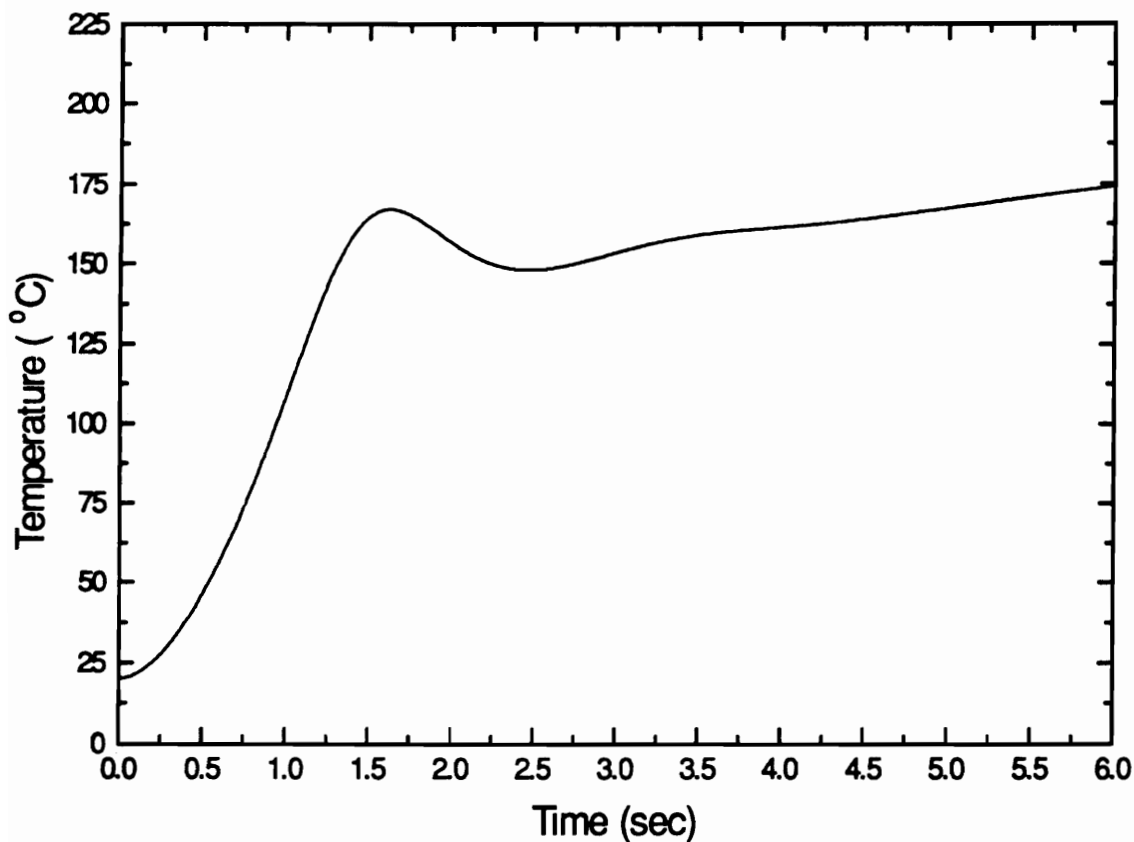
Figure 7.11 (b) Predicted temperature vs time

Figure 7.11 Variations in air pressure and temperature for Wa Jing Wan Colliery: case 2

(input parameters: initial height of workings = 4 m, plan area = 404 m x 404 m, thickness of the falling block = 10 m, rock density = 2500kg/m^3. and resistance of connecting airways = 0.0006 m^{-4})

mining operations [Song and Xu, 1992]. There were no further windblast events occurred afterwards.

7.4.2 Case 3: Moura No. 4 Coal Mine

On July 16th, 1986, an area of room and pillar goaf (gob) estimated at some 10,000 m^2, within a larger total goaf, collapsed at Moura No. 4 Coal Mine in Queensland, Australia. The seam was extracted to a total height of 5 m. The overlying strata consisted of some 60 m thickness of laminated sandstone up to the next superadjacent coal seam. The rectangular goaf area was 150 m long and 170 m wide, bounded by solid coal on three sides with five entries connected to the operating (face) zone on the fourth side. The windblast that swept through the section was either accompanied or followed immediately by a coal dust explosion. All twelve miners within the section were killed. The adiabatic compression analysis applied to the Moura conditions produced the results shown on Figure 7.12.

7.5 Summary

The work described in this chapter indicates that the compression of air under an areally large fall of roof can develop dangerous high air pressure in the collapse area and initiate a mine explosion. For this to occur, the following conditions must exist simultaneously. Firstly, the plan area of the fall roof slab must be large. More precisely, the dominant path length of air escape actually under the falling roof must be sufficient to offer significant resistance to displacement of that air. The numerical simulation developed during this work becomes unstable at plan areas of less than 20 m x 20 m. Secondly, the overlying strata should be sufficiently strong to inhibit excessive fragmentation of the roof as it descends. Since such fragmentation will produce additional areas of rock / air surface and encourage heat transfer, the process will deviate from
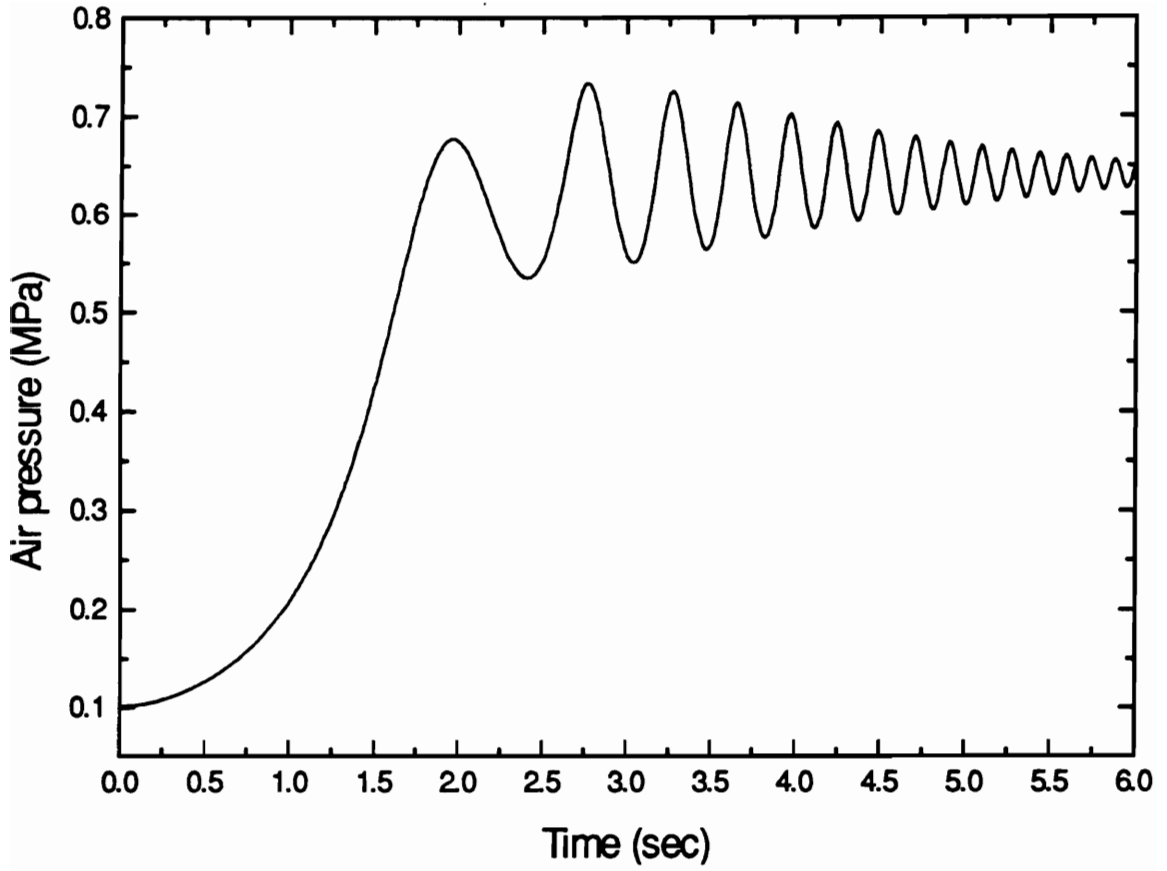
Figure 7.12 (a) Predicted air pressure vs time
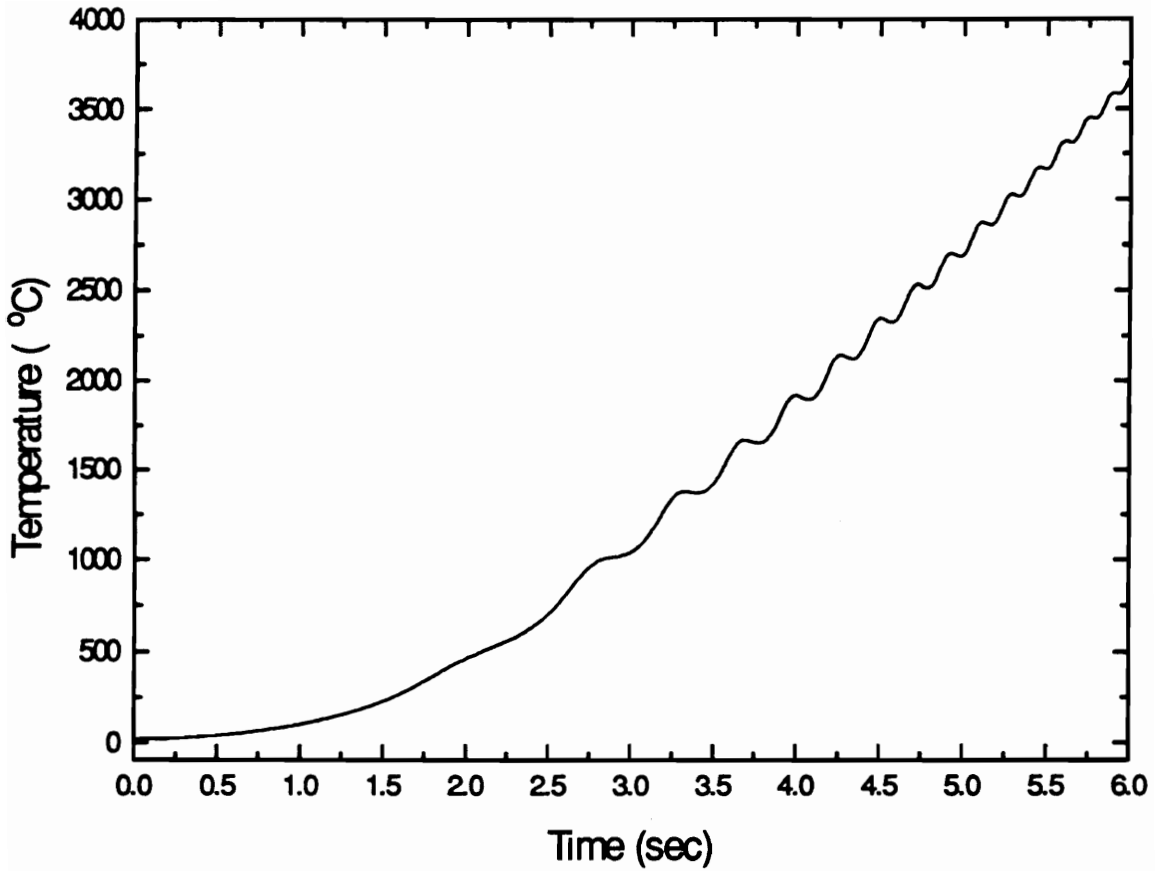
Figure 7.12 (b) Predicted temperature vs time

Figure 7.12 Variations in air pressure and temperature for Moura No. 4 mine

(input parameters: initial height of workings = 5 m, plan area = 100 m x 100 m, thickness of the falling block = 25 m, rock density = 2200 kg / m^3. and resistance of connecting airways = 0.0006 m^{-4}).

adiabatic compression and, hence, reduce the levels of air pressure and temperature. And thirdly, within the collapsing zone there must exist combinations of air, gases and / or dusts that provide a flammable mixture.

Sensitivity analysis shows that the behavior of pressure and temperature associated with roof collapse is affected by a number of variables. These include dimensions of the falling block, damping characteristics, initial falling height. The presence of the fragmented material on the floor greatly changes the pressure and temperature behavior after the peak pressure. In contrast to the no gob materiel condition, shortly after the recompaction process commences, the resistance of the fragmented material builds up rapidly and the compacted material supports the entire block. The air pressures drop down to the initial values in a very short period, and the corresponding temperatures cease to escalate and becomes stable.

This analysis has involved certain simplifications. The approximations of damping of the process and the treatment of air escape from the collapsing zone following steady-flow relationships. Further work is required to investigate these matters to improve the precision of the analysis. From current investigation, it is recommended that when an areally large collapse is anticipated in a mine where flammable gas or dust may be present, then it should be assumed the possibilities of inducing high air pressure and triggering an explosion.

CHAPTER 8 CONCLUSIONS AND RECOMMENDATIONS

8.1 Conclusions

This investigation has been conducted to study the behavior of competent roofs directly overhanging longwall and retreat room-and-pillar working faces, and the bump and airblast problems associated with their delayed caving. The major conclusions from this research work are summarized below.

In contrast with conventional treatment of the roof bed as simple or fixed-end beams on a rigid foundation under a uniform load, the strong roof beds are modeled as either cantilevering or bridging beams on elastic foundations (coal or weak roof) under exponentially decaying abutment stresses. These models incorporate the elastic deformation of the foundation, as well as the high stress concentrations around the working faces. The introduction of elastic foundation and stress concentration along the front abutment gives a more accurate representation of interaction between the roof, the foundation, and the loading conditions for an underground excavation. Further parametric analysis shows the importance of foundation compression and abutment stress concentration in contributing to roof caveability and strain energy storage.

Based on elastic beam theory, mathematical solutions of deflection lines have been developed for the single-layer elastically supported cantilevering and bridging roof beams. These solutions provide an analytical basis for determining critical spans of roof beds and

evaluating the strain energy stored in the roof and the foundation. The analysis also reveals that the difference in the moduli of elasticity in tension and compression for rock material alters the position of the neutral axis, decreases the actual flexural rigidity, and results in non-symmetric stress redistributions in the rock beam. Following the analysis of single-layer roof models, an analytical approach has been given for transformation of a double-layer roof to a single-layer roof by constructing an equivalent layer with a T-shape cross-section consisting of same material as the layer with a smaller value of the elastic modulus. A method for determining equivalent elastic constants, i.e., modulus of elasticity, Poisson's ratio, and modulus of the foundation, of a double-layer foundation has been discussed.

Design formulae have been developed to determine the critical spans of cantilevering and bridging strong roof beds under tension failure. A set of design curves were generated to provide a tool for determining critical spans that is quick and simple to use. Investigations on roof caveability show that:

- The critical spans for both cantilevering and bridging models increase with increasing tensile strength of rock materials, ratio of the elastic modulus in compression to the elastic modulus in tension, and decreasing overburden;

- In the cases of the bridging roofs, the caveability is also affected by the foundation (coal) characteristics. The critical spans increase with decreasing foundation height or increasing foundation modulus; and

- For a given roof formation under the same overburden loading, the bridging roof has a greater span than the cantilevering roof, indicating that the initial caving intervals are greater than the periodic caving intervals during longwall operations.

Applying the developed strain energy formulae, a comprehensive parametric analysis

is conducted to examine the factors influencing the energy buildup and distributions caused by the cantilevering and bridging of the strong roofs. The parametric analysis identifies that the strain energy accumulation in the roof and the foundation is affected by the following four categories of factors:

- Mechanical properties of the strong roofs (tensile strength and ratio of elastic modulus in compression to modulus in tension);

- Foundation (coal) properties (elasticity modulus and height);

- Applied stress characteristics (overburden depth and stress concentration); and

- Roof configurations.

The analysis further reveals the following facts pertaining to energy accumulations:

- The stored strain energy increases with increasing roof thickness, overburden depth, E_c / E_t ratio, tensile strength, stress concentration factor, foundation height, and decreasing foundation modulus; and

- Under the same conditions the energy storage associated with the bridging roof model is always greater than that for the cantilevering roof model, which translates into a greater bump potential for the first weighting stage as compared to the periodic weighting stage during longwall extraction.

The fact that different roof models have distinctive energy distributions in the roof and the coal may guideline the design of practical bump control measures. Bump control methods, such as drillhole blasting and hydraulic fracturing are aimed at releasing strain energy in the stress concentrated regions by artificially inducing cracks in the strong roof or the coal ahead of the working faces. From energy analysis, for the cantilevering models, the roof carries only small percentage of the total energy, therefore, efforts taken to alleviate bump hazards should be focused on control of the energy stored in the coal. The energy stored in a thicker and massive bridging roof bed with a higher tensile strength

may exceed the energy stored in the coal, control of both the roof and the foundation energy accumulation should be concurrently taken into account. It is recommended that when a bump possibility is anticipated at the mine planning or design stage, energy analysis based on site-specific geological and mining conditions should be conducted to examine the energy distributions. Then appropriate bump control measures can be designed, or adjustments of mine design parameters can be made to alleviate energy accumulations.

A quantitative parameter, the local Richter magnitude, is proposed as a predictive index for the likeliness and severity of coal bumps associated with mining under competent roofs. Criteria for pressure and shock bump events are suggested. Evaluation of the amount of released energy together with the particle velocity damage model provides a quantitative estimate of the possibility and extent of shock and pressure bumps. Five case studies from U.S. bump-prone coal mines show that the theoretical predictions of the bump potential agree well with the field data.

A Windows-based software package "CBPEP" is developed to facilitate determination of roof spans, stored strain energy, and coal bump possibility caused by delayed caving of strong roof beds. Eight single- and double-layer roof models are implemented in the package.

The behavior of air pressure and temperature caused by roof falls in large areas is investigated using the adiabatic air compression theory. The investigation reveals that the compression of air beneath a areally large fall of roof could develop dangerously high air pressure in the collapse area and initiate a mine explosion. For this to occur, the following conditions must exist simultaneously. Firstly, the plan area of the falling roof slab must be large. More precisely, the dominant path length of air escape actually under the falling roof must be sufficient to offer significant resistance to displacement of that air. Secondly, the overlying strata should be sufficiently strong to inhibit excessive fragmentation of the roof as it descends. And thirdly, within the collapsing zone there must exist combinations

of air, gases and / or dusts that provide a flammable mixture. Sensitivity analysis shows that the behavior of pressure and temperature associated with roof collapse is affected by a number of variables. These include dimensions of the falling block, damping characteristics, initial falling height. The presence of the fragmented material on the floor greatly changes the pressure and temperature behavior after air pressure reaches the peak value. In contrast to the no gob material condition, shortly after the recompaction process commences, the resistance of the fragmented material builds up rapidly and the compacted material supports the entire block. The air pressures drop down to the initial values in a very short period, and the corresponding temperatures cease to escalate and become stable. From the current investigation, it is recommended that when a sufficiently large collapse is anticipated in a mine where flammable gas or dust may be present, it should be assumed that the possibilities of inducing high air pressure and triggering an explosion exist.

8.2 Recommendations

The investigation carried out this far indicates that additional studies may be needed in the following areas:

In the roof beam models, the rock materials are treated as a purely elastic, isotropic, and homogeneous medium. This approximation is not valid for rock materials which include distinct discontinuities. A no-tension voussoir beam or plate may be appropriate for the modeling of discontinuous rocks. In those cases where the length of the roof is less than twice its width, the strong roof no longer behaves as beam. Consequently, plate theory should be applied to study its behavior.

It is a well-known fact that all laboratory test results of rock properties have a salient feature of variations and uncertainties. Considering the probabilistic nature of the rock

parameters used in coal bump prediction, a probability and statistics approach should be used to improve the prediction process. The proposed methodology based on statistical concepts is to construct a frequency distribution of the parameter in question, and then to determine a measure of central tendency and variability. The main idea involved is that the central tendencies of each input parameter are used in the calculations, and their variabilities constitute a basis for the estimating the probability of the output parameter.

Analysis of the air compression process under large roof falls has involved certain simplifications: the approximations of damping of the process, and the treatment of air escape from the collapsing area following steady-flow relationships. While the fragmented material is present on the floor, the additional area of rock / air surface may encourage heat transfer. Hence, the air compression may not follow the adiabatic law. Further work is required to investigate these matters to improve the precision of the analysis.

REFERENCES

Adler, L., 1970, "Evaluating Double Elasticity in Drill Cores Under Flexure," Int. J. Rock Mech. & Min. Sci., Vol. 4, pp. 357-370.

Adler, L., and Sun, M., 1976, "Ground Control in Bedded Formations," Bulletin 28, Research Division, VPI & SU, Dec., 266 pp.

Avershin, S. G., and Petukhov, I. M., 1964, "Rock Bump Conditions and Ways of Combating Them in Soviet Mines," Proceedings, Fourth International Conference of Strata Control and Rock Mechanics, New York, pp. 412-418.

Barker, R. M. and Hatt, F., 1972, "Joint Effects in Bedded Formation Roof Control," In New Horizons in Rock Mechanics, Proceedings, 14th Symp. Rock Mech., New York: Am. Soc. Civ. Engrs., pp. 247-261.

Beer, G. and Meek, J. L., 1982, "Design Curves for Roofs and Hanging Walls in Bedded Rock Based on Voussoir Beam and Plate Solutions," Transactions of the Institution of Minerals and Metallurgy, 91, A18-22.

Blight, G. E., 1984, "Soil Mechanics Principles in Underground Mining," J. Geotech. Engng Div., ASCE, 110, pp. 567-581.

Board, M. P., and Fairhurst, C., 1983, "Rockburst Control Through Destressing - A Case Example," Rockbursts: Prediction and Control, Institution of Mining and Metallurgy, London, pp. 91-101.

Brady, B. H. G., and Brawn, E. T., 1993, "Rock Mechanics for Underground Mining," Chapman & Hall, 571 pp.

Brady, B. T., and Haramy K. Y., 1994, "High Amplitude Stress Wave Generation and Damage Induced by Roof Caving in Mines," Proceedings, 1st North American Rock Mechanics Symposium, Austin, Texas, pp. 1033-1040.

Brady B. T., and Rowell, G. A., 1986, "Laboratory Investigation of the Electrodynamics of Rock Fracture," Nature, v. 321, pp. 488-492.

Buchanan, G. R., 1988, "Mechanics of Materials," Holt, Rinehard and Winston, Inc, pp. 582-590.

Campoli, A. A., Barton, T. M., Dyke, F. C. V., and Gauna, M., 1993, "Gob and Gate Road Reaction to Longwall Mining in Bump-Prone Strata," BuMines RI 9445, 48 pp.

Caudle, R. D., and Clark, G. B., 1955, "Stress Around Mine Openings in Some Simple Geologic Structures," Univ. of Ill. Eng. Exp. Stat. Bull., No. 430, 42 pp.

Cook, N. G. W., 1967a, "The Design of Underground Excavations," Proceedings, 8th Symposium on Rock Mechanics, University of Minnesota, AIME, New York, pp. 167-193.

Cook, N. G. W., 1967b, "Contribution to Discussion on Pillar Stability," J. S. Afr. Inst. Min. Metall., 68, pp. 192-195.

Cook, N. G. W., 1978, "Rockburst and Rockfills," Chamber of Mines of S. Afr. Publn No. 216.

Cook, N. G. W., 1983, "Origin of Rockbursts," Rockbursts: Prediction and Control, Institution of Mining and Metallurgy, London, pp. 1-9.

Crouch, S. L., and Fairhurst, C., 1972, "The Mechanics of Coal Bumps and the Interaction Between Coal Pillars, Mine Roof and Floor," Report Research Contract H0101778 to U.S. Bureau of Mines, Washington, DC.

Crouch, S. L., and Fairhurst, C., 1973, "The Mechanics of Coal Mine Bumps," U.S. Bureau of Mines Open File Report 53/73.

Evans, W. H., 1941, "The Strength of Undermined Strata," Trans. Bull. of Inst. Min. and Met., Vol. L, pp. 475-532.

Farmer, I. W., 1985, "Coal Mine Structures," Chapman & Hall, 310 pp.

Fine, J. E., E. Maurin, Michel, B., Sinou, P., Tincelin, E., and Vigier, G., 1964, "Instability of Mine Workings - Bumps, Rockbursts in the Floor and Generalized Collapse," Proceedings, Fourth International Conference of Strata Control and Rock Mechanics, New York, pp. 44-66.

Gay, N., and Ortlepp, W. D., 1979, "Anatomy of a Mining-Induced Fault Zone," Bull. Geo. Soc. Amer., pp. 47-58.

Goode, C. A., Zona, A., and Campoli, A. A., 1984, "Causes and Control of Coal Mine Bumps," Proceedings, 15th Annual Institute on Coal Mining Health, Safety and Research, pp. 155-166.

Hackett, P., 1962, "Rock Mechanics and Mining Engineering," Mine and Quarry Engineering, Vol. 28, No. 5, pp. 215-219.

Haramy, K. Y., Magers, J. A., and McDonnell, J. P., 1988, "Mining Under Strong Roof," Proceedings, 7th International Conference on Ground Control in Mining, West Virginia University, Morgantown, pp. 179-194.

Haramy, K. Y. and McDonnell, J. P., 1988, "Cause and Control of Coal Mine Bumps," BuMines RI 9225, 35 pp.

Heasley, K. A., 1991, "An Examination of Energy Calculations Applied to Coal Bump Prediction," Proceedings, 32nd U.S. Symposium on Rock Mechanics : Rock Mechanics as a Multidisciplinary Science, July, University of Oklahoma, pp. 481-490.

Hetenyi, M., 1946, "Beams on Elastic Foundation," University of Michigan Press, Ann Arbor, Mich., 255 pp.

Holden, W., 1982, "Explosible Dusts," Chap 28, Environmental Engineering in South African Mines, Pub. The Mine Ventilation Society of South Africa, pp. 763-771.

Holland, C. T., 1955, "Rock Burst or Bumps in Coal Mines," Colliery Eng., Apr., pp. 145-153.

Holland, C. T., 1958, "Causes and Occurrence of Coal Mine Bumps," Trans. A.I.M.E., 211, pp. 994-1004B.

Holland, C. T., and Thomas, E., 1954, "Coal Mine Bumps: Some Aspects of Occurrence, Cause, and Control," USBM Bull. 535, 37 pp.

Hopkins, H. G., 1960, "Dynamic Expansion of Spherical Cavities in Metals," Prog. Solid Mech., 1, pp. 84-164.

Hsing, S. M., and Peng, S. S., 1985, "First Caving and its Effects -- A Case Study," Proceedings, 4th Conference on Ground Control in Mining, West Virginia University, Morgantown, pp. 83-93.

Hua, A., 1987, "Rock Burst and Energy Release Rate," Proceedings, 6th International Congress on Rock Mechanics," Montreal, Canada, pp. 971-974.

Iannacchione, A. T. and DeMarco, J. M., 1992, "Optimum Mine Design to Minimize Coal Bumps: a Review of Past and Present U.S. Practice," Proceedings, New Technology in Mine Health and Safety, SME Annual Meeting, Phoenix, Arizona, Feb., pp. 235-247.

Iannacchione, A. T. and Mark, C., 1990, "Possible Mechanism for Surface Vibrations

Near Maxwell Hill, West Virginia," Proceedings, Mine Subsidence - Prediction and Control. 33rd Annual Meeting of Association of Engineering Geologists, Pittsburgh, Pennsylvania, Oct., 20 pp.

Iannacchione, A. T. and Zelanko, J. C., 1995, "Occurrence and Remediation of Coal Mine Bumps: A Historical Review," USBM Special Publication 01-95, pp. 27-67.

Jacobi, O., 1966, "Occurrence, Cause, and Control of Rock Bursts in the Ruhr District," Int. J. Rock. Min. Sci., Vol 3, pp. 205-219.

Jaeger, C., 1979, "Rock Mechanics and Engineering," Cambridge Univ. Press.

Karfakis, M. G., and Wu, X., 1995, "Prediction of Bump Hazards Associated With Coal Mining Under Competent Roofs," Proceedings, 35th U.S. Rock Mechanics Symposium, University of Nevada, Reno, June, pp. 599-604.

Khair, A. W., 1985, "An Analysis of Coal Bump Liability in a Bump Prone Mine," International Journal of Mining Engineering, 3, pp. 243-259.

Kidybinski, A., 1982, "Classification of Rocks for Longwall Caveability," Proceedings, State-of-the-Art of Ground Control in Longwall Mining and Mining Subsidence, ed. by Chugh Y. P. and Karmis M., pp. 31-37.

Kusznir, N. J., 1983, "Rockburst Phenomena in British Coal Mines," Rockbursts: Prediction and Control, Papers Presented at a Symposium organized by the Institution of Mining and Metallurgy in Association with the Institution of Mining Engineers, London, Oct., pp. 103-115.

Lama, R. D., 1966, "Rock Bursts, a Comparison of the in situ Mechanical Properties of Coal Seams," Colliery Engineering, pp. 20-25.

Lama, R. D., Blackwood, R. L., Hebblewhite, B. K., and Bhattacharyya, A. K., 1984, "Monitoring the Effect of Massive Sandstone Roof in a Longwall Operation at West Cliff Colliery," Coal Journal, Aug., pp. 5-15.

Langefors, H., and Kihlstrom, B., 1963, "Rock Blasting," John Willey and Sons, Inc., New York, 425 pp.

Lippmann, H., 1988, "Mechanical Considerations of Bumps in Coal Mines: Keynote Lecture," Proceedings, 2nd International Symposium on Rockbursts and Seismicity In Mines, University of MN, Minneapolis, MN, June, Balkema, 1990, pp. 279-284.

Maleiki, H., 1995, "An Analysis of Violent Failure in U.S. Coal Mines - Case Studies," USBM Special Publication 01-95, pp. 5-25.

Maleiki, H., Aggson, J. R., Miller, F., and Agapito, J. F. T., 1987, "Mine Design Layout for Coal Bump Control," Proceedings, 6th International Conference on Ground Control in Mining, University of West Virginia, Morgantown, WV, June, pp. 32-46.

McGarr, A., 1984, "Some Applications of Seismic Source Mechanism Studies to Assessing Underground Hazard," Rockbursts and Seismicity in Mines, Balkama, pp. 199-208.

McPherson, M. J., 1980, "Air Pressures Developed in Collapsing Workings," Transaction: 2nd International Mine Ventilation Congress, Reno, Nevado, pp. 317-325.

McPherson, M. J., 1995, "The Adiabatic Compression of Air by Large Falls of Roof," Proceedings, 7th U.S. Symposium on Mine Ventilation, Lexington, KY, (in press).

McPherson, M., Wu, X., and Karfakis, M. G., 1995, "The Compression of Air Under Large Falls of Roof," Proceedings, 26th International Conference of Safety in Mines Research Institutes, Katowice, Poland, pp. 145-159.

Mei, J. and Lu, J., 1987, "The Phenomenona, Prediction and Control of Rockbursts in China," Proceedings, Sixth International Congress on Rock Mechanics, Montreal, Canada, pp. 1135-1140.

Naismith, W. A., 1984, "The Influence of Large-scale Surface Blasting on the Stability of Underground Coal Mine Workings," Rockbursts and Seismicity in Mines, Balkama, pp. 183-191.

Napier, J. A. L., 1991, "Energy Changes in a Rockmass Containing Multiple Discontinuities," J. S. Afr. Inst. Min. Metall., Vol. 91, no. 5, pp. 145-157.

Neyman, B., Szecowka, A., and Zuberek, W., 1972, "Effective Methods for Fighting Rock Bursts in Polish Collieries," 5th Int. Strata Control Conf., 9 pp. (preprint).

Obert, L., Duvall, W. L., and Merill, R. H., 1960, "Design of Underground Openings in Competent Rock," USBM Bull. 587.

Ortlepp, W. D., 1983, "The Mechanism and Control of Rockbursts," Rock Mechanics in Mining Practice, Afr. Inst. Min. Metall., Johannesburg, pp. 257-281.

Ortlepp, W. D., 1992, "Note on Fault-slip Motion Inferred from a Study of Microcataclastic Particles from an Underground Shear Rupture," Pure and Appl. Geophys., V. 139, pp. 677-695.

Pappas, D. M., and Mark, C., 1993, "Behavior of Simulated Longwall Gob Material," BuMines RI 9458, 31 pp.

Petukhov, I. M., 1987, "Forecasting and Combating Rockbursts: Recent Developments," Proceedings, Sixth International Congress on Rock Mechanics, Montreal, Canada, pp. 1207-1210.

Phillips, D. W., 1944, Rock Bursts and Bumps in Coal Mines," Trans. Inst. of Mining Eng., 104, pp. 55-84.

Rice, G. S., 1934, "Bumps in Coal Mines of the Cumberland Field, Kentuchy, Virginia - Causes and Remedy," USBM Rept. Invest. 3267, 36 pp.

Richter, C. F., 1956, "Elementary Seismology," W. H. Freeman and Company, San Francisco, California, pp. 338-374.

Rupert, G. B., and Clark, C. B., 1977, "Criterion for the Proximity of Surface Blasting to Underground Coal Mines," Proceedings, 18th US Symposium on Rock Mechanics, pp. 3C310-3C331.

Rzhevsky, V. and Nasik, G., 1971, "The Physics of Rocks," Mir, Moscow, 62 pp.

Salamon, M. D. G., 1974, "Rock Mechanics of Underground Excavations," Proceedings, 3rd Congr. Int. Soc. Rock Mech., Denver, 1B, Nat. Acad. Sci., Washington DC, pp. 951-1099.

Salamon, M. G. D., 1983, "Rockburst Hazard and Fight for its Alleviation in Southern African Goldmine," Rockbursts: Prediction and Control, Institution of Mining and Metallurgy, London, pp. 11-36.

Salamon, M. G. D., 1984, "Energy Considerations in Rock Mechanics: Fundamental Results," J. S. Afr. Inst. Min. Metall., Vol. 84, No. 8, pp. 223-246.

Sames, G. P., 1995, "Bump Hazard Criteria Derived From Basic Geologic Data," USBM Special Publication 01-95, pp. 69-89.

Schofield, A. N., and Wroth, C. P., 1968, "Critical State Soil Mechanics," McGraw-hall, London.

Seedsman, R., 1987, "Back-analysis of Roof Conditions in the Great Northern Seam, Newcastle Coal Measures, Australia, Using Voussoir Beam Theory," International Journal of Mining and Geological Engineering, 5, pp. 15-27.

Sibol, M. S., Bollinger, G. A., and Birch, J. B., 1987, "Estimation of Magnitude in Central and Eastern North America Using Intensity and Felt Area," Bulletin, the Seismological Society of America, Vol. 77, No. 5, pp. 1635-1654.

Singh, T. N. and Dubey, B. K., 1994, "Caveability Study of a Competent Roof - A Case

Study," <u>Proceedings</u>, 13th Conference on Ground Control in Mining, West Virginia University, Morgantown, WV, pp. 121-129.

Singh, J. G., Upadhway, P. C., and Saluja, S. S., 1980, "The Bending of Rock Plates," <u>Int. J. Rock Mech. Min. Sci. & Geomech. Abstr.</u>, Vol. 17, pp. 377-381.

Song, Z. C., Deng, T. L., Liu, Y. S., Zhen, M. K., Chen, M. B., Lin, Z. Y., Yu, L. Z., and Song, Y., 1982, "Manifestation of Mine Pressure and Its Relations to Overlying Strata Movements," <u>Proceedings</u>, 2nd Conference on Ground Control in Mining, ed. by S. S. Peng and Jay H. Kelley, July 19-21, West Virginia University, Morgantown, WV, pp. 22-35.

Song, Y. and Xu, L., 1992, "Study of the Impact of Mining Under Massive Roof at Datong Coal Mines, China," <u>Proceedings</u>, 11th International Conference. on Ground Control in Mining, University of Wollongong, Wollongong, NSW, Australia, July, pp. 540-547.

Stephansson, O., 1971, "Stability of Single Opening in Horizontally Bedded Rock," <u>Engineering Geology</u>, 5, pp. 5-71.

Sterling, R. L., 1980, "The Ultimate Load Behaviour of Laterally Constrained Rock Beams," In The State of the Art in rock Mechanics, <u>Proceedings</u>, 21st US Symp. Rock Mech., Rolla: University of Missouri, pp. 533-542.

Sugawara, K., Kaneko, K., Obara, Y., and Aoki, T., 1987, "Prediction of Coal Outburst," <u>Proceedings</u>, Sixth International Congress on Rock Mechanics, Montreal, Canada, pp. 1251-1254.

Talman, W. G., and Shrooder, J. L., 1958, "Control of Maintain Bumps in the Pocahontas No. 4 Seam," <u>Trans. Soc. Min. Eng.</u>, AIME, Vol. 211, pp. 888-891.

Timoshenko, S. P., 1983, "Strength of Materials, Part II, Advanced Theory and Problems," <u>Robert E. Krieger Publishing Company</u>, Malabar, Florida, pp. 1-15, 346-386.

Timoshenko, S. P., and Goodier, J. N., 1970, "Theory of Elasticity," <u>John Wiley & Sons, Inc</u>.

Unrug, K. F., 1982, "Roof Falls and Caving in Longwall Mining Operations," <u>Proceedings</u>, 2nd Conference on Ground Control in Mining, ed. by S. S. Peng and Jay H. Kelley, July 19-21, West Virginia University, Morgantown, WV, pp. 45-52.

Walsh, J. B., 1977, "Energy Changes due to Mining," <u>Int. J. Rock. Mech. Min. Sci. and Geomech. Abstr.</u>, Vol. 14, pp. 25-33.

Wilson, A. H., 1986, "Keynote Address: the Problems of Strong Roof Beds and Water Bearing Strata in the Control of Longwall Faces," Proceedings, Ground Movement and Control Related to Coal Mining, pp. 1-8.

Wright, F. D., 1974, "Design of Roof Bolt Patterns for Jointed Rock," USBM Open File Report 61-75.

Wu, X., and Karfakis M. G., 1993a, "Mathematical Modeling of Strong Roof Beds in Longwall Mining," Proceedings, 12th International Conference on Ground Control in Mining, West Virginia University, Morgantown, pp. 175-183.

Wu, X., and Karfakis, M. G., 1993b, "Critical Spans Determination for Strong Roof Beds in Longwall Mining," Proceedings, 11th Annual Workshop, Generic Mineral Technology Center, Mine Systems Design and Ground Control, University of Alabama, Tuscaloosa, pp. 133-146.

Wu, X., and Karfakis, M. G., 1994a, "An Analysis of Strain Energy Accumulation Around Longwall Panels Under Strong Roofs," Proceedings, 5th Conference on Ground Control for Midwestern U.S. Coal Mines, Collinsville, Illinois, pp. 230-253.

Wu, X., and Karfakis, M. G., 1994b, "A Proposed Method to Evaluate the Impact of Strong Roofs in Longwall Mining," Proceedings, 12th Annual Workshop, Generic Mineral Technology Center, Mine Systems Design and Ground Control, University of Alaska, Fairbanks, pp. 67-78.

Wu, X., Karfakis, M. G., Haramy, K. Y., and Brady, B. T., 1995, "Ground Motion Parameters Associated with Coal Mine Tremors," 1995 Annual Meeting of SME, Denver, Colorado, Preprint Number 95-49, 9 pp.

Yu, C., and Xian, X., 1991, "Numerical Analyses for Latent Energy of Outbursts in Coal Seams," Proceedings, 7th International Conference Computer Methods and Advances in Geomechanics, Balkema, Rotterdam, pp. 1429-1433.

Zipf, R. K., Jr., and K. A. Heasley, 1990, "Decreasing Coal Bump Risk Through Optimal Cut Sequencing With a Non-linear Boundary Element Program," Proceedings, 31st U.S. Symposium on Rock Mechanics: Rock Mechanics Contributions and Challenges, Colorado School of Mines, Golden, CO, June, Balkema, pp. 947-954.

Zou, D., Miller, H. D. S., 1987, "A Proposed Mechanism of Rock Failure and Rockbursting," Proceedings, Sixth International Congress on Rock Mechanics, Montreal, Canada, pp. 971-974.

APPENDIX   COAL BUMP POTENTIAL EVALUATION
PROGRAM (Visual Basic Version 3.0)

beam.bas

```
'Global variable definition section.
Global Model_Type
Global Span
Global Roof_Energy
Global Foundation_Energy
Global Total_Energy
Global Richter_Scale
Global Foundation_Stress
Global Seismic_Ratio
Global C0
Global W

'Local variable definition section.
Dim Eav, Iav, Dav, T0, h1, Hr, d2, Eav1, Eav2
Dim P, Pmax, f, r, L
Dim C, Ee, Ve, He
Dim alpha, beta
Dim S, H0

Sub alpha_beta ()
    'Evaluate alpha and beta values.
    alpha = Pmax / (Dav * f ^ 4 + C)
    beta = (C / (4 * Dav)) ^ .25
End Sub

Sub bridge_energy ()
    'Calculate the Q value.
    Q = (Dav * alpha * f ^ 3 - P * Span) / (2 * Dav * beta ^ 3)
    'Calculate initial values y0, y01, A1, and A2.
```

Term1 = P * Span ^ 3 / (48 * Dav)
Term2 = -1 / 8 * (alpha * f ^ 3 - 2 * beta ^ 3 * Q) * Span ^ 2
Term3 = Span * (alpha * f ^ 2 / 2 - alpha * beta ^ 2 + Q * beta ^ 2)
Term4 = -alpha * f - beta * (2 * alpha - Q)
y0 = -(Term1 + Term2 + Term3 + Term4) / (beta * (Span * beta + 2))
y01 = alpha * f - beta * (2 * y0 - 2 * alpha + Q)
A1 = (y01 - alpha * f) / beta + y0 - alpha
A2 = y0 - alpha
'Calculate strain energy stored in supported part of the roof beam, Wr1.
C1 = -2 * Dav * alpha * f ^ 2 * beta ^ 2
C1 = C1 / (f ^ 2 - 2 * f * beta + 2 * beta ^ 2)
C2 = -.25 * Dav * beta ^ 3
C3 = -.25 * Dav * alpha ^ 2 * f ^ 3
C4 = .5 * Dav * beta ^ 3 * (A1 ^ 2 + A2 ^ 2)
C5 = C1 * (beta * A1 - A1 * f - beta * A2)
C6 = C2 * (A2 ^ 2 - A1 ^ 2 + 2 * A1 * A2)
CC = C3 + C4 + C5 + C6
F1 = -C1 * (f * A2 - beta * A2 - beta * A1)
F2 = -C1 * (beta * A1 - beta * A2 - f * A1)
F3 = -C2 * (A2 ^ 2 - A1 ^ 2 + 2 * A1 * A2)
F4 = -C2 * (A1 ^ 2 + 2 * A1 * A2 - A2 ^ 2)
F5 = 2 * C2 * (A1 ^ 2 + A2 ^ 2)
Var1 = Exp((f - beta) * L) * Sin(beta * L)
Var2 = Exp((f - beta) * L) * Cos(beta * L)
Var3 = Exp(-2 * beta * L) * Cos(2 * beta * L)
Var4 = Exp(-2 * beta * L) * Sin(2 * beta * L)
Sum1 = -C3 * Exp(2 * f * L) + F1 * Var1 + F2 * Var2 + F3 * Var3
Sum2 = F4 * Var4 + F5 * Exp(-2 * beta * L) + CC
Wr1 = Sum1 + Sum2
'Calculate strain energy stored in unsupported part of the roof beam, Wr2.
Term5 = (y01 - alpha * f) / beta + 2 * y0 - alpha
Term6 = (y01 - alpha * f) / beta + y0 - alpha
K1 = alpha * f ^ 3 / 6 + Term5 * beta ^ 3 / 3
K2 = alpha * f ^ 2 / 2 - beta ^ 2 * Term6
Sum3 = P ^ 2 * Span ^ 5 / (40 * Dav) - 3 / 4 * P * K1 * Span ^ 4
Sum4 = 1 / 6 * (2 * P * K2 + 36 * K1 ^ 2 * Dav) * Span ^ 3
Sum5 = -6 * K1 * K2 * Dav * Span ^ 2 + 2 * K2 ^ 2 * Dav * Span
Wr2 = Sum3 + Sum4 + Sum5
'Calculate strain energy in roof beam, Roof_Energy in MJ.
Roof_Energy = (2 * Wr1 + Wr2) * W / 10 ^ 6
'Calculate strain energy stored in foundation, Foundation_Energy in MJ.
G1 = He * C * C * (1 - Ve - 2 * Ve * Ve) / (2 * Ee * (1 - Ve))
G2 = -2 * alpha / (f * f - 2 * f * beta + 2 * beta ^ 2)

219

```
    G3 = -alpha ^ 2 / (2 * f)
    G4 = .25 * (A1 ^ 2 + A2 ^ 2) / beta
    G5 = G2 * (f * A2 - beta * A2 - beta * A1)
    G6 = (A2 ^ 2 - A1 ^ 2 + 2 * A1 * A2) / (8 * beta)
    G7 = G2 * (beta * A2 + f * A1 - beta * A1)
    G8 = (A2 ^ 2 - A1 ^ 2 - 2 * A1 * A2) / (8 * beta)
    GG = G3 + G4 + G5 + G6
    Sum6 = -G3 * Exp(2 * f * L) - G4 * Exp(-2 * beta * L)
    Sum7 = -G5 * Var2 - G6 * Var3 - G7 * Var1 + G8 * Var4
    Foundation_Energy = 2 * G1 * W * (Sum6 + Sum7 + GG) / 10 ^ 6
    'Calculate total strain energy, Total_Energy.
    Total_Energy = Roof_Energy + Foundation_Energy
    'Calculate the local Richter Magnitude, Richter_Scale.
    Richter_Scale = (Log(10 ^ 13 * Seismic_Ratio * Total_Energy)
    / 2.302585 - 11.8) / 1.5
    'Calculate maximum foundation stress in MPa.
    Foundation_Stress = Ee * y0 / (He * 10 ^ 6)
End Sub


Sub bridge_span ()
    'Determine the critical spans of bridging roof beds.
    A1 = P * beta ^ 2
    A2 = 6 * P * beta
    Select Case Model_Type
        Case 2, 6
            A3 = 12 * P - 24 * beta ^ 2 * T0 * Iav / h1
            A4 = -48 * beta * T0 * Iav / h1
        Case 4, 8
            If Eav1 < Eav2 Then
                A3 = 12 * P - 24 * beta ^ 2 * T0 * Iav / (Hr - d2)
                A4 = -48 * beta * T0 * Iav / (Hr - d2)
            ElseIf Eav1 > Eav2 Then
                A3 = 12 * P - 24 * beta ^ 2 * T0 * Iav / d2
                A4 = -48 * beta * T0 * Iav / d2
            Else
                A3 = 12 * P - 24 * beta ^ 2 * T0 * Iav / (.5 * Hr)
                A4 = -48 * beta * T0 * Iav / (.5 * Hr)
            End If
    End Select
    A2 = A2 / A1
    A3 = A3 / A1
    A4 = A4 / A1
    A1 = A1 / A1
```

```
    Span = 0#
    Span = solution(A1, A2, A3, A4, Span)
End Sub


Sub cantilever_energy ()
    'Evaluate bending moment M0 and shear force V0 at x = 0.
    M0 = -P * Span * Span / 2
    V0 = -P * Span
    'Calculate initial values y0, y01,A1, and A2.
    C1 = alpha * (1 - (f ^ 3 + f * f * beta) / (2 * beta ^ 3))
    C2 = alpha * f * (1 + (f ^ 2 + 2 * beta * f) / (2 * beta ^ 2))
    y0 = C1 - (V0 + beta * M0) / (2 * Dav * beta ^ 3)
    y01 = C2 + (V0 + 2 * beta * M0) / (2 * Dav * beta ^ 2)
    A1 = (y01 - alpha * f) / beta + y0 - alpha
    A2 = y0 - alpha
    'Calculate strain energy stored in supported part of the roof beam, Wr1.
    C3 = -2 * Dav * alpha * f ^ 2 * beta ^ 2
    C3 = C3 / (f ^ 2 - 2 * f * beta + 2 * beta ^ 2)
    C4 = -.25 * Dav * beta ^ 3
    C5 = -.25 * Dav * alpha ^ 2 * f ^ 3
    C6 = .5 * Dav * beta ^ 3 * (A1 ^ 2 + A2 ^ 2)
    C7 = C3 * (beta * A1 - A1 * f - beta * A2)
    C8 = C4 * (A2 ^ 2 - A1 ^ 2 + 2 * A1 * A2)
    CC = C5 + C6 + C7 + C8
    F1 = -C3 * (f * A2 - beta * A2 - beta * A1)
    F2 = -C3 * (beta * A1 - beta * A2 - f * A1)
    F3 = -C4 * (A2 ^ 2 - A1 ^ 2 + 2 * A1 * A2)
    F4 = -C4 * (A1 ^ 2 + 2 * A1 * A2 - A2 ^ 2)
    F5 = 2 * C4 * (A1 ^ 2 + A2 ^ 2)
    Var1 = Exp((f - beta) * L) * Sin(beta * L)
    Var2 = Exp((f - beta) * L) * Cos(beta * L)
    Var3 = Exp(-2 * beta * L) * Cos(2 * beta * L)
    Var4 = Exp(-2 * beta * L) * Sin(2 * beta * L)
    Sum1 = -C5 * Exp(2 * f * L) + F1 * Var1 + F2 * Var2 + F3 * Var3
    Sum2 = F4 * Var4 + F5 * Exp(-2 * beta * L) + CC
    Wr1 = Sum1 + Sum2
    'Calculate strain energy stored in unsupported part of roof beam, Wr2.
    Wr2 = P * P * Span ^ 5 / (40 * Dav)
    'Calculate strain energy in roof beam, Roof_Energy in MJ.
    Roof_Energy = W * (Wr1 + Wr2) / 10 ^ 6
    'Calculate strain energy in foundation, Foundation_Energy in MJ.
    G1 = C * C * (1 - Ve - 2 * Ve ^ 2) / (2 * Ee * (1 - Ve))
    G2 = -2 * alpha / (f * f - 2 * f * beta + 2 * beta ^ 2)
```

```
        G3 = -alpha ^ 2 / (2 * f)
        G4 = .25 * (A1 ^ 2 + A2 ^ 2) / beta
        G5 = G2 * (f * A2 - beta * A2 - beta * A1)
        G6 = (A2 ^ 2 - A1 ^ 2 + 2 * A1 * A2) / (8 * beta)
        G7 = G2 * (beta * A2 + f * A1 - beta * A1)
        G8 = (A2 ^ 2 - A1 ^ 2 - 2 * A1 * A2) / (8 * beta)
        GG = G3 + G4 + G5 + G6
        Sum3 = -G3 * Exp(2 * f * L) - G4 * Exp(-2 * beta * L)
        Sum4 = -G5 * Var2 - G6 * Var3 - G7 * Var1 + G8 * Var4
        Foundation_Energy = W * He * G1 * (Sum3 + Sum4 + GG) / 10 ^ 6
        'Calculate total strain energy, Total_Energy.
        Total_Energy = Roof_Energy + Foundation_Energy
        'Calculate the local Richter Magnitude, Richter_Scale.
        Richter_Scale = (Log(10 ^ 13 * Seismic_Ratio * Total_Energy)
        / 2.302585 - 11.8) / 1.5
        'Calculate the maximum foundation stress in MPa.
        Foundation_Stress = Ee * y0 / (He * 10 ^ 6)
End Sub


Sub cantilever_span ()
    'Determine the critical spans of cantilevering roof beds.
    Select Case Model_Type
        Case 1, 5                       'Single-layer cantilevering roof.
            Span = Sqr((2 * Iav * T0) / (P * h1))
        Case 3, 7                       'Double-layer cantilevering roof.
            If Eav1 < Eav2 Then
                Span = Sqr(2 * Iav * T0 / (P * (Hr - d2)))
            ElseIf Eav1 > Eav2 Then
                Span = Sqr(2 * Iav * T0 / (P * d2))
            Else
                Span = Sqr(2 * Iav * T0 / (P * Hr / 2))
            End If
        Case Else
            Msg = "Critical span can not be determined !"
            MsgBox Msg
    End Select
End Sub


Sub foundation_property1 ()
    Select Case Model_Type
        Case 1, 2
            'Assign foundation parameters for Model 1 and Model 2.
            Ee = Val(frmInput1!txtText(4)) * 10 ^ 9 'Young's modulus of foundation.
```

```
        Ve = Val(frmInput1!txtText(5))      'Poisson's ratio of foundation.
        C0 = Val(frmInput1!txtText(6)) * 10 ^ 6 'Compressive strength of foundation.
        He = Val(frmInput1!txtText(7))      'Foundation thickness.
    Case 3, 4
        'Assign foundation parameters for Model 3 and Model 4.
        Ee = Val(frmInput2!txtText(7)) * 10 ^ 9 'Young's modulus of foundation.
        Ve = Val(frmInput2!txtText(8))      'Poisson's ratio of foundation.
        C0 = Val(frmInput2!txtText(9)) * 10 ^ 6 'Compressive strength of foundation.
        He = Val(frmInput2!txtText(10))     'Foundation thickness.
    End Select
    'Evaluate foundation property C for Models 1, 2, 3, 4.
    C = Ee / (He * (1 - Ve * Ve))
End Sub

Sub foundation_property2 ()
    Select Case Model_Type
    Case 5, 6
        'Assign foundation parameters for Model 5 and Model 6.
        Ee1 = Val(frmInput3!txtText(4)) * 10 ^ 9    'Young's modulus of coal seam.
        Ee2 = Val(frmInput3!txtText(5)) * 10 ^ 9    'Young's modulus of weak roof.
        Ve1 = Val(frmInput3!txtText(6))      'Poisson's ratio of coal seam.
        Ve2 = Val(frmInput3!txtText(7))      'Poisson's ratio of weak roof.
        C01 = Val(frmInput3!txtText(8)) * 10 ^ 6    'Compressive strength of coal seam.
        C02 = Val(frmInput3!txtText(9)) * 10 ^ 6    'Compressive strength of weak roof.
        He1 = Val(frmInput3!txtText(10))      'Thickness of coal seam.
        He2 = Val(frmInput3!txtText(11))      'Thickness of weak roof.
    Case 7, 8
        'Assign foundation parameters for Model 7 and Model 8.
        Ee1 = Val(frmInput4!txtText(7)) * 10 ^ 9    'Young's modulus of coal seam.
        Ee2 = Val(frmInput4!txtText(8)) * 10 ^ 9    'Young's modulus of weak roof.
        Ve1 = Val(frmInput4!txtText(9))      'Poisson's ratio of coal seam.
        Ve2 = Val(frmInput4!txtText(10))      'Poisson's ratio of weak roof.
        C01 = Val(frmInput4!txtText(11)) * 10 ^ 6  'Compressive strength of coal seam.
        C02 = Val(frmInput4!txtText(12)) * 10 ^ 6  'Compressive strength of weak roof.
        He1 = Val(frmInput4!txtText(13))      'Thickness of coal seam.
        He2 = Val(frmInput4!txtText(14))      'Thickness of weak roof.
    End Select
    'Evaluate equivalent foundation properties for Models 5, 6, 7, 8.
    He = He1 + He2
    Ee = He * Ee1 * Ee2 / (He1 * Ee2 + He2 * Ee1)
    Temp = He * Ee1 * Ee2 * (Ve1 * He1 + Ve2 * He2)
    Ve = Temp / ((He1 * Ee2 + He2 * Ee1) * (He1 * Ee1 + He2 * Ee2))
    C = Ee / (He * (1 - Ve * Ve))
```

223

```
      C0 = C01
End Sub

Sub main ()
   Const MB_OK = 0                'Define buttons.
   Const MB_ICONSTOP = 16          'Define Icons.
   Dim DgDef, Response, Msg, Title    'Declare variables.
   DgDef = MB_ICONSTOP              'Describe dialog.
   Title = "Roof Span Error"
   'Get input of roof parameters.
   'Evaluate equivalent roof properties Eav, Iav, and Dav.
   Select Case Model_Type
      Case 1, 2, 5, 6          'Single-layer roof.
         Call roof_property1
      Case 3, 4, 7, 8          'Double-layer roof.
         Call roof_property2
      Case Else
         Msg = "Roof parameter input error !"
         MsgBox Msg
   End Select
   'Get input of foundation parameters.
   'Evaluate equivalent foundation properties c, Ee, and Ve.
   Select Case Model_Type
      Case 1, 2, 3, 4            'Single-layer foundation.
         Call foundation_property1
      Case 5, 6, 7, 8            'Double-layer foundation.
         Call foundation_property2
   End Select
   'Get input of overburden and abutment stress parameters.
   Call stress
   'Evaluate alpha and beta values.
   Call alpha_beta
   'Determine the critical spans of roof beds.
   Select Case Model_Type
      Case 1, 3, 5, 7            'Cantilevering roof beam.
         Call cantilever_span
      Case 2, 4, 6, 8            'Bridging roof beam.
         Call bridge_span
         If Span <= 0# Then
            Msg = "The critical span of roof beds can not be determined !"
            Response = MsgBox(Msg, DgDef, Title)
            Exit Sub
         End If
```

```
        Case Else
            Msg = "Roof type error !"
            MsgBox Msg
        End Select
        'Evaluate strain energies stored in roof and foundation.
        Select Case Model_Type
            Case 1, 3, 5, 7              'Cantilevering roof beam.
                Call cantilever_energy
            Case 2, 4, 6, 8             'Bridging roof beam.
                Call bridge_energy
        End Select
End Sub

Sub roof_property1 ()
    Select Case Model_Type
        Case 1, 2
            'Assign roof parameters for Model 1 or Model 2.
            Ec = Val(frmInput1!txtText(0)) * 10 ^ 9   'Young's modulus in compression.
            Et = Val(frmInput1!txtText(1)) * 10 ^ 9    'Young's modulus in tension.
            Hr = Val(frmInput1!txtText(2))             'Roof thickness.
            T0 = Val(frmInput1!txtText(3)) * 10 ^ 6   'Tensile strength of roof bed.
        Case 5, 6
            'Assign roof parameters for Model 5 and Model 6.
            Ec = Val(frmInput3!txtText(0)) * 10 ^ 9   'Young's modulus in compression.
            Et = Val(frmInput3!txtText(1)) * 10 ^ 9    'Young's modulus in tension.
            Hr = Val(frmInput3!txtText(2))             'Roof thickness.
            T0 = Val(frmInput3!txtText(3)) * 10 ^ 6   'Tensile strength of roof bed.
    End Select
    'Evaluate equivalent roof properties Eav, Iav, and Dav
    'and neutral axis position h1 for Models 1, 2, 5, 6.
    h1 = (Hr * Sqr(Ec)) / (Sqr(Et) + Sqr(Ec))
    Eav = 4 * Et * Ec / (Sqr(Et) + Sqr(Ec)) ^ 2
    Iav = h1 ^ 3 * (Sqr(Et) + Sqr(Ec)) / (3 * Sqr(Ec))
    Dav = Eav * Iav
End Sub

Sub roof_property2 ()
    Select Case Model_Type
        Case 3, 4
            'Assign roof parameters for Model 3 and Model 4.
            Ec1 = Val(frmInput2!txtText(0)) * 10 ^ 9   'Young's modulus in compression
                                                        'of upper layer.
            Ec2 = Val(frmInput2!txtText(1)) * 10 ^ 9   'Young's modulus in compression
```

225

```
                                                             'of lower layer.
       Et1 = Val(frmInput2!txtText(2)) * 10 ^ 9    'Young's modulus in tension of
                                                             'upper layer.
       Et2 = Val(frmInput2!txtText(3)) * 10 ^ 9    'Young's modulus in tension of
                                                             'lower layer.
       Hf1 = Val(frmInput2!txtText(4))             'Roof thickness of upper layer.
       Hf2 = Val(frmInput2!txtText(5))             'Roof thickness of lower layer.
       T0 = Val(frmInput2!txtText(6)) * 10 ^ 6     'Tensile strength of lower layer.
   Case 7, 8
     'Assign roof parameters for Model 7 and Model 8.
       Ec1 = Val(frmInput4!txtText(0)) * 10 ^ 9    'Young's modulus in compression
                                                             'of upper layer.
       Ec2 = Val(frmInput4!txtText(1)) * 10 ^ 9    'Young's modulus in compression
                                                             'of lower layer.
       Et1 = Val(frmInput4!txtText(2)) * 10 ^ 9    'Young's modulus in tension of
                                                             'upper layer.
       Et2 = Val(frmInput4!txtText(3)) * 10 ^ 9    'Young's modulus in tension of
                                                             'lower layer.
       Hf1 = Val(frmInput4!txtText(4))             'Roof thickness of upper layer.
       Hf2 = Val(frmInput4!txtText(5))             'Roof thickness of lower layer.
       T0 = Val(frmInput4!txtText(6)) * 10 ^ 6     'Tensile strength of lower layer.
End Select
'Evaluate equivalent roof properties Eav, Iav, and Dav
'and neutral axis position h1 for Models 3, 4, 7, 8.
Eav1 = 4 * Et1 * Ec1 / (Sqr(Et1) + Sqr(Ec1)) ^ 2
Eav2 = 4 * Et2 * Ec2 / (Sqr(Et2) + Sqr(Ec2)) ^ 2
Hr = Hf1 + Hf2
Temp = Eav1 / Eav2
temp1 = (Temp * Hr ^ 2 + (1 - Temp) * Hf2 ^ 2)
temp2 = 2 * (Temp * Hr + (1 - Temp) * Hf1)
d2 = temp1 / temp2
If Eav1 < Eav2 Then
   Eav = Eav2
   D = Hf1 - d2
   Iav = ((Hr - d2) ^ 3 - (1 - Temp) * D ^ 3 + Temp * d2 ^ 3)
ElseIf Eav1 > Eav2 Then
   Eav = Eav1
   D = Hf2 - d2
   Iav = ((Hr - d2) ^ 3 - (1 - Temp) * D ^ 3 + Temp * d2 ^ 3)
Else
   Eav = Eav1
   Iav = Hr ^ 3 / 12
End If
```

```
      Dav = Eav * Iav
   End Sub
   Function solution (A, B, C, D, Span)
      x = 100
      For j = 1 To 1000
         sum = 0
         psum = 0
         sum = sum + A * x ^ 3 + B * x ^ 2 + C * x + D
         psum = psum + 3 * A * x ^ 2 + 2 * B * x + C
         If Abs(sum) <= .1 Then
            solution = x
            Exit Function
         ElseIf psum = 0 Then
            solution = 0#
            Exit Function
         Else
            x = x - sum / psum
         End If
      Next
   End Function


   Sub stress ()
      Select Case Model_Type
         Case 1, 2                       'Model 1 and Model 2.
            'Assign overburden properties.
            H0 = Val(frmInput1!txtText(8))        'Overburden depth.
            S = Val(frmInput1!txtText(9))         'Specific gravity of overburden.
            'Assign abutment stress characteristics.
            r = Val(frmInput1!txtText(10))        'Abutment stress concentration ratio.
            L = Val(frmInput1!txtText(11))        'Stress concentration length.
            'Assign width of longwall face.
            W = Val(frmInput1!txtText(12))        'Width of longwall face.
            'Assign seimic efficiency.
            Seismic_Ratio = Val(frmInput1!txtText(13)) 'Seismic efficiency.
         Case 3, 4                       'Model 3 and Model 4.
            'Assign overburden properties.
            H0 = Val(frmInput2!txtText(11))       'Overburden depth.
            S = Val(frmInput2!txtText(12))        'Specific gravity of overburden.
            'Assign abutment stress characteristics.
            r = Val(frmInput2!txtText(13))        'Abutment stress concentration ratio.
            L = Val(frmInput2!txtText(14))        'Stress concentration length.
            'Assign width of longwall face.
            W = Val(frmInput2!txtText(15))        'Width of longwall face.
```

```vb
                'Assign seimic efficiency.
                Seismic_Ratio = Val(frmInput2!txtText(16))  'Seismic efficiency.
        Case 5, 6                        'Model 5 and Model 6.
                'Assign overburden properties.
                H0 = Val(frmInput3!txtText(12))          'Overburden depth
                S = Val(frmInput3!txtText(13))           'Specific gravity of overburden.
                'Assign abutment stress characteristics.
                r = Val(frmInput3!txtText(14))           'Abutment stress concentration ratio.
                L = Val(frmInput3!txtText(15))           'Stress concentration length.
                'Assign width of longwall face.
                W = Val(frmInput3!txtText(16))           'Width of Longwall face.
                'Assign seimic efficiency.
                Seismic_Ratio = Val(frmInput3!txtText(17))  'Seismic efficiency.
        Case 7, 8                        'Model 7 and Model 8.
                'Assign overburden properties.
                H0 = Val(frmInput4!txtText(15))          'Overburden depth.
                S = Val(frmInput4!txtText(16))           'Specific gravity of overburden.
                'Assign abutment stress characteristics.
                r = Val(frmInput4!txtText(17))           'Abutment stress concentration ratio.
                L = Val(frmInput4!txtText(18))           'Stress concentration length.
                'Assign width of longwall face.
                W = Val(frmInput4!txtText(19))           'Width of Longwall face.
                'Assign seimic efficiency.
                Seismic_Ratio = Val(frmInput4!txtText(20))  'Seismic efficiency.
        Case Else
                Msg = "Stress parameter input error."
                MsgBox Msg
    End Select
    'Calculate the overburden pressure P, maximum abutment pressure
    'Pmax, and load characterics f.
    P = S * H0
    Pmax = P * r
    f = Log(1 / r) / L
End Sub



start.frm


Sub cmdContinue_Click ()
    'Hide the start up screen.
    frmStart.Hide
    'Show the model form and prompt user to choose a roof model.
```

```
        frmClaim.Show
    End Sub

    Sub cmdExit_Click ()
        'End the execution of the program.
        End
    End Sub

    Sub cmdHelp_Click ()
        'Show a help screen that describes the general information about the program.
        frmStart.Hide
        frmHelp1.Show
    End Sub
```

claim.frm

```
    Sub cmdAccept_Click ()
        frmClaim.Hide
        frmInfo.Show
    End Sub

    Sub cmdReject_Click ()
        frmClaim.Hide
        frmStart.Show
    End Sub
```

help1.frm

```
    Sub cmdExit_Click ()
        frmHelp1.Hide
        frmStart.Show
    End Sub

    Sub cmdPrint_Click ()
        PrintForm
    End Sub
```

help2.frm

```
Sub cmdExit_Click ()
    'Hide the current help form.
    frmHelpInput.Hide
End Sub

Sub cmdPrint_Click (Index As Integer)
    PrintForm
End Sub
```

help3.frm

```
Sub cmdExit_Click ()
    'Hide the current help form and show the previous form.
    frmHelpOutput.Hide
    frmOutput.Show
End Sub

Sub cmdPrint_Click (Index As Integer)
    PrintForm
End Sub
```

info.frm

```
Sub cmdBack_Click (Index As Integer)
    frmInfo.Hide
    frmClaim.Show
End Sub

Sub cmdContinue_Click (Index As Integer)
    frmInfo.Hide
    frmModel1.Show
End Sub

Sub cmdExit_Click (Index As Integer)
    End
End Sub
```

```
Sub cmdPrint_Click (Index As Integer)
    PrintForm
End Sub


input1.frm


Sub cmdBack_Click ()
    'Hide the input screen and show the model form frmModel 1.
    Model_Type = 0
    frmInput1.Hide
    frmModel1.Show
End Sub

Sub cmdExit_Click ()
    'End the excution of the program.
    End
End Sub

Sub cmdHelp_Click ()
    'Show a help form that describes the input parameter.
    frmHelpInput.Show
End Sub

Sub cmdOutput_Click ()
    'Input error-checking section.
    Const MB_OK = 0                    'Define buttons.
    Const MB_ICONSTOP = 16             'Define Icons.
    Dim DgDef, Response, Msg, Title    'Declare variables.
    Title = "Input Error"
    DgDef = MB_ICONSTOP                'Describe dialog.
    Title = "Input Error"
    par = Val(txtText(0))
    Msg = "Check input -- Roof Parameter: Young's modulus in compression."
        If par <= 0 Then
            Response = MsgBox(Msg, DgDef, Title)
            Exit Sub
        End If
    par = Val(txtText(1))
    Msg = "Check input -- Roof Parameter: Young's modulus in tension."
        If par <= 0 Then
            Response = MsgBox(Msg, DgDef, Title)
```

```
            Exit Sub
        End If
par = Val(txtText(2))
Msg = "Check input -- Roof Parameter: thickness."
        If par <= 0 Then
            Response = MsgBox(Msg, DgDef, Title)
            Exit Sub
        End If
par = Val(txtText(3))
Msg = "Check input -- Roof Parameter: effective tensile strength."
        If par <= 0 Then
            Response = MsgBox(Msg, DgDef, Title)
            Exit Sub
        End If
par = Val(txtText(4))
Msg = "Check input -- Coal Parameter: Young's modulus."
        If par <= 0 Then
            Response = MsgBox(Msg, DgDef, Title)
            Exit Sub
        End If
par = Val(txtText(5))
Msg = "Check input -- Coal Parameter: Poisson's ratio."
        If par <= 0 Or par > 1# Then
            Response = MsgBox(Msg, DgDef, Title)
            Exit Sub
        End If
par = Val(txtText(6))
Msg = "Check input -- Coal Parameter: compressive strength."
        If par <= 0 Then
            Response = MsgBox(Msg, DgDef, Title)
            Exit Sub
        End If
par = Val(txtText(7))
Msg = "Check input -- Coal Parameter: thickness."
        If par <= 0 Then
            Response = MsgBox(Msg, DgDef, Title)
            Exit Sub
        End If
par = Val(txtText(8))
Msg = "Check input -- Other Parameter: overburden depth."
        If par <= 0 Then
            Response = MsgBox(Msg, DgDef, Title)
            Exit Sub
```

```
        End If
    par = Val(txtText(9))
    Msg = "Check input -- Other Parameter: specific gravity of overburden."
        If par <= 0 Then
            Response = MsgBox(Msg, DgDef, Title)
            Exit Sub
        End If
    par = Val(txtText(10))
    Msg = "Check input -- Other Parameter: abutment stress concentration (> 1.0)."
        If par < 1 Then
            Response = MsgBox(Msg, DgDef, Title)
            Exit Sub
        End If
    par = Val(txtText(11))
    Msg = "Check input -- Other Parameter: stress concentration length."
        If par <= 0 Then
            Response = MsgBox(Msg, DgDef, Title)
            Exit Sub
        End If
    par = Val(txtText(12))
    Msg = "Check input -- Other Parameter: width of working face."
        If par <= 0 Then
            Response = MsgBox(Msg, DgDef, Title)
            Exit Sub
        End If
    par = Val(txtText(13))
    Msg = "Check input -- Other Parameter: seismic efficiency (0 < n <= 1.0)."
        If par <= 0 Or par > 1# Then
            Response = MsgBox(Msg, DgDef, Title)
            Exit Sub
        End If
    'Hide the present input form, show the output form.
    frmInput1.Hide
    frmOutput.txtCase = frmInfo.txtInfo(0)
    If Model_Type = 1 Then
        frmOutput.lblTitle.Caption = "Analysis Results: Single Layer Cantilevering Roof -
Single Layer Foundation"
    Else
        frmOutput.lblTitle.Caption = "Analysis Results: Single Layer Bridging Roof -
Single Layer Foundation"
    End If
    Call main
    'Output the results of the program.
```

```
    frmOutput!txtText(0).Text = Format$(Span, "####0.00")
    frmOutput!txtText(1).Text = Format$(Roof_Energy, "0.00E+00")
    frmOutput!txtText(2).Text = Format$(Foundation_Energy, "0.00E+00")
    frmOutput!txtText(3).Text = Format$(Total_Energy, "0.00E+00")
    frmOutput!txtText(4).Text = Format$(Richter_Scale, "##0.00")
    frmOutput!txtText(5) = Format$(Foundation_Stress, "###0.00")
    frmOutput!txtText(6) = Format$(Seismic_Ratio, "#0.00%")
    'Evaluate and output the bump likeliness.
    If Richter_Scale >= 2# Then
        If Foundation_Stress >= C0 / 10 ^ 6 Then
            Msg = "Foundation failure is predicted."
            Msg = Msg + "  Local Richter magnitude is over 2.0."
            Msg = Msg + "  Pressure bump condition may exist."
        Else
            Msg = "Roof failure is predicted."
            Msg = Msg + "  Local Richter magnitude is over 2.0."
            Msg = Msg + "  Shock bump condition may exist."
        End If
    Else
        Msg = "Coal bump condition may not exist."
    End If
    frmOutput.txtBump = Msg
    frmOutput.Show
End Sub


Sub cmdPrint_Click ()
    'Print the current input form.
    PrintForm
End Sub



input2.frm


Sub cmdBack_Click ()
    'Hide the current input form and show the previous model form frmModel1.
    Model_Type = 0
    frmInput2.Hide
    frmModel1.Show
End Sub


Sub cmdExit_Click ()
    'End the excution of the program.
```

```
      End
End Sub

Sub cmdHelp_Click ()
   'Show a help form that describes the input parameter.
   frmHelpInput.Show
End Sub

Sub cmdOutput_Click ()
   'Input error-checking section.
   Const MB_OK = 0            'Define buttons.
   Const MB_ICONSTOP = 16         'Define Icons.
   Dim DgDef, Msg, Title      'Declare variables.
   Title = "Input Error"
   DgDef = MB_ICONSTOP            'Describe dialog.
   Title = "Input Error"
   par = Val(txtText(0))
   Msg = "Check input -- Roof Parameter: Young's modulus in compression
          (upper layer)."
     If par <= 0 Then
        Response = MsgBox(Msg, DgDef, Title)
        Exit Sub
     End If
   par = Val(txtText(1))
   Msg = "Check input -- Roof Parameter: Young's modulus in compression
          (lower layer)."
     If par <= 0 Then
        Response = MsgBox(Msg, DgDef, Title)
        Exit Sub
     End If
   par = Val(txtText(2))
   Msg = "Check input -- Roof Parameter: Young's modulus in tension (upper layer)."
     If par <= 0 Then
        Response = MsgBox(Msg, DgDef, Title)
        Exit Sub
     End If
   par = Val(txtText(3))
   Msg = "Check input -- Roof Parameter: Young's modulus in tension (lower layer)."
     If par <= 0 Then
        Response = MsgBox(Msg, DgDef, Title)
        Exit Sub
     End If
   par = Val(txtText(4))
```

235

```
Msg = "Check input -- Roof Parameter: thickness (upper layer)."
   If par <= 0 Then
      Response = MsgBox(Msg, DgDef, Title)
      Exit Sub
   End If
par = Val(txtText(5))
Msg = "Check input -- Roof Parameter: thickness (lower layer)."
   If par <= 0 Then
      Response = MsgBox(Msg, DgDef, Title)
      Exit Sub
   End If
par = Val(txtText(6))
Msg = "Check input -- Roof Parameter: effective tensile strength."
   If par <= 0 Then
      Response = MsgBox(Msg, DgDef, Title)
      Exit Sub
   End If
par = Val(txtText(7))
Msg = "Check input -- Coal Parameter: Young's modulus."
   If par <= 0 Then
      Response = MsgBox(Msg, DgDef, Title)
      Exit Sub
   End If
par = Val(txtText(8))
Msg = "Check input -- Coal Parameter: Poisson's ratio."
   If par <= 0 Or par > 1# Then
      Response = MsgBox(Msg, DgDef, Title)
      Exit Sub
   End If
par = Val(txtText(9))
Msg = "Check input -- Coal Parameter: compressive strength."
   If par <= 0 Then
      Response = MsgBox(Msg, DgDef, Title)
      Exit Sub
   End If
par = Val(txtText(10))
Msg = "Check input -- Coal Parameter: thickness."
   If par <= 0 Then
      Response = MsgBox(Msg, DgDef, Title)
      Exit Sub
   End If
par = Val(txtText(11))
Msg = "Check input -- Other Parameter: overburden depth."
```

```
   If par <= 0 Then
      Response = MsgBox(Msg, DgDef, Title)
      Exit Sub
   End If
par = Val(txtText(12))
Msg = "Check input -- Other Parameter: specific gravity of overburden."
   If par <= 0 Then
      Response = MsgBox(Msg, DgDef, Title)
      Exit Sub
   End If
par = Val(txtText(13))
Msg = "Check input -- Other Parameter: abutment stress concentration (> 1.0)."
   If par < 1 Then
      Response = MsgBox(Msg, DgDef, Title)
      Exit Sub
   End If
par = Val(txtText(14))
Msg = "Check input -- Other Parameter: stress concentration length."
   If par <= 0 Then
      Response = MsgBox(Msg, DgDef, Title)
      Exit Sub
   End If
par = Val(txtText(15))
Msg = "Check input -- Other Parameter: width of working face."
   If par <= 0 Then
      Response = MsgBox(Msg, DgDef, Title)
      Exit Sub
   End If
par = Val(txtText(16))
Msg = "Check input -- Other Parameter: seismic efficiency (0 < n <= 1.0)."
   If par <= 0 Or par > 1# Then
      Response = MsgBox(Msg, DgDef, Title)
      Exit Sub
   End If
'Hide the present input form, show the output form.
frmInput2.Hide
frmOutput.txtCase = frmInfo.txtInfo(0)
If Model_Type = 3 Then
   frmOutput.lblTitle.Caption = "Analysis Results: Double Layer Cantilevering
                              Roof - Single Layer Foundation"
Else
   frmOutput.lblTitle.Caption = "Analysis Results: Double Layer Bridging Roof
                              - Single   Layer Foundation"
```

```vb
      End If
      Call main
      'Output the results of the program.
      frmOutput!txtText(0).Text = Format$(Span, "####0.00")
      frmOutput!txtText(1).Text = Format$(Roof_Energy, "0.00E+00")
      frmOutput!txtText(2).Text = Format$(Foundation_Energy, "0.00E+00")
      frmOutput!txtText(3).Text = Format$(Total_Energy, "0.00E+00")
      frmOutput!txtText(4).Text = Format$(Richter_Scale, "##0.00")
      frmOutput!txtText(5) = Format$(Foundation_Stress, "###0.00")
      frmOutput!txtText(6) = Format$(Seismic_Ratio, "#0.00%")
      'Evaluate and output the bump likeliness.
      If Richter_Scale >= 2# Then
         If Foundation_Stress >= C0 / 10 ^ 6 Then
            Msg = "Foundation failure is predicted."
            Msg = Msg + " Local Richter magnitude is over 2.0."
            Msg = Msg + " Pressure bump condition may exist."
         Else
            Msg = "Roof failure is predicted."
            Msg = Msg + " Local Richter magnitude is over 2.0."
            Msg = Msg + " Shock bump condition may exist."
         End If
      Else
         Msg = "Coal bump condition may not exist."
      End If
      frmOutput.txtBump = Msg
      frmOutput.Show
End Sub


Sub cmdPrint_Click ()
   'Print the current input form.
   PrintForm
End Sub



input3.frm


Sub cmdBack_Click ()
   'Hide the current input form and show the previous model form frmModel2.
   Model_Type = 0
   frmInput3.Hide
   frmModel2.Show
End Sub
```

```vb
Sub cmdExit_Click ()
    'End the excution of the program.
    End
End Sub

Sub cmdHelp_Click ()
    'Show a help form that describes the input parameter.
    frmHelpInput.Show
End Sub

Sub cmdOutput_Click ()
    'Input error-checking section.
    Const MB_OK = 0             'Define buttons.
    Const MB_ICONSTOP = 16      'Define Icons.
    Dim DgDef, Msg, Title       'Declare variables.
    Title = "Input Error"
    DgDef = MB_ICONSTOP         'Describe dialog.
    Title = "Input Error"
    par = Val(txtText(0))
    Msg = "Check input -- Roof Parameter: Young's modulus in compression."
        If par <= 0 Then
            Response = MsgBox(Msg, DgDef, Title)
            Exit Sub
        End If
    par = Val(txtText(1))
    Msg = "Check input -- Roof Parameter: Young's modulus in tension."
        If par <= 0 Then
            Response = MsgBox(Msg, DgDef, Title)
            Exit Sub
        End If
    par = Val(txtText(2))
    Msg = "Check input -- Roof Parameter: thickness."
        If par <= 0 Then
            Response = MsgBox(Msg, DgDef, Title)
            Exit Sub
        End If
    par = Val(txtText(3))
    Msg = "Check input -- Roof Parameter: effective tensile strength."
        If par <= 0 Then
            Response = MsgBox(Msg, DgDef, Title)
            Exit Sub
        End If
```

239

```
par = Val(txtText(4))
Msg = "Check input -- Foundation Parameter: Young's modulus (coal seam)."
   If par <= 0 Then
      Response = MsgBox(Msg, DgDef, Title)
      Exit Sub
   End If
par = Val(txtText(5))
Msg = "Check input -- Foundation Parameter: Young's modulus (weak roof)."
   If par <= 0 Then
      Response = MsgBox(Msg, DgDef, Title)
      Exit Sub
   End If
par = Val(txtText(6))
Msg = "Check input -- Foundation Parameter: Poisson's ratio (coal seam)."
   If par <= 0 Or par > 1# Then
      Response = MsgBox(Msg, DgDef, Title)
      Exit Sub
   End If
par = Val(txtText(7))
Msg = "Check input -- Foundation Parameter: Poisson's ratio (weak roof)."
   If par <= 0 Or par > 1# Then
      Response = MsgBox(Msg, DgDef, Title)
      Exit Sub
   End If
par = Val(txtText(8))
Msg = "Check input -- Foundation Parameter: compressive strength (coal seam)."
   If par <= 0 Then
      Response = MsgBox(Msg, DgDef, Title)
      Exit Sub
   End If
par = Val(txtText(9))
Msg = "Check input -- Foundation Parameter: compressive strength (weak roof)."
   If par <= 0 Then
      Response = MsgBox(Msg, DgDef, Title)
      Exit Sub
   End If

par = Val(txtText(10))
Msg = "Check input -- Foundation Parameter: thickness (coal seam)."
   If par <= 0 Then
      Response = MsgBox(Msg, DgDef, Title)
      Exit Sub
   End If
```

```
par = Val(txtText(11))
Msg = "Check input -- Foundation Parameter: thickness (weak roof)."
   If par <= 0 Then
      Response = MsgBox(Msg, DgDef, Title)
      Exit Sub
   End If
par = Val(txtText(12))
Msg = "Check input -- Other Parameter: overburden depth."
   If par <= 0 Then
      Response = MsgBox(Msg, DgDef, Title)
      Exit Sub
   End If
par = Val(txtText(13))
Msg = "Check input -- Other Parameter: specific gravity of overburden."
   If par <= 0 Then
      Response = MsgBox(Msg, DgDef, Title)
      Exit Sub
   End If
par = Val(txtText(14))
Msg = "Check input -- Other Parameter: abutment stress concentration (> 1.0)."
   If par < 1 Then
      Response = MsgBox(Msg, DgDef, Title)
      Exit Sub
   End If
par = Val(txtText(15))
Msg = "Check input -- Other Parameter: stress concentration length."
   If par <= 0 Then
      Response = MsgBox(Msg, DgDef, Title)
      Exit Sub
   End If
par = Val(txtText(16))
Msg = "Check input -- Other Parameter: width of working face."
   If par <= 0 Then
      Response = MsgBox(Msg, DgDef, Title)
      Exit Sub
   End If
par = Val(txtText(17))
Msg = "Check input -- Other Parameter: seismic efficiency (0 < n <= 1.0)."
   If par <= 0 Or par > 1# Then
      Response = MsgBox(Msg, DgDef, Title)
      Exit Sub
   End If
'Hide the present input form, show the output form.
```

```vb
    frmInput3.Hide
    frmOutput.txtCase = frmInfo.txtInfo(0)
    If Model_Type = 5 Then
        frmOutput.lblTitle.Caption = "Analysis Results: Single Layer Cantilevering
                                    Roof - Double Layer Foundation"
    Else
        frmOutput.lblTitle.Caption = "Analysis Results: Single Layer Bridging Roof
                                    - Double Layer Foundation"
    End If
    Call main
    'Output the results of the program.
    frmOutput!txtText(0).Text = Format$(Span, "####0.00")
    frmOutput!txtText(1).Text = Format$(Roof_Energy, "0.00E+00")
    frmOutput!txtText(2).Text = Format$(Foundation_Energy, "0.00E+00")
    frmOutput!txtText(3).Text = Format$(Total_Energy, "0.00E+00")
    frmOutput!txtText(4).Text = Format$(Richter_Scale, "##0.00")
    frmOutput!txtText(5) = Format$(Foundation_Stress, "###0.00")
    frmOutput!txtText(6) = Format$(Seismic_Ratio, "#0.00%")
    'Evaluate and output the bump likeliness.
    If Richter_Scale >= 2# Then
        If Foundation_Stress >= C0 / 10 ^ 6 Then
            Msg = "Foundation failure is predicted."
            Msg = Msg + "  Local Richter magnitude is over 2.0."
            Msg = Msg + "  Pressure bump condition may exist."
        Else
            Msg = "Roof failure is predicted."
            Msg = Msg + "  Local Richter magnitude is over 2.0."
            Msg = Msg + "  Shock bump condition may exist."
        End If
    Else
        Msg = "Coal bump condition may not exist."
    End If
    frmOutput.txtBump = Msg
    frmOutput.Show
End Sub

Sub cmdPrint_Click ()
    'Print the current input form.
    PrintForm
End Sub
```

input4.frm

```
Sub cmdBack_Click ()
    'Hide the current input form and show the previous model form frmModel2.
    Model_Type = 0
    frmInput4.Hide
    frmModel2.Show
End Sub


Sub cmdExit_Click ()
    'End the excution of the program.
    End
End Sub


Sub cmdHelp_Click ()
    'Show a help form that describes the input parameter.
    frmHelpInput.Show
End Sub


Sub cmdOutput_Click ()
    'Input error-checking section.
    Const MB_OK = 0            'Define buttons.
    Const MB_ICONSTOP = 16      'Define Icons.
    Dim DgDef, Msg, Title       'Declare variables.
    Title = "Input Error"
    DgDef = MB_ICONSTOP          'Describe dialog.
    Title = "Input Error"
    par = Val(txtText(0))
    Msg = "Check input -- Roof Parameter: Young's modulus in compression
           (upper layer)."
        If par <= 0 Then
            Response = MsgBox(Msg, DgDef, Title)
            Exit Sub
        End If
    par = Val(txtText(1))
    Msg = "Check input -- Roof Parameter: Young's modulus in compression
           (lower layer)."
        If par <= 0 Then
            Response = MsgBox(Msg, DgDef, Title)
            Exit Sub
        End If
    par = Val(txtText(2))
    Msg = "Check input -- Roof Parameter: Young's modulus in tension (upper layer)."
```

243

```
      If par <= 0 Then
         Response = MsgBox(Msg, DgDef, Title)
         Exit Sub
      End If
par = Val(txtText(3))
Msg = "Check input -- Roof Parameter: Young's modulus in tension (lower layer)."
      If par <= 0 Then
         Response = MsgBox(Msg, DgDef, Title)
         Exit Sub
      End If
par = Val(txtText(4))
Msg = "Check input -- Roof Parameter: thickness (upper layer)."
      If par <= 0 Then
         Response = MsgBox(Msg, DgDef, Title)
         Exit Sub
      End If
par = Val(txtText(5))
Msg = "Check input -- Roof Parameter: thickness (lower layer)."
      If par <= 0 Then
         Response = MsgBox(Msg, DgDef, Title)
         Exit Sub
      End If
par = Val(txtText(6))
Msg = "Check input -- Roof Parameter: effective tensile strength."
      If par <= 0 Then
         Response = MsgBox(Msg, DgDef, Title)
         Exit Sub
      End If
par = Val(txtText(7))
Msg = "Check input -- Foundation Parameter: Young's modulus (coal seam)."
      If par <= 0 Then
         Response = MsgBox(Msg, DgDef, Title)
         Exit Sub
      End If
par = Val(txtText(8))
Msg = "Check input -- Foundation Parameter: Young's modulus (weak roof)."
      If par <= 0 Then
         Response = MsgBox(Msg, DgDef, Title)
         Exit Sub
      End If
par = Val(txtText(9))
Msg = "Check input -- Foundation Parameter: Poisson's ratio (coal seam)."
      If par <= 0 Or par > 1# Then
```

```
        Response = MsgBox(Msg, DgDef, Title)
        Exit Sub
    End If
  par = Val(txtText(10))
  Msg = "Check input -- Foundation Parameter: Poisson's ratio (weak roof)."
    If par <= 0 Or par > 1# Then
        Response = MsgBox(Msg, DgDef, Title)
        Exit Sub
    End If
  par = Val(txtText(11))
  Msg = "Check input -- Foundation Parameter: compressive strength (coal seam)."
    If par <= 0 Then
        Response = MsgBox(Msg, DgDef, Title)
        Exit Sub
    End If
  par = Val(txtText(12))
  Msg = "Check input -- Foundation Parameter: compressive strength (weak roof)."
    If par <= 0 Then
        Response = MsgBox(Msg, DgDef, Title)
        Exit Sub
    End If
  par = Val(txtText(13))
  Msg = "Check input -- Foundation Parameter: thickness (coal seam)."
    If par <= 0 Then
        Response = MsgBox(Msg, DgDef, Title)
        Exit Sub
    End If
  par = Val(txtText(14))
  Msg = "Check input -- Foundation Parameter: thickness (weak roof)."
    If par <= 0 Then
        Response = MsgBox(Msg, DgDef, Title)
        Exit Sub
    End If
  par = Val(txtText(15))
  Msg = "Check input -- Other Parameter: overburden depth."
    If par <= 0 Then
        Response = MsgBox(Msg, DgDef, Title)
        Exit Sub
    End If
  par = Val(txtText(16))
  Msg = "Check input -- Other Parameter: specific gravity of overburden."
    If par <= 0 Then
        Response = MsgBox(Msg, DgDef, Title)
```

```
            Exit Sub
        End If
    par = Val(txtText(17))
    Msg = "Check input -- Other Parameter: abutment stress concentration (> 1.0)."
        If par < 1 Then
            Response = MsgBox(Msg, DgDef, Title)
            Exit Sub
        End If
    par = Val(txtText(18))
    Msg = "Check input -- Other Parameter: stress concentration length."
        If par <= 0 Then
            Response = MsgBox(Msg, DgDef, Title)
            Exit Sub
        End If
    par = Val(txtText(19))
    Msg = "Check input -- Other Parameter: width of working face."
        If par <= 0 Then
            Response = MsgBox(Msg, DgDef, Title)
            Exit Sub
        End If
    par = Val(txtText(20))
    Msg = "Check input -- Other Parameter: seismic efficiency (0 < n <= 1.0)."
        If par <= 0 Or par > 1# Then
            Response = MsgBox(Msg, DgDef, Title)
            Exit Sub
        End If
'Hide the present input form, show the output form.
    frmInput4.Hide
    frmOutput.txtCase = frmInfo.txtInfo(0)
    If Model_Type = 7 Then
        frmOutput.lblTitle.Caption = "Analysis Results: Double Layer Cantilevering
                                Roof - Double Layer Foundation"
    Else
        frmOutput.lblTitle.Caption = "Analysis Results: Double Layer Bridging
                                Roof - Double Layer Foundation"
    End If
    Call main
    'Output the results of the program.
    frmOutput!txtText(0).Text = Format$(Span, "####0.00")
    frmOutput!txtText(1).Text = Format$(Roof_Energy, "0.00E+00")
    frmOutput!txtText(2).Text = Format$(Foundation_Energy, "0.00E+00")
    frmOutput!txtText(3).Text = Format$(Total_Energy, "0.00E+00")
    frmOutput!txtText(4).Text = Format$(Richter_Scale, "##0.00")
```

```
   frmOutput!txtText(5) = Format$(Foundation_Stress, "###0.00")
   frmOutput!txtText(6) = Format$(Seismic_Ratio, "#0.00%")
   'Evaluate and output the bump likeliness.
   If Richter_Scale >= 2# Then
      If Foundation_Stress >= C0 / 10 ^ 6 Then
         Msg = "Foundation failure is predicted."
         Msg = Msg + "  Local Richter magnitude is over 2.0."
         Msg = Msg + "  Pressure bump condition may exist."
      Else
         Msg = "Roof failure is predicted."
         Msg = Msg + "  Local Richter magnitude is over 2.0."
         Msg = Msg + "  Shock bump condition may exist."
      End If
   Else
      Msg = "Coal bump condition may not exist."
   End If
   frmOutput.txtBump = Msg
   frmOutput.Show
End Sub


Sub cmdPrint_Click ()
   'Print the current input form.
   PrintForm
End Sub
```

model1.frm

```
Sub cmdBack_Click ()
   frmModel1.Hide
   frmInfo.Show
End Sub


Sub cmdContinue_Click ()
   Const MB_OK = 0                  'Define buttons.
   Const MB_ICONEXCLAMATION = 48          'Define Icons.
   Dim DgDef, Response, Msg, Title       'Declare variables.
   DgDef = MB_ICONEXCLAMATION           'Describe dialog.
   Title = "Model Selection Error"
   'Hide the model form and show the input form, depending on the model type chosen.
   frmModel1.Hide
   Select Case Model_Type
```

```
      Case 1
        frmInput1.Caption = "Model 1 : Input Parameter"
        frmInput1.txtCase = frmInfo.txtInfo(0)
        frmInput1.fraFrame1.Caption = "Roof Parameter:  " & frmInfo.txtInfo(1)
        frmInput1.fraFrame2.Caption = "Coal Parameter:  " & frmInfo.txtInfo(2)
        frmInput1.Show
      Case 2
        frmInput1.Caption = "Model 2 : Input Parameter"
        frmInput1.txtCase = frmInfo.txtInfo(0)
        frmInput1.fraFrame1.Caption = "Roof Parameter:  " & frmInfo.txtInfo(1)
        frmInput1.fraFrame2.Caption = "Coal Parameter:  " & frmInfo.txtInfo(2)
        frmInput1.Show
      Case 3
        frmInput2.Caption = "Model 3 : Input Parameter"
        frmInput2.txtCase = frmInfo.txtInfo(0)
        frmInput2.fraFrame1.Caption = "Roof Parameter:  " & frmInfo.txtInfo(1)
        frmInput2.fraFrame2.Caption = "Coal Parameter:  " & frmInfo.txtInfo(2)
        frmInput2.Show
      Case 4
        frmInput2.Caption = "Model 4 : Input Parameter"
        frmInput2.txtCase = frmInfo.txtInfo(0)
        frmInput2.fraFrame1.Caption = "Roof Parameter:  " & frmInfo.txtInfo(1)
        frmInput2.fraFrame2.Caption = "Coal Parameter:  " & frmInfo.txtInfo(2)
        frmInput2.Show
      Case Else
        frmModel1.Show
        Msg = "You must select one of roof models to continue."
        Msg = Msg + Chr(10) + "Or choose More Models button to show
        more roof models."
        Response = MsgBox(Msg, DgDef, Title)
    End Select
End Sub

Sub cmdExit_Click ()
  'End the execution of the program.
  End
End Sub

Sub cmdModel1_Click ()
  Model_Type = 1    'Global variable.
End Sub

Sub cmdModel2_Click ()
```

```
      Model_Type = 2    'Global variable.
End Sub


Sub cmdModel3_Click ()
      Model_Type = 3
End Sub


Sub cmdModel4_Click ()
      Model_Type = 4    'Global variable.
End Sub


Sub cmdMore_Click ()
      'Hide the form Model1 and show the more roof models.
      frmModel1.Hide
      frmModel2.Show
End Sub


Sub cmdPrint_Click ()
      'Print the form.
      PrintForm
End Sub
```

model2.frm

```
Sub cmdBack_Click ()
      'Hide the current form and show the previous form for roof models 1 to 4.
      frmModel2.Hide
      frmModel1.Show
End Sub


Sub cmdContinue_Click ()
      Const MB_OK = 0                      'Define buttons.
      Const MB_ICONEXCLAMATION = 48        'Define Icons.
      Dim DgDef, Response, Msg, Title      'Declare variables.
      DgDef = MB_ICONEXCLAMATION           'Describe dialog.

      Title = "Model Selection Error"

      'Hide the model form and show the input form, depending on the model type chosen.
      frmModel2.Hide
      Select Case Model_Type
```

```
        Case 5
            frmInput3.Caption = "Model 5 : Input Parameter"
            frmInput3.txtCase = frmInfo.txtInfo(0)
            frmInput3.fraFrame1.Caption = "Roof Parameter:  " & frmInfo.txtInfo(1)
            frmInput3.fraFrame2.Caption = "Coal Parameter:  " & frmInfo.txtInfo(2)
            frmInput3.Show
        Case 6
            frmInput3.Caption = "Model 6 : Input Parameter"
            frmInput3.txtCase = frmInfo.txtInfo(0)
            frmInput3.fraFrame1.Caption = "Roof Parameter:  " & frmInfo.txtInfo(1)
            frmInput3.fraFrame2.Caption = "Coal Parameter:  " & frmInfo.txtInfo(2)
            frmInput3.Show
        Case 7
            frmInput4.Caption = "Model 7 : Input Parameter"
            frmInput4.txtCase = frmInfo.txtInfo(0)
            frmInput4.fraFrame1.Caption = "Roof Parameter:  " & frmInfo.txtInfo(1)
            frmInput4.fraFrame2.Caption = "Coal Parameter:  " & frmInfo.txtInfo(2)
            frmInput4.Show
        Case 8
            frmInput4.Caption = "Model 8 : Input Parameter"
            frmInput4.txtCase = frmInfo.txtInfo(0)
            frmInput4.fraFrame1.Caption = "Roof Parameter:  " & frmInfo.txtInfo(1)
            frmInput4.fraFrame2.Caption = "Coal Parameter:  " & frmInfo.txtInfo(2)
            frmInput4.Show
        Case Else
            frmModel2.Show
            Msg = "You must select one of roof models to continue."
            Response = MsgBox(Msg, DgDef, Title)
    End Select
End Sub

Sub cmdExit_Click ()
    'End the excution of the program.
    End
End Sub

Sub cmdModel5_Click ()
    Model_Type = 5    'Global variable.
End Sub

Sub cmdModel6_Click ()
    Model_Type = 6    'Global variable.
End Sub
```

```
Sub cmdModel7_Click ()
   Model_Type = 7    'Global variable.
End Sub

Sub cmdModel8_Click ()
   Model_Type = 8    'Global variable.
End Sub

Sub cmdPrint_Click ()
   'Print the form
   PrintForm
End Sub
```

output.frm

```
Sub cmdAnother_Click ()
   Model_Type = 0
   frmOutput.Hide
   frmInfo.Show
End Sub

Sub cmdBack_Click ()
   'Hide the current output form and show the previous form.
   frmOutput.Hide
   Select Case Model_Type
      Case 1, 2
         frmInput1.Show
      Case 3, 4
         frmInput2.Show
      Case 5, 6
         frmInput3.Show
      Case 7, 8
         frmInput4.Show
   End Select
End Sub

Sub cmdExit_Click ()
   'End the excution of the program.
   End
End Sub
```

251

```
Sub cmdHelp_Click ()
    'Show a help form for output.
    frmOutput.Hide
    frmHelpOutput.Show
End Sub

Sub cmdPrint_Click ()
    'Print the current output form.
    PrintForm
End Sub
```

Vita

Xiaolin Wu was born on January 19, 1964, in Yueshan, the People's Republic of China. He graduated with a Bachelor degree in Mining Engineering from the Southern College of Metallurgy, Ganzhou, in 1983. One year later, he attended the China University of Geosciences, Beijing, where he received a Master degree in Mining Engineering in 1987. He subsequently worked four years as a mining engineer for the Jiangxi Bureau of Geology and Mineral Resources. In September, 1991, He entered the Virginia Polytechnic Institute and State University to study a doctoral program in the Department of Mining and Mineral Engineering. He expects to complete the requirements for the Ph.D. degree in Mining Engineering in December, 1995.